Volume II, 1958

TRANSACTIONS of the SOCIETY OF RHEOLOGY

Editor: R. D. ANDREWS
Massachusetts Institute of Technology

Preface 1
ARTHUR S. NOWICK: Presentation of the Bingham Medal to Clarence M. Zener 3
J. J. BIKERMAN and WILLIAM YAP: Rheology of Peeling in a Newtonian Liquid 9
KENNETH E. OWENS and CARL A. DAHLQUIST: Dynamic Mechanical Properties of Fluorochemical Elastomers 23
DONALD J. PLAZEK, M. N. VRANCKEN, and JOHN W. BERGE: A Torsion Pendulum for Dynamic and Creep Measurements of Soft Viscoelastic Materials 39
ROBERT F. LANDEL: The Dynamic Mechanical Properties of a Model Filled System: Polyisobutylene-Glass Beads 53
J. C. MILLER and R. R. MYERS: A Photographic Study of Liquid Flow in a Roll Nip 77
B. ALBRECHT and A. M. FREUDENTHAL: On Relaxation Spectra in High Polymers 95
THOR L. SMITH: Approximate Equations for Interconverting the Various Mechanical Properties of Linear Viscoelastic Materials 131
COSIMO TORRE: The Principles of Plastico-Dynamics 153
J. K. LANDAUER: The Creep of Snow under Combined Stress 175
BERNARD D. COLEMAN: Time Dependence of Mechanical Breakdown in Bundles of Fibers. III. The Power Law Breakdown Rule 195
LAWRENCE M. EPSTEIN and ROBERT P. SMITH: The Tensile Strength of GR-S Elastomers 219
A. B. METZNER and MALCOLM WHITLOCK: Flow Behavior of Concentrated (Dilatant) Suspensions 239
P. R. PASLAY and A. SLIBAR: Flow of an Incompressible Visco-Plastic Layer on an Inclined Plane 255
WLADIMIR PHILIPPOFF and FREDERICK H. GASKINS: The Capillary Experiment in Rheology 263
JOHN G. BRODNYAN, FREDERICK H. GASKINS, WLADIMIR PHILIPPOFF, and E. G. LENDRAT: The Rheology of Various Solutions of Cellulose Derivatives 285
Abstracts of Additional Papers Presented at the Society of Rheology Meeting, November 7–9, 1957 303
Corrigenda: BERNARD D. COLEMAN: A Stochastic Process Model for Mechanical Breakdown (*Trans. Soc. Rheology*, 1, 153–168, 1957) 313

INTERSCIENCE PUBLISHERS NEW YORK • LONDON

F. H. Wetzel

TRANSACTIONS of the SOCIETY OF RHEOLOGY

VOLUME II · 1958

INTERSCIENCE PUBLISHERS · NEW YORK · LONDON

Copyright © 1959 by
INTERSCIENCE PUBLISHERS, INC.

Library of Congress Catalog
Card Number 57-11926

INTERSCIENCE PUBLISHERS, INC.
250 Fifth Avenue, New York 1, N. Y.

For Great Britain and Northern Ireland:
INTERSCIENCE PUBLISHERS LTD.
88/90 Chancery Lane, London, W. C. 2

PRINTED IN THE UNITED STATES OF AMERICA BY MACK PRINTING CO., EASTON, PA.

Preface

Volume II of the *Transactions of the Society of Rheology* (1958) is a collection of the papers presented at the annual meeting of the Society held at the Textile Research Institute in Princeton, New Jersey, on November 7–9, 1957. In cases where the papers in full are not included, abstracts are given. The address of presentation of the Bingham Medal to Dr. Clarence M. Zener, by Dr. Arthur S. Nowick, is included at the beginning of the volume, following the custom established in Volume I.

The Society of Rheology was founded almost thirty years ago, on December 19, 1929, largely through the vision and efforts of the late Professor Eugene C. Bingham of Lafayette College. The founding of the Society was an outgrowth of a series of Viscosity and Plasticity Symposia dating back to 1924, which indicated a lively and widespread interest in this general field. The word "Rheology" was suggested (by Professor Bingham) as an official name for the science of the deformation and flow of matter. The Society is a member of the American Institute of Physics, and, in fact, was one of the founder Societies of the Institute. The Society is also affiliated with the American Association for the Advancement of Science.

Collections of papers presented at annual meetings in the past have been published as Symposia in other journals—notably the *Journal of Colloid Science* and the *Journal of Applied Physics*. However, in 1957 it was decided to initiate a new journal, *Transactions of the Society of Rheology*, which would publish the papers from the annual meeting under an expanded and more flexible editorial policy. Volume I, published in 1957, contained papers presented at the annual meeting held at the Mellon Institute in Pittsburgh, Pennsylvania, on November 7–9, 1956, together with the presentation address of the Bingham Medal to Professor Arthur V. Tobolsky by Dean Sir Hugh S. Taylor. Volume I was well received, and this encouraged the Society to establish *Transactions of the Society of Rheology* as a permanent publication.

The other publication of the Society is the *Rheology Bulletin*, which is ordinarily issued three times a year, one issue of which gives abstracts of papers to be presented at the annual meeting together with details concerning the meeting.

Current officers of the Society are as follows:

President:

J. H. Dillon
Textile Research Institute
Princeton, N. J.

Vice-President:

J. H. Elliott
Hercules Experiment Station
Wilmington, Del.

Secretary-Treasurer:

W. R. Willets
Titanium Pigment Corp.
99 Hudson Street
New York 13, N. Y.

Editor:

R. D. Andrews, Jr.
Plastics Research Laboratory
Room 7-006, M. I. T.
Cambridge 39, Mass.

The governing body of the Society is the Executive Committee, which consists of the Officers, the most recent living Past President (F. D. Dexter, Union Carbide Plastics), and two other members elected by the Society. For 1958–59 the latter are: R. S. Marvin (National Bureau of Standards) and R. S. Rivlin (Brown University).

R. D. Andrews, Jr.

Cambridge, Massachusetts
December 30, 1958

TRANSACTIONS OF THE SOCIETY OF RHEOLOGY II, 3-7 (1958)

Presentation of the Bingham Medal to Clarence M. Zener

ARTHUR S. NOWICK, *I.B.M. Watson Laboratory, Columbia University, New York, New York*

In 1937 our medalist, as a young theoretical physicist, decided to step down from the lofty heights of the quantum theory to attack an interesting problem in rheology. At that time Dr. Zener had behind him a succession of significant achievements in the field of quantum mechanics. He had made important contributions to the theory of the hydrogen molecule as a graduate student at Harvard University, and to the theory of the lithium atom during a postdoctoral fellowship in Germany. In subsequent work at Princeton and then in England he had become interested in the solid state and had made contributions to the theory of the optical and electrical properties of solids. Much of this work of his early period of research is now classic and may be found quoted in any textbook on quantum mechanics or solid state physics. The abrupt change of interest in 1937 came about as a result of an attempt to determine the origin of internal friction (or damping) in metals. In seeking possible mechanisms for this damping, he noted that a reed vibrating in flexure would show an energy loss due to the heat flow from the stretched (or cooled) side across to the compressed (or heated) side. He showed that internal friction as a function of frequency goes through a maximum and related the fre-

quency of the maximum to the thermal diffusivity and the thickness of the reed.

After this work, Dr. Zener was prompted to move in two directions. On the one hand he sought to generalize his theory to other related mechanisms. In particular, he recognized that in polycrystalline metals there would be a similar source of energy loss due to thermal currents between grains, originating in the elastic anisotropy of the metal. On the other hand he realized that the data required to confirm his predictions concerning these mechanisms of internal friction were not available and would require experiments designed specifically to look for the effects in question. He therefore turned experimentalist for a period of time, and together with some of his colleagues and students at the City College of New York, carried out a series of experiments which confirmed in all details his theory of damping originating in thermal currents.

About the same time Dr. Zener became interested in a strongly temperature-dependent internal friction found in polycrystalline metals. He concluded that this behavior could be attributed to a viscous property of grain boundaries at high temperatures. Such ideas were not readily accepted by many metallurgists to whom the concept of treating a grain boundary as a viscous layer seemed to be at variance with the prevalent notions of the structure of the grain boundary. Subsequent experiments by Dr. Zener and his collaborators (particularly the later work at the Institute for the Study of Metals with the Chinese physicist T. S. Kê), vindicated the concept of the viscous grain boundary and demonstrated the generality of the phenomenon. Today this source of internal friction is an important metallurgical tool for the study of the grain boundaries of metals. Even the minutest changes of composition in the grain boundary which cannot be detected by any other means will have a profound effect on the grain boundary internal friction.

Dr. Zener's work on the various mechanisms of internal friction was interrupted by the war when he left academic life to take up work at the Watertown Arsenal in Massachusetts. Here he worked on problems of flow and fracture, particularly of steel, and his contributions in this field are still widely quoted.

In 1945 he joined the staff of the newly formed Institute for the Study of Metals at the University of Chicago. Here he began to systematize the work that he had done before the war on various

mechanical relaxation phenomena. After experimenting with some of his ideas in the form of an article called "Anelasticity of Metals," he finally published his book entitled "Elasticity and Anelasticity of Metals" in 1948. The term "anelasticity" he defined as linear viscoelastic behavior which involves limited strain that is completely recoverable after removal of all the stresses. Dr. Zener's insight in separating "anelastic" behavior from other types of viscoelastic effects were made apparent as he showed how the same formal theory permitted one to treat a variety of relaxation phenomena in metals. The word "anelasticity" is now standard terminology among metal physicists, and Dr. Zener's book, though nearly 10 years old, is still the basic reference in this field. The various phenomena discussed in this book were so simply and directly interpreted that they have served as the starting point for those working with complex materials. One of the most beautiful relaxation effects was discovered in 1943 by Dr. Zener during his experimental work at Washington State College. He found that a single crystal of alpha-brass showed a sharp symmetrical peak of internal friction versus reciprocal absolute temperature such as to suggest an anelastic phenomenon controlled by a single time of relaxation. In the paper in which the data were presented, possible interpretations were offered for the effect in terms of clusters of solute atoms or crystal imperfections. Evidently Zener did not believe these mechanisms himself, for he used a modified explanation in a publication three years later. Finally, while at the Institute, an interpretation as appealing and as simple as the phenomenon itself occurred to him, namely, the concept of stress-induced reorientation of pairs of solute atoms. According to this concept, each pair of foreign atoms in the crystal has a preferred direction under an applied stress, and therefore a relaxation in the distribution of such pairs will take place if sufficient time is allowed for diffusion. This phenomenon, which has since been shown to be common to essentially all substitutional solid solutions, is now referred to as the Zener relaxation, and the internal friction peak as Zener's peak. Of course, peaks have been named after their discoverers before; but it may be consoling to Dr. Zener to know that long after Pike's peak has disappeared from the face of the earth, Zener's peak will still be with us.

The period at the Institute for the Study of Metals was a most exciting one. Here "anelasticity" was born and grew to maturity as it quickly became recognized as a powerful tool of the metal physicist.

Dr. Zener's keen physical insight always seemed to point to the problems that were most worth investigating. He showed how a diffusion coefficient could be obtained from the measurement of an internal friction peak or of stress relaxation at temperatures so low that conventional diffusion measurements would have taken an inconceivably long time. He also showed how the growth of particles of a second phase could be studied by anelastic techniques. Those of us who were fortunate enough to work with Dr. Zener during this period found that there were so many exciting experiments to be done that no one of us could find time to improve the appearance of the apparatus or to make it more automatic in its operation. For low frequency and static measurements, the group continued to use a very simple type of torsion pendulum (originally designed by Kê), consisting of a specimen in the form of a wire hanging in a tubular furnace with an inertia member at the bottom. It was such a simple piece of equipment that Dr. Cyril Smith, Director of the Institute for the Study of Metals, remarked that he used to enjoy surprising visitors by taking them to see the pendulum right after they had been shown the great 450 m.e.v. cyclotron at the University of Chicago. Indeed, the remarkable results derived from this simple pendulum under Zener's guidance made it almost the trademark of the Institute.

After 14 years devoted to the study of viscoelasticity, Dr. Zener developed a fear of stagnation. He made a conscious effort to do something totally different and found himself returning to his original field of study, the quantum theory of solids. This time he tackled the theory of ferromagnetism and was daring enough to ask the question "Why are some metals ferromagnetic?" This question had not been raised seriously for twenty-two years, since Heisenberg had proposed his mechanism to interpret ferromagnetism. Zener quickly ruled out Heisenberg's theory and substituted an entirely new idea of his own. It appears that the conflict thus engendered has not yet died down, but there seems to be no question that the stirring up of the magnetic pot did much to put new life into an old field of study.

The latest period in Dr. Zener's career began in 1951 when he left the Institute for the Study of Metals to take a position as Associate Director of Research at Westinghouse. Subsequently he has become Director of the Westinghouse Research Laboratory. This change has decreased the amount of time available to him to do work that is entirely his own, but if my own contact with him is any indication, he is

capable of filling even as large an organization as the Westinghouse Laboratory with ideas and inspiration.

It seems remarkable that one who has made important theoretical contributions in such diverse fields as ferromagnetism, diffusion, and phase transformations, as well as several others, could still have found the opportunity to carry out extensive enough work in the field of rheology to earn the highest award of the Society of Rheology. Although Dr. Zener's work in rheology may total only about 40% or less of his scientific output, his work in this field represents the founding of a new branch of the physics of metals. The impact of his work, however, is by no means confined to the study of metallic solids, since the mechanisms that he has introduced are usually related to elementary atomic movements in simple atomic structures, and are therefore of general interest. I believe that the Society of Rheology could not have chosen more wisely in selecting for this year's Bingham medalist, Dr. Clarence Zener.

TRANSACTIONS OF THE SOCIETY OF RHEOLOGY II, 9-21 (1958)

Rheology of Peeling in a Newtonian Liquid

J. J. BIKERMAN and WILLIAM YAP, *Department of Civil and Sanitary Engineering, Massachusetts Institute of Technology, Cambridge 39, Massachusetts*

I. INTRODUCTION

In experiments on adhesive joints, the force required to peel off (or strip off) a ribbon glued to a rigid plate[1] or to separate by peeling two ribbons glued together,[2] or the work expended on any of these peeling operations are often measured and the results are considered to represent the "force of adhesion" or "the work of adhesion"[3]: far-reaching conclusions have been drawn from data thus obtained.[4] On another view, however, the force and the work of stripping are largely of rheological nature[5] as are the force and the work of tensile rupture.[6] In this paper, an approximate rheological theory of peeling is derived for a Newtonian liquid as the adhesive, and experiments which seem to confirm the theory are described. A theory of peeling through a Hookean solid has been presented elsewhere.[7]

II. AN APPROXIMATE THEORY

1. The experiments reported in Section IV were done on systems outlined in Figure 1, in which P is a rigid plate, R is a flexible ribbon, W and W are weights attached to or near the ends of the ribbon, and A is the adhesive film. The experiment consists in pressing the

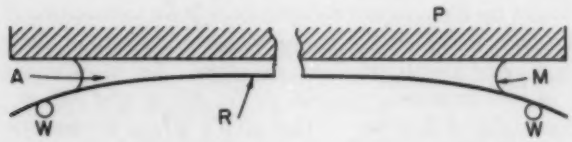

Fig. 1. Side view of a joint being peeled. P, rigid plate; R, flexible ribbon; A, adhesive; W, weights; M, menisci.

ribbon against the plate until a definite thickness (y_0) of the film is attained, releasing the pressure, and determining the time (t_m) until the ribbon falls off. Analogous experiments with two rigid plates (instead of plate and ribbon) have been described earlier.[5]

As soon as weights W are free to act, several processes start. The curvature of the ribbon increases. The liquid film, which initially was y_0 cm. thick over the whole pressed area, is forced to assume a wedge-like shape, and the wedge gets thicker and shorter as time goes on. This flow naturally is retarded by the viscosity η of the liquid, and the time t_m is determined by the rate at which the viscous fluid can follow the movement of the ribbon. The bending of the ribbon in its turn must depend on the product EI, E being the modulus of elasticity of the ribbon material and I the moment of inertia of the ribbon; if the width of the ribbon (normal to the plane of paper in Fig. 1) is w and its thickness is δ, then $I = w\delta^3/12$.

The main phenomenon described in the foregoing paragraph was associated with two secondary processes. The liquid menisci M (see Fig. 1) gave rise to capillary pressure γ/r, where γ is the surface tension of the liquid and r is the radius of curvature of line M. If $2l$ stands for the length of the ribbon, this capillary pressure exerted an upward force $2w\gamma l/r$ on the ribbon so that only the force $2W - (2wl\gamma/r)$ was available for moving the liquid. On the other hand, liquid flowed toward the center of the system not only from right and left in Figure 1 but also in the perpendicular direction (i.e., normal to the plane of paper) since an excess of liquid was present along the edges of the ribbon. This effect, contrary to that of capillary pressure, accelerated the fall. In the following mathematical treatment it is assumed that the values used have already been corrected for these influences. For the technique adopted in these corrections, see Subsection II,4.

2. The relation between time of separation t_m on one hand and corrected weight W_1, rigidity EI, and viscosity η on the other hand can be found by dimensional analysis only if an assumption is made as to the form in which the various lengths present in the system (i.e., l, w, y_0, and δ) enter the final equation. Let us express t_m as a product of two functions, namely, $f_1(W_1, EI, \eta)$ and $f_2(l, w, y_0, \delta)$. If the dimension of f_2 is cm.$^{-1}$, then $f_1(W_1, EI, \eta)$ is constant times $\eta(EI)^{2/3}W_1^{-1/3}$. If f_2 is a pure number, then f_1 is constant times $\eta EI/W_1^2$, and so on.

The experiments are in better agreement with the second than with the other possible expressions, and indicate that

$$t_m = \kappa \frac{\eta w E I}{W_1^2 y_o} \tag{1}$$

κ being a pure number. As $I = w\delta^3/12$,

$$t_m = \frac{\kappa}{12} \frac{\eta w^2 E \delta^3}{W_1 y_0} \tag{2}$$

Equation (1) can be derived if a suitable assumption is made as to the shape of the ribbon during its separation process. For this derivation refer to Figure 2, which represents one-half of the symmetrical system of Figure 1 plus an imaginary continuation of the

Fig. 2. Side view of a half-joint. The part left of x_0 is imaginary. $X-x_0$ is the half-length of the adhesive film. W is weight.

ribbon, which is needed to simplify the equations. The real ribbon is situated to the right of x_0.

Suppose that the actual shape of the half-ribbon can be approximated by

$$y = kx^n \tag{3}$$

At x_0 and time $t = 0$, y is

$$y_0 = k_0 x_0^n \tag{4}$$

y_0 being, as above, the initial thickness of the film; this equation defines the value of x_0. Suppose further that during the separation process n does not change, that is that

$$\frac{dy}{dt} = x^n \frac{dk}{dt} \tag{5}$$

The volume V of the liquid present to the left of any x (smaller than X) is

$$V = w\int_{x_0}^{x} y dx = \frac{wk}{n+1}(x^{n+1} - x_0^{n+1})$$

The volume of liquid crossing the plane of any x toward the left in unit time is

$$\frac{dV}{dt} = \frac{w(x^{n+1} - x_0^{n+1})}{n+1}\frac{dk}{dt}$$

Except very near x_0, the term x_0^{n+1} is much smaller than x^{n+1} and may be neglected. Now, dk/dt is supposed to be independent of x; let it be denoted by letter c. Thus,

$$\frac{dV}{dt} = \frac{wcx^{n+1}}{n+1}$$

On the other hand, for a Newtonian liquid,

$$\frac{dV}{dt} = \frac{wy^3}{12\eta}\frac{dP}{dx} \tag{6}$$

if P is the pressure in the liquid. Hence,

$$\frac{dP}{dx} = \frac{12\eta c}{(n+1)k^3x^{2n-1}} \tag{7}$$

Integrating and neglecting X^{2-2n} in comparison with x^{2-2n} leads to the equation

$$P = P_0 - \frac{6\eta c}{(n^2-1)k^3x^{2n-2}} \tag{8}$$

in which P_0 is the atmospheric pressure minus the capillary pressure. The pressure deficiency $P_0 - P$ is what keeps the ribbon up against gravitation. As long as the fall of the ribbon takes place without marked acceleration, the integral

$$\int_{x_0}^{X} w(P_0 - P)dx$$

must be equal to weight W_1, that is, neglecting X^{3-2n} and retaining x_0^{3-2n},

$$W_1 = \frac{6\eta w(dk/dt)}{(n^2-1)(2n-3)k^3x_0^{2n-3}} \tag{9}$$

Integration of eq. (9) yields

$$\frac{1}{k_0^2} - \frac{1}{k_1^2} = \frac{(n^2 - 1)(2n - 3)x_0^{2n-3}W_1}{3\eta w} t_m$$

if k_0 is the value of k at $t = 0$ [more exactly: when the steady flow represented by eq. (6) has been established] and k_1 is the value of k at $t = t_m$. Since k_1 is much larger than k_0, we have, introducing eq. (3),

$$t_m = \frac{3\eta w}{(n^2 - 1)(2n - 3)k_0^{3/n}y_0^{2-(3/n)}W_1} \tag{10}$$

The only possible n which gives whole numbers for $3/n$ and $2 - (3/n)$ is 3. With $n = 3$, eq. (10) affords

$$t_m = \frac{\eta w}{8k_0 y_0 W_1} \tag{11}$$

When a ribbon is bent in the absence of an adhesive, the distance of the free end from the plate, i.e., the greatest y, is

$$y = W_1 l^3/3EI \tag{12}$$

corresponding to $k = W_1/3EI$ [see eq. (3)]. We assume that k_0 in eq. (11) also is proportional to W_1 and inversely proportional to EI and call $1/8\kappa$ the proportionality constant*; thus,

$$k_0 = \frac{W_1}{8\kappa EI} \tag{13}$$

Equations (11) and (13) yield eq. (1).

3. It is instructive to compare the value of t_m with time t_t of tensile separation as given by Stefan's equation, see, e.g., ref. 6, which for a rectangular plate would be

$$t_t = \kappa_1 \frac{\eta w^2 l^2}{W_1 y_0^2} \tag{14}$$

κ_1 being a numerical constant of the order of one. From eqs. (2) and (14),

$$\frac{t_m}{t_t} = \frac{\kappa}{12\kappa_1} \frac{E\delta^2 y_0}{W_1 l^2} \tag{15}$$

* The neglect of the lateral contraction (due to Poisson ratio being different from zero) would affect the numerical value of k but not the form of the equation.

Introduction of usual values for the quantities E, δ, y_0, W_1, and l shows that t_m, as a rule, is smaller than t_t unless κ/κ_1 is large. In the present work, $E\delta y_0$ was of the order of magnitude of $12W_1$. As κ/κ_1 seems to be not far from unity, the ratio t_m/t_t would be of the order of magnitude of $(\delta/l)^2$, i.e., usually between 10^{-5} and 10^{-7}.

From eqs. (11) and (14), $t_m/t_t = y_0/8\kappa_1 k_0 w l^2$. Let the y at the meniscus be equal to Y when eq. (6) starts to be valid. Then $Y = k_0 l^3$. Consequently,

$$\frac{t_m}{t_t} = \frac{l}{8\kappa_1 w}\frac{y_0}{Y} \tag{16}$$

Thus, t_m usually is much shorter than t_t because Y is much greater than y_0.

4. The corrected load W_1 occurring in the above equations is different from the total load W because of at least three considerations, namely, (*a*) the weight of the ribbon itself is not concentrated at its ends, (*b*) capillary pressure acts, and (*c*) liquid flows parallel to the menisci (see Section II,1 above). An exact calculation of these three effects would be difficult and hardly justify the effort. Therefore, an empirical procedure was worked out.

As Figures 5 and 6 demonstrate, $t_m^{-1/3}$ is a linear function of W but the straight line crosses the abscissa at some finite value of W. Let this value be denoted W_0. Then, for $W_1 = W - W_0$ the equation $W_1^2 t_m$ = constant, which follows from eq. (1), is seen to be valid. Thus, W_0 is the correction to be subtracted from W to arrive at W_1.

III. EXPERIMENTAL PROCEDURE

1. The Principle

The experiments conformed to the scheme of Figure 1. A drop of Newtonian liquid was placed on the center of a metal ribbon, the ribbon was pressed (for a time t_0 proportional to the viscosity of the liquid) against the bottom of a horizontal steel plate (compare ref. 8) so as to spread the liquid over the whole area under pressure, the pressing device removed, a stop watch started, and t_m determined. This time (t_m) naturally was sensitive to the position of the weights W. When these were attached 0.5 cm. from the edge of the oil film (e.g., the film length was 5 cm. and the distance between the weights was 6 cm.), t_m was about 2–10 times as long as when the points of attach-

ment were 2.4 cm. from this edge. As the results at the longer distance had better reproducibility, they are the only ones reported in the following unless otherwise noted.

Of the other quantities in eq. (1), viscosity η was determined in a rolling-ball viscometer and E was taken from published tables. The value of y_0 was found by placing various volumes of the oil on the ribbon, pressing this for t_0 seconds with the standard force, and observing the minimum volume (v) which still gave rise to spreading over the whole area $2wl$; the ratio $v/2wl$ was approximately equal to y_0.

2. The Materials

Metal ribbons of three types were used. Aluminum 1145-H19* and steel (not further identified) were 0.0051 cm. thick and used without annealing. Copper† (electrolytic tough pitch, over 99.9% Cu) was about 0.0080 cm. thick; it was stress-relieved at 350–360°C. for 60 minutes. The ribbons were 6–10 cm. long and 2.5 to 7.5 cm. wide.

Three viscous liquids were employed: a solution of Chlorowax 70‡ (a chlorinated paraffin wax) in Chlorowax LV‡ with the viscosities of 350 and 79 g./cm. sec. at 18.0° and 24.0° and two polybuteneS§ (H-35 and H-100) whose viscosities were about 75 and 300 g./cm. sec., respectively, at the average temperature (21°C.) of the air-conditioned room in which the main experiments were performed. Only these experiments are reported in Section IV. The apparent viscosity of these polybutenes slightly varied with the rate of shear, but the variability was deemed not serious enough to disqualify these liquids.

3. The Reproducibility

The reproducibility of the experiments was poor. In many instances, one end of the ribbon with its load pulled the other end as shown in Figure 3; these experiments were disregarded. As the efforts to improve the reproducibility were not successful, every experiment was repeated many times (usually more than ten), all sus-

* Donated by Aluminum Company of America.
† Donated by Chase Copper and Brass Company.
‡ Donated by Diamond Alkali Company.
§ Donated by Indoil Chemical Company.

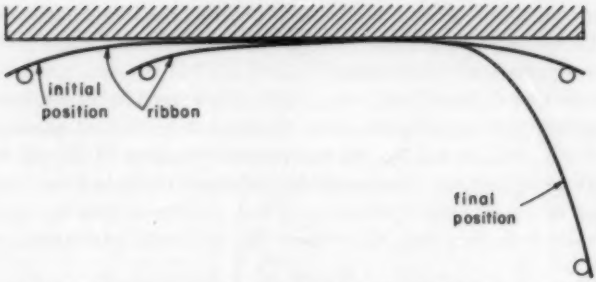

Fig. 3. Scheme of an unsuccessful experiment. The initial shape of the ribbon was symmetrical, and the final asymmetrical.

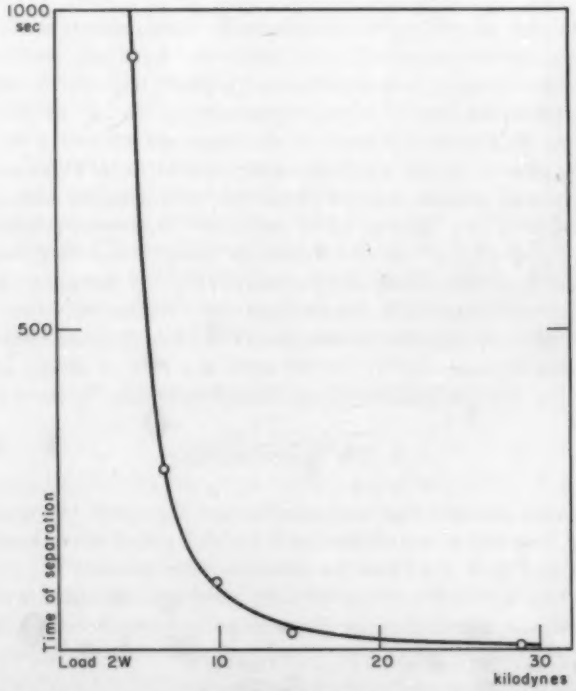

Fig. 4. Time of separation as function of applied load. Aluminum: 2.5 cm. wide and 0.0051 cm. thick. Initial film length: 5.0 cm. Initial film thickness: approximately 0.0018 cm. Polybutene, η = 300 poises.

pect data eliminated, and the averages of the more reliable results used in Section IV.

Apparently the nonuniformity of the metal ribbons used was the main source of error. Since the external forces applied were so small (down to 500 dynes for 1 cm. ribbon width), the actual curvature of the ribbon was determined not only by these forces (as assumed in Section II) but also by the internal stresses in the metal; for instance, rolling a metal cylinder over the ribbon (to smooth out the visible folds in the latter's surface) altered the time of separation.

IV. EXPERIMENTAL RESULTS

Figure 4 illustrates the typical dependence of the time of separation (t_m) on the applied load $2W$. The five circles represent the experimental data (that is, averages of 3 to 5 more reliable measurements), while the curve is calculated assuming that $(W - W_0)^2 t_m$ was constant and determining W_0 as in Section II,4.

Figure 5 presents analogous data for another ribbon, in an arrangement showing that W really is an approximately linear function of $t_m^{-1/3}$. The upper line of this graph is for an oil of 75, and the lower, for an oil of 300 g./cm.sec. viscosity. It is seen that, in agreement with eq. (1), the ordinates of the upper line are about twice those of the lower; that is, the t_m values for $\eta = 75$ are about one-quarter those for $\eta = 300$.

In Figure 6 steel ribbons are compared with copper ribbons in a graph analogous to Figure 5. The data of this figure and the upper line of Figure 5 permits a test of eq. (1) as far as the rigidity EI of the ribbons is concerned. According to eq. (1), the tangents of the lines drawn in Figures 5 and 6 should be inversely proportional to $(EI)^{1/3}$. Table I shows the extent of agreement between experiment and theory.

The values shown in the last column for aluminum and steel are sufficiently close to each other, but the value for copper is decidedly too great. This discrepancy, however, confirms rather than refutes the theory. Equation (12) and the use of the product EI in general are predicated on the constancy of E. The range of stresses, in which E is approximately independent of stress, is wide for steel and aluminum but relatively narrow for annealed copper, and the stresses applied in this study usually were outside this range for Cu. To de-

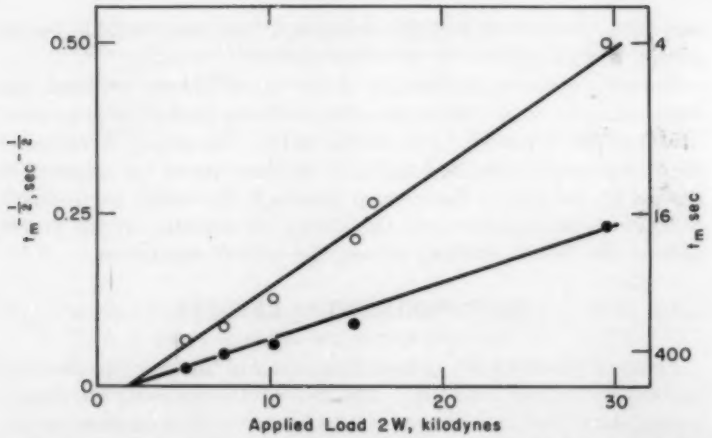

Fig. 5. Time of separation t_m as function of applied load at different viscosities. Aluminum: 5.0 cm. wide and 0.0051 cm. thick. Initial film: 5.0 cm. long and 0.0037 cm. thick. Polybutenes. Upper line: η = 75; lower line: η = 300 poises.

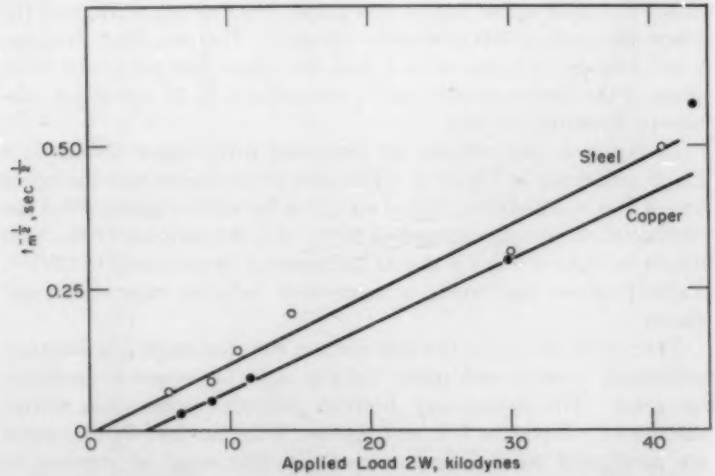

Fig. 6. Time of separation t_m as function of applied load for different ribbons. Polybutene, η = 75 poises. Initial film: 5.0 cm. long and 0.0037 cm. thick. Upper line: steel, 5.0 cm. wide and 0.0051 cm. thick. Lower line: copper, 5.0 cm. wide and 0.008 cm. thick.

termine a more suitable value of EI, one of the copper ribbons was bent without an adhesive but about as much as during the peeling experiments, and the ratio $W_1l^3/3y$ was assumed to be equal to EI [see eq. (12)]. This ratio proved to be 6.99×10^4 g.cm.^{3}/sec.^{2}, i.e., $(EI)^{1/2}$ was 264, and the product of $(EI)^{1/2}$ and $d(t_m^{-1/2})/2dW$ was 0.0031, not greatly different from the values obtained for aluminum and steel.

With polybutene of $\eta = 300$, the derivative $d(t_m^{-1/2})/2dW$ was 0.84×10^{-5} for aluminum and 0.54×10^{-5} for copper, for the same w and y_0 as above.

Equation (2) predicts that the corrected forces W_1 needed to attain a constant t_m will be proportional to the width of the ribbon. This

TABLE I

Comparison of $d(t_m^{-1/2})/2dW$ with $(EI)^{1/2}$ for Different Ribbons
Polybutene, $\eta = 75$ g./cm.sec. Initial film thickness about 0.0037 cm.

Ribbons	$d(t_m^{-1/2})/2dW$, sec.$^{3/2}$/g. cm.	$(EI)^{1/2}$, g.$^{1/2}$ cm.$^{3/2}$/sec.	$(EI)^{1/2}d(t_m^{-1/2})/2dW$, (cm. sec./g.)$^{1/2}$
Aluminum	1.75×10^{-5}	194	0.0034
Steel	1.22×10^{-5}	312	0.0038
Copper	1.18×10^{-5}	464	0.0055

conclusion was not well confirmed by experiment. Aluminum ribbons 2.5, 5.0, and 7.5 cm. wide were used for polybutene of $\eta = 300$ g./cm.-sec., the points of application of the weights being 1.5 cm. from the edge of the oil film (see Section III,1), and the initial film thickness being about 0.0036 cm. The *total* weight $2W$ was approximately proportional to w; for instance, at $t_m = 25$ sec. the interpolated values of $2W$ were 13.8 and 40.0 kilodynes for $w = 2.5$ and 7.5 cm., respectively; and at $t_m = 100$ sec. they were 8.2 and 25.6 kilodynes; but the proportionality was not observed for the corrected weights.

V. THE MEANING OF THE RESULTS

It is believed that, in spite of the crudeness of the theory and the low precision of the experimental data, the above results do prove that peeling of an adhesive joint (as long as the adhesive is liquid) is a rheological phenomenon depending on the viscosity of the liquid and

the rigidity of the ribbon, and cannot give any information on the molecular forces of adhesion between the solid and the glue. The commercial adhesives are not Newtonian liquids but they usually flow when the stresses used in testing are not too weak and not too strong, and the above conclusion should be valid for all customary adhesives.

Two additional remarks should be made in conclusion.

(*1*) In the above experiments the liquid flowed toward the center of the ribbon both parallel to the ribbon length $2l$ and parallel to its width w. The pressure gradient which causes the flow parallel to w will have an analogue in a stress (parallel to w) along the ribbon edges, when the adhesive is too viscous for eq. (6) to hold. Consequently, there will be stress concentrations at the edges, as indicated in Figure 7, in which again A, P, and R are the adhesive, the rigid plate, and the ribbon, respectively, and a are the most stressed points. Thus, failure may originate at a.

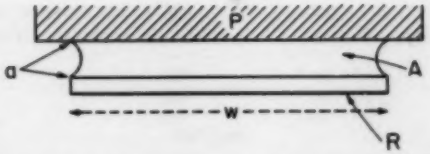

Fig. 7. Cross section of a joint being peeled parallel to its width, w. P, rigid plate; R, flexible ribbon; A, adhesive. The most stressed points are marked a.

(*2*) Let the distance between the plate and the ribbon at the weights W be y_m just before the final separation takes place. Then the gravitational work done during separation (for both weights) is $2W(y_m - y_0)$. The major part of this work is $2W_1(y_m - y_0)$, and for this part eq. (2) gives the expression

$$2W_1(y_m - y_0) = \left(\frac{\kappa\eta E\delta^2}{3t_m}\right)^{1/2} \frac{w(y_m - y_0)}{y_0^{1/2}} \tag{17}$$

It is clear that any conclusions as to the molecular forces of adhesion, derived from the consideration of the value of $W(y_m - y_0)$, are not likely to be valid.

The authors thank Lord Manufacturing Company of Erie, Pennsylvania, for sponsorship and assistance in the execution of the research described in this paper.

References

1. E.g., A.S.T.M., Test D 903–49; *Book of Standards 1955*, Part 7, p. 1182.
2. E.g., *ibid.*, Test D 825–54, p. 939.
3. E.g., A. I. Shapovalova, S. S. Voyutskii, and A. P. Pisarenko, *Kolloid. Zhur.*, **18**, 485 (1956); S. S. Voyutskii, A. I. Shapovalova, and A. P. Pisarenko, *Kolloid. Zhur.*, **19**, 274 (1957).
4. E..g, N. A. Krotova, Yu. M. Kirillova, and B. V. Deryagin, *Zhur. Fiz. Khim.*, **30**, 1921 (1956).
5. J. J. Bikerman in *Adhesion and Adhesives, Fundamentals and Practice*, Wiley, New York, 1954, p. 72.
6. J. J. Bikerman, *J. Colloid Sci.*, **2**, 163 (1947).
7. J. J. Bikerman, *J. Appl. Phys.* **28**, 1484 (1957).
8. J. J. Bikerman, *Trans. Soc. Rheology*, **1**, 3 (1957).

Synopsis

A metal ribbon was pressed against a rigid plate, the space between the plate and the ribbon being filled with a viscous liquid (two hydrocarbon oils and chlorinated paraffin oil were used). Then the ribbon was peeled off, and time t_m of separation measured as a function of the applied load W. An approximate rheological theory of the function $t_m = f(W)$ was developed, analogous to Stefan's theory for tensile separation. The equations derived were in satisfactory agreement with experiment as far as the modulus of elasticity of the ribbons (aluminum, copper, and steel foils) and the viscosity of the liquids were concerned. Thus, tackiness measured by peeling, similarly to tackiness measured by tensile pull, has no connection with the theoretical forces of adhesion.

TRANSACTIONS OF THE SOCIETY OF RHEOLOGY II, 23–38 (1958)

Dynamic Mechanical Properties of Fluorochemical Elastomers*

KENNETH E. OWENS and CARL A. DAHLQUIST, *Minnesota Mining and Manufacturing Company, St. Paul, Minnesota*

INTRODUCTION

Elastomers containing fluorine have achieved importance as engineering materials because of their resistance to solvents and their excellent high temperature aging characteristics. To use these elastomers effectively for structural purposes, data concerning their mechanical properties must be known. Since data concerning the dynamic mechanical properties of this class of elastomers are meager or nonexistent, work was performed to provide such information. The effects of a fluorocarbon side chain and of the polymer backbone upon the dynamic mechanical properties were examined and contrasted with those of the familiar hydrocarbon elastomer, polyisobutylene. The three fluorocarbon elastomers studied were chosen because they are significantly different in side chain or backbone structure. There are now too many commercial or experimental fluorine-containing elastomers to cover in a single paper. Others will be discussed in a subsequent publication.

MATERIALS

Three elastomeric materials containing fluorine were studied. Fluororubbers Nos. 1 and 2 were prepared by the Chemical Products Group of Minnesota Mining and Manufacturing Company, St. Paul, Minnesota. Both are essentially homopolymers; Fluororubber No. 1 was prepared from 1,1-dihydroperfluorobutyl acrylate, and Fluororubber No. 2 was prepared from 3-trifluoromethoxy-1,1-dihydroperfluoropropyl acrylate. Fluororubber No. 1 is available

* Contribution No. 149.

commercially as 3M Brand Fluororubber 1F4. The uncured gums used in these experiments are white, rather soft, rubbery solids. The polymers were unfractionated, but the molecular weight, even considering the high molecular weight of the monomers, was very high. Complete descriptions of preparation details and properties are available in earlier publications from this Laboratory.[1–4] Fluororubber No. 3 is Silastic LS 53, a fluorosilicone rubber produced by the Dow Corning Corporation, Midland, Michigan. It was studied as a compounded cured rubber which contained silica and ferric oxide as fillers. Although its exact structure has not been disclosed, a product brochure published by the Dow Corning Corporation reports data pertaining to the effect of temperature on elasticity. Physical data concerning the three fluorocarbon elastomers are given in Table I.

TABLE I
Properties of the Fluororubbers

	No. 1	No. 2	No. 3[a]
Combined fluorine, %	52	49	26
Volume coefficient of expansion	9.4×10^{-4}	8.1×10^{-4}	4.5×10^{-4}
Density	1.54	1.53	1.39
Class transition temperature, °C.	−30	−55	—
Gehman T_{10}, °C.	−12	−32	−60
ASTM brittle point D746–54T, °C.	−15	−38	−68
$[\eta]$, intrinsic viscosity	2.2	2.3	—
Molecular weight, light scattering	15,000,000	—	—

[a] Properties shown are for the compounded, cured stock.

EXPERIMENTAL METHOD

The "real" (J') and "imaginary" (J'') components of the complex compliance in cyclic shear were obtained over a temperature range of −40 to 100°C. and a frequency range of 24 to 5200 cycles/sec. It was not practicable to obtain measurements at all of the available frequencies in the entire temperature range, but sufficient data were obtained to define the master dispersion curves adequately for each material. The electromagnetic transducer used was the Fitzgerald Apparatus. This instrument, a commercial model of the transducer originally described by Fitzgerald and Ferry,[5] is manufactured

by Atlantic Research Corporation, Alexandria, Virginia. The calibration of the apparatus was performed in the manner indicated by these authors and verified independently by comparing the results obtained with National Bureau of Standards polyisobutylene (PIB) with published data for this material.[6] Table II shows these results. Although the calibration measurements were probably not as precise as the original measurements, the agreement of the data for polyisobutylene was satisfactory. Later rechecks of instrument constants showed no significant change in the instrument over the period of the experiments.

TABLE II

Verification of Calibration of Fitzgerald Apparatus Using NBS Polyisobutylene at 25°C.

Frequency, cycles/sec.	Experimental		Literature	
	$J' \times 10^6$, cm.²/dyne	$J'' \times 10^6$, cm.²/dyne	$J' \times 10^6$, cm.²/dyne	$J'' \times 10^6$, cm.²/dyne
24	0.0246	0.0104		
30	0.0213	0.0108	0.0204	0.0102
45	0.0183	0.0110	0.0182	0.0107
72	0.0151	0.0112		
100	0.0122	0.0100	0.0119	0.00952
140			0.00984	0.00881
200	0.0086	0.0079	0.00790	0.00779
280			0.00653	0.00650
400	0.0048	0.0062	0.00512	0.00564
600	0.0036	0.0048	0.00385	0.00469
800	0.0029	0.0041	0.00321	0.00410
1000	0.0026	0.0033	0.00271	0.00364
1400		0.0034	0.00207	0.00301
2000			0.00157	0.00263

Specimens of Fluororubbers Nos. 1 and 2 were prepared by solution casting in a disc-shaped mold, air drying, and subsequently vacuum drying at 60°C. for 24 hours. Discs of Fluororubber No. 3 were molded and cured at 124°C. for 5 minutes under pressure. They were then post cured for 24 hours at 150°C. Polyisobutylene was hot molded directly from the sheet as received from the National Bureau of Standards. Several sets of discs, differing in cross-sectional area and thickness, were molded from each elastomer. Since the mechan-

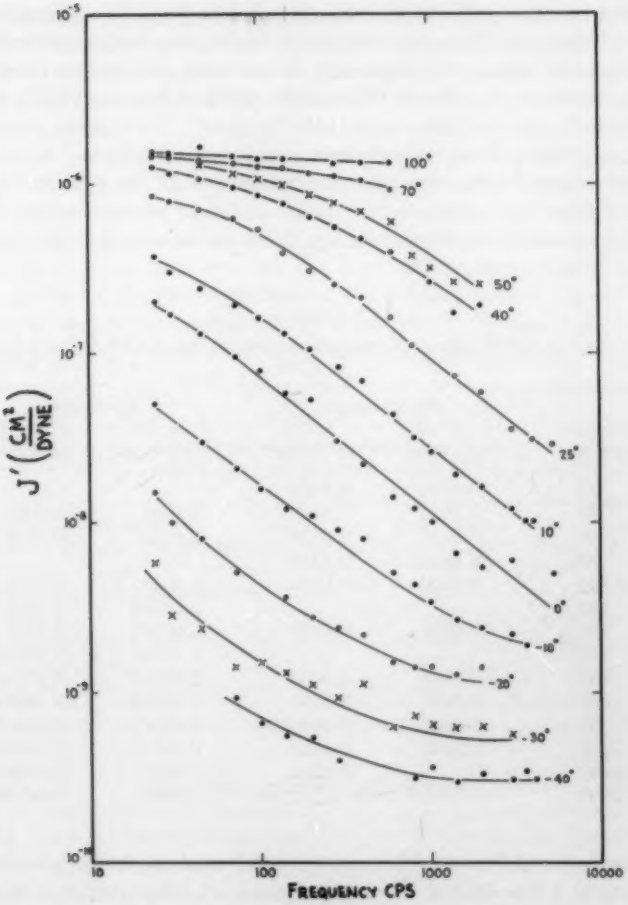

Fig. 1. Variation of the real part of the dynamic shear compliance with frequency of Fluororubber No. 2 at the temperatures indicated.

ical properties of the elastomers are sensitive to temperature and frequency, several sets of discs with different thickness to area ratios

must be used to obtain data over broad ranges of temperature and time.

EXPERIMENTAL RESULTS

The reduced variables treatment as outlined by Ferry[7] was applied to the compliance data of each elastomer. At each of several uniformly spaced temperatures, values of J'_p and J''_p were plotted as functions of circular frequency. Values of J'_p and J''_p are obtained directly from the measured compliance values by the use of:

$$J'_p = (T\rho/T_0\rho_0)J'$$
$$J''_p = (T\rho/T_0\rho_0)J''$$

where T and ρ refer to absolute temperature and density, respectively, at the temperature of the measurements. T_0 and ρ_0 refer to the reference temperature and density at 25°C., respectively. These curves at the several temperatures were then superimposed to form a single composite dispersion curve by shifting horizontally along the circular frequency axis. This assumes

$$\omega_p = \omega a_T$$

where ω is the circular frequency and a_T is the factor expressing the ratio of any retardation time at temperature T to that at the reference temperature T_0. The contribution of the glassy compliance was neglected. This treatment standardizes the observed compliances at the various temperatures by correcting for the different contributions of the configurational entropy to the total compliance of the elastomer. Also the effect of changing the number of retardation mechanisms in a unit cube due to changes in temperature is corrected by the ratio of densities. The use of the shift factor, a_T, for all frequencies at a given temperature assumes that all retardation times have the same temperature dependence. Plots of J' and J'' as functions of circular frequency are shown for Fluororubber No. 2 in Figures 1 and 2, and master dispersion curves of the reduced real, J'_p, and imaginary, J''_p, components of the complex shear compliance as functions of log ωa_T are shown in Figures 3 and 4. The master dispersion curves of log J'_p, log J''_p, and J'_p/J''_p each plotted against log ωa_T, for the three fluororubbers are shown in Figures 5, 6, and 7. For comparison, the dispersion curves of polyisobutylene obtained from published data[7] are plotted on the same figures.

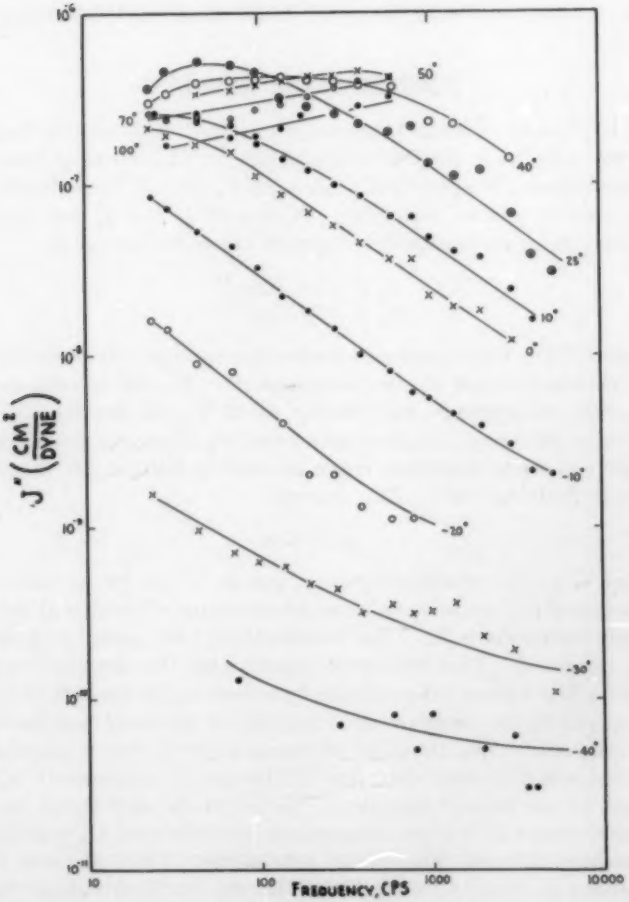

Fig. 2. Variation of the imaginary part of the dynamic shear compliance with frequency for Fluororubber No. 2 at the temperatures indicated.

DISCUSSION

Since these three elastomers differ markedly in structure from well-known hydrocarbon elastomers, it is of interest for a preliminary

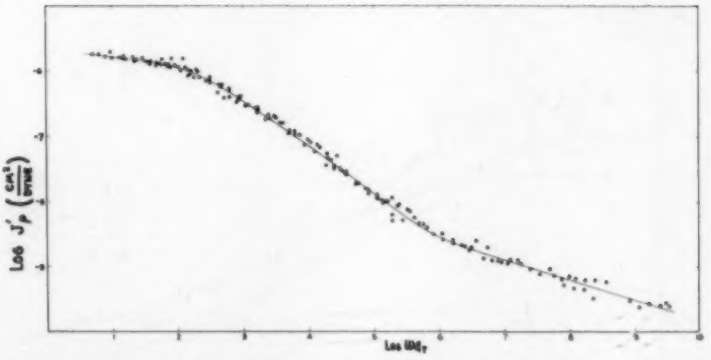

Fig. 3. Real part of the complex compliance of Fluororubber No. 2 reduced to 25°C., plotted logarithmically against reduced frequency.

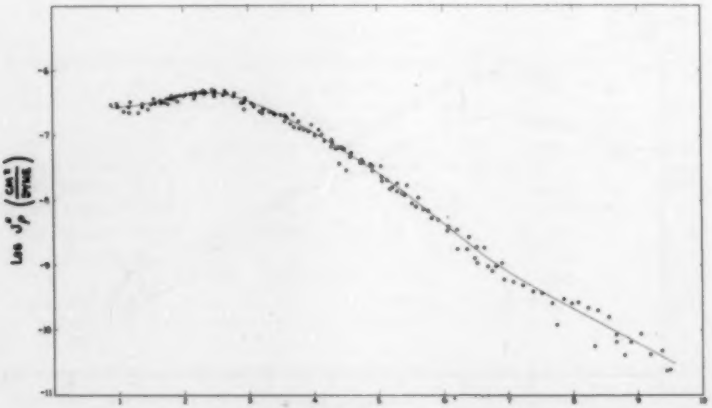

Fig. 4. Imaginary part of the complex compliance of Fluororubber No. 2 reduced to 25°C., plotted logarithmically against reduced frequency. Abscissa: Log ωa_T.

orientation to compare their dynamic mechanical properties with those of some conventional elastomers. Table III shows the room temperature complex compliance values and the loss tangents at 100 and 1000 cycles/sec. of the three fluororubbers, polyisobutylene,

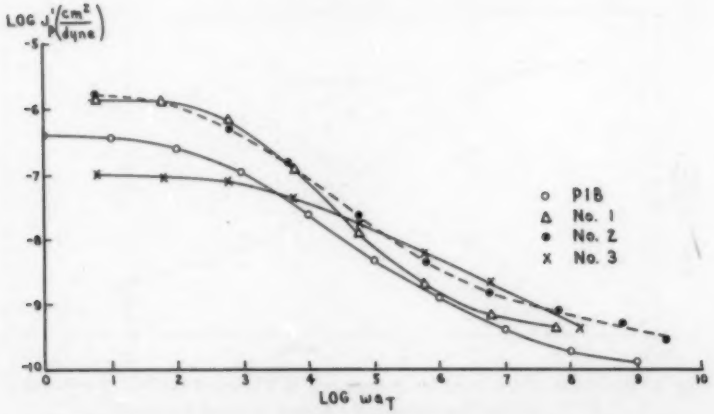

Fig. 5. Master dispersion curves of real compliance reduced to 25°C.

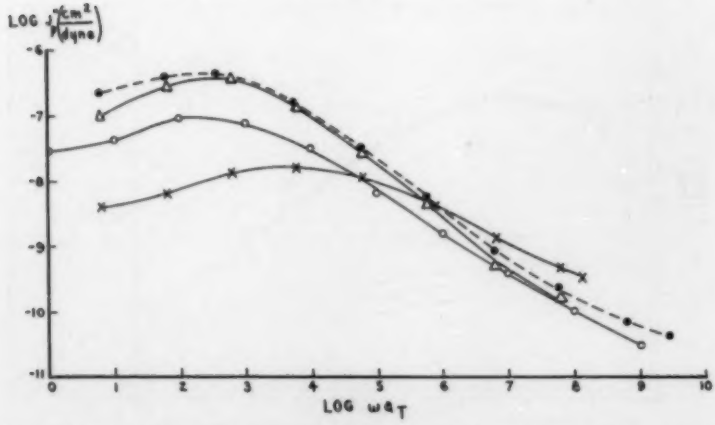

Fig. 6. Master dispersion curves of imaginary compliance reduced to 25°C. (O) PIB. (Δ) No. 1. (●) No. 2. (×) No. 3.

natural rubber, and GR-S.[8] Fluororubber No. 3 is a filled, cured stock, and would be expected to be less compliant than the uncured gums, as, indeed, it is; though not far different from polyisobutylene. Fluororubbers Nos. 1 and 2, which are rather soft gums, are

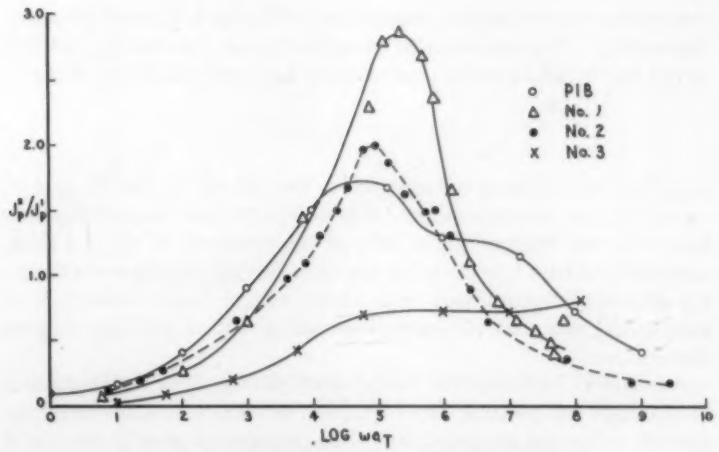

Fig. 7. Loss tangent curves reduced to 25°C.

TABLE III

Comparative Mechanical Data on Fluorocarbon and Hydrocarbon Elastomers at 25°C.

	100 cycles/sec.		1000 cycles/sec.	
	$J^* \times 10^8$cm.^{2}/dyne	Tan	$J^* \times 10^8$ cm.^{2}/dyne	Tan
Fluororubber No. 1	0.74	0.56	0.185	0.79
Fluororubber No. 2	0.70	0.81	0.166	1.23
Fluororubber No. 3	0.062	0.18	0.039	0.42
Polyisobutylene	0.152	0.80	0.045	1.33
GR-S	0.10	0.06	0.086	0.07
Natural Rubber	0.30	0.05	0.25	0.04

most compliant of the group at 100 cycles/sec.: but at 1000 cycles/sec. they fall between natural rubber and GR-S. Mechanical loss is high in fluororubbers Nos. 1 and 2, with fluororubber No. 2 approaching polyisobutylene at 1000 cycles/sec. Fluororubber No. 3 is intermediate between polyisobutylene and GR-S.

The plots of J'_p, J''_p, and J''_p/J'_p as functions of log ωa_T provide a more detailed comparison of the three fluororubbers and polyisobutylene. A great deal of similarity is noted between polyisobutylene and the fluorine-containing polyacrylates, particularly between polyisobutylene and Fluororubber No. 2. Polyisobutylene has a some-

what broader loss tangent distribution. Figures 5, 6, and 7 illustrate these data. The temperature insensitivity and low internal friction of the fluorosilicone rubber, presumably due to the flexibility of the

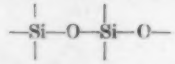

backbone chain, show up strongly in the flatness of the J'_p and J''_p versus log ωa_T plots and in the broadness of the loss tangent distribution. In the fluoroacrylate rubbers, replacement of the 1,1-dihydroperfluorobutyl side chain by the more flexible 3-trifluoromethoxy-1,1-dihydroperfluoropropyl side chain effects some reduction in mechanical loss, but no marked spreading out of the loss tangent distribution.

A better indication of the temperature sensitivity of the elastomers is obtained by plotting the logarithm of the reduction factor a_T against reciprocal temperature. This brings out clearly the rapid change of elastic properties with temperature in Fluororubber No. 1, and the closer similarity in temperature sensitivity of Fluororubber No. 2, polyisobutylene, and Fluororubber No. 3. Fluororubber No. 2 is somewhat more sensitive than polyisobutylene and the Fluororubber No. 3 is least temperature sensitive of the four. This is illustrated in Figure 8.

The use of these elastomers for structural applications requires familiarity with the extent of the mechanical dispersion regions and their positions in the time and temperature scales. It is best to avoid the regions of major dispersion, if possible, by remaining on the rubbery side of the dispersion in the time scale. If the dispersion region cannot be avoided, then due consideration and compensation for the changes in properties must be made. In this case, use of a material with relatively small extent of dispersion is most desirable mechanically. However, in any application of these rubbers, other nonmechanical considerations must be made. Among these are solvent resistance, ultimate strength, high temperature aging characteristics, and processability. Use of the master dispersion curves of these three fluororubbers reduced to 25°C., the temperature reduction factor, a_T, and the corrections due to changes in density and in configurational entropy permit the determination of the time-dependent mechanical properties at other temperatures that may be required.

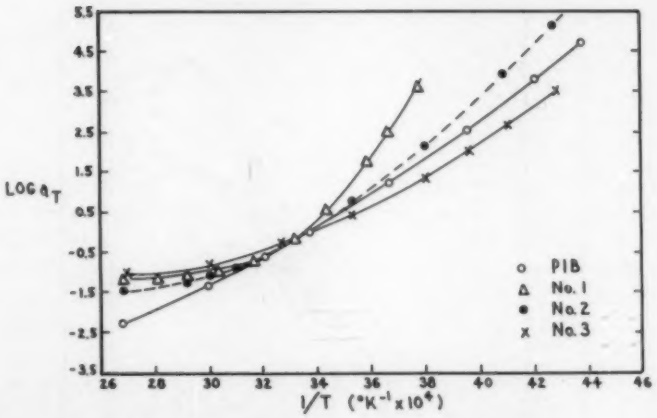

Fig. 8. Temperature dependence of reduction factor, a_T.

TABLE IV

Apparent Activation Energies of the Fluororubbers

Temperature, °C.	ΔH_a, Kcal./mole			
	PIB	No. 1	No. 2	No. 3
−40	24.4	—	33	22
0	18.5	44	23	15
25	17.0	21	18	12
100	12.0	9.0	5.3	2.8

A further indication of the temperature sensitivity is the temperature dependence of the apparent activation energy per moving polymer segment, ΔH_a. This is obtained by use of the expression:

$$\Delta H_a = Rd(\ln a_T)/d(1/T)$$

Table IV shows values for the four rubbers at four temperatures over the range −40 to 100°C. Fluororubbers Nos. 2 and 3 have apparent activation energies very comparable to that of polyisobutylene at −40°C. Fluororubber No. 1 shows a very sharp rise in activation energy at 0°C. and is glassy at −40°C., but above 25°C. it shows least decrease in ΔH_a with increasing temperature.

The retardation and relaxation distribution functions were determined from the data for the three fluororubbers using the second

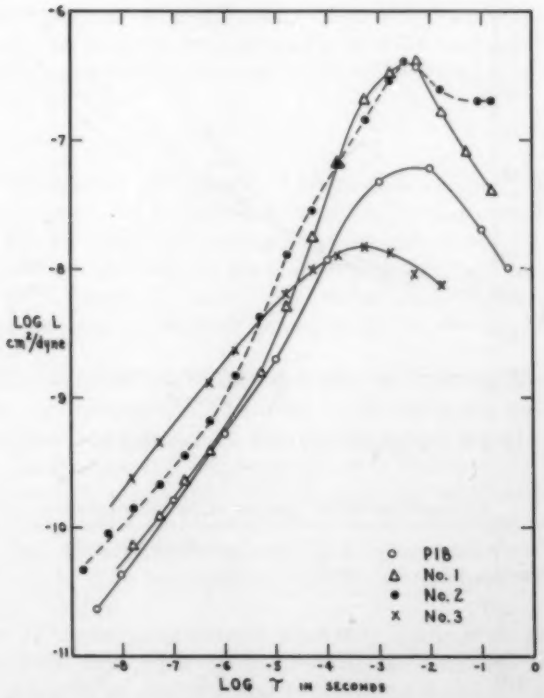

Fig. 9. Distribution functions of retardation times, L, plotted logarithmically reduced to 25°C.

approximation method of Ferry and Williams.[7,9] Excellent checks were obtained between values obtained from the real and imaginary compliance data. Figure 9 shows the retardation distribution functions at 25°C. plotted against log τ. The similarity in the shape of the curves is striking. Exact methods for obtaining the response under various conditions of stress application from the distribution functions have been published.[10,11] However, visual inspection indicates that all three fluororubbers show a higher degree of compliance than polyisobutylene in the high frequency range at 25°C. At larger values of log τ, Fluororubber No. 3 has least compliance of the four,

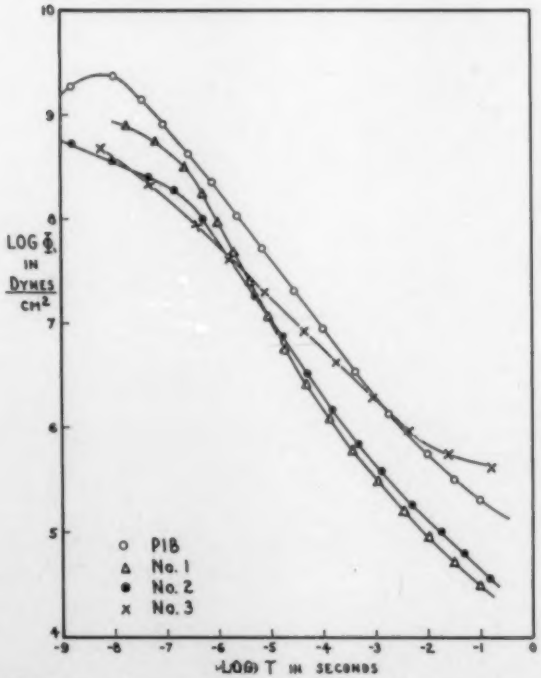

Fig. 10. Distribution functions of relaxation times, Φ, plotted logarithmically reduced to 25°C.

but this is to be expected since it is a filled and cured stock. The high compliance of Fluororubbers Nos. 1 and 2 at large values of log τ is probably a result of the internal plasticizing action of the bulky side chains. Figure 10 shows the relaxation distribution functions for the three fluororubbers and polyisobutylene. Again, there is a general similarity between Fluororubbers Nos. 1 and 2 and polyisobutylene. The modifications of the rigidity at high values of log τ by crosslinking and reinforcing is evident in Fluororubber No. 3. The slope of the logarithm of the relaxation distribution functions approaches $-1/2$ over several orders of magnitude in log τ. The Rouse theory concerning the viscoelastic properties of isolated polymer molecules and the Blizard theory concerning viscous coupling of poly-

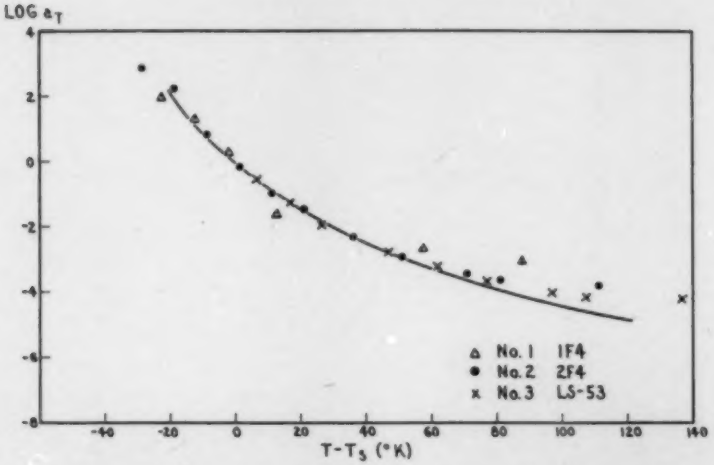

Fig. 11. Logarithm of a_T plotted against $T - T_s$ for the three fluororubbers.

mer molecules predict that in the region of short times the distribution function should be proportional to $\tau^{-1/2}$.

The treatment of Williams, Landel, and Ferry[12] concerning the temperature dependence of relaxation mechanisms in polymers was extended to the three fluororubbers. The parameters given by these authors are:

$$\log a_T = -8.86(T - T_s)/(101.6 + T - T_s)$$

where T is the absolute temperature and T_s is an empirically chosen reference temperature such that the equation is valid. Plots of $\log a_T$ versus T were obtained for each of the three rubbers, and each plot was shifted horizontally and vertically to best fit the equation as represented graphically. The results of the curve fitting are shown in Figure 11. The parameter, T_s, obtained from the horizontal shifting, was as follows for each of the three rubbers: No. 1, +12°C.; No. 2, −11°C.; No. 3, −37°C. An interesting comparison with other rubbers is the difference between T_s, and T_g, the glass transition temperature. The differences obtained

are 42, 44, and 43°C., respectively, for the three rubbers. In the case of Fluororubber No. 3, the glass transition temperature was estimated as −80°C. The overall fit of the data to the empirical curve and the agreement of values of $T_s - T_g$ with values published for other elastomers is excellent. This indicates that the fluorocarbon elastomeric materials studied behave similarly to hydrocarbon elastomers as far as the temperature dependence of their relaxation mechanisms is concerned.

CONCLUSIONS

The dynamic mechanical properties of the two fluoroacrylate rubbers are not markedly different from those of polyisobutylene at room temperature. The perfluoro alkoxy alkyl side chain affords greater segmental mobility, hence somewhat less mechanical loss and somewhat greater elasticity at low temperature than the perfluoro alkyl side chain. The

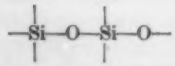

backbone chain provides still greater mobility, with attendant low loss factor and low sensitivity to temperature change. The modern theories of viscoelastic behavior developed by Ferry and others have been extended to the fluororubbers and found to apply as well as to hydrocarbon elastomers. The retardation and relaxation distribution functions for the uncured polyacrylate gums are very similar in shape to those for polyisobutylene, though displaced somewhat in the time scale. Although crosslinking and addition of reinforcing fillers to the fluorosilicone elastomer modify the distribution functions somewhat, they generally show less time sensitivity than those of the other fluororubbers studied.

The authors are indebted to R. E. Bade for assistance in collecting data and performing calculations.

References

1. U. S. Patent 2,642,416, A. H. Ahlbrecht, T. S. Reid, and D. R. Husted; British Patent 703,435, Minnesota Mining and Manufacturing Company.

2. F. A. Bovey, J. F. Abere, G. B. Rathmann, and C. L. Sandberg, *J. Polymer Sci.*, **15**, 520 (1955).

3. P. J. Stedry, J. F. Abere, and A. M. Borders, *J. Polymer Sci.*, **15**, 558 (1955).
4. F. A. Bovey and J. F. Abere, *J. Polymer Sci.*, **15**, 537 (1955).
5. E. R. Fitzgerald and J. D. Ferry, *J. Colloid Sci.*, **8**, 1 (1953).
6. E. R. Fitzgerald, L. D. Grandine, Jr., and J. D. Ferry, *J. Appl. Phys.*, **24**, 650 (1953).
7. J. D. Ferry, L. D. Grandine, Jr., and E. R. Fitzgerald, *J. Appl. Phys.*, **24**, 911 (1953).
8. L. J. Zapas, S. L. Shufler, and T. W. DeWitt, *J. Polymer Sci.*, **18**, 245 (1955).
9. J. D. Ferry and M. L. Williams, *J. Colloid Sci.*, **7**, 347 (1952).
10. J. D. Ferry, E. R. Fitzgerald, L. D. Grandine, Jr., and M. L. Williams, *Ind. Eng. Chem.*, **44**, 703 (1952).
11. J. D. Ferry, *Record Chem. Progr.*, **16**, 85 (1955).
12. M. L. Williams, R. F. Landel, and J. D. Ferry, *J. Am. Chem. Soc.*, **77**, 3701 (1955).

Synopsis

The dynamic mechanical properties of three fluorinated elastomers were determined by use of the double transducer of Fitzgerald and Ferry. The measurements cover a temperature range of −40 to 100°C. and a frequency range of 24 to 5200 cycles/sec. The elastomers studied are the acrylic 3M Brand Fluororubber 1F4, a homopolymer of 3-trifluoromethoxy-1,1-dihydroperfluoropropyl acrylate, and Dow Corning Silastic Rubber LS-53. Master dispersion curves of the compliances at 25°C. versus time have been obtained using the reduced variables treatment of Ferry. The position in the time scale and extent of the dispersion regions are discussed. The apparent heats of activation per chain segment and relaxation distribution functions were determined and are discussed in reference to the reported values for polyisobutylene. The universal function for the temperature dependence of mechanical relaxations in amorphous polymers applies to these fluorinated elastomers.

TRANSACTIONS OF THE SOCIETY OF RHEOLOGY II, 39–51 (1958)

A Torsion Pendulum for Dynamic and Creep Measurements of Soft Viscoelastic Materials

DONALD J. PLAZEK,* M. N. VRANCKEN,† and JOHN W. BERGE, *University of Wisconsin, Madison, Wisconsin*

INTRODUCTION

The freely damped torsion pendulum method has been widely used to investigate dynamic mechanical properties of high polymers.[1–5] Up to the present time, the instruments used have not been designed to measure storage moduli much below 10^7 dynes/cm.^{2}. Necessity of clamping the sample under slight tension is the principal reason for the lower limit. The instrument described here can be used to investigate systems with storage moduli at least as low as 10^5 dynes/cm.^{2}, if their loss tangents are sufficiently small (less than 0.8). It can also be used to measure creep of such soft systems in the range of small applied stresses and hence small final sample strains.

Very few low frequency measurements have been made on gels,[3] and there has been little progress in understanding the role of cross-linking in very slow viscoelastic mechanisms. It is hoped that this instrument will help ascertain the phenomenological nature of the mechanical behavior of gels in the region of long times.

DESCRIPTION AND OPERATION OF APPARATUS

In the apparatus, pictured in Figure 1, a disc-shaped sample is sinusoidally sheared in torsion between two circular metal surfaces. The bottom surface is fixed, while the other is suspended from above and can oscillate freely. Self-adhesion or a normal force causes the sample surfaces to be held immobile relative to the shearing plates.

* Present address: Mellon Institute, Pittsburgh, Pennsylvania.
† Present address: Gevaert Photo Producten, N. V., Belgium.

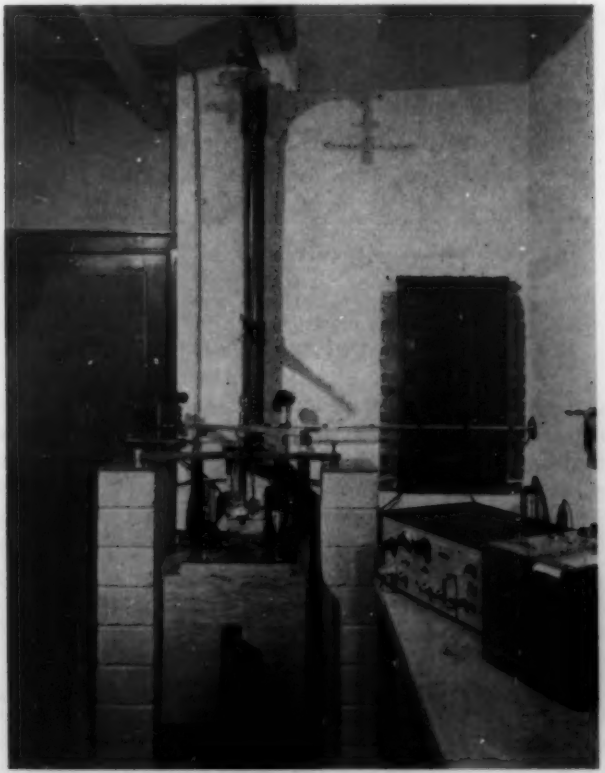

Fig. 1. Photograph of apparatus and recorder. The constant temperature bath has been lowered to reveal the cell housing. The telemicroscope is on the left pillar and the light source and the photocell housing are, respectively, to the left and right sides of the steel post.

It has been our experience that at normal operating torques one need worry about slipping only with gels that exhibit syneresis and possibly those polymers that have a soapy texture, such as Teflon. In a doubtful case, a series of creep runs at various torques would have to be made to ascertain the maximum operating torque. The fact that the sample is not clamped is the most distinguishing feature of this torsional apparatus and allows measurements to be made on

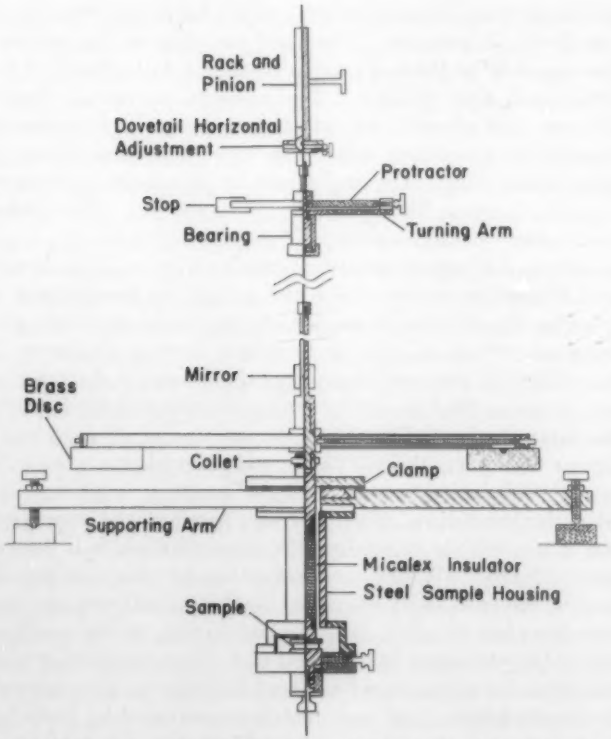

Fig. 2. Half-section of torsion head, sample housing, and inertial system.

very soft gels and on solutions if the viscosities of the latter are sufficiently high so that the sample will retain its shape for the duration of a series of runs. Samples of different dimensions are used to obtain data covering about two decades of logarithmic frequency at a particular temperature. Their heights vary from $^1/_{32}$ to $^1/_2$ in. and diameters from $^1/_2$ to 2 in.; weights usually range between 1 and 4 grams.

The sample position can be seen in Figure 2 to be near the bottom of a stainless steel housing. A window, cemented in place with an epoxy resin (Armstrong's A-2 Adhesive), and lights in the housing are necessary for sample installation. Secured to the bottom of the

flanged housing is a brass base plate which holds and fixes the stainless steel sample cylinder. The rigid coupling of the moment of inertia assembly to the top sample plate is a 1-in. diameter rod of stainless steel and Micalex. The moment of inertia assembly, which is removed when the instrument functions as a creep apparatus, consists of an aluminum tube with two detachable brass discs, weighing about 2 kg. each, which can be positioned symmetrically at various distances from the axis of oscillation. The accessible range of moment of inertia is 1.0×10^5 to 1.8×10^7 g. cm.^{2}.

Piano wire, 0.012 in. in diameter and about 90 cm. long, is used to suspend the entire system above the sample for the dynamic runs. Its restoring force is always less than $^1/_2\%$ of that of the sample and is neglected. Wires of the same length having diameters from 0.008 to 0.029 in. are used to produce the torque in the creep runs. Stresses as low as 100 dynes/cm.^{2} can be attained with the former.

The clamp shown in Figure 2 holds the steel shaft fixed and perpendicular during sample installation and removal, and when any adjustments or changes are made after the sample is in place; e.g., removal of the brass discs. Since the wire supports the entire inertial system, it is necessary to produce the proper tension in it before the clamp is released. Weights compensating for the clamped lower sections of the steel shaft are added to the inertial system and the collet is loosened to allow the wire to stretch to its equilibrium length. After the collet is tightened and the compensating weights are removed, the clamp may be opened and the run may proceed.

The sample housing and base plate are supported by three heavy steel arms whose ends rest on cement block pillars. A $^1/_2$-in. steel plate lies under the pillars and is cushioned underneath with Unisorb "H" felt (The Felters Co.) to minimize vibrations arising from the concrete floor. A steel pipe $3^1/_2$ in. in diameter and 9 feet high, filled with cement and welded to the steel plate, provides the support for the cantilever arm that holds the top end of the wire.

The torsion head, shown in the top half of Figure 2, functions only during creep runs. It serves to apply the required constant stress in a manner which will be described later. Alignment and vertical adjustment are accomplished with two mutually perpendicular dovetail slides and a vertical rack and pinion, respectively.

Since this torsion pendulum was built to measure low loss materials, the use of bearings was avoided where possible. Normally, the only

damping resistance outside that of the sample is due to the air; that of the wire is completely negligible. Because the wire and the inertial system are entirely free except at the upper point of suspension and the sample surface, occasionally the oscillating system tends to rock. When this rocking is observable in the recorded motion a friction bearing is closed about the wire. Duplicate determinations made with and without the bearing, when possible, agree within experimental error. The bearing is never used in creep runs and only when necessary for dynamic measurements.

The oscillatory motion is followed by recording the angular deflection of a light beam reflected from a mirror fixed near the axis of oscillation. A vertical straight edge that cuts off part of the beam is focused on the surface of a barrier-type photocell. The rest position of the uniform semicircular light beam is such that approximately half of the one inch square surface of the cell is illuminated. As the inertial system oscillates, a damped sinusoidal current is generated by the cell. The light intensities used are relatively low so that no detectable error has been traced to photocell fatigue. A resistor shunts the photocell and the voltage drop across this resistor is amplified and recorded with a Sanborn recording system: recorder assembly 151-100A, power supply and amplifier 150-200A/400, and preamplifier 150–1500. The maximum angular deformation in the sample for both dynamic and creep measurements can be varied from 0.5° to 1.5° by changing the length of the reflected light beam.

For creep measurements detection of the strain is identical to the preceding except that the cell is illuminated to about 3% before the stress is applied. During the run the proportion of the area illuminated gradually increases, and just before total illumination the stress must be removed and recovery begun.

A constant intensity light source is essential for both dynamic and creep measurements. An auto headlight lamp was tried with a Sola constant voltage transformer. At times it proved satisfactory for the dynamic measurements, but was not dependable enough for creep runs. A mercury vapor lamp is now being used instead of the tungsten lamp and is proving satisfactory. To correct for drifts in the recorder and the light source, a movable second photocell, placed above the measuring cell, is used to recalibrate the recorder during creep runs which are longer than just a few minutes.

The sample coefficient and the various values of the moment of

inertia must be known for the dynamic determinations. The former is calculated from the sample volume and height. The height is monitored during the runs with a telemicroscope that is used to read a scale machined into the one inch diameter stainless steel shaft, so that the sample height at room temperature is known to ± 0.001 in. At temperatures above and below that of room, the measured value has to be corrected for the difference in the thermal expansions of the stainless steel housing and the Micalex insulating shaft. The Micalex section is 9 in. long, but its expansion coefficient is so close to that of the steel used that the height correction 125°C. from room temperature is only 0.007 in.

The moments of inertia are accurately known from their dimensions and their distance from the axis of oscillation, R. The geometry of the rest of the inertial system is not simple; therefore its calculated moment, I_c, was checked by determining the periods of oscillation, T, in the absence of a sample with the discs at a number of positions. The equation, $T^2 = (4\pi^2/k)(I_c + I_0 + MR^2)$, where I_0 is the moment of inertia of the discs about their own axis and M is their combined mass, shows that a plot of T^2 versus R^2 yields I_c and k, the wire constant (dyne cm.). Determinations of I_c made with several wires checked among themselves and with the calculated value to within 1%.

The torques applied in creep experiments are calculated from the determined wire constant and the known angle through which the wire has been manually twisted with the torsion head at time zero. This angle is so large that the angular sample deformation will not decrease as much as 1%. The stress, therefore, is sufficiently constant for the creep portion of a run, but since in practice it is impossible to remove the stress exactly, the recovery portion at long times is in doubt. The strain at 100% cell illumination is known from geometrical considerations and the smaller strains are recorded as fractions of this value.

An advantage peculiar to this kind of bifunctional instrument is the fact the sample can remain *in situ*, untouched and unchanged, while the transformation from a dynamic to a creep instrument takes place. It is particularly useful in the execution of creep measurements, for no assumptions about the maintenance of the sample shape need be made. Quick dynamic check runs at a few frequencies can be made at appropriate times, and so long as the frequencies are repro-

duced it can be concluded that neither change in the nature of the sample nor in the sample shape has occurred. The latter is far more frequent, but if there is any doubt the loss tangent, which is independent of sample shape, will furnish the necessary information. Finally, if the sample shape has changed one need not begin with a new sample, because the dynamic check run has provided an empirical correction to the calculated sample coefficient. In practice, dynamic check runs are always made before and after long creep runs. A series of dynamic runs ends at the starting temperature and other checks are usually made.

Constant temperature to within ±0.2°C. is maintained with a bath which is raised into position beneath the supporting arms by means of a hydraulic jack. A two-junction copper-constantan thermocouple resides in the bottom sample cylinder. To investigate the possibility of a thermal gradient across the sample at the extremes of the temperature range of the instrument (−45 to 160°C.), a dummy run was made with a second thermocouple above a sample, $^1/_8$ in. high, and no detectable gradient was found.

Originally the instrument was designed with a reinforced Lucite sample housing and a coupling shaft with only a short Bakelite insulating section. With these features the temperature range was restricted to less than half of the present accessible range; at the extremes the height corrections were appreciably larger and the measured thermal gradient was about 1.5°C.

CALCULATIONS

Frequencies, ν, and logarithmic decrements, Δ, are obtained from the recorded damped sinusoidal curves. Figure 3 pictures examples of some experimental curves obtained on a polyvinyl chloride gel which will be discussed later. The four curves illustrate about half of the range of frequencies attainable from a single sample by changing the moment of inertia.

The usual approximate relations[6] for the case of small damping are used to calculate the real component of the complex dynamic rigidity, G' (storage modulus), and the ratio of the imaginary to real components or loss tangent, G''/G':

$$G' = K\omega^2 I(1 + \Delta^2/4\pi^2) \quad (1)$$

and

$$G''/G' = \Delta/\pi(1 + \Delta^2/4\pi^2), \tag{2}$$

where K is the sample coefficient and ω is the circular frequency, $2\pi\nu$. The sample coefficient in the case of a right circular cylinder is h/j, where h is the sample height and j is the second moment of the cross-sectional area, $\pi r^4/2$. In terms of h and V, the volume, $K = 2\pi h^3/V^2$.

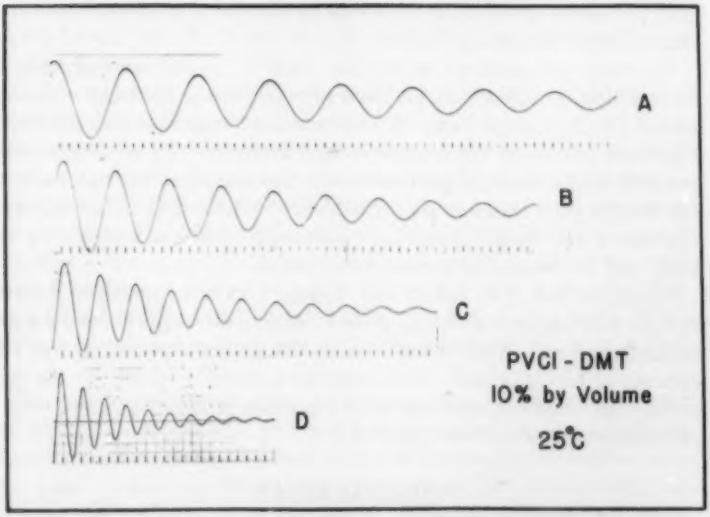

Fig. 3. Examples of experimental curves of a gel of polyvinyl chloride and dimethylthianthrene recorded with different moments of inertia, I. (A) I = 3.3×10^6; (B) 1.8×10^6; (C) 8.2×10^6; (D) 3.1×10^6 g. cm.^{2}. One-second timing pips are indicated. Approximate sample dimensions: height, $^1/_8$ in.; diameter $1^1/_8$ in.

The exact relations are available,[7] but are difficult for normal data analysis. It is felt that as long as the recorded curves follow within experimental error the equation of motion, from which eqs. (1) and (2) are derived, the results may be considered accurate.

The logarithmic decrement is determined from the slope of a semi-logarithmic plot of the peak amplitudes against the ordinal number of the peak. However, a special procedure is necessary for very soft

materials. In exciting the oscillations manually, it is impossible to give the inertial system the proper amount of kinetic energy to avoid an initial deformation that complicates the motion of the system. Essentially, a short time creep and recovery experiment is superimposed on the damped sinusoidal motion which causes the base line to drift. The effect of the drifting base line is eliminated in the following manner. The logarithms of peak amplitudes above and below a tentative base line are plotted separately versus peak number. Then

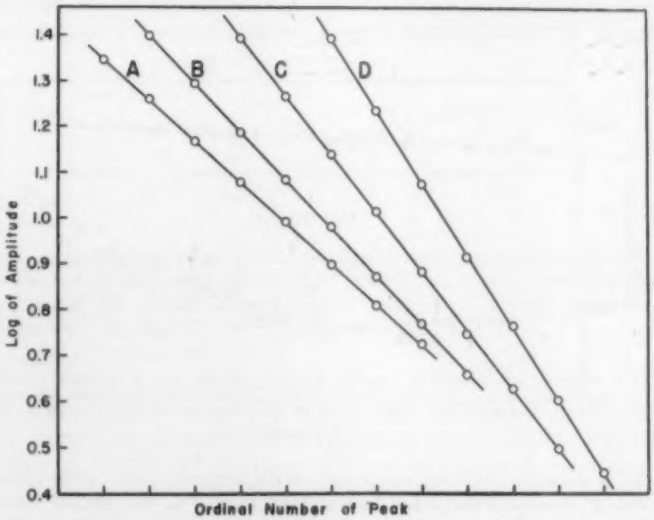

Fig. 4. Logarithmic decrement curves derived from experimental curves of Fig. 3. Letters A through D indicate the correspondence of curves.

the antilogarithm of each reading interpolated midway between two successive peaks on one curve is averaged with the amplitude, γ, of the opposite peak on the other curve. Half the distance between the two envelopes of the damped sine wave at each peak is then known and is the true amplitude of that peak. The actual decrements, $\ln \gamma_n/\gamma_{n+1}$, are determined from these values. Figure 4 illustrates the precision of the final curves derived from the experimental curves of Figure 3.

The creep compliance, $J(t)$, is obtained very simply from

$$J(t) = \Theta/SK$$

where Θ is the angular deformation and S is the torque exerted by the wire.

ILLUSTRATIVE RESULTS

To establish the accuracy of the apparatus, measurements were made on the polyisobutylene which was distributed by Dr. Robert S. Marvin of the National Bureau of Standards.[8] These dynamic

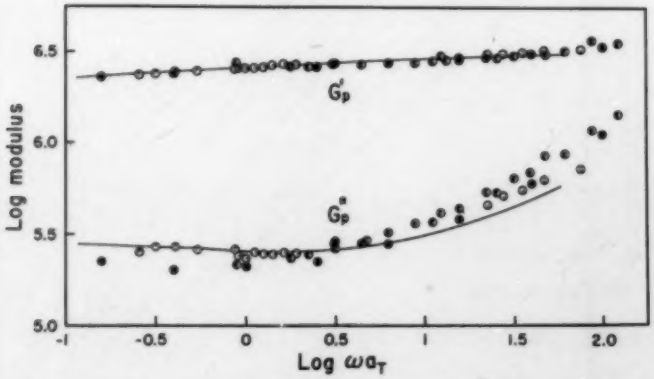

Fig. 5. Real and imaginary components of the dynamic rigidity of the National Bureau of Standards polyisobutylene reduced to 25.0°C. and plotted logarithmically against the reduced frequency: Black circles, NBS averages; half-filled circles, Ferry, Grandine, and Fitzgerald[9]; lines, Philippoff[10]; this paper, pip down, 5.2°; pip right, 34.6°; pip up, 48.9°.

measurements were made on a single sample ($1^1/_8$ in. in diameter and 0.35 in. high) at three temperatures: 5.2, 34.6, and 48.9°C. Values of G' and G'' were reduced to 25.0°C. with the relations $G'_p = G' \cdot (T_0\rho_0/T\rho)$ and $G''_p = G''(T_0\rho_0/T\rho)$, where ρ and ρ_0 are the densities at the operating and reference temperatures, T and T_0, respectively. The logarithms of the reduced values are plotted in Figure 5 against the logarithm of the reduced circular frequency, log ωa_T. The shift factors, a_T, used are those of Ferry, Grandine, and Fitzgerald.[9] Also

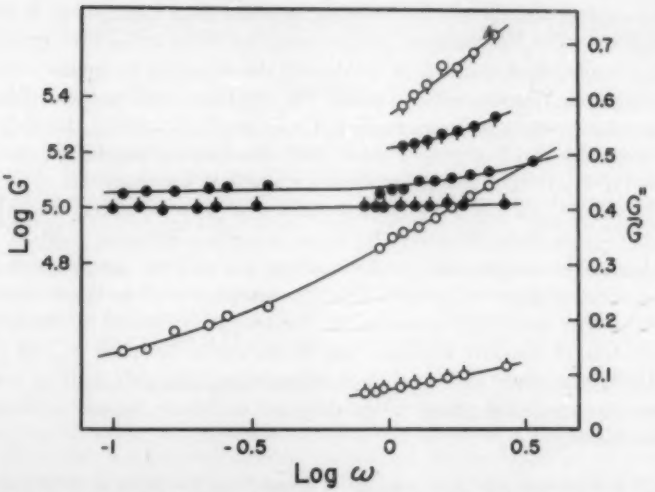

Fig. 6. Loss tangents (open circles) and logarithms of real components of dynamic rigidity (black circles) of polyvinyl chloride gel in dimethylthianthrene (10% polymer by volume) plotted against logarithm of circular frequency: pip down, 4.6°; no pip, 9.5°; pip up, 25.0°.

shown in Figure 5 are the averaged values of previous studies computed at the National Bureau of Standards.[8] The double transducer data of Ferry, Grandine, and Fitzgerald,[9] and the low frequency measurements of Philippoff[10] are presented as two examples of the compiled results included in the NBS averages. The agreement between all sources of the G'_p data is excellent. The G''_p values show more scatter between the various sources in such a manner that the torsion pendulum data may be considered as justified as any of the others. It may be concluded, therefore, that the accuracy of the instrument is satisfactory.

A gel of polyvinyl chloride in dimethylthianthrene (10% polymer by volume) has also been studied to complement measurements obtained previously on this same system by Ferry and Fitzgerald using the double-transducer method.[11] Figure 6 presents values of log G' and G''/G' obtained from two samples. Their diameters were $1^1/_8$ and $^1/_2$ in. and their heights $^1/_8$ and $^3/_8$ in., respectively. The higher frequency data, measured at 4.6, 9.5, and 25.0°C., were obtained from

the shorter sample, and the lower from the longer sample at 9.5 and 25.0°C. The loss tangent values from the latter at 25.0°C. were unattainable because drafts of air caused the damping to appear erratic, though the frequencies and hence the rigidities were not so affected. The data, when reduced to 25.0°C.,[12] smoothly extend the data of Fitzgerald and Ferry and show that the torsion pendulum can be used to study the type of material for which it was designed.

Although no creep results are shown, it may be noted that their accuracy is dependent on the same sample coefficient used in the calculation of dynamic results and on the torque applied and the measured angular deformation of the sample. Unless there is creep in the wire itself, the accuracy of the torque is limited by the determination of the wire constant which can easily be made within 1%. The largest errors thus arise in readings of angular deformation taken near the resolving power of the detector and from sample coefficient uncertainty.

This work was part of a program of research on the physical structure and properties of cellulose derivatives and other polymers supported by the Allegany Ballistics Laboratory, Cumberland, Maryland, an establishment owned by the United States Navy and operated by Hercules Powder Company under Contract NOrd 10431. It was also supported in part by a grant from the National Science Foundation, and by the Research Committee of the Graduate School of the University of Wisconsin from funds supplied by the Wisconsin Alumni Research Foundation. The authors are indebted to Dr. John D. Ferry for his guidance in the design of the apparatus, to Mr. Robert Schmelzer for help in its construction, and to Miss Shirley Pomeroy for assistance with some of the calculations.

References

1. W. Kuhn and O. Künzle, *Helv. Chim. Acta*, **30**, 839 (1947).
2. L. E. Nielsen, *Rev. Sci. Instr.*, **22**, 690 (1951).
3. K. Schmieder and K. Wolf, *Kolloid-Z.*, **127**, 65 (1952).
4. J. Koppelmann, *Kolloid-Z.*, **144**, 12 (1955).
5. N. Tokita, *J. Polymer Sci.*, **20**, 515 (1956).
6. A. J. Staverman and F. Schwarzl, in H. A. Stuart, *Die Physik der Hochpolymeren*, Band IV, Springer-Verlag, Berlin, Germany, 1956, pp. 86–88.
7. H. C. Brinkman, to be published.
8. R. S. Marvin, *Proc. 2nd Intern. Congr. Rheology*, Butterworths, London, England, 1953, p. 156.
9. J. D. Ferry, L. D. Grandine, Jr., and E. R. Fitzgerald, *J. Appl. Phys.*, **24**, 911 (1953).
10. W. Philippoff, *J. Appl. Phys.*, **24**, 685 (1953).

11. J. D. Ferry and E. R. Fitzgerald, *J. Colloid Sci.*, **8**, 224 (1953).
12. J. D. Ferry, D. J. Plazek, and G. E. Heckler, *J. chim. phys.*, **55**, 152 (1958).

Synopsis

An instrument designed to measure the mechanical properties of soft viscoelastic materials with low loss has been built and tested. It is used as a free vibration torsion pendulum for obtaining low frequency dynamic mechanical properties (0.02 to 10 cycles/sec.) and as a torsional creep apparatus capable of measurements involving low stresses (e.g., 100 dynes/cm.^{2}). Since the disc-shaped samples are held between two parallel surfaces by means of a normal force, measurements can be made on materials whose consistencies defy clamping. The maximum angular deformation of the sample can be varied from 0.5 to 1.5°. The accessible temperature range is −45 to 160°C. Detection of the motion is accomplished with a reflected light beam, a barrier-type photocell and a Sanborn chart recorder.

Dynamic measurements made on the widely studied National Bureau of Standards polyisobutylene sample compared favorably with previous measurements from this laboratory and elsewhere. Similar experiments on a 10% gel of polyvinyl chloride in dimethylthianthrene showed that storage moduli as low as 10^5 dyne/cm.^{2} and loss tangents as low as 0.07 could be satisfactorily measured.

TRANSACTIONS OF THE SOCIETY OF RHEOLOGY II, 53–75 (1958)

The Dynamic Mechanical Properties of a Model Filled System: Polyisobutylene-Glass Beads*

ROBERT F. LANDEL, *Jet Propulsion Laboratory, California Institute of Technology, Pasadena, California*

INTRODUCTION

The effects of fillers on the tensile strength, ultimate elongation, and equilibrium modulus of rubbers have been extensively studied. On the other hand, relatively little work has been done on the time-dependent mechanical properties of filled rubbers. Becker,[1] studying the response of a vulcanized natural rubber in the rubber-to-glass transition zone, found that the addition of an unspecified amount of silica increased the equilibrium modulus and the low-frequency dynamic modulus but had little effect on the dynamic modulus at high frequencies. Blatz[2] found that the quasi-equilibrium creep compliance of a crosslinked, plasticized synthetic rubber decreased with increasing amounts (50 to 70 wt.-%) of an inorganic salt as filler. In both of these studies the time-temperature superposition principle[3–5] was found to be applicable, and data obtained at different temperatures could be superposed by a simple translation along the time scale. Nielsen and co-workers[6] used a torsion pendulum to measure the dynamic modulus and damping as a function of temperature for polystyrene filled with a variety of materials. However, they were mainly concerned with properties in the glassy region and did not attempt to separate the effects of time and of temperature.

In order to provide experimental data on the effects of fillers on mechanical properties in the transition zone as a function of filler concentration, we have studied the dynamic shear compliance and

* This paper presents the results of one phase of research carried out at the Jet Propulsion Laboratory, California Institute of Technology, under Contract No. DA-04-495-Ord 18, sponsored by the Department of the Army, Ordnance Corps.

modulus of a model filled system. To avoid the question of "reinforcing" versus "nonreinforcing" fillers as well as possible side effects related to the type and density of crosslinks, we have chosen an uncrosslinked polymer—polyisobutylene (PIB)—containing a nonreinforcing, noninteracting filler—small glass beads.

As a first approximation crystalline polymers can probably be considered to be like highly crosslinked and highly filled systems with temperature dependent crosslink and filler densities. Thus, in addition to its intrinsic value, a study of simple filled systems might give some insight into the mechanical properties of crystalline polymers.

MATERIALS AND METHODS

The polyisobutylene (a standard sample obtained from the National Bureau of Standards (NBS) through the courtesy of Dr. R. S. Marvin) has a weight-average molecular weight of 1.56×10^6. Its mechanical behavior has been extensively studied in a number of laboratories.[7-10] The glass beads are essentially spherical and polydisperse, having an average diameter of 40 microns as determined with a Micromerigraph. The size distribution is fairly narrow, 94% of the beads being between 20 and 60 microns in diameter. The beads were washed in carbon tetrachloride to remove any surface oil which might be present and then were dried in a stream of filtered tank nitrogen. Weighed amounts of clean beads were then stirred into viscous carbon tetrachloride solutions of polyisobutylene to give 20, 40, and 60 weight-% beads in the PIB. The high viscosity of the solutions prevented the beads from settling during mixing. After the uniform dispersions were frozen in liquid nitrogen, the carbon tetrachloride was removed by lyophilization to give a spongy product. The residual carbon tetrachloride in a sample of the composite containing 60% beads was less than 0.001% as determined by ultraviolet absorption. The exact weight concentration of beads in each preparation was determined by ignition. Designating the three preparations as Systems I, II, and III, the glass-bead concentrations in each were: System I, 19.92% by weight or 8.68% by volume; System II, 39.95% by weight or 20.30% by volume; and System III, 60.24% by weight or 36.65% by volume.

The complex shear compliance $[J^*(\omega) = J' - iJ'']$ was measured at frequencies between 24 and 6000 cycles/sec. and at various tem-

peratures between −45 and 70°C. with a Fitzgerald Transducer Apparatus (Atlantic Research Corp., Alexandria, Va.), which is similar to the double transducer of Fitzgerald and Ferry.[11] Bubble-free disks suitable for study in the apparatus were prepared by molding the spongy lyophilizate at 125°C. and 2000 p.s.i. Microscopic examination of the disks, especially those prepared from System I, showed the beads to be uniformly dispersed. The sample coefficients $2\bar{m}/\rho\bar{h}^2$ were calculated from the average disk weights $\bar{m}$, the average thicknesses measured *in situ* $\bar{h}$, and the densities ρ. The latter were calculated on the assumption of additive volumes and zero volume expansion coefficient for the beads. The density of the beads, 2.39 g./cm.^{3} at 25°C., was determined experimentally. The density and volume expansion coefficient of PIB are 0.913 g./cm.^{3} and 6.2×10^{-4} deg.$^{-1}$, respectively.[12]

The polymer is easily pulled away from the beads at the higher bead concentrations. When this happens, voids form around the beads and the samples turn white. The disks must therefore be handled carefully to preserve their integrity. Disks of System III, for example, cannot be compressed more than about 6 or 7% before the separation occurs. The separation might also occur on subjecting

TABLE I
Dimensions, Per Cent Compression, and Sample Coefficients for the Glass-Bead-Filled PIB Systems Studied

System	Concentration of beads, Wt.-%	Concentration of beads, Vol.-%	Sample no.	Approximate dimensions, in.	Compression, %	Sample coefficients at 25°C., cm. Calculated	Sample coefficients at 25°C., cm. Correction factor
I	19.9	8.68	27	7/8 × 1/10	4.7	33.92	—
			28	1/4 × 1/8	3.9	1.662	0.82
			29	1/2 × 3/64	4.0	22.44	—
			30	1/4 × 1/16	5.9	6.88	—
II	39.9	20.3	25	1/4 × 1/16	6.8	4.248	—
			26	1/4 × 1/8	5.6	1.644	0.95
III	60.2	36.7	13	7/8 × 7/64	2.5	28.88	1.21
			14	1/4 × 1/8	3.1	1.556	1.04
			15	1/4 × 1/5	3.4	1.645	0.95
			19	1/4 × 5/64	4.6	3.865	—

the samples to high or low temperatures because the beads have a smaller thermal expansion coefficient than the polymer. Since the separation would change the dynamic compliance, measurements were repeated at several intermediate temperatures in a given temperature sequence in order to test for such changes. Ordinarily a check run is made only at the initial temperature to insure that the samples have not pulled away from the driving surfaces. The latter effect would give a vertical shift to the compliance-frequency curve at a given temperature while the PIB-bead separation would be expected to give both a vertical shift and a changed slope. Only after going to 70°C. with Sample 13 of System III was there a slight change in the slope of the check run curve to indicate a separation.

All systems were run at essentially the temperatures indicated for System III in Figure 1. In some cases, the results for the different samples of the same composition did not agree at overlapping temperatures. This was taken to indicate incomplete adhesion to the shearing surfaces. To correct for this effect, the sample coefficients were corrected by small factors to bring the data into agreement. A complete description of the various samples including the nominal coefficient values and correction factors is given in Table I. In the two extreme cases, a correction of 20% was necessary, but other samples of the same composition required only a small or zero correction.

When the transducer housing was opened at the conclusion of measurements on System II, a small amount of isopropanol was found to have leaked in from the thermostat bath. However it should not have affected the results because the final check runs agreed so well with the initial runs, and the leak was so slow that it seems doubtful that the initial data could have been in error. The average gain in weight of the two disks comprising Sample 25 was 0.2 mg. and, for Sample 26, 0.5 mg.—a gain of 0.4% in each case. Thus the PIB can contain at best only a trace of diluent.

RESULTS

For economy of space, only the initial data for System III containing 36.7% by volume of beads are illustrated. Values of J' and J'' for this system are shown in Figure 1. The results for the other two systems are similar: at any given temperature the compliance increases with decreasing filler concentration.

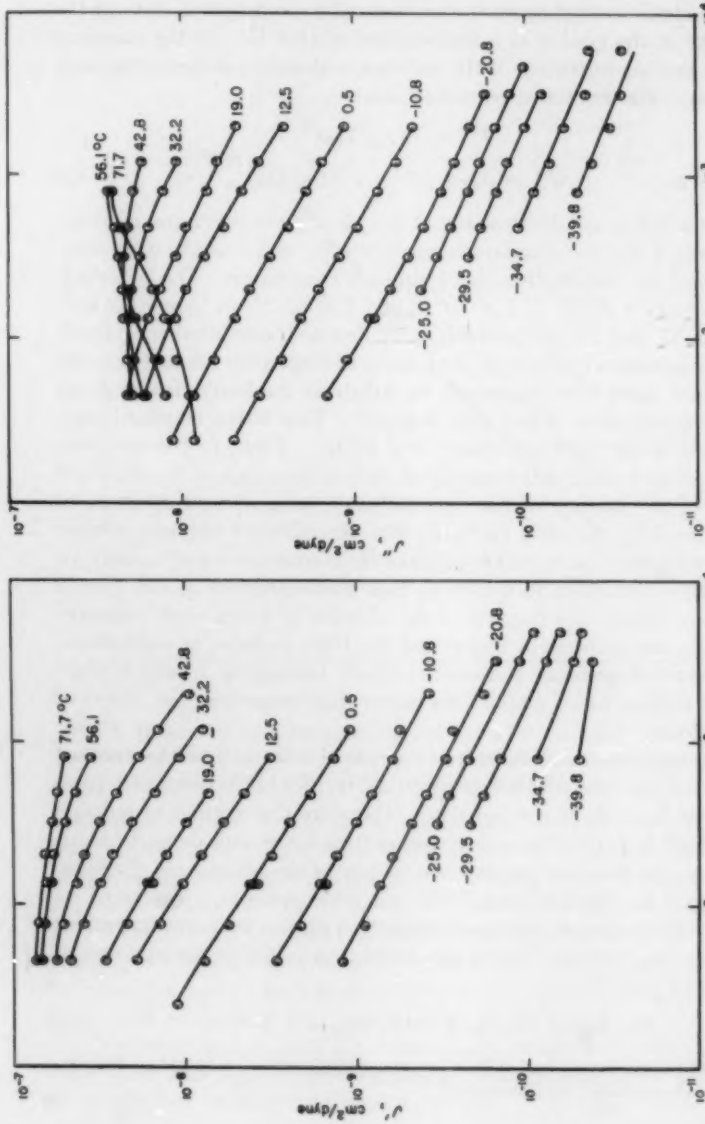

Fig. 1. Variation of the shear storage compliance J' (left) and loss compliance J'' (right) at the indicated temperatures for NBS polyisobutylene containing 36.7 vol.-% of small glass beads as a filler.

The data for each system were reduced to a standard state of the density of the system at a temperature of 12.5°C. At the standard state, the concentration of the polymer is therefore different for each system. The reduction equations are:[13]

$$J_c'' = J''T\rho/T_0\rho_0 \tag{1}$$

$$J_c' = J_g + (J' - J_g)T\rho/T_0\rho_0 \tag{2}$$

where ρ and ρ_0 are the densities at the absolute temperature of measurement T and the standard temperature T_0, and J_g is the glass compliance,* i.e., the limiting high-frequency compliance. The latter was taken to be 5×10^{-11}, 2×10^{-11}, and 2×10^{-11} cm.²/dyne for Systems I, II, and III, respectively. We denote the reduced compliance by the subscript c instead of the usual p to emphasize the fact that the standard state here represents an arbitrary concentration and not the concentration of the pure polymer. This is the standard state implicit in the work of Becker[1] and Blatz.[2] Thus, to convert from the standard state of the density of each system $(\rho_0)_c$ to the standard state of the density of the pure polymer $(\rho_0)_p$, J' and J'' must be multiplied by the ratio $(\rho_c/\rho_p)_0$. But the effective polymer density may not always be available to make the conversion—particularly for polymers containing moderate to high concentrations of soft porous fillers or crystallites because of the absence of a clear-cut boundary between the amorphous region and the filler particles or crystallites. We therefore prefer to present the results initially in a more directly useful fashion which emphasizes rather than suppresses the effects of the filler.

The temperature-shift factor a_T required to superpose the reduced data was the same within experimental error for both compliance components for a given composition. Therefore the method of reduced variables[5] is applicable and all retardation times still depend identically on the absolute temperature in spite of the presence of the filler, as found by Becker[1] and Blatz[2] on their systems. Values of a_T at any given temperature vary slightly with the filler concentration, but the temperature dependence in each case follows an equation of the WLF form:[15]

$$\log a_T = -c_1(T - T_s)/(c_2 + T - T_s) \tag{3}$$

* The nomenclature used is that recommended by the Committee on Nomenclature of the Society of Rheology.[14]

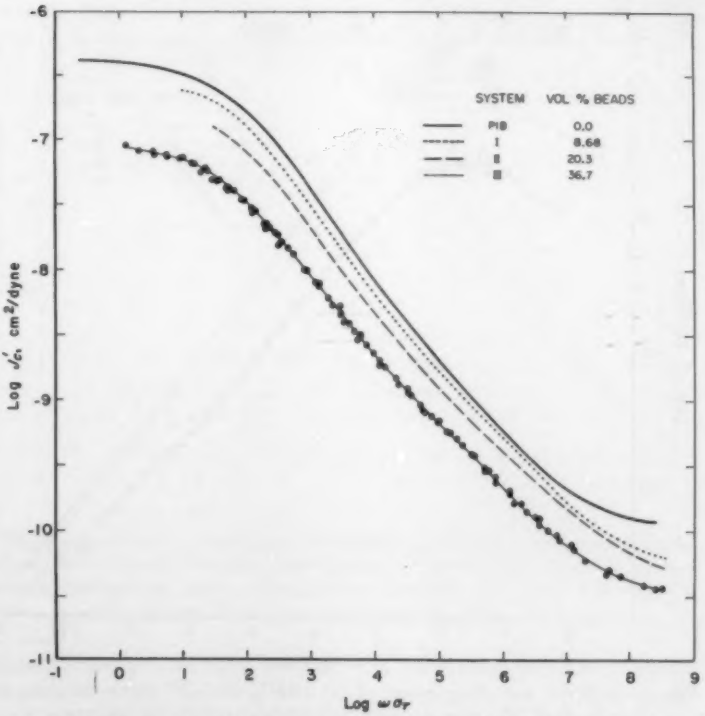

Fig. 2. Reduced storage compliance J'_c at 12.5°C. of NBS polyisobutylene at four levels of filler concentration as indicated, plotted against reduced frequency. Data for pure PIB from Ferry, Grandine, and Fitzgerald.[9]

Here c_1 and c_2 are approximately universal constants, and T_s is a standard reference temperature which is about 50°C. greater than the glass transition temperature T_g. For pure PIB, T_s is 41° higher than T_g. By plotting the log a_T values for the three composites against $T - T_0$ and fitting the data to a corresponding plot of the WLF equation, T_g can be approximated. However a more reliable estimate can be obtained by comparing the curves with a similar plot for pure PIB,[9] and on doing so one finds that the beads raise T_g by 2, 5, and 7°C. for Systems I, II, and III, respectively. Such an increase seems reasonable because the regions of polymer adsorption will act as weak crosslinks and crosslinking raises T_g.[16,17]

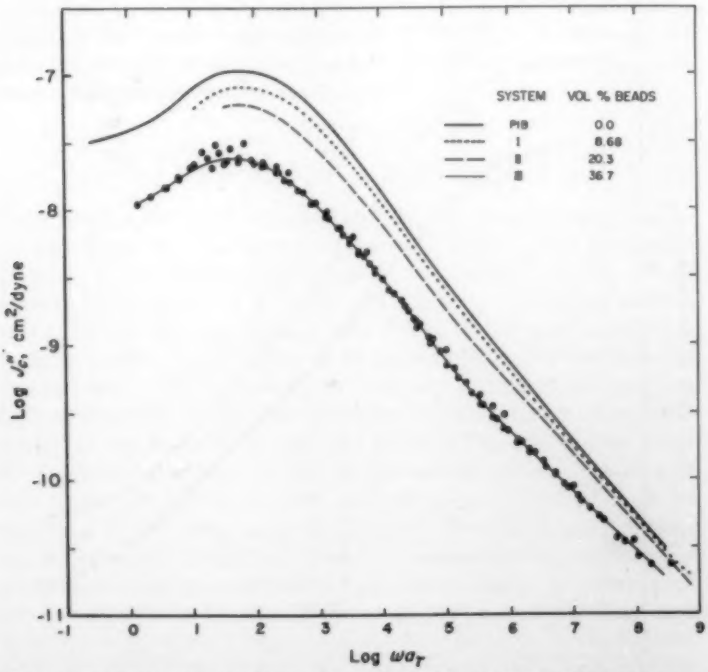

Fig. 3. Reduced loss compliance J''_c at 12.5°C. of NBS polyisobutylene at four levels of filler concentration, plotted against reduced frequency.

The superposed data for System III are illustrated in Figures 2 and 3. Also indicated are the corresponding dispersion curves for the filled systems of lower concentrations. The curves for pure PIB were obtained from the data of Ferry, Grandine, and Fitzgerald[9] after reduction from 25 to 12.5°C. The factor $T\rho/T_0\rho_0$ was included in the reduction.

These results show that the magnitude of J'_c and J''_c diminishes steadily with increasing filler concentration. At the same time the dispersion zones are broadened; the decrease in slope of the curves is plainly evident in the J''_c curves. A portion of the difference in magnitude can be attributed to the fact that the comparison is not being made at corresponding temperature states, i.e., at the same number of

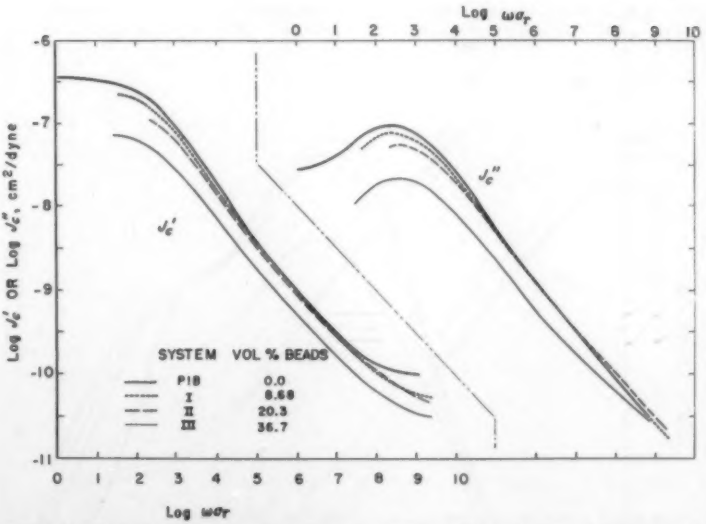
Log ωa_T
0 1 2 3 4 5 6 7 8 9 10
-6 -7 -8 -9 -10 -11
Log J_c' OR Log J_c'', cm²/dyne
J_c'
J_c''
SYSTEM VOL % BEADS
PIB 0.0
I 8.68
II 20.3
III 36.7
0 1 2 3 4 5 6 7 8 9 10
Log ωa_T

Fig. 4. Variation of reduced storage compliance J'_c and reduced loss compliance J''_c with reduced frequency after converting data of Figs. 2 and 3 to corresponding temperature states. Standard temperatures are: pure PIB, 25°C.; System I, 27°C.; System II, 30°C.; and System III, 32°C.

degrees above T_g for each system. On converting to corresponding temperature states equivalent to 25°C. for pure PIB, i.e., 27, 30, and 32°C. for Systems I, II, and III, respectively, one finds, as shown in Figure 4, that Systems I and II actually show little change in properties from those of pure PIB. Barring the changes in J_g, the results at reduced circular frequencies ωa_T greater than 10^4 sec.$^{-1}$ are nearly identical to those for PIB. The progressive decrease in the slope of the log J''_c versus log ωa_T plots above $\omega a_T = 10^6$ is now somewhat more sharply revealed, since J''_c for System II lies *above* the results for pure PIB and System I. A comparison of the loss tangents J''/J' at corresponding temperature states (Fig. 5) also illustrates the fact that there is little change in going from 0 to 20.3 volume-% beads other than the broadening effect already noted; the shoulder found in pure PIB steadily widens. However on increasing the bead content to 36.7%, the primary maximum drops markedly and the shoulder separates into a second maximum.

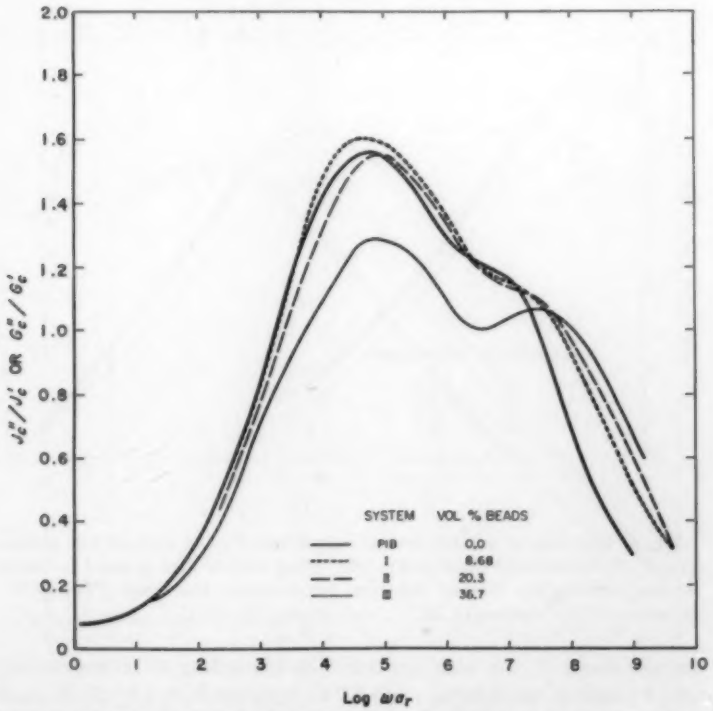

Fig. 5. Reduced loss tangents at corresponding temperature states plotted against reduced frequency.

DISCUSSION

Dependence of Modulus on Filler Concentration

To facilitate the following discussion we recast the results in terms of the storage modulus G'_e and the loss modulus G''_e (Fig. 6). Note that at high reduced frequencies the beads affect G'' more than G', whereas they influence J' more than J''.

According to the Guth-Smallwood[18,19] theory of the reinforcement of rubber, the equilibrium modulus M of a filled system should be related to the modulus M_0 of the unfilled rubber as follows:

$$M = M_0(1 + 2.5\phi + 14.1\phi^2) \tag{3}$$

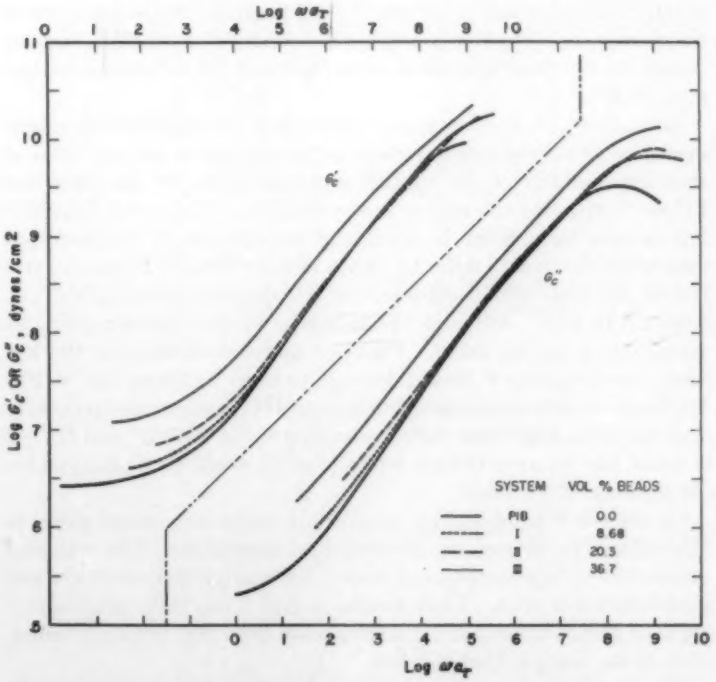

Fig. 6. Reduced storage modulus G'_c and reduced loss modulus G''_c at corresponding temperature states plotted against reduced frequency.

where ϕ is the volume fraction of filler particles. This equation is derived for the case of spherical filler particles in a medium which wets but does not react with the particle surface. A. M. Bueche[20] treats the case in which there are strong interactions between the rubber and the filler, but the Guth-Smallwood model seems more directly applicable here.

Assuming that eq. (3) holds for dynamic as well as static conditions, we then divide the data for the three compositions by an appropriate correction factor $F(= 1 + 2.5\phi + 14.1\phi^2)$. The results (Fig. 7) show that the modulus in the rubbery region is predicted extremely well by eq. (3). The dispersion curves for System III, containing 36.7% beads, now agree within a tenth of a log unit with those

of pure PIB up to $\omega a_T = 10^4$ sec.$^{-1}$. At progressively higher reduced frequencies, eq. (3) overcorrects for the presence of the filler, and the curves for the filled systems diverge from and fall below that for unfilled PIB.

Actually eq. (3) as given is not applicable in the region of high rubber modulus. Two assumptions made in its derivation are not valid in that the modulus of the rubber approaches that of the filler and Poisson's ratio for the rubber is less than 0.5. However, Eshelby[21] has treated this problem in detail, and from his results it is clear that even when the moduli differ by only a factor of 10 and Poisson's ratio is 0.33, the first virial coefficient in F will decrease only slightly, i.e., from 2.5 to 1.76. Although the change is in the right direction, its magnitude is far too small. Figures 4 and 6 show that for the low bead concentrations F should decrease to unity at about $\omega a_T = 10^4$. Furthermore the loss tangent for System III demonstrates pointedly that the same correction factor *cannot* apply to both G' and G''. If it could, the shape of the tan δ plot (Fig. 5) would be unchanged by the presence of the filler.

On the other hand, eq. (3) is certainly useful as a rough guide to filler effects in spite of its acknowledged limitations. The adjusted curves for the four systems in Figure 7 are nearly identical at low and moderate frequencies. Their spread at high frequencies after applying the correction factor is not much greater than that originally found, even at the highest filler content.

When strong polymer-filler bonds exist and eq. (3) is not applicable, it is to be expected that the use of the appropriate theory relating M and M_0 will serve to predict the dynamic properties in the rubbery end of the transition zone. Thus A. M. Bueche's[20] theory would predict a variable first virial coefficient instead of 2.5 and zero for the second virial coefficient. The numerical value of the coefficient would depend on the number of polymer-filler bonds and could be evaluated experimentally. It can be very large, e.g., 80 for a silicone rubber containing Aerosil as a filler.[20]

Relaxation Spectra H

The relaxation spectra H_e at corresponding temperatures were calculated from the composite curves of Figure 7 by the usual second approximation methods.[22,23] For each system, except System I at the shortest times, values calculated from G_e' were in good agreement

TABLE II

Logarithm of Relaxation Spectra H at Corresponding Temperatures for NBS Polyisobutylene Containing Small Glass Beads as Filler

Log τ, sec.	Unfilled PIB,[a] T_0 = 298°K.		8.68 vol.-% beads, T_0 = 300°K.		20.3 vol.-% beads, T_0 = 303°K.		36.6 vol.-% beads, T_0 = 305°K.	
	From G'	From G''	From G'	From G''	From G'	From G''	From G'	From G''
−1.0	5.30	5.28						
−2.0	5.71	5.74	5.75	5.74			6.18	6.21
−3.0	6.28	6.32	6.29	6.30	6.34	6.46	6.78	6.79
−4.0	6.89	6.91	6.88	6.95	6.96	7.01	7.38	7.37
−5.0	7.63	7.60	7.59	7.62	7.63	7.67	7.96	8.01
−6.0	8.25	8.30	8.28	8.29	8.29	8.33	8.62	8.60
−7.0	8.84	8.84	8.79	8.80	8.78	8.86	9.02	9.10
−8.0	9.25	9.36	9.37	9.40	9.31	9.34	9.49	9.62
−9.0	8.97	9.18	9.34	9.64	9.67	9.75	9.78	9.94

[a] Data for unfilled PIB from Ferry, Grandine, and Fitzgerald.[9]

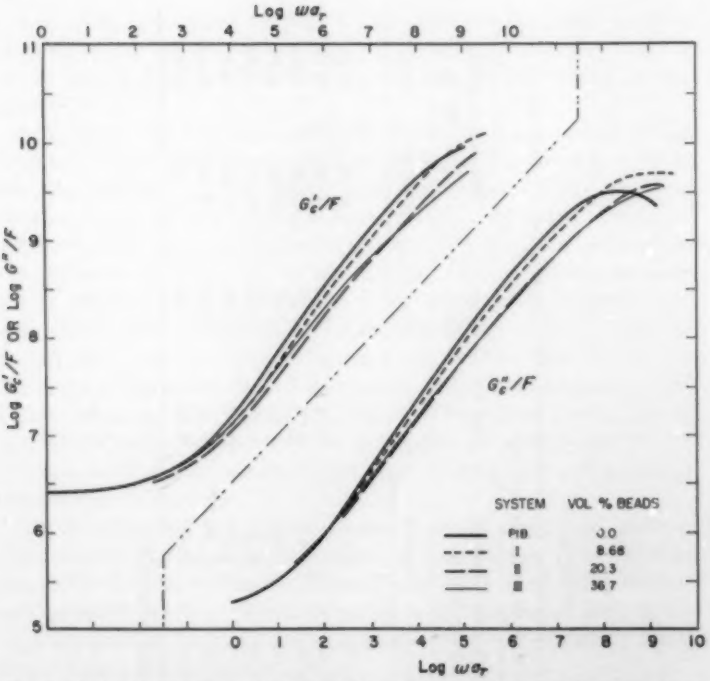

Fig. 7. Reduced storage and loss moduli at corresponding temperature states divided by the Guth-Smallwood factor F and plotted against reduced frequency.

with those from G''_c. The results are given in Table II, where the data of Ferry, Grandine, and Fitzgerald[9] for pure PIB are included for completeness. The weighted curves* through these points are shown in Figure 8. As with G'' of Figure 6 the addition of the beads causes a slight decrease in the slopes of the curves and a progressive increase in the overall magnitude of H.

Retardation Spectra L

The retardation spectra L_e were calculated from the composite curves of Figure 4 by the second approximation methods.[22,23] The

* The values calculated from G' and J' are more accurate on the long-time side of a region of curvature.[23]

TABLE III

Logarithm of Retardation Spectra L at Corresponding Temperatures for NBS Polyisobutylene Containing Small Glass Beads as Filler

Log τ, sec.	Unfilled PIB,[a] T_0 = 298°K.		8.68 vol.-% beads, T_0 = 300°K.		20.3 vol.-% beads, T_0 = 303°K.		36.6 vol.-% beads, T_0 = 305°K.	
	From J'	From J''	From J'	From J''	From J'	From J''	From J'	From J''
−1.0	−7.68	−7.53						
−2.0	−7.22	−7.20	−7.26	−7.14			−7.92	−7.87
−3.0	−7.31	−7.32	−7.22	−7.16	−7.48	−7.46	−7.86	−7.86
−4.0	−7.83	−7.92	−7.86	−7.79	−8.08	−8.01	−8.37	−8.39
−5.0	−8.69	−8.70	−8.53	−8.51	−8.74	−8.69	−9.03	−9.01
−6.0	−9.26	−9.27	−9.17	−9.12	−9.40	−9.32	−9.62	−9.64
−7.0	−9.89	−9.79	−9.64	−9.63	−9.87	−9.75	−10.08	−10.03
−8.0	−10.59	−10.37	−10.24	−10.18	−10.36	−10.30	−10.67	−10.47
−9.0			−10.83	−10.72	−10.92	−10.82	−10.16	−10.90

[a] Data for unfilled PIB from Ferry, Grandine, and Fitzgerald.[9]

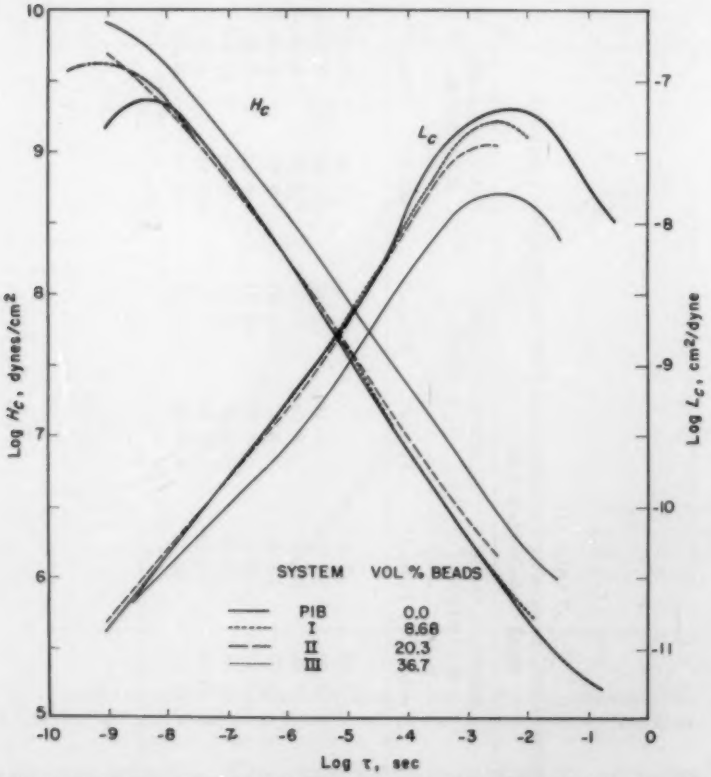

Fig. 8. Relaxation and retardation spectra H_c and L_c reduced to the densities of the systems at corresponding temperature states.

values are given in Table III and are also plotted in Figure 8. Again, those calculated from J_c' are in good agreement with those from J_c''.

The beads depress the magnitude of L_c and broaden the peak. They do not change the ratio of the maximum value of L_c to the equilibrium compliance from the value of 0.20 found for pure PIB.[24] Thus, although the polymer may be absorbed on the surface of the beads, it is too weakly bound to reduce this ratio to a value of about 0.14 as found in a crosslinked polyurethane rubber[25] and in gels of

cellulose tributyrate and polyvinyl chloride, which are crosslinked by crystallites.[24]

Influence of Fillers on Relaxation and Retardation Times

Application of the Guth-Smallwood treatment to H_c or L_c for the purpose of evaluating the effects of the filler would be unsatisfactory, even though it would certainly account for the separation of the spectra at $\tau > 10^{-4}$ sec. as it does for G_c' and G''_c. The underlying theory is that of elastic bodies, and considerations on a molecular scale do not appear. To find such a molecular explanation for the differences between the spectra, we first convert to the standard state of the pure polymer, e.g., to H_p, so that the effects of different amounts of beads are partially removed and the spectra represent the polymer only. While we can convert formally by multiplying by the density ratio as previously indicated, it is instructive to consider the conversion in more detail with the aid of a hypothetical model.

Suppose we have a rubber strip which elongates, say, 100% under a given force. Now apply the same force to a composite strip of the same total length, consisting of a strip of rubber half as long as the first piece and joined at its end to a strip of glass. The rubber section will still elongate 100% but the overall elongation will be only 50%, and the overall modulus will be twice that of the all-rubber strip. Formally, the rubber had been diluted; its concentration per unit total length has decreased, but in contrast to the usual effect of dilution the overall modulus has increased. Yet the modulus of the rubber in the strip is the same. To see whether there is any real change in the properties, the modulus has to be compared on the basis of the unit of the length which is *effective* in the deformation, i.e., that of rubber only.

Similarly the comparison between the filled and unfilled PIB should be made on the basis of the effective or deformable volume. More specifically, the comparison should be made in terms of the number of polymer chains per unit effective volume. Therefore H_c has to be corrected by the factor ρ_c/ρ_p. This reduction to the state of the pure polymer for the glass-filled composite is equivalent to displacing all of the beads to one end of the sample and fusing them to a solid mass. By doing so, we account for what might be called the pure concentration effects but ignore all interaction effects. Any remaining dif-

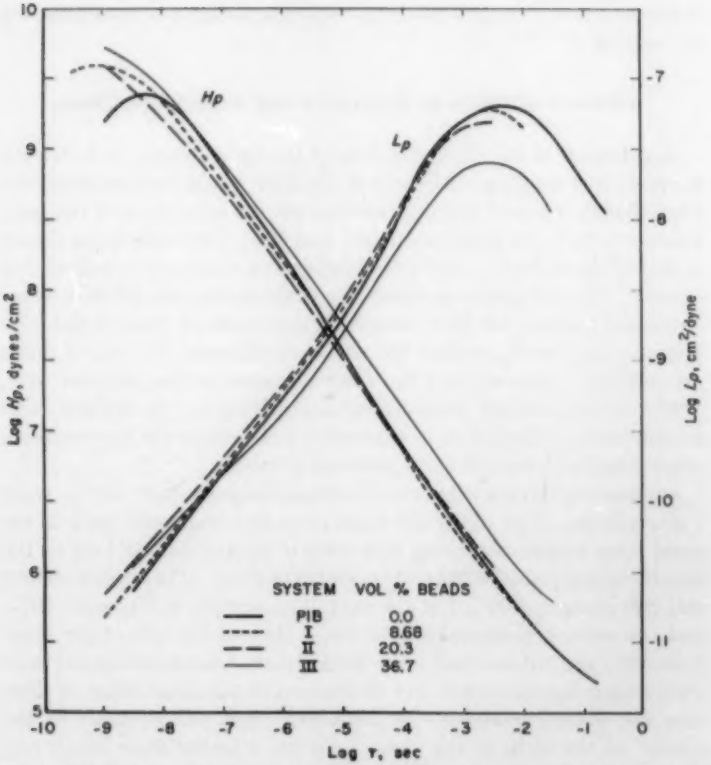

Fig. 9. Relaxation and retardation spectra H_p and L_p reduced to the standard state of the pure polymer at corresponding temperature states.

ferences between H_p for pure PIB and H_p for the composite must therefore originate in these interactions.

Figure 9 shows the results of the reduction. The spectra are essentially unaffected by the beads at short times but diverge at longer times. We interpret this divergence as the result of the partial immobilization of portions of the polymer chains by adhesion. This pinning of the chains reduces the average segmental mobility just as entanglements do,[26,27] and causes a portion of the spectrum to be shifted toward longer times. As a result there is a tendency for a

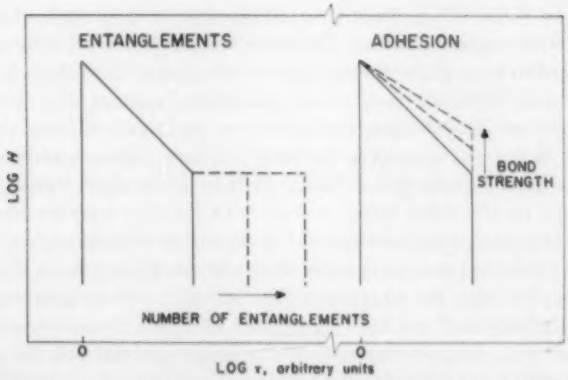

Fig. 10. Idealized description of the effects of entanglements and adhesion on the shape of the distribution function.

plateau to be formed, just as it is by entanglements. But while entanglements actually produce a plateau—the box of the idealized wedge-box distribution—the effects of adhesion merely change the wedge angle. This is indicated schematically in Figure 10. For either entanglements or adhesion the location on the time scale of the maximum in H found at short times (the apex of the wedge) is unchanged but for smaller values of H there is a shift toward longer times. The main differences between the two mechanisms are that (*a*) the effects of adhesion do not enter so abruptly as they do with entanglements, and (*b*) the magnitude of the effect is less. These differences can be explained as follows:

(*a*) The effects of entanglements appear rather abruptly because a critical chain length is required before chains can entangle efficiently. (For PIB, the molecular weight between entanglements is about 13,400.[36]) Thus entanglements are restricted to longer chains. The shorter segments are oblivious to conditions at the ends of the chains, and their average friction coefficient for motion is unchanged. As a result, when studies are made at progressively longer times there is a transition from a response characteristic of the unhindered segmental motions to a response in which the entanglements prolong the relaxation times. The region of the transition is evident in H as a change in the slope of a $\log H - \log \tau$ plot from a value near -0.5 to a value near zero.

On the other hand, there is no limitation to the length of a chain between adsorption points. Therefore the effects of adhesion are not restricted to long segments and there is no abrupt transition from unhindered to hindered motion. In addition, most of the short segments are in the bulk polymer phase, so far removed from the filler surface that only a small percentage of them suffer a reduced mobility. Hence, there will be little shift in H at short times. Long segments, on the other hand, will be both fewer in number and have more adsorption sites per segment than the short segments. Therefore, not only will relatively more of the long segments have a reduced mobility, but also the amount of the reduction will be greater. As a result, shifting of H is relatively greater at longer times, where H has lower values. This changes the wedge angle and flattens the relaxation spectrum in the transition zone.

(*b*) The lesser magnitude of the shift resulting from adhesion can be explained as follows. According to F. Bueche's[28] theory of the increase in macroscopic viscosity associated with entanglements, the increase in the segmental friction coefficient (and thus the extent of the shift of H on the time scale) will depend both on the number of secondary molecules pulled along by a primary molecule and on a slippage factor which is determined by the strength of the binding of two chains at an entanglement point. For the case of a primary molecule adsorbed on a filler particle, so long as the segment remains adsorbed the number of secondary molecules is enormous, consisting as it does of all other molecules adsorbed to the same particle. However, it will be easier to desorb a weakly held chain than it will be to disentangle two chains, and so the slippage factor will be much smaller. Therefore the overall increase in the friction coefficient is less for segments bound to a filler surface by van der Waals forces than it is for segments involved in entanglements. (The reverse is true for tightly bound segments.) As a corollary then, the magnitude of the shift in H toward longer times will also be reduced.

Thus the net effect of adhesion is to decrease the slope of H by shifting the smaller H values toward longer times, with the extent of the shift depending on the strength of the bond between the chain and the filler surface.* In the present case the bond is weak and the

* In the discussion following the presentation of this paper, Mr. L. Zapas reported that this prediction is confirmed by unpublished experiments at the Mellon Institute on natural rubber and GR-S containing both active and inactive carbon blacks. The more active blacks do indeed flatten the modulus dispersion curves.

shift is small, but in crystalline polymers the bond is a primary chemical bond and H should be quite flat. We believe this shifting effect possibly in conjunction with the non-Gaussian statistics of short-chain segments between crystallites, explains the relatively flat spectra in the transition zone which Tokita[29] finds for nylon 6 of varying degrees of crystallinity. The slopes of the log H − log τ plots at long times are about $-1/4$, half that predicted by the Rouse[30] theory.

In this connection note that the Rouse theory applies to free-draining coils while the Zimm[31] theory applies to partially shielded coils and predicts a slope of $-2/3$. In the latter case the monomeric friction coefficient does not have a constant value but increases toward the center of the coil according to the Kirkwood-Riseman[32] theory for hydrodynamic interactions within the coil. On the other hand, in crystalline or highly filled systems the lower segmental mobility for longer segments means that the friction coefficient *decreases* toward the center of the coil. Thus a coil effectively acts like a "shell," more free-draining in the center than at the periphery. Since, with the exception of the increasing friction coefficient, the Zimm and Rouse treatments are formally identical, it seems likely that an analogous treatment with a decreasing coefficient would predict the lower value of the log H − log τ slope which is experimentally observed. Moreover it might permit a correlation between the magnitude of the slope and the extent to which the coils behave like "shells."

On the other hand, the extremely flat spectra for polyethylene[33] at 17 to 20°C. represent the response in what is equivalent to the rubbery region for amorphous systems. Ferry[33] surmises that the molecular origin of the relaxation mechanism ". . . may well involve separations of chains from the periphery of crystallites and subsequent ordering in other positions."

Since the moduli of Systems I, II, and III differ from those of PIB by constant factors at long times, the relaxation distribution functions of Figure 9 must be parallel in this same region. Therefore the distribution functions for the composite systems follow the Rouse slope of $-1/2$ just as does pure PIB, and the effect of the filler on the average monomeric friction coefficient ζ_0[21] can be calculated. For the 60% composite it turns out that ζ_0 is increased approximately threefold.

CONCLUSIONS

(*1*) The filler increases the modulus and broadens the dispersion zone. The increase in modulus at long times can be interpreted quantitatively in terms of classical elasticity theory, i.e., the Guth-Smallwood equation. A qualitative molecular interpretation assigns the increase in modulus at short times to concentration effects and the broadening of the dispersion zone to an increased average segmental friction coefficient for longer segments as a result of the adsorption of the polymer to the filler surface. The stronger the adsorption, the broader the dispersion zone, thus accounting for the much flatter modulus-frequency curves for crystalline systems, where the chains are "bound" to the "filler" by primary valence bonds.

(*2*) The form of the temperature dependence of the relaxation times is not changed by the addition of the filler, although T_g is. Thus in crystalline systems, where the "filler concentration" is temperature-dependent, temperature superposition cannot hold because of changes in both the modulus and time scales due to the changing degree of crystallinity. It is implied, therefore, that data obtained on filled systems over a wide time scale might not obey time-temperature superposition, especially if the strength and extent of the adsorption to the filler are temperature-sensitive.

References

1. G. W. Becker and H. Oberst, *Kolloid-Z.*, **148,** 6 (1956).
2. P. J. Blatz, *Ind. Eng. Chem.*, **48,** 727 (1956).
3. H. Leaderman, *Elastic and Creep Properties of Filamentous Materials and Other High Polymers*, Textile Foundation, Washington, D.C., 1943, p. 175.
4. A. V. Tobolsky and R. D. Andrews, *J. Chem. Phys.*, **13,** 3 (1945).
5. J. D. Ferry, *J. Am. Chem. Soc.*, **72,** 3746 (1950).
6. L. E. Nielsen, R. A. Wall, and P. G. Richmond, *Society of Plastics Engineers Journal*, **11,** 22 (1955).
7. R. S. Marvin, *Proceedings of the Second International Congress on Rheology*, V. G. W. Harrison, ed., Academic Press, New York, 1954, p. 156.
8. E. R. Fitzgerald, L. D. Grandine, and J. D. Ferry, *J. Appl. Phys.*, **24,** 650 (1953).
9. J. D. Ferry, L. D. Grandine, and E. R. Fitzgerald, *J. Appl. Phys.*, **24,** 911 (1953).
10. A. V. Tobolsky, *J. Am. Chem. Soc.*, **74,** 3786 (1952).
11. E. R. Fitzgerald and J. D. Ferry, *J. Colloid Sci.*, **8,** 1 (1953).
12. G. S. Whitby, C. E. Davies, and R. F. Dunbrook, eds., *Synthetic Rubber*, Wiley, New York, 1954, p. 350.
13. J. D. Ferry and E. R. Fitzgerald, *J. Colloid Sci.*, **8,** 224 (1953).

14. H. Leaderman, *Trans. Soc. Rheology*, **1**, 213 (1957).
15. M. L. Williams, R. F. Landel, and J. D. Ferry, *J. Am. Chem. Soc.*, **77**, 3701 (1955).
16. T. G. Fox and S. Loshaek, *J. Polymer Sci.*, **15**, 371 (1955).
17. S. Loshaek, *J. Polymer Sci.*, **15**, 391 (1955).
18. E. Guth, *J. Appl. Phys.*, **16**, 20 (1945).
19. H. M. Smallwood, *J. Appl. Phys.*, **15**, 758 (1944).
20. A. M. Bueche, *J. Polymer Sci.*, **25**, 139 (1957).
21. J. D. Eshelby, *Proc. Roy. Soc., London*, **241A**, 376 (1957).
22. J. D. Ferry and M. L. Williams, *J. Colloid Sci.*, **7**, 347 (1952).
23. M. L. Williams and J. D. Ferry, *J. Polymer Sci.*, **11**, 169 (1953).
24. R. F. Landel and J. D. Ferry, *J. Phys. Chem.*, **60**, 294 (1956).
25. R. F. Landel, *J. Colloid Sci.*, **12**, 308 (1957).
26. J. D. Ferry, R. F. Landel, and M. L. Williams, *J. Appl. Phys.*, **26**, 359 (1955).
27. F. Bueche, *J. Appl. Phys.*, **26**, 738 (1955).
28. F. Bueche, *J. Chem. Phys.*, **20**, 1959 (1952).
29. N. Tokita, *J. Polymer Sci.*, **20**, 515 (1956).
30. P. E. Rouse, Jr., *J. Chem. Phys.*, **21**, 1272 (1953).
31. B. Zimm, *J. Chem. Phys.*, **24**, 269 (1956).
32. J. G. Kirkwood and J. Riseman, *J. Chem. Phys.*, **16**, 565 (1948).
33. J. D. Ferry, in *Die Physik der Hochpolymeren*, Vol. IV, H. A. Stuart, ed., Springer-Verlag, 1956, p. 425.

Synopsis

The dynamic mechanical properties of three dispersions of 40-micron-diameter glass beads in NBS polyisobutylene were studied in the rubber-to-glass transition zone. These dispersions contained 8.7, 20.3, and 36.7% beads by volume. The real and imaginary components of the complex shear compliances were measured in a Fitzgerald Transducer Apparatus at frequencies between 24 and 6000 cycles/sec. and at temperatures between −45 and 70°C. The temperature shift factors required to superpose the compliance data for the three dispersions are nearly identical to those for unfilled polyisobutylene. The reinforcement in the long-time end of the transition zone is predicted by the Guth-Smallwood equation:

$$M = M_0(1 + 2.5\phi + 14.1\phi^2)$$

where M_0 is the modulus of the unfilled polymer and ϕ is the volume concentration of the filler. However the filler broadens the dispersion curves, and consequently the equation does not hold at shorter times. Certain similarities between the properties of the dispersions and those of crystalline polymers are described.

TRANSACTIONS OF THE SOCIETY OF RHEOLOGY II, 77–93 (1958)

A Photographic Study of Liquid Flow in a Roll Nip

J. C. MILLER* and R. R. MYERS, *Chemistry Department, Lehigh University, Bethlehem, Pennsylvania*

INTRODUCTION

Variables which are known[1] to influence the amount of transfer and perhaps the quality of films applied to substrates by rolls are the porosity of the two surfaces, the speed, the amount of material, and the rheological properties of the coating. These variables influence the amount of material transferred via a mechanism involving the compression of a thin wedge of liquid and its subsequent splitting on the downstream side of the nip.

The work reported here differs from previously reported studies of flow between rolls in that it covers the transition region between laminar shear in the nip and the behavior of the free boundary downstream from the nip. In the first mentioned region, Gaskell[2] has provided a mathematical analysis of flow from the point where the two wetted roll surfaces come into contact to the point where the surfaces are no longer separated by a continuous liquid layer. Gaskell's work has been amplified by Finston[3] and Gatcombe,[4] and has been confirmed experimentally by Bergen and Scott.[5] For the second, filamentation, region, the equation of Stefan[6] appears more appropriate, but is not applicable to the present problem without extensive revision. The intermediate region in roll kinematics in which the laminar shear of the region of continuous liquid contact gives way to cavitation involves a highly complex flow pattern leading eventually to the formation and elongation of filaments.

Figure 1 shows the velocity gradients and pressure profile derived by Gaskell for the nip region where the surfaces are separated by a

* Present Address: Union Carbide Plastics Co., Division of Union Carbide Corporation, Bound Brook, New Jersey.

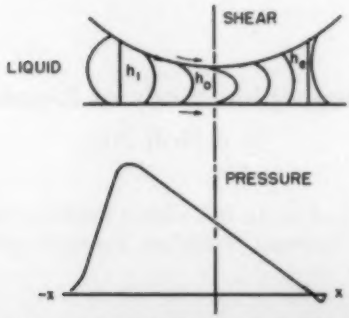

Fig. 1. Pressure and shear profiles in the roll nip for the cone and disc (after Gaskell).

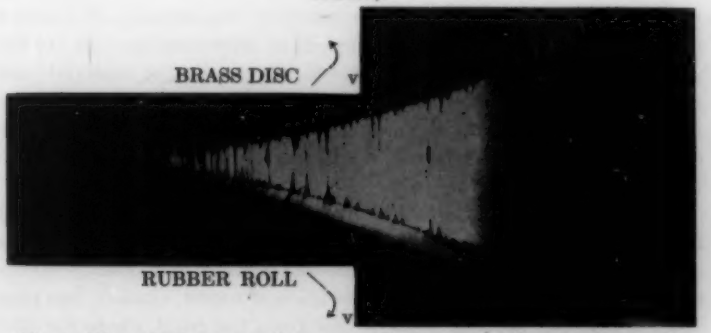

Fig. 2. Film splitting on a roll system. Exposure, 1/millionth of a second. (Courtesy of R. R. Donnelly; taken by O. G. Linnell.)

continuous liquid film. The extreme right-hand portion of the pressure profile is of major interest because it shows that the liquid undergoes tension in that part of the roll coating process which determines the quality of the applied coating.

Early attempts to photograph nip flow have captured only the filaments; never the cavities which were postulated as the precursors of filaments.[7–9] The first experimental efforts directed towards observing the mechanism by which a film splits were done by Sjodahl, who suggested that the interior of the nip be investigated by the present method. Figure 2 is an early high-speed photograph of a roll system taken parallel to the axis of rotation. Filaments of liquid many times the original film thickness can be seen clearly on

this photograph, and are also evident on a motion picture made by the Interchemical Corporation.[9] Banks and Mill[10] photographed an immersed roll system and advanced the hypothesis that the sequence of action of a splitting film on rolls involved cavitation and then elongation of the resulting filaments.

EXPERIMENTAL

The requirements for the roll system used in the present photographic investigation are that one of the rolls be transparent to permit photography and that it be large enough to admit the camera. The modified roll system designed from these requirements is shown schematically in Figure 3. One of the rolls is flattened into a circular glass disc, while the other is a steel cone, whose largest diameter is one-fourth the diameter of the disc. The disc rotates around its axis perpendicular to the plane of the circle, while the apex of the cone is positioned at the center of the disc and rotates without slippage against the surface of the disc. This construction gives an area of observation of the nip which is motionless with respect to an external observer, while both rolls rotate around their axes.

Figure 4 is a photograph of the cone and disc apparatus assembled, and Figure 5 is a detailed drawing of the construction of the assembly holding the cone. The yoke is self-aligning with respect to the disc surface and the liquid film. Force is applied to the cone through the spring assembly marked *S*. Both the disc and the cone were rim-driven with variable speed Graham transmissions.

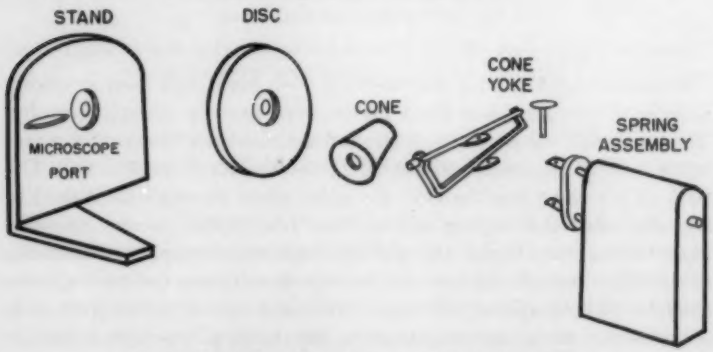

Fig. 3. Exploded view of cone and disc roll system.

For detailed information on the nip flow, low power microscope, a high intensity (short duration) flash lamp, and a recording camera were necessary. The microscope was a simple tube with interchangeable objectives and eyepieces. The eyepieces were 5, 10, and 15 power, and the objectives 2 and 4 power with working distances of 48 and 32 mm., respectively. Long working distances were necessary because the objective had to be at least one inch (the thickness of the glass plate) from the subject. The camera was a mirror reflex 35 mm. Alpa Alnea Model 4 with a focal plane shutter.

Fig. 4. Disc and cone roll system.

Reflected light from a microsecond flash lamp was used in taking individual pictures, and flood lamps were used in cinematography. The flash bulb was placed near the surface of the disc beside the microscope and positioned to about 30° from the microscope axis. The path of the light was through the glass plate, through the liquid in the nip, onto the surface of the cone from which it was reflected back through the liquid and glass into the microscope. The microsecond flash equipment used in the experiments was designed specifically for photographing roll nips. The light and reflector were only 3 inches in diameter and connected to the electrical source by a flexible cable. The small size of the lamp and flexible cable made a versatile

unit for work in small spaces and was ideal for this study. A discharge of 40,000 volts across the lamp in 2 to 3 microseconds produced a flash of sufficient intensity to obtain good photographs with a fast film. The shutter of the camera and the flash were synchronized, so that the flash duration determined the exposure time.

The film used for recording was the fastest commercial film available, Eastman Kodak Tri X with an ASA rating of 160 tungsten, 200 daylight. The developer was a low contrast, fine grain developer producing the best detail possible from the latent image.

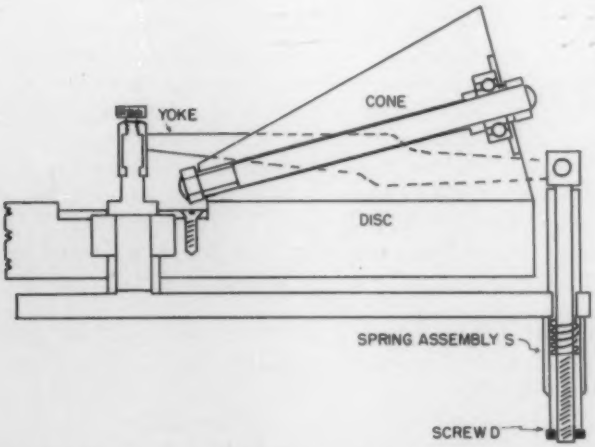

Fig. 5. Detail of cone yoke and spring assembly of disc cone. This mechanism was designed to be self aligning with the liquid film.

The high speed motion pictures were taken at 2000 frames/sec. on duPont film with a Fastax high-speed camera in the Bell Laboratories in New York.

The problem of lighting the subject in high-speed motion pictures is usually the greatest experimental difficulty. Photographing through a microscope increased this problem considerably. In order to supply adequate light to the cone and plate, four 1000 watt lights were focused on a small area of the plate, two on either side of the microscope and two behind the glass disc.

The liquid investigated was a low molecular weight polybutene supplied by Oronite Chemical Co., designated as 24, and a dispersion of hydrophobic silica in the same polybutene. Both the polybutene and the dispersion were transparent with little color, a prerequisite for photographic work.

To distribute these films on the cone and disc, a volume of liquid from a pipet was spread on the plate, a portion of each of the quadrants. The drive to the plate was engaged and the roller system run until the film appeared to be evenly spread over the surfaces of both cone and disc. After distribution of the film on the disc and cone, the equipment was stopped and the microscope focused on the cone surface and adjusted so that the liquid film contact area in the roller nip was in the center of the photograph. The desired force was applied by tightening the screw *D* on the spring *S* shown in Figure 5.

Operation of the cone and disc while photographing consisted of matching the tangential velocities of each member at the desired velocity and then taking photographs under each experimental condition. All photographs for a given film thickness were taken on the same area of the glass disc to minimize the effect of surface variations of the disc (as much as 0.005 in.). The average film thickness was determined by scraping the area of the plate where the photographs were taken with a razor blade and weighing the liquid material removed.

A vacuum tank large enough to hold the roll system and driving motors was designed to take pictures at pressures lower than atmospheric. The problem of taking the pictures in the evacuated tank was solved by including a glass viewing port which was built close enough to the disc surface to enable focusing of the microscope on the cone. A differential mercury manometer was used to measure the pressure inside the tank.

Because of the possibility of temperature changes during a run due to heating from the motors, a calibrated thermistor was taped to the cone holder and its resistance recorded during the run. In general, heating did not occur until the pressure was increased after prolonged operation under vacuum. The temperature of the apparatus during an experiment was room temperature (25–27° C.) since enclosing the apparatus resulted in large temperature increases due to the heat developed by the electric motors.

RESULTS

Figure 6 is a group of low magnification photographs taken at three different roll velocities with a 200 poise polybutene. Figure 6a is approximately 0.2 cm./sec. and the direction of motion is towards the bottom of the photograph. The splitting boundary is at the bottom of the photograph in the form of arches which are open in the direction of motion, and the merging boundary of the films is represented by the wavy line at the top of the photograph. The smooth area with striations in the center of the photograph is the contact area or nip of the rolls. These striations are polishing marks on the metal cone.

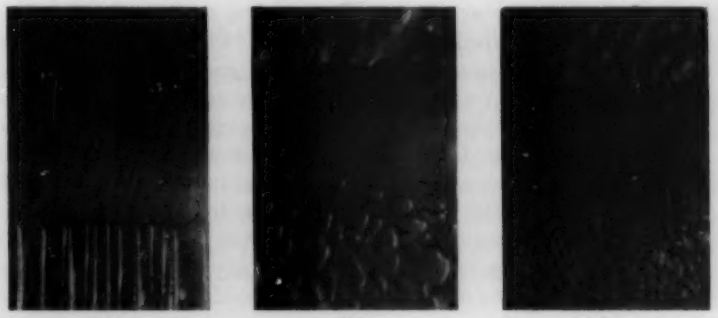

(a) (b) (c)

Fig. 6. Typical photographs of splitting. (a) Low shear. (b) Moderate shear. (c) High shear.

Fig. 7. Structure and flow of web at low shear. The webs are spaced regularly across the roll at the nip exit.

Separation of the film at low speeds proceeds by simple flow into a unique pattern of webs perpendicular to rolls. Figure 7 depicts the structure and flow pattern in the web. This pattern of flow is called the first regime of splitting.

Figure 6c shows the splitting mechanism as it appears at roll velocities above 20 cm./sec. The formerly clear-cut boundary flow at the nip exit has disappeared and in its place is a rough discontinuous pattern which is the result of the filamentation shown in Figure 2. In the contact area can be seen cavities whose size depends on the distance from the splitting or cavitation line. A definite increase in size can be observed from the line where the cavity is first visible and where its life ends. A large number of photographs has shown that cavities appear at a definite line parallel to the roll axis. This pattern of flow is called the second regime. Figure 6b portrays the transition region between the web splitting and the cavitation-filamentation sequence. Only a few cavities are formed and these grow elliptically as they move out of the nip. The origin and growth of the cavities were observed most clearly in the high-speed motion pictures and confirmed the interpretation of the still photographs that growth was related to the distance of the cavity from the nip center.

The high-speed motion pictures also showed two additional characteristics of the free boundary which can only be observed by projection. The position of the free boundary on the splitting side of the nip can be observed to vary slightly in and out of the nip; and when a cavity grows to a large size and approaches the splitting interface, an implosion of the cavity occurs because its pressure is considerably less than atmospheric. The distance from the nip at which this implosion occurs is not apparent from the still photographs, but is evident in the motion pictures.

As liquid is added to a roll system with a fixed clearance, the excess liquid accumulates at the entrance of the nip until a bank of rotating liquid becomes visible. For limited amounts of liquid no bank is visible to the unaided eye and the presence of a bank could not be proved, although all theoretical developments pointed out the necessity of the bank.[11] With the development of photomicrography of the nip area, the investigation of microscopic banks became feasible. At the low speeds depicted in Figure 6a, where the limit of the bank is a straight line, microscopic bubbles can be seen which follow a path towards the nip, then away from the nip, and illustrate the flow pat-

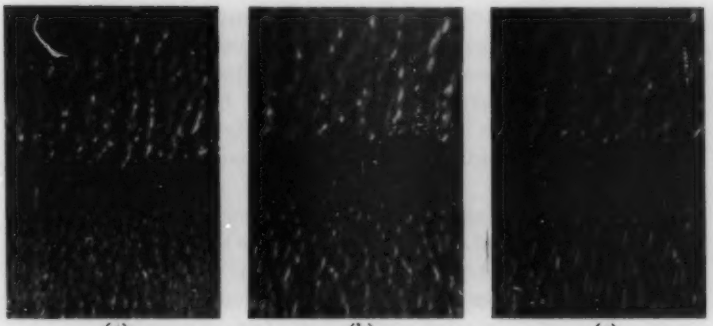

(a) (b) (c)

Fig. 8. Influence of roll speed ratio on splitting mechanism. Differential velocities have a pronounced effect on number of cavities. (a) 1:1. (b) 1.2:1. (c) 1.4:1.

tern in the bank. Photographs at higher speeds show no bubbles at the entrance; furthermore, the line representing the entrance free boundary is irregular as in Figures 6b and 6c. The serrations in the line are the result of the irregular film left on the roll after splitting. From the theory of flow on a roller system and the nondeviation of the line of cavity formation, the conclusion has been reached that a bank does indeed exist, and that the appearance of an irregular line of contact must mean that the bank is small compared to the fluctuations in the film thickness.

The influence of differential roll speeds is remarkable. Three photographs taken with constant disc velocity and decreasing cone velocity are shown in Figure 8 where roll speed ratio defines the velocity differential. The number of cavities decreases rapidly as the roll speed ratio increases until the flow reverts from the second regime to the first regime. The change suggests that laminar shear imposed on the separation alters the pressure profile and reduces the forces necessary to separate the film. Heidebroek and Pietsch[12] discovered a similar phenomenon in the separation of parallel plates. A small lateral shearing motion before separation drastically reduced the force required for splitting the film.

One observation which is difficult to explain in terms of Gaskell's[2] theory is the apparent decrease in the bank size with increased speed. This may be due to an increase in clearance with increased speed.

Quantitative results on cavity formation as a function of the instrument variables were obtained by counting the number of cavities

formed at the cavitation line. Although the average number of cavities produced in the cavitation zone was the measurement desired and the main effort was devoted to developing a suitable counting technique, other measurements which could be made include: (*1*) Distribution of cavity sizes; (*2*) rate of cavity expansion; (*3*) position of the line of contact at the nip entrance; and (*4*) position of cavitation line.

All these data were obtained in selected experiments, but the major effort was concentrated on developing a simple technique for counting cavities which would be linearly related to the number of cavities in the area defined by the length of the expansion zone per unit of roll length. The data presented represent hundreds of exposures.

The first counting method attempted was to count the number of cavities, $\bar{B}$, per centimeter touching a line placed randomly in the field parallel to the line of cavity formation. The technique was later changed to placing lines at 0.5 cm. intervals in the expansion field. Where the cavity diameter was greater than 0.5 cm. at 40× magnification, this method produced data indicating that nucleation continued in the expansion region, while no nucleation persisted beyond the cavitation line when the cavities were less than 0.5 cm. in diameter. Table I lists the line counts at increasing distance from the nucleation line for three speeds.

TABLE I
Values of $\bar{B}$ for Three Roll Speeds

Rev./sec. →	0.27	0.65	1.21
Distance from nucleation line (cm.)	Ave. no. of bubbles/cm. (40×)		
0.012	8	32	68
0.025	12	36	60
0.037	14	44	60
0.050	18	32	56

The following technique was adopted for small numbers of cavities in the field. All the cavities in an area behind the first line position were counted and the line moved 0.5 cm. away from the nucleation line. The total number of cavities behind this new line was counted and the difference between the two counts was adopted as the number

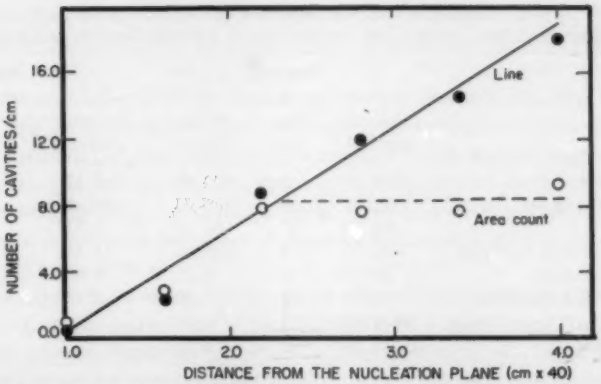

Fig. 9. Comparison of line and difference counts for low bubble count showing the effect of increased bubble size on line count.

of cavities formed at the nucleation line. Figure 9 is a comparison of the line and area counts as a function of distance from the cavitation line. The area count established that the apparent nucleation in the expansion field was an artifact of the line counting technique.

A large number of qualitative observations had established that roll speed was the major influence on the number of cavities per centimeter and that film thickness and force on the cone altered the speed effects in a complicated manner. Quantitative investigation and separation of the variables of speed, force, and film thickness was accomplished by designing a factorial experiment[12] which involved three levels of each variable. The levels were chosen to encompass the range of each variable unless limited by the cavity counting pro-

TABLE II
Cavity Counts from the Factorial Experiment

Film thickness (cm. × 10^4)	Velocity (rev./sec.) 0.96/2π			1.95/2π			2.97/2π		
	Force (kg.)								
	1.7	3.4	6.9	1.7	3.4	6.9	1.7	3.4	6.9
12	2.3	1.4	2.2	5.2	6.5	5.8	8.1	12.8	10.9
18	3.4	5.5	2.0	12.5	12.7	3.9	19.3	16.5	14.0
22	3.2	2.1	1.7	18.2	14.0	10.2	29.5	28.8	21.3

TABLE III
Variance of Main Effects and Interactions in Average Number of Cavities

	Sum of squares	Degrees of freedom	Mean square	Variance ratio	Significance level, %
Velocity	1049.73	2	524.86	126.47	99
Film thickness	302.83	2	151.41	36.48	99
Force	62.27	2	31.13	7.51	95
Velocity-film thickness	193.71	4	48.43	11.66	99
Velocity-force	16.68	4	4.17	1.00	<90
Force-film thickness	45.73	4	11.43	2.75	<90
Total	1670.95				
Residual	33.24	8	4.15		

cedure. Three photographs were taken at each of the 27 permutations of variables included in the experimental design and the data analyzed for the effects of the major variables and any interactions between two of the variables. The data presented in Table II are the average number of cavities per centimeter counted on three exposures. The three factor interaction was small and, consequently, used to test

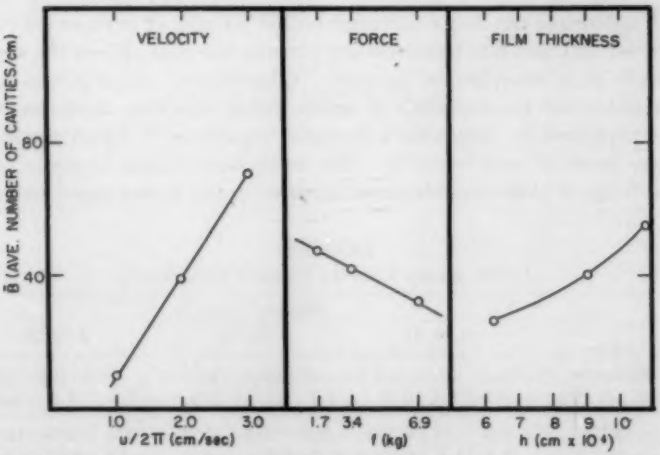

Fig. 10. Influence of operational variables on bubble formation. Speed represents the major influence on cavitation rate.

the significance of the two factor interactions and main effects. Table III lists the results of the analysis of variance for the experimental results.

Only one interaction is found significant, the velocity-film thickness, whose components also are highly significant as main effects. Interpretation of this result on the basis of mean square magnitudes suggests that film thickness is probably not significant as a main effect. The low significance level of the force effect may be due to the limited range of pressure in the nip, a factor which should be influential on the formation of cavities.

Averaged data for the three main effects are shown in Figure 10 where the cavitation rate is plotted versus the instrument variables. These curves illustrate graphically the relative importance of the variables as indicated by the range of the cavity count associated with the variable. The influence of speed on the cavitation can be explained by analogy with nucleation phenomena in precipitation reactions. Previously it had been explained that a critical velocity is necessary to produce cavities and now the results show a marked increase in cavitation rate with increasing velocity. This behavior is markedly similar to the results of a precipitation reaction where a certain concentration of compound is necessary to produce precipitation and the size of the precipitate is influenced by the speed with which the precipitation occurs.

Another similarity to precipitation reactions was discovered in the bubble distribution curve shown in Figure 12. The apparent log normal distribution is the same type of distribution found by Kottler[16] for silver halide precipitates. Figure 11 illustrates the increase in cavity size as a function of the distance from the cavitation line. The result is linear as might be expected from the roughly linear increase in clearance between the roll and disc for small arcs.

One external variable, ambient pressure, was investigated because of experiments reported previously[15] which established that the work necessary to split a film increased with decreased ambient pressure. A hypothesis that dissolved or dispersed air was the primary nucleant in the rapid splitting of thin films was developed from this finding and also from Banks' data[10] that unpurified liquids would only support one atmosphere tension. This hypothesis of air nuclei suggests that an alteration in the film splitting pattern should occur with decreasing pressure, but numerous photographs of splitting down to 0.1 atmos-

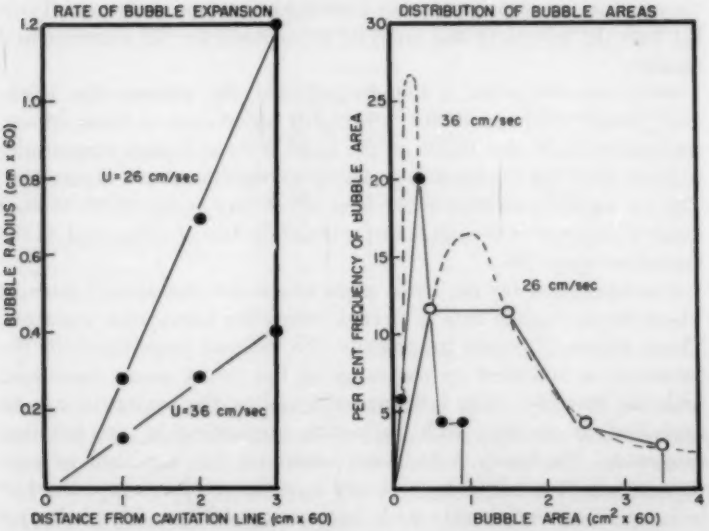

Fig. 11 (left). Rate of bubble expansion after cavity formation in the roll nip.
Fig. 12 (right). Logarithmic normal distribution of bubble areas for two velocities.

phere pressure revealed no change in splitting behavior. The increased work apparently reflects a decreased contribution from expansion of the gas inside the cavity.

DISCUSSION

One of the major goals of this kinematic study is the development of concepts which will help ultimately to define the forces involved in the rapid splitting of liquid films.

Flow in the nip can be divided conveniently into four regions: laminar flow, cavitation, cavity expansion, and filamentation. The dynamics of these regions may or may not be amenable to practical measurement on a roll system, but calculation of the forces based on reasonable assumptions have led to the design of experiments based on the temperature dependence of $\bar{B}$ and its relation to the temperature dependence of the viscosity, surface tension, and pressure-volume product which contribute to $\bar{B}$ and the cavity expansion. Gas-

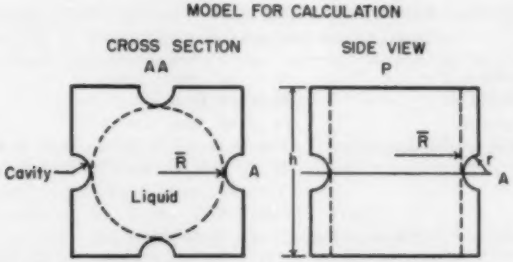

Fig. 13. Model for calculation of bubble pressure, surface tension, and viscosity stresses. Motion is in upward direction.

kell[2] has adequately described the dynamics of the laminar flow region in the absence of temperature changes, Banks and Mill[10] have attempted to determine experimentally the tension a liquid will support before cavitation occurs, and Voet[17] has discussed the dynamics of the filamentation region when the filament elongation is viscoelastic. The dynamics of the expansion have not been considered previously and will be discussed here.

There are at least three forces contributing to or retarding the expansion of the cavity after its formation. Resisting the expansion are surface tension γ and viscosity η. If air is contained in the cavity, then the air will provide PV work to the system during expansion. The order of magnitude of these terms and their relative importance in the expansion zone are to be investigated.

The model to be utilized in the following discussion is shown in Figure 13 which is representative of a small block of liquid just after the cavities are formed. The major characteristic of the block is that the volume of cavities is much smaller than the volume of liquid, a limitation necessary to realize the assumptions of the equations. A number of defects are recognizable in this calculation: the total liquid flow is not accounted for and the flow process may be accompanied by elastic effects since this liquid is slightly viscoelastic.

Table IV lists the dimensions taken from a photograph which will be used, and Table V the physical properties of the polybutene. The $U_s\eta$ product arises because the velocity important in the splitting forces is the separation velocity U_s of the roll and disc, and not the tangential velocity of the rolls.

TABLE IV
Approximate Measurements of Bubbles

Radius of bubble, r	10×10^{-4} cm.
Radius of liquid, $\hat{R}$	80×10^{-4} cm.
Film thickness, h	70×10^{-4} cm.
Rate of bubble expansion, dr/dt	0.40 cm./cm. $\times$ 26 cm./sec. = 10 cm./sec.

TABLE V
Physical Properties of Polybutene 24

Surface tension, γ	30 dynes/cm.
Density, ρ	0.88 g./cm.^{3}
$U_{s\eta}$ Product (η = 200 poises)	50 dynes/cm.

The contributions of the various force components are shown in Table VI. The viscous term is a modification of Stefan's equation for the separation of parallel plates developed by Banks and Mill;[10] the expressions which represent surface tension and rate of cavity expansion were derived by Plesset[18] and substantiated by Dergarabedian;[19] and the ideal gas law is used for the estimation of cavity pressure where m is the number of gas molecules in the cavity.

TABLE VI
Tension Contributed by Viscosity, Surface Tension, and Gas Pressure in the Bubble

Viscosity	$-(3U_{s\eta}\hat{R}^2/h^3)$	-28×10^9 dynes/cm.^{2}
Surface tension	$-(4\gamma/r)$	-12×10^4 dynes/cm.^{2}
Rate of expansion	$-\rho\left[\frac{3\,dr}{2\,dt}\right]$	$-0.88(3/2) \times 10 = 13$ dynes/cm.^{2}
Bubble pressure	$3mkT/4\pi r^3$	$m \times 10^{-9}$ dynes/cm.^{2}

Surface tension appears to be an overwhelming effect except for known influence of the enclosed gas[15] which represents a significant portion of the total work in film splitting. An average concentration of at least 10^9 molecules/cavity is necessary to get a gas pressure sufficiently large to exert an effect on the splitting. The cavity pressure is then about 5×10^{-3} atm., which probably represents a lower limit.

This work was supported by the Francis McD. Sinclair Fellowship and the National Printing Ink Research Institute.

The high-speed motion pictures were obtained through the cooperation of Mr. R. Haard and Mr. T. Musca of the Bell Laboratories in New York. The authors also wish to thank the Interchemical Corporation for the loan of the microflash.

References

(1) Walker, W. C., and Fetsko, J. M., *Am. Ink Maker* **33,** No. 12, 38 (1955).

(2) Gaskell, R. E., *Trans. ASME*, **72,** 334 (1950).

(3) Finston, M., *J. Appl. Mech.*, **18,** 12 (1951).

(4) Gatcombe, E. K., *Trans. ASME*, **67,** 177 (1945).

(5) Bergen, J. T., and Scott, G. W., Jr., *J. Appl. Mech.*, **18,** 101 (1951).

(6) Stefan, M. J., *Sitzker Akad. Wiss. Wien*, II, **69,** 713 (1874).

(7) Sjodahl, L., Paper presented at the First Annual Meeting of The Tech. Assn. of The Lithographic Industry, April 15, 1949.

(8) Banks, W. H., and Mill, C. C., *Proc. Roy. Soc.* **222A,** 414 (1954).

(9) Interchemical Corporation Laboratories, *Am. Ink Maker*, **33,** No. 1, 51 (1951).

(10) Banks, W. H., and Mill, C. C., *J. Colloid Sci.*, **8,** 37 (1954).

(11) Maus, L., Walker, W. C., and Zettlemoyer, A. C., *Ind. Eng. Chem.*, **53,** 46 (1955).

(12) Heidebroek, E., and Pietsch, E., *Forsch. Gebieten Igenieurw.*, **12,** 74 (1941).

(13) Moroney, J. M., *Facts from Figures*, Penguin Books, Inc., Baltimore, Maryland.

(14) Myers, R. R., Miller, J. C., and Zettlemoyer, A. C., *Preprint Div. PPPI, Am. Chem. Soc.*, **17,** No. 2 (1957).

(15) Myers, R. R., Miller, J. C., and Zettlemoyer, A. C., *Preprint Div. PPPI, Am. Chem. Soc.*, **15,** No. 1, 69 (1955).

(16) Kottler, F., *J. Franklin Institute*, **251,** 499 (1951).

(17) Voet, A., and Geffken, C., *Ind. Eng. Chem.*, **43,** 1614 (1951).

(18) Plesset, M. S., *J. Appl. Mech. Trans. ASME*, **71,** 227 (1949).

(19) Dergarabedian, P. J., *J. Appl. Mech.*, **20,** 537 (1953).

TRANSACTIONS OF THE SOCIETY OF RHEOLOGY II 95–130 (1958)

On Relaxation Spectra in High Polymers

B. ALBRECHT and A. M. FREUDENTHAL, *Columbia University, New York, New York*

1. INTRODUCTION

The interpretation in terms of polymer structure of the deformational response of high polymers to applied forces requires a clear distinction between the effects related to change of density and those related to change of shape (distortion). While the assumption that volume change is perfectly elastic, and that, therefore, in the absence of non-mechanical phenomena the volume viscosity is zero, has governed the general approach to the study of visco-elastic materials, recent investigations have provided strong evidence for the presence of volume-viscosity in simple as well as in polymeric liquids.[1] It is reasonable to assume that a similar mechanism of compressional or dilatational dissipation exists in the polymeric solid. Therefore the simplest viscoelastic response under conditions of small strain probably must be described by at least four physical constants (K, G, η and η_{vl}) instead of the usual three (K, G, η). Hence an effective experimental study of the mechanical behavior of high polymers requires the establishment of such conditions of the experiment that the effects of volume-change and distortion can be clearly distinguished. Since the present understanding relating molecular structure of solid or pseudo-solid high polymers to their viscoelastic behavior is based entirely on mechanisms of deformation in shear, it appears desirable, at this stage of the study of polymers, to eliminate the volumetric component entirely and to perform the experiments in shear.

The best way to produce such conditions in a mechanical test is by applying a torque to a hollow cylinder of ratio of wall-thickness to radius small enough to justify the assumption of uniform stress distribution over the wall thickness, but large enough to ensure de-

formation to fracture without local instability. By subjecting the specimen to a purely deviatoric state of stress, the direct proportionality for small strains of the torque twist diagram observed in the torsion test to the shear-stress/shear-strain relation for the volume element is ensured; this proportionality does not exist in other mechanical tests. Moreover, because of the elimination of the dilatation as well as of the necking effect generally associated with the tension test, the total strain that can be applied in a torsion test prior to fracture, though small, exceeds the strain which the same material can sustain in a tension test.

2. PURPOSE AND PROGRAM OF INVESTIGATION

The purpose of the investigation was to establish the deformational response to rapidly applied shear and the fracture strength of molded crosslinked phenolic polymers with different fillers, and to correlate the observed behavior with the assumed structure of the polymer and action of the filler. Since the filled molded resin has a structure consisting of filler particles or threads impregnated and bound together by the resinous matrix of spherocolloid embedded in a less highly polymerized substance and crosslinked probably by methylene bonds and Van der Waals' forces, its deformation and strength will be strongly influenced by the nature (length and shape of particles) and quantity of filler present. Because of the characteristic behavior of the resinous matrix as a supercooled liquid, the mechanical response, including the strength, of phenolic polymers is significantly temperature and strain-rate sensitive.

Because of the complexity of the interaction between filler and resin and of its variation with temperature and strain-rate, it appeared necessary to carry out the investigation over the widest possible range of strain-rates and of temperatures. It was assumed that a spectrum of relaxation times of a shape that would probably not be unimodal would be required to formulate adequately the equations governing the mechanical response of such materials. The establishment of the relaxation spectrum of the resinous matrix therefore appeared to be the principal purpose of the experimental investigation.

In experiments with polymers covering a relatively wide range of applied strain-rates, the physical "constants" show very significant

variations,[2] the extent of which depends on the temperature level, on the configuration of the molecular structure, and on the extent of molecular motion under the applied stress. Deformation and strength under various strain rates reflect the facility with which, under the action of the load, the spatial relationship between polymer molecules can be altered by diffusion, by local changes of shape of molecular chain segments (stress biased micro-Brownian motion), and by displacements of segments of various length with respect to each other (stress biased macro-Brownian motion).

The frequency of an applied vibratory force or the duration of an applied impulsive force determines the frequency of the molecular motion that can be excited. The apparent relaxation time, as well as the viscosity of the polymer as a whole, produced by a certain load are therefore functions of the duration and, to a certain extent, of the shape of the load impulse. Because of this interaction of applied force and molecular structure, the dynamic resistance of polymers depends on the existence of regions in which extensive local deformation is not inhibited at high strain-rates.

The mobility of molecules and molecular groups is usually defined in terms of their "retardation"—or "relaxation"—times rather than directly by their velocities of motion; the dynamic behavior of high polymers can therefore be related to a spectrum of relaxation or retardation times, which indicates the distribution, within the solid, of an inverse parameter of the mobility of molecules and molecular groups of various sizes and masses. Thus the dynamic performance of a high polymer—its toughness, shock resistance and strength, all of which depend on its capacity to dissipate, without cracking, energy applied at very high rates—will necessarily be related to the spectrum of relaxation times. This dependence can also be expressed by the change, with the rate of applied shear-strain, of the shear viscosity η and shear modulus G of the substance. Only for a homogeneous and isotropic monomer could both parameters remain constant over a wide range of conditions.

Because of the variation of parameters with testing conditions due to the expected wide spectrum of relaxation times, it is reasonable to assume that a specific testing condition can only provide the response within the range of this condition. Hence stress-relaxation tests will provide information on relaxation times within their time scale, limited on one side by the time required to induce the initial stress

and on the other by the period of observation; resonant vibration tests, on the other hand, will reflect the viscoelastic response within a narrow range limited by the change of frequency that is practically possible. Thus the results obtained from such tests alone do not permit the establishment of more than relatively narrow portions of the relaxation spectrum. It appears, therefore, that only by a combination of experiments in which the applied strain or stress rates can be varied between a maximum that still permits a reliable observation of the strain as the upper limit and zero strain rates as the lower limit (relaxation test) can the full spectrum be established.

In order to study the various aspects of the problem, it was decided to select three phenolics of widely different "impact resistance," as established by conventional impact (Izod) tests, differing by their filler content and character. However, the brittleness of the cotton-flock filled phenolic selected as the first type made strain readings at high velocities unreliable, and the investigation had to be limited to two materials: one a fabric-filled phenolic classified as of intermediate shock resistance (designated as FM-1132) and one a cord-filled phenolic classified as of high shock resistance (designated as Fiberite FM-11678).

The reported data refer to the fabric-filled phenolic; they indicate that its response up to stress levels rather close to the fracture stress is fairly linear and can therefore be represented with the aid of a spectrum of relaxation times.

3. SPECIMENS AND INSTRUMENTATION

A special testing machine for the rapid application of a torque $T(t)$ to a tubular specimen has been designed. The machine is capable of delivering a torque sequence closely approximated by the function

$$T(t) = T_0(1 - e^{-\omega t} \cos \omega t) \tag{1}$$

where the amplitude T_0 can be varied and the peak can be reached in a few milliseconds. The exponent n depends on the material tested and its value is close to $n = 0.1$; the frequency ω can be determined from the record of the actual tests. A family of torque sequences for different values of n is shown in Figure 1.

The machine is also able to apply to the specimen a nearly uniform rate of deformation through the preload mechanism at rates of the

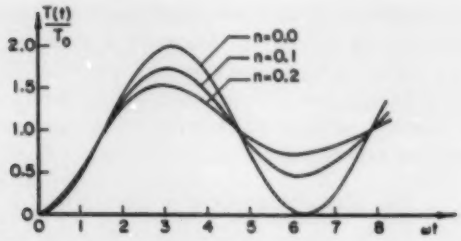

Figure 1.

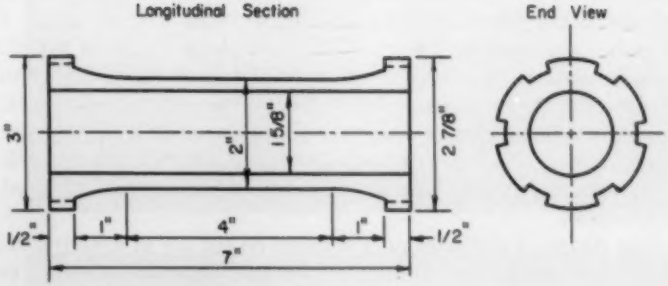

Figure 2.

order of magnitude of the so-called "static" tests. The order of magnitude of the strain rates applied to the phenolics can thus be varied between 1–4 in./in./sec. for high-speed and 10^{-4}–10^{-6} in./in./sec. for low-speed tests.

The specimen can be enclosed in an insulated box within which the temperature can be controlled within ±2°F. Tests were performed at three temperature levels, −70, +72, and +200°F., which delimit the temperature range of most applications of high polymers.

(a) Specimens

Tubular specimens of 2 in. o.d. and 7 in. overall length with fluted flanges were designed and molded. Figure 2 shows the specimen shape. A relatively short and stiff specimen had to be selected so as to keep the period of vibration in the lowest mode of the specimen short in relation to the shortest expected period of torque application.

An approximate analysis of the elastic stability of the specimen following the procedure developed by Donnell[3] has shown the critical (buckling) stress for an elastic specimen of $^1/_8$ in. wall thickness to be roughly $\sigma_B = 0.1\,G$. This value is considerably higher than the expected fracture stress in shear which, even for the most resistant hard phenolics, does not exceed a value of roughly $\sigma_F = 0.02\,G$.

(b) The Torque Testing Apparatus

The capacity of the testing machine designed was determined on the assumption of a maximum fracture stress in shear of $0.02\,G$ in a specimen of $^1/_8$ in. wall-thickness and $r_0 = 1.0$ in. outer radius, assuming the elastic value of G to be of the order of 4×10^6 p.s.i. The machine was designed for a maximum working torque of 500 ft.lb. to be applied within a period of between 2 and 10 millisec., producing a maximum twist of an order of magnitude of 0.02 radians/in. of specimen length, which is equivalent to a shear strain of an order of magnitude $\gamma = 0.02$, or roughly 4.5° over the measuring length of 4 in. The total twist angle on the machine constructed is limited to 0.2 radians.

The design of the machine was based on the use of compressed air for energy storage and transfer, which has the advantage that even when considerable forces have to be applied, the moving masses are very light. The design developed is shown in Figure 3.

A piston moving within a cylinder is connected by a rod and link to a lever which, in turn, is fastened to one end of the specimen. A small tank of approximately half a gallon is filled with compressed air under pressures up to 300 p.s.i. and is connected to the cylinder through a small valve held in closed position by an armature attracted by an electromagnet. As long as this magnet is energized, the valve remains closed, and the pressure in the tank can be adjusted to the desired value. When the electrical current of the magnet is cut, the valve is released and high pressure air admitted into the cylinder, pushing the piston down and thus applying the torque to the specimen.

The torque to be applied can be predetermined directly by measuring the pressure of the air and can be adjusted by changing the air pressure. In order to measure the torque actually applied to the specimen unaffected by piston friction and air leakage, the "fixed" end of the specimen is connected to a "weighbar" in the shape of a

(a)

(b)

Figure 3.

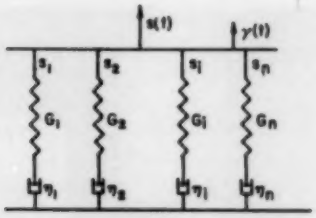

Figure 4.

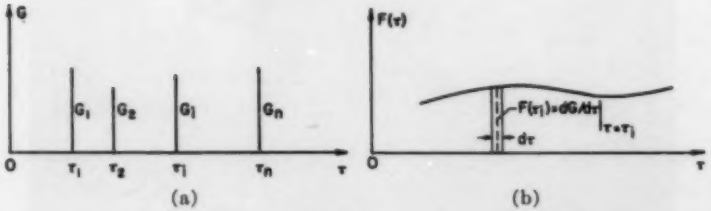

Figure 5.

steel cylinder, the twist of which is recorded by two pairs of crossed strain gages mounted on it. The output of these strain gages is amplified and applied to the deflecting plate of a CRT-oscilloscope and recorded in the usual way. The weighbar is made stiff enough to permit only a negligibly small angular motion of the specimen.

4. THEORY OF MECHANICAL RESPONSE OF HIGH POLYMERS

A real polymer possesses many elastic and dissipative mechanisms; by coupling a sufficient number of Maxwell elements in parallel, a good approximation of its behavior within the linear range can be obtained.

To visualize the response in shear of a complex linear viscoelastic body, it is expedient to replace the elastic mechanism of the ith of n elements by a spring with spring constant G_i, and the corresponding dissipative mechanism by a dashpot with coefficient of viscosity η_i (Fig. 4), and to plot the values of G_i against the values of the relaxation time τ_i on the axis of τ, obtaining a discrete spectrum of relaxation times (Fig. 5a). Increasing the number of coupled Maxwell

bodies to infinity, the discrete spectrum of relaxation times is transformed into a continuous distribution of relaxation times[4] $F(\tau)$ (Fig. 5b) where $dG/d\tau = F(\tau)$ is the density of shear modulus along the τ axis, and $\int_0^\infty (dG/d\tau)d\tau = G_0$ is the shear modulus of all elements added together. These spectra usually cover several orders of magnitude of τ and therefore it is expedient to plot them against $\ln \tau$ or $\log_{10} \tau$.

Since the shear modulus $G(\tau)$ is equal to the area between τ and ∞ under the function $F(\tau)$, the following relations hold in the interval $\tau_1 \leqslant \tau \leqslant \tau_2$:

$$G_0 = \int_0^\infty F(\tau)d\tau = \int_{\tau_1}^{\tau_2} F(\tau)d\tau = \int_{\ln \tau_1}^{\ln \tau_2} F(\tau)\tau d \ln \tau$$
$$= \int_{\ln \tau_1}^{\ln \tau_2} F_1(\ln \tau)d \ln \tau = 2.303 \int_{\log_{10} \tau_1}^{\log_{10} \tau_2} F_1(2.303 \log_{10} \tau)d \log_{10} \tau$$
$$= \int_{\log_{10} \tau_1}^{\log_{10} \tau_2} F_2(\log_{10} \tau)d \log_{10} \tau$$

provided $F(\tau)$ does not exist outside of this interval. G_0 therefore represents the instantaneous shear modulus, the true value of which can be obtained only if the duration of the test is much shorter than the shortest relaxation time in the material.

In the case of a rectangular distribution $F_2(\log_{10} \tau) = b_0$, which is the simplest possible assumption,[5] the corresponding distribution is

$$F(\tau) = \frac{b_0}{2.303} \frac{1}{\tau}$$

I. Discrete Spectra of Relaxation Times

The equations of the model shown in Figure 4a are

$$\frac{d\gamma(t)}{dt} = \frac{1}{G_i}\left[\frac{ds_i(t)}{dt} + \frac{1}{\tau_i} s_i(t)\right] \quad \text{and} \quad \sum_{i=1}^{n} s_i(t) = s(t) \qquad (1)$$

with the initial conditions $\gamma(0) = 0$ and $s_i(0) = 0$. Using the Laplace transform and substituting the initial conditions, eqs. (1) become

$$p\Gamma(p) = \frac{1}{G_i}\left(p + \frac{1}{\tau_i}\right) S_i(p) \quad \text{and} \quad \sum_{i=1}^{n} S_i(p) = S(p) \qquad (2)$$

where the capitals Γ, S_i and S denote the transforms of γ, s_i and s. The resulting system of $(n + 1)$ simultaneous equations is solved for $\Gamma(p)$:

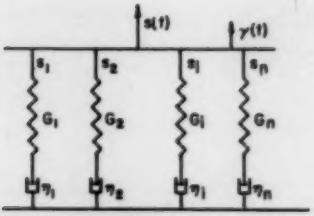

Figure 4.

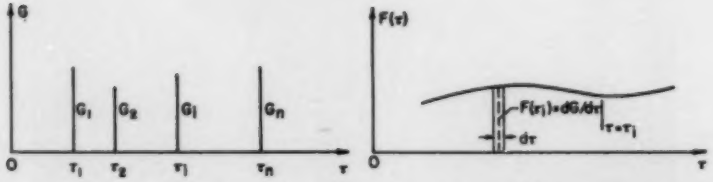

Figure 5.

steel cylinder, the twist of which is recorded by two pairs of crossed strain gages mounted on it. The output of these strain gages is amplified and applied to the deflecting plate of a CRT-oscilloscope and recorded in the usual way. The weighbar is made stiff enough to permit only a negligibly small angular motion of the specimen.

4. THEORY OF MECHANICAL RESPONSE OF HIGH POLYMERS

A real polymer possesses many elastic and dissipative mechanisms; by coupling a sufficient number of Maxwell elements in parallel, a good approximation of its behavior within the linear range can be obtained.

To visualize the response in shear of a complex linear viscoelastic body, it is expedient to replace the elastic mechanism of the ith of n elements by a spring with spring constant G_i, and the corresponding dissipative mechanism by a dashpot with coefficient of viscosity η_i (Fig. 4), and to plot the values of G_i against the values of the relaxation time τ_i on the axis of τ, obtaining a discrete spectrum of relaxation times (Fig. 5a). Increasing the number of coupled Maxwell

bodies to infinity, the discrete spectrum of relaxation times is transformed into a continuous distribution of relaxation times[4] $F(\tau)$ (Fig. 5b) where $dG/d\tau = F(\tau)$ is the density of shear modulus along the τ axis, and $\int_0^\infty (dG/d\tau)d\tau = G_0$ is the shear modulus of all elements added together. These spectra usually cover several orders of magnitude of τ and therefore it is expedient to plot them against $\ln \tau$ or $\log_{10} \tau$.

Since the shear modulus $G(\tau)$ is equal to the area between τ and ∞ under the function $F(\tau)$, the following relations hold in the interval $\tau_1 \leqslant \tau \leqslant \tau_2$:

$$G_0 = \int_0^\infty F(\tau)d\tau = \int_{\tau_1}^{\tau_2} F(\tau)d\tau = \int_{\ln \tau_1}^{\ln \tau_2} F(\tau)\tau d \ln \tau$$
$$= \int_{\ln \tau_1}^{\ln \tau_2} F_1(\ln \tau)d \ln \tau = 2.303 \int_{\log_{10} \tau_1}^{\log_{10} \tau_2} F_1(2.303 \log_{10} \tau)d \log_{10} \tau$$
$$= \int_{\log_{10} \tau_1}^{\log_{10} \tau_2} F_2(\log_{10} \tau)d \log_{10} \tau$$

provided $F(\tau)$ does not exist outside of this interval. G_0 therefore represents the instantaneous shear modulus, the true value of which can be obtained only if the duration of the test is much shorter than the shortest relaxation time in the material.

In the case of a rectangular distribution $F_2(\log_{10} \tau) = b_0$, which is the simplest possible assumption,[5] the corresponding distribution is

$$F(\tau) = \frac{b_0}{2.303} \frac{1}{\tau}$$

I. Discrete Spectra of Relaxation Times

The equations of the model shown in Figure 4a are

$$\frac{d\gamma(t)}{dt} = \frac{1}{G_i}\left[\frac{ds_i(t)}{dt} + \frac{1}{\tau_i} s_i(t)\right] \quad \text{and} \quad \sum_{i=1}^{n} s_i(t) = s(t) \qquad (1)$$

with the initial conditions $\gamma(0) = 0$ and $s_i(0) = 0$. Using the Laplace transform and substituting the initial conditions, eqs. (1) become

$$p\Gamma(p) = \frac{1}{G_i}\left(p + \frac{1}{\tau_i}\right) S_i(p) \quad \text{and} \quad \sum_{i=1}^{n} S_i(p) = S(p) \qquad (2)$$

where the capitals Γ, S_i and S denote the transforms of γ, s_i and s. The resulting system of $(n + 1)$ simultaneous equations is solved for $\Gamma(p)$:

$$\Gamma(p) = \frac{1}{\sum_{i=1}^{n} \frac{G_i}{\left(p + \frac{1}{\tau_i}\right)}} \frac{S(p)}{p} \tag{3}$$

where $S(p)$ is the transform of any applied stress sequence. Alternatively, solving for $S(p)$:

$$S(p) = \sum_{i=1}^{n} p\Gamma(p)G_i \frac{1}{\left(p + \frac{1}{\tau_i}\right)} \tag{4}$$

where $\Gamma(p)$ is the transform of any applied strain sequence. The forms of eqs. (3) and (4) indicate that the inverse transforms of the first type become cumbersome when the number of Maxwell elements is large.

Two stress sequences are of interest:

$$s(t) = s_0(1 - e^{-\kappa\omega t} \cos \omega t) \tag{5}$$

and

$$s(t) = q + \frac{s_0}{\tau_0} t \tag{5a}$$

the first closely approximating the torque sequence produced by the testing machine, the second reproducing conditions of uniform rate of loading, including creep.

For a three-Maxwell-element model, eq. (3) has the form

$$\Gamma(p) = \frac{1}{G} \left\{ 1 + \frac{1}{\tau_0} \frac{1}{\left[p - \frac{1}{2\tau_0} (-a + \sqrt{a^2 - 4b}) \right]} A \right.$$
$$\left. + \frac{1}{\tau_0} \frac{1}{\left[p - \frac{1}{2\tau_0} (-a - \sqrt{a^2 - 4b}) \right]} B + \frac{1}{\tau_0} \frac{1}{p} C \right\} S(p) \tag{6}$$

where

$$\tau_i = k_i\tau_0,\ g_i = G_i/G,\ G = \sum_{j=1}^{3} G_j$$

$$a = g_1\left(\frac{1}{k_2}+\frac{1}{k_3}\right)+g_2\left(\frac{1}{k_1}+\frac{1}{k_3}\right)+g_3\left(\frac{1}{k_1}+\frac{1}{k_2}\right)$$

$$b = g_1\frac{1}{k_2k_3}+g_2\frac{1}{k_1k_3}+g_3\frac{1}{k_1k_2}$$

$$c = \frac{1}{k_1}+\frac{1}{k_2}+\frac{1}{k_3}$$

$$d = \frac{1}{k_1k_2}+\frac{1}{k_1k_3}+\frac{1}{k_2k_3}$$

$$e = \frac{1}{k_1k_2k_3}$$

and

$$A = \frac{[(a^2-2b)-a\sqrt{a^2-4b}]\,(-a+\sqrt{a^2-4b})}{2[(a^2-4b)-a\sqrt{a^2-4b}]}$$

$$+\frac{c(-a+\sqrt{a^2-4b})}{2\sqrt{a^2-4b}}+\frac{d}{\sqrt{a^2-4b}}+\frac{2e}{(a^2-4b)-a\sqrt{a^2-4b}}$$

$$B = \frac{[(a^2-2b)+a\sqrt{a^2-4b}]\,(-a-\sqrt{a^2-4b})}{2[(a^2-4b)+a\sqrt{a^2-4b}]}$$

$$-\frac{c(-a-\sqrt{a^2-4b})}{2\sqrt{a^2-4b}}-\frac{d}{\sqrt{a^2-4b}}+\frac{2e}{(a^2-4b)+a\sqrt{a^2-4b}}$$

$$C = e/b$$

Using the convolution theorem, the inverted transform is

$$\gamma(t) = \frac{1}{G}\left\{s(t)+\frac{1}{\tau_0}A\int_0^t s(\lambda)\exp\left\{\frac{-a+\sqrt{a^2-4b}}{2\tau_0}(t-\lambda)\right\}d\lambda\right.$$

$$+\frac{1}{\tau_0}B\int_0^t s(\lambda)\exp\left\{\frac{-a-\sqrt{a^2-4b}}{2\tau_0}(t-\lambda)\right\}d\lambda$$

$$\left.+\frac{1}{\tau_0}C\int_0^t s(\lambda)d\lambda\right\} \quad (7)$$

For the stress sequence $s(t) = s_0(1 - e^{-n\omega t}\cos\omega t)$, the solution is

$$\gamma(t) = \frac{s_0}{G}\left\{\left[1 - \frac{2}{(-a + \sqrt{a^2 - 4b})}A - \frac{2}{(-a - \sqrt{a^2 - 4b})}B - \frac{n}{(1 + n^2)\omega\tau_0}C\right]\right.$$

$$+\left[\frac{\left(n\omega\tau_0 + \frac{-a + \sqrt{a^2 - 4b}}{2}\right)}{\omega^2\tau_0^2 + \left(n\omega\tau_0 + \frac{-a + \sqrt{a^2 - 4b}}{2}\right)^2}A + \frac{\left(n\omega\tau_0 + \frac{-a - \sqrt{a^2 - 4b}}{2}\right)}{\omega^2\tau_0^2 + \left(n\omega\tau_0 + \frac{-a - \sqrt{a^2 - 4b}}{2}\right)^2}B\right.$$

$$\left.\left. + \frac{n}{(1 + n^2)\omega\tau_0}C - 1\right]e^{-n\omega t}\cos\omega t\right.$$

$$+\left[-\frac{\omega\tau_0}{\omega^2\tau_0^2 + \left(n\omega\tau_0 + \frac{-a + \sqrt{a^2 - 4b}}{2}\right)^2}A - \frac{\omega\tau_0}{\omega^2\tau_0^2 + \left(n\omega\tau_0 + \frac{-a - \sqrt{a^2 - 4b}}{2}\right)^2}B\right.$$

$$\left.\left. - \frac{1}{(1 + n^2)\omega\tau_0}C\right]e^{-n\omega t}\sin\omega t\right.$$

$$+\left[\frac{2}{(-a+\sqrt{a^2-4b})}-\frac{\left(n\omega\tau_0+\dfrac{-a+\sqrt{a^2-4b}}{2}\right)}{\omega^2\tau_0^2+\left(n\tau_0\omega+\dfrac{-a+\sqrt{a^2-4b}}{2}\right)^2}\right]$$

$$\times A\exp\left\{\frac{-a+\sqrt{a^2-4b}}{2\tau_0}t\right\}$$

$$+\left[\frac{2}{(-a-\sqrt{a^2-4b})}-\frac{\left(n\omega\tau_0+\dfrac{-a-\sqrt{a^2-4b}}{2}\right)}{\omega^2\tau^2+\left(n\omega\tau_0+\dfrac{-a-\sqrt{a^2-4b}}{2}\right)^2}\right]$$

$$\times B\exp\left\{\frac{-a-\sqrt{a^2-4b}}{2\tau_0}t\right\}+C\,(t/\tau_0)\Big\} \quad (8)$$

The stress sequence $s(t) = q + (s_0/\tau_0)t$ leads to the solution

$$\gamma(t)=\frac{1}{G}\Big\{q\left[1+C\left(\frac{t}{\tau_0}\right)-\frac{2}{(-a+\sqrt{a^2-4b})}\right.$$

$$\times A\left(1-\exp\left\{\frac{-a+\sqrt{a^2-4b}}{2\tau_0}t\right\}\right)-\frac{2}{(-a-\sqrt{a^2-4b})}$$

$$\left.\times B\left(1-\exp\left\{\frac{-a-\sqrt{a^2-4b}}{2\tau_0}t\right\}\right)\right]$$

$$+s_0\left[\left(1-\frac{2}{(-a+\sqrt{a^2-4b})}A-\frac{2}{(-a-\sqrt{a^2-4b})}B\right)\left(\frac{t}{\tau_0}\right)\right.$$

$$+\frac{1}{2}C\left(\frac{t}{\tau_0}\right)^2-\left(\frac{2}{-a+\sqrt{a^2-4b}}\right)^2$$

$$\times A\left(1-\exp\left\{\frac{-a+\sqrt{a^2-4b}}{2\tau_0}t\right\}\right)$$

$$\left.-\left(\frac{2}{-a-\sqrt{a^2-4b}}\right)^2 B\left(1-\exp\left\{\frac{-a-\sqrt{a^2-4b}}{2\tau_0}t\right\}\right)\right]\Big\} \quad (9)$$

Equation (4), solved for $\gamma(t) = \gamma_0$, gives

$$s(t) = G\gamma_0\{g_1 e^{-t/k_1\tau_0} + g_2 e^{-t/k_2\tau_0} + g_3 e^{-t/k_3\tau_0}\} \quad (10)$$

while for $\gamma(t) = (\delta_0/\tau_0)\, t$,

$$s(t) = G\delta_0\{k_1g_1(1 - e^{-t/k_1\tau_0}) + k_2g_2(1 - e^{-t/k_2\tau_0}) + k_3g_3\,(1 - e^{-t/k_3\tau_0})\} \quad (11)$$

II. Continuous Spectra of Relaxation Times

A polymer characterized by a distribution function $F(\tau) = dG/d\tau$ along the τ axis can be represented by the equation of a Maxwell "element" associated with any increment along the τ axis:

$$\frac{d\gamma(t)}{dt} = \frac{1}{\dfrac{dG}{d\tau}\,d\tau}\left\{\frac{\partial^2 s(\tau,t)}{\partial t\partial\tau}\,d\tau + \frac{1}{\tau}\frac{\partial s(\tau,\,t)}{\partial\tau}\,d\tau\right\}$$

and

$$s\ (t) = \int_0^\infty \frac{\partial s(\tau,t)}{\partial\tau}\,d\tau \quad (12)$$

where $[\partial s(\tau, t)/\partial\tau]d\tau$ is the contribution of the "element" with relaxation time τ to the shear stress $s(t)$.

Taking as initial conditions $\gamma(0) = 0$ and $[\partial s(\tau, 0)/\partial\tau]d\tau = 0$, the Laplace transform of eq. (12) is

$$p\ \Gamma(p) = \frac{1}{\dfrac{dG}{d\tau}\,d\tau}\left(p + \frac{1}{\tau}\right)\frac{\partial S(\tau,p)}{\partial\tau}\,d\tau \quad (13)$$

and

$$S(p) = \int_0^\infty \frac{\partial S(\tau,p)}{d\tau}\,d\tau$$

Solving eqs. (13) for $[\partial S(\tau, p)/\partial\tau]d\tau$ and integrating

$$\int_0^\infty p\Gamma(p)\,\frac{1}{\left(p + \dfrac{1}{\tau}\right)}\frac{dG}{d\tau}\,d\tau = \int_0^\infty \frac{\partial S(\tau,p)}{\partial\tau}\,d\tau = S(p) \quad (14)$$

considering that $\Gamma(p)$ is not a function of τ, then

$$\Gamma(p) = \frac{1}{\int_0^\infty \frac{1}{\left(p + \frac{1}{\tau}\right)} \frac{dG}{d\tau} d\tau} \frac{S(p)}{p} \tag{15}$$

Solutions (14) and (15) can be developed further when the distribution of relaxation times is specified.

Assuming the simplest possible (rectangular) distribution of relaxation times (Fig. 6), then

$$\frac{dG}{d\tau} = F(\tau) = \frac{b_0}{2.303} \frac{1}{\tau} = \frac{b}{\tau} \qquad \tau_1 \leqslant \tau \leqslant \tau_2$$

$$\frac{dG}{d\tau} = F(\tau) = 0 \qquad \tau_1 > \tau, \tau > \tau_2$$

with the integral

$$\int_0^\infty \frac{1}{\left(p + \frac{1}{\tau}\right)} \frac{dG}{d\tau} d\tau = b \int_{\tau_1}^{\tau_2} \frac{1}{p\tau + 1} d\tau = \frac{b}{p} \ln \frac{p\tau_2 + 1}{p\tau_1 + 1} \tag{16}$$

and eq. (15) becomes

$$\Gamma(p) = \frac{1}{b} \frac{1}{p \ln \frac{p\tau_2 + 1}{p\tau_1 + 1}} p\, S(p) \tag{17}$$

The transform

$$H(p) = \frac{1}{p \ln \frac{p\tau_2 + 1}{p\tau_1 + 1}}$$

is not a standard form and its inverse transform $h(t)$ has to be evaluated by integration in the complex plane; the inversion is shown in the Appendix. The result is:

$$h(t) = \frac{t}{\tau_2 - \tau_1} + \frac{\tau_2 + \tau_1}{2(\tau_2 - \tau_1)} - \int_{1/\tau_2}^{1/\tau_1} \frac{e^{-\rho t}}{\left\{\left[\ln \frac{\tau_2\rho - 1}{1 - \tau_1\rho}\right]^2 + \pi^2\right\}\rho}\, d\rho \tag{18}$$

With $\tau_1 = k_1\tau_0$ and $\tau_2 = k_2\tau_0$ and change of the variable of integration to $\tau_0\rho = \theta$, this expression becomes

$$h(t) = \frac{k_2 + k_1}{2(k_2 - k_1)} + \frac{1}{k_2 - k_1}\left(\frac{t}{\tau_0}\right) - \int_{1/k_2}^{1/k_1} \frac{e^{-\theta(t/\tau_0)}}{\left\{\left[\ln \frac{k_2\theta - 1}{1 - k_1\theta}\right]^2 + \pi^2\right\}\theta}\, d\theta \tag{19}$$

Substitution of eq. (19) into eq. (17) gives

$$\Gamma(p) = \frac{1}{b}\left[\mathfrak{L}\left\{\frac{ds(t)}{dt}\right\} + s(0)\right]\left[\mathfrak{L}\left\{\frac{k_2 + k_1}{2(k_2 - k_1)} + \frac{1}{k_2 - k_1}\left(\frac{t}{\tau_0}\right) - \int_{1/k_2}^{1/k_1} \frac{e^{-\theta(t/\tau_0)}}{\left\{\left[\ln \frac{k_2\theta - 1}{1 - k_1\theta}\right]^2 + \pi^2\right\}\theta}\, d\theta\right\}\right] \tag{20}$$

and by inversion

$$\gamma(t) = \frac{s(0)}{b}\left[\frac{k_2 + k_1}{2(k_2 - k_1)} + \frac{1}{(k_2 - k_1)}\left(\frac{t}{\tau_0}\right) - \int_{1/k_2}^{1/k_1} \frac{e^{-\theta(t/\tau_0)}}{\left\{\left[\ln \frac{k_2\theta - 1}{1 - k_1\theta}\right]^2 + \pi^2\right\}\theta}\, d\theta\right] + \frac{1}{b}\int_0^t \frac{ds(\lambda)}{d\lambda}\left\{\frac{k_2 + k_1}{2(k_2 - k_1)} + \frac{1}{(k_2 - k_1)}\left(\frac{t - \lambda}{\tau_0}\right) - \int_{1/k_2}^{1/k_1} \frac{e^{-\theta(t-\lambda)/\tau_0}}{\left\{\left[\ln \frac{k_2\theta - 1}{1 - k_1\theta}\right]^2 + \pi^2\right\}\theta}\, d\theta\right\} d\lambda \tag{21}$$

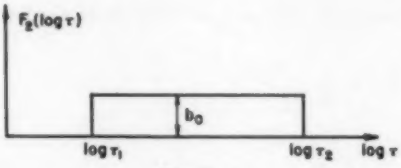

Figure 6.

Inserting the stress sequence $s(t) = s_0(1 - e^{-nat} \cos \omega t)$ into eq. (21) yields:

$$\gamma(t) = \frac{s_0}{b} - \Bigg[\frac{k_2 + k_1}{2(k_2 - k_1)} (1 - e^{-nat} \cos \omega t) + \frac{1}{k_2 - k_1} \left\{ \left(\frac{t}{\tau_0} \right) - \frac{1}{(1 + n^2)\omega\tau_0} [n(1 - e^{-nat} \cos \omega t) + e^{-nat} \sin \omega t] \right\}$$

$$+ e^{-nat} \cos \omega t \int_{1/k_1}^{1/k_2} \frac{1 - \dfrac{\dfrac{\theta}{\omega\tau_0}\left(\dfrac{\theta}{\omega\tau_0} - n\right)}{1 + \left(\dfrac{\theta}{\omega\tau_0} - n\right)^2}}{\left\{ \left[\ln \dfrac{k_2\theta - 1}{1 - k_1\theta} \right]^2 + \pi^2 \right\} \theta} d\theta$$

$$- e^{-nat} \sin \omega t \int_{1/k_1}^{1/k_2} \frac{\dfrac{\dfrac{\theta}{\omega\tau_0}}{1 + \left(\dfrac{\theta}{\omega\tau_0} - n\right)^2}}{\left\{ \left[\ln \dfrac{k_2\theta - 1}{1 - k_1\theta} \right]^2 + \pi^2 \right\} \theta} d\theta$$

$$- \int_{1/k_1}^{1/k_2} \frac{\left[1 - \dfrac{\dfrac{\theta}{\omega\tau_0}\left(\dfrac{\theta}{\omega\tau_0} - n\right)}{1 + \left(\dfrac{\theta}{\omega\tau_0} - n\right)} \right] e^{-\theta(t/\tau_0)}}{\left\{ \left[\ln \dfrac{k_2\theta - 1}{1 - k_1\theta} \right]^2 + \pi^2 \right\} \theta} d\theta \Bigg] \quad (22)$$

For the stress sequence $s(t) = q + (s_0/\tau_0)t$, the solution obtained is:

$$\gamma(t) = \frac{q}{b}\left\{\frac{k_2 + k_1}{2(k_2 - k_1)} + \frac{1}{(k_2 - k_1)}\left(\frac{t}{\tau_0}\right) - \int_{1/k_2}^{1/k_1} \frac{e^{-\theta(t/\tau_0)}}{\left\{\left[\ln\frac{k_2\theta - 1}{1 - k_1\theta}\right]^2 + \pi^2\right\}\theta}\, d\theta\right\} + \frac{s_0}{b}\left\{\frac{k_2 + k_1}{2(k_2 - k_1)}\left(\frac{t}{\tau_0}\right) + \frac{1}{2(k_2 - k_1)}\left(\frac{t}{\tau_0}\right)^2 - \int_{1/k_2}^{1/k_1} \frac{1 - e^{-\theta(t/\tau_0)}}{\left\{\left[\ln\frac{k_2\theta - 1}{1 - k_1\theta}\right]^2 + \pi^2\right\}\theta^2}\, d\theta\right\} \tag{23}$$

Substituting $dG/d\tau = b/\tau$ into eq. (14) and noting the limits of the distribution:

$$S(p) = \int_{\tau_1}^{\tau_2} p\Gamma(p)\,\frac{b}{\tau}\,\frac{1}{\left(p + \frac{1}{\tau}\right)}\, d\tau \tag{24}$$

with the strain sequence $\gamma(t) = \gamma_0$, eq. (24) becomes

$$S(p) = \gamma_0 b \int_{k_1\tau_0}^{k_2\tau_0} \frac{1}{\tau}\,\frac{1}{\left(p + \frac{1}{\tau}\right)}\, d\tau \tag{25}$$

Inversion and integration yields the solution

$$s(t) = \gamma_0 b\left\{\left[-E_i\left(-\frac{t}{k_2\tau_0}\right)\right] - \left[-E_i\left(-\frac{t}{k_1\tau_0}\right)\right]\right\}$$

where
$$-E_i(-x) = \int_x^\infty \frac{e^{-\lambda}}{\lambda}\, d\lambda \tag{26}$$

With the strain sequence $\gamma(t) = (\delta_0/\tau_0)t$, eq. (24) becomes

$$S(p) = \frac{b\delta_0}{\tau_0} \int_{k_1\tau_0}^{k_2\tau_0} \frac{1}{\tau} \frac{1}{p\left(p + \frac{1}{\tau}\right)} d\tau \tag{27}$$

which after inversion and integration yields

$$s(t) = b\delta_0 \left\{ k_2(1 - e^{-t/k_2\tau_0}) - k_1(1 - e^{-t/k_1\tau_0}) - \left(\frac{t}{\tau_0}\right) \left\{ \left[- E_i\left(-\frac{t}{k_1\tau_0}\right)\right] - \left[-E_i\left(-\frac{t}{k_2\tau_0}\right)\right] \right\} \right\} \tag{28}$$

5. DISCUSSION OF THEORETICAL RESULTS

The evaluation and interpretation of experimental data in terms of a continuous distribution of relaxation times of the polymer investigated is based on the comparison of the experimental stress-strain curves with a set of theoretical curves obtained by numerical evaluation of the expressions (24) and (25). The amount of numerical work involved in covering a large variety of conditions would be prohibitive and a simpler substitute method has been used for this evaluation.

The most expedient approach appears to be to replace the continuous distribution by an equivalent discrete spectrum, replacing a certain area under the function $F(\tau)$, or $F_2(\log_{10} \tau)$, by individual constants proportional to the area replaced. Care must, however, be exercised in the selection of discrete relaxation times as by spacing the elements too far from each other along the τ axis of the spectrum the discrete spectrum may no longer approximate the continuous one. A comparison of relaxation curves that can be evaluated quite readily for both types of models exhibits clearly the degree of approximation achieved by this replacement.

Figure 7 shows the relaxation curves of models with uniform distributions of relaxation times covering two and four orders of magnitude of τ, and the relaxation curves of the replacing models with two and three elements. It is obvious from the diagrams that the two element model offers a good approximation of the two decade distribution, but is not adequate to replace the four decade distribution. The degree of approximation is improved by considering a three element model.

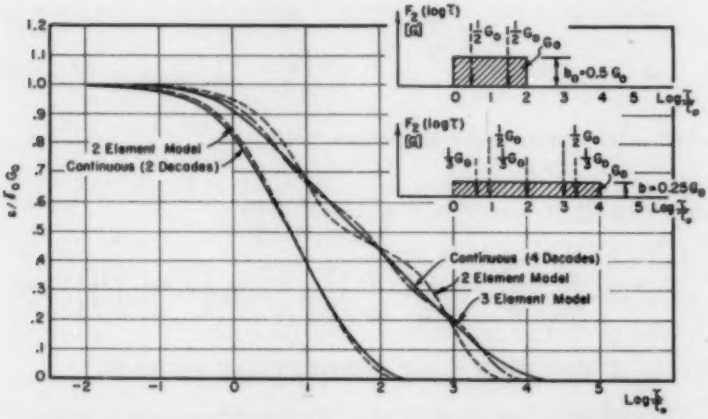

Fig. 7. Relaxation curves for continuous and discrete distributions.

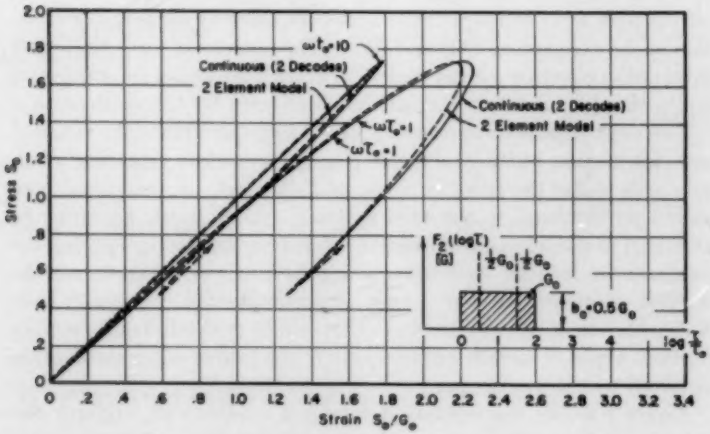

Fig. 8. Stress-strain relations for applied stress $S = S_0(1 - e^{-0.1\omega t} \cos \omega t)$.

Figure 8 shows the response of the two decade distribution and of the two-Maxwell-element model to the stress sequence $s = s_0 (1 - e^{-0.1\omega t} \cos \omega t)$ for two sets of conditions: $\omega\tau_0 = 1$ and $\omega\tau_0 = 10$. The curves of the two element model can be considered, for all prac-

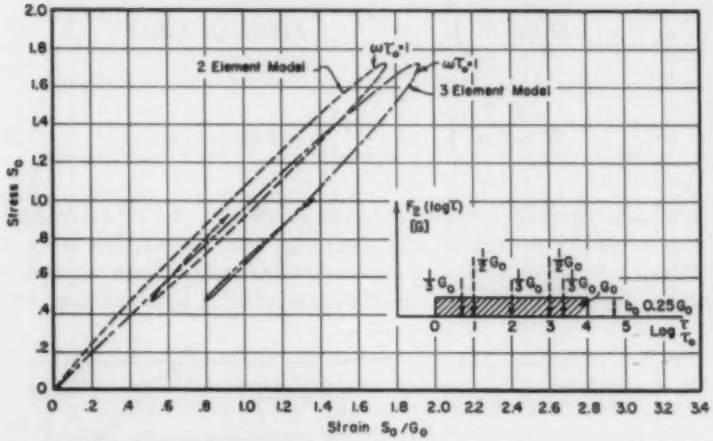

Fig. 9. Stress-strain relations for applied stress $S = S_0(1 - e^{-0.1\omega t} \cos \omega t)$.

tical purposes, as a good approximation of those of the two decade distribution. Figure 9 shows the difference between the two and three element models replacing the four decade uniform distribution of relaxation times under the above stress sequence.

Prior to the actual evaluation of the test results, it was hoped that the use of a rectangular spectrum of relatively limited extent or the equivalent three-Maxwell-element model would produce a reasonable approximation of the test results. This hope was based on the fact that (trapezoidal and rectangular) spectra of limited range have been used rather successfully in the interpretation of relaxation tests.[6]

It seems obvious, however, that good agreement between the theoretical and experimental relaxation curves can be expected only if the spectrum of relaxation times more or less coincides with the time range of the relaxation test. It was therefore assumed that since fair agreement was reported for various polymers, their relaxation spectra would necessarily be of rather limited extent, with minor contributions outside the usual range of relaxation tests. This assumption is implied in the commonly accepted procedure of deriving the complex dynamic shear modus $G(\omega) = G'(\omega) + iG''(\omega)$ as a function of the angular frequency of vibration ω from a distribution function of relaxation times $F(\tau)$ or $F(\log_{10} \tau)$ obtained from the interpretation of a relaxation test. While the form of the respective equations

$$G'(\omega) = \int_{-\infty}^{+\infty} \frac{\omega^2\tau^2}{1+\omega^2\tau^2} F(\log_{10}\tau)d\log_{10}\tau$$

and

$$G''(\omega) = \int_{-\infty}^{+\infty} \frac{\omega\tau}{1+\omega^2\tau^2} F(\log_{10}\tau)d\log_{10}\tau \qquad (29)$$

implies integration over the complete range of τ, the actual integration is usually performed over the range of an incomplete function $F(\log_{10}\tau)$ in which all contributions shorter than the time required to apply the initial strain in the relaxation test are automatically lost.

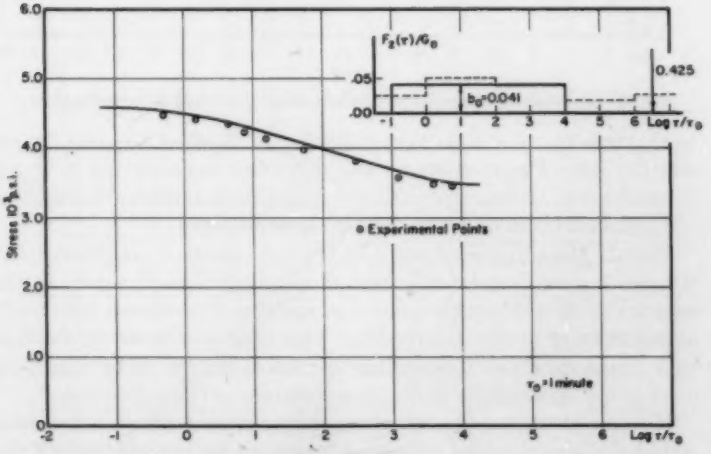

Figure 10.

As the period of one cycle $(1/\omega)$ is usually much shorter than this time, eqs. (29) can, in general, not be used unless the complete function $F(\log_{10}\tau)$ is known.

This is illustrated in Figure 10 in which an observed relaxation diagram has been used to establish a three-element approximation of $F(\tau)$. Using the same model to predict the stress-strain diagram in a dynamic test, the discrepancy between the theoretical and experimental diagram is demonstrated (Fig. 11). Thus, the existence of a very

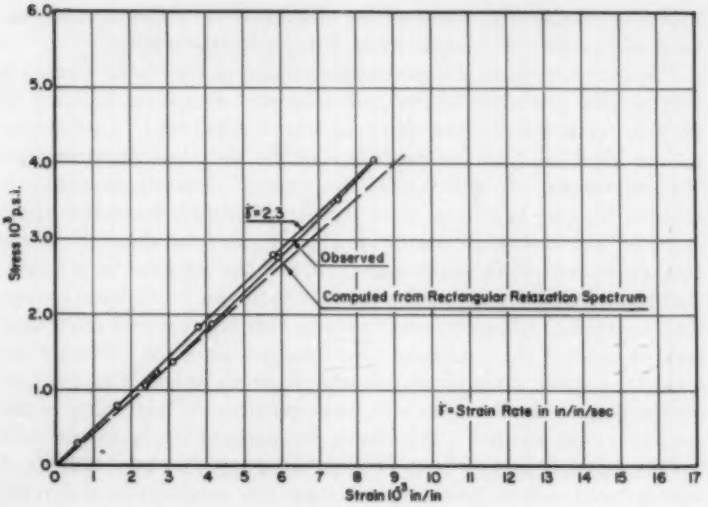

Figure 11.

wide and probably nonuniform spectrum of relaxation times had to be assumed as a basis for the evaluation of the test results.

6. TESTS AND EVALUATION OF EXPERIMENTAL RESULTS

A relatively large number of specimens of the fabric-filled phenolic designated as FM-1132 (average tensile strength 6000 p.s.i., average impact value of $^1/_2$" specimens 1.5) was tested both under dynamic conditions with strain rates of 2 to 3 in./in./sec. and under slow uniform loading with strain rates of the order of 10^{-6} in./in./sec. at each of the three temperature levels of -70, $+72$, and $+200$°F. A stress-strain diagram was constructed from the oscilloscope records for each test.

The test results showed a certain amount of scatter; this must be expected because of unavoidable differences in the molding process of individual specimens. Therefore a few specimens representing well the average trend of the results were selected for the actual evaluation of the relaxation spectrum of this polymer. Samples of the experi-

mentally established stress-strain diagrams for different temperatures and strain rates are shown in Figures 12 through 17.

The construction of the spectrum of relaxation times is an extremely cumbersome procedure of trial and error and consists of building up models, composed of a few elements, whose responses to a set of conditions identical with the conditions of the test closely approximate the test results. In this way the number of elements momentarily involved can be kept low, since the elements with relaxation times three or four orders of magnitude shorter than the duration of the test considered can be safely neglected, and the elements with relaxation times longer by about the same amount can be replaced by one elastic element. Models constructed in this way covered more than eight decades of the relaxation spectrum and, since the difference between the strain rates employed was about six orders of magnitude, overlapping of these models and, consequently, the continuity of the spectrum were insured. Combining the parts of the spectrum built up from models derived from the test data at +72 and +200°F., it was deduced that in first approximation this temperature difference is equivalent, on the logarithmic scale, to a shift of the spectrum[7] of 8 decades. Assuming that the viscosity dependence on the temperature in this range is governed by the relation

$$\eta = \eta_0^{E_a/RT}$$

where E_a is the activation energy, R the gas constant, and T the temperature in °K., and since $\tau = \eta/G$, we can write

$$\ln \tau = \ln \frac{\eta_0}{G} + \frac{E_a}{R}\frac{1}{T}$$

Denoting the value of the relaxation time at room temperature T_0 (+72°F.) as τ_0, and at temperature T_1 as τ_0', the following relation holds

$$\ln \frac{\tau_0'}{\tau_0} = \frac{E_a}{R}\left(\frac{1}{T_1} - \frac{1}{T_0}\right)$$

Substituting for $\tau_0'/\tau_0 = 10^8$, $R = 1.986$ cal./°K./mole, $T_0 = 295$°K. (+72°F.), and $T_1 = 366$°K. (+200°F.), the value of the activation energy was computed as $E_a = 55.6$ kg.cal./mole.

Denoting the value of the relaxation time at the temperature $T_2 =$

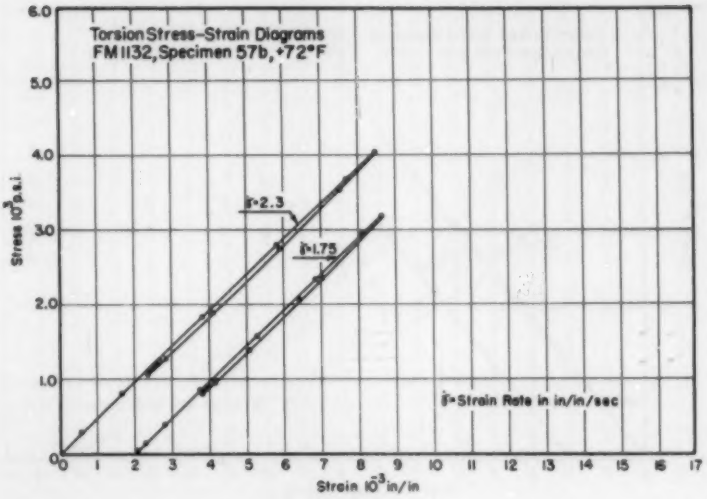

Figure 12.

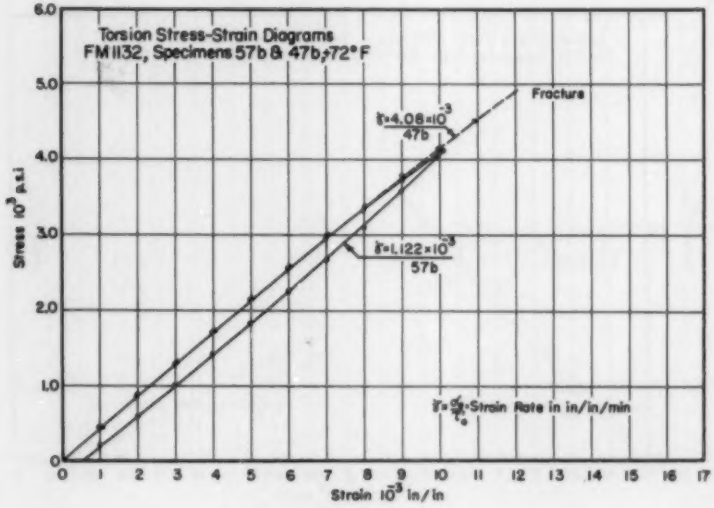

Figure 13.

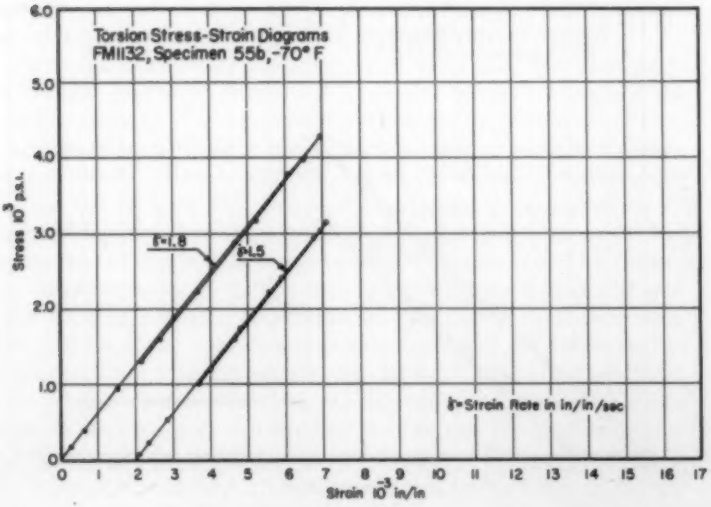

Figure 14.

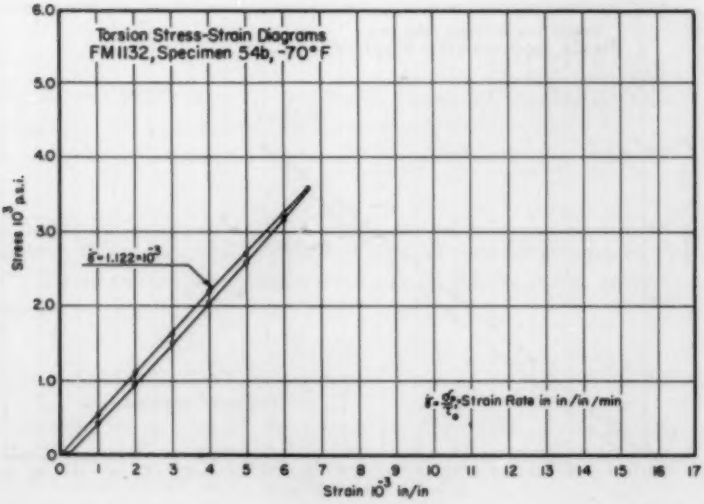

Figure 15.

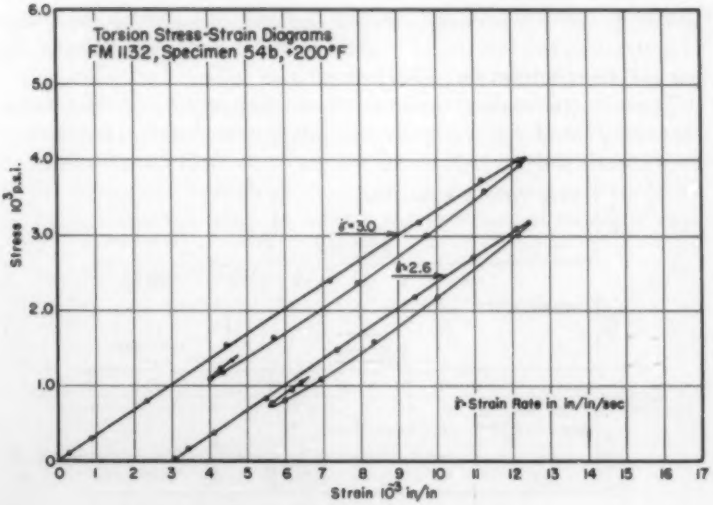

Figure 16.

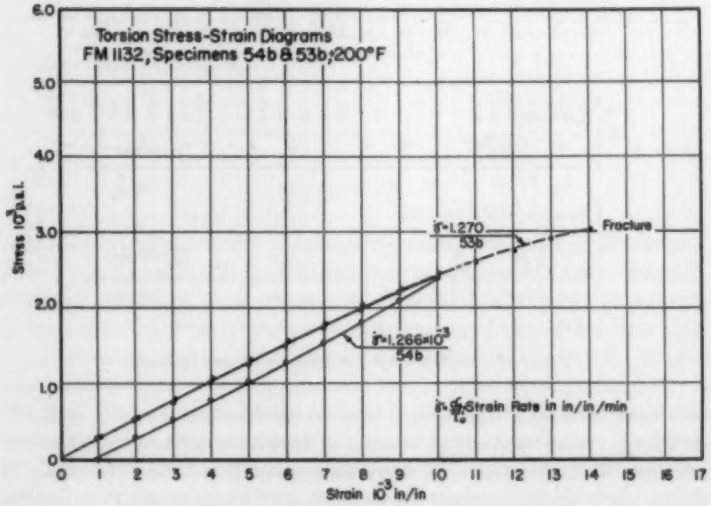

Figure 17.

216°K. (−70°F.) as τ_0'' and using the computed value for the energy of activation, the ratio $\tau_0/\tau_0'' = 8.33 \times 10^{-16}$ was evaluated and the part of the spectrum for −70°F. located.

The assumption of a constant activation energy E_a over the entire range of T or of τ is obviously only an approximation, necessary at

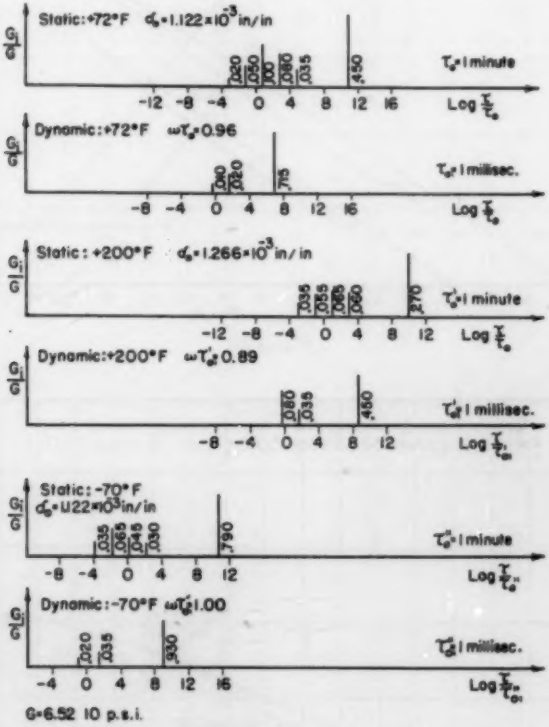

Fig. 18. Models used for analysis of test results.

this time because of the lack of reliable information concerning $E_a(T)$ or $E_a(\tau)$. As a result of increasing molecular weight of the elements presumably associated with increasing relaxation times, the value of E_a per mole might be expected to increase with increasing τ. On the other hand, this tendency could be reversed over the range of small

τ, when the interaction between elements associated with very small values of τ might change in character.

The individual models used in the interpretation of the tests are shown in Figure 18, and the spectrum of relaxation times derived in this fashion is presented in Figure 19. It was impossible to determine the actual form of the spectrum for extremely long relaxation times by the foregoing procedures; this part of the spectrum is therefore shown by a dotted line. It reflects the existence of elements with

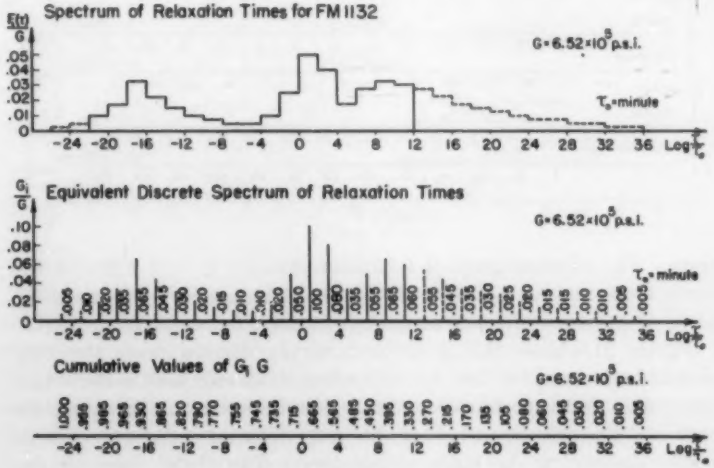
Spectrum of Relaxation Times for FM 1132
G = 6.52×10⁵ p.s.i.
τ₀ = minute
Equivalent Discrete Spectrum of Relaxation Times
G = 6.52×10⁵ p.s.i.
τ₀ = minute
Cumulative Values of Gᵢ G
G = 6.52×10⁵ p.s.i.

Figure 19.

very long relaxation times which are necessary for building up the observed shear modulus G, as well as the assumption that the number of elements continues to decrease with increasing relaxation times, but it can not reliably show the exact distribution of these elements. In order to establish this part of the distribution more accurately, relaxation tests of extremely long duration would have to be performed.

Figure 20 shows the location of the test ranges for both the static and dynamic tests with respect to the constructed spectrum of relaxation times for the three temperature levels. The magnitudes of the shifts due to the temperature changes are shown, as well as the shifts due to the change of time scales between the static and the dynamic

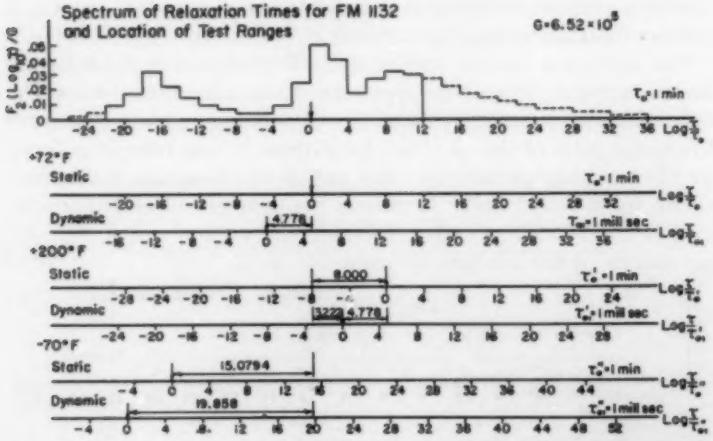

Figure 20.

tests. The selected units of relaxation times: $\tau_0 = 1$ min. for the static tests, and $\tau_{01} = 1$ millisec. for the dynamic tests, were chosen to be of the same order of magnitude as the time scales of the tests.

Figure 21 shows the theoretical curves derived from the constructed spectrum for the various loading conditions used in the actual tests, with the experimental points superimposed on the respective curves. The agreement between the experimental and the theoretical results appears to be quite satisfactory. The slight discrepancies occurring at the very high stress levels suggest that in this region the assumption of *linear* viscoelasticity for the constitutive phases of this polymer may no longer be valid. Finally, in Figure 22 a relaxation curve is derived from the spectrum constructed in Figure 19 by first analyzing the straining to the predetermined "initial" strain (Fig. 22a) and subsequently establishing the stress-relaxation at this strain (Fig. 22b). The comparison of this curve with the results of relaxation tests performed under the same conditions shows satisfactory agreement. (It should be noted that while the fit shown in Figure 22b is not significantly better than that shown in Figure 10, the dynamic stress-strain diagram cannot be reproduced by the rectangular spectrum.)

Considering the relaxation spectrum derived for the material in-

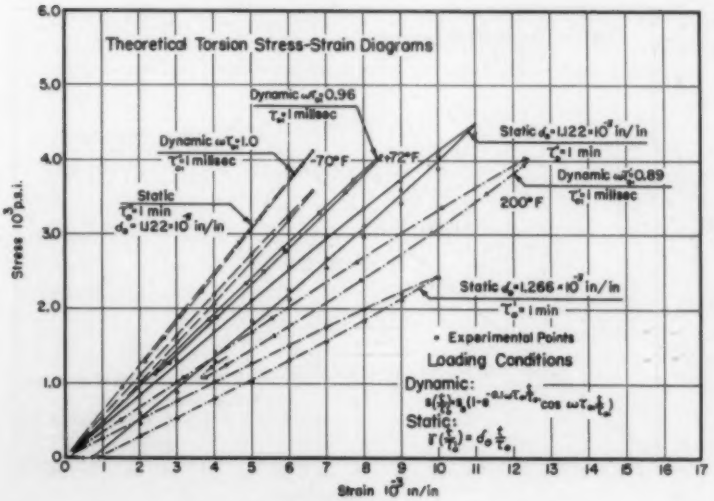

Figure 21.

vestigated, which is a commercially produced filled phenolic and thus representative of a relatively large group of materials, it is immediately obvious that no simple correlation of the results of mechanical tests at various speeds and temperatures can be expected. The so-called "equations of state" disregarding the extremely wide and, at best, bimodal distribution of relaxation times can, for such materials, be used only to correlate tests of similar time scale at constant temperatures, thus losing much of their value. The idealization of real viscoelastic materials by the Maxwell body or even by a two-Maxwell-element model can reproduce the behavior only within the same narrow time scale for which the model parameters have been determined.

It is interesting to note that the first relatively sharp mode of the spectrum appears to be in the range of the velocity of motion of very light particles of atomic or monomolecular size, while the second, much less sharp, mode is in the range of motion of long molecular chain segments. The shape of this part of the spectrum is probably an indication of the character and the extent of the polymerization process.

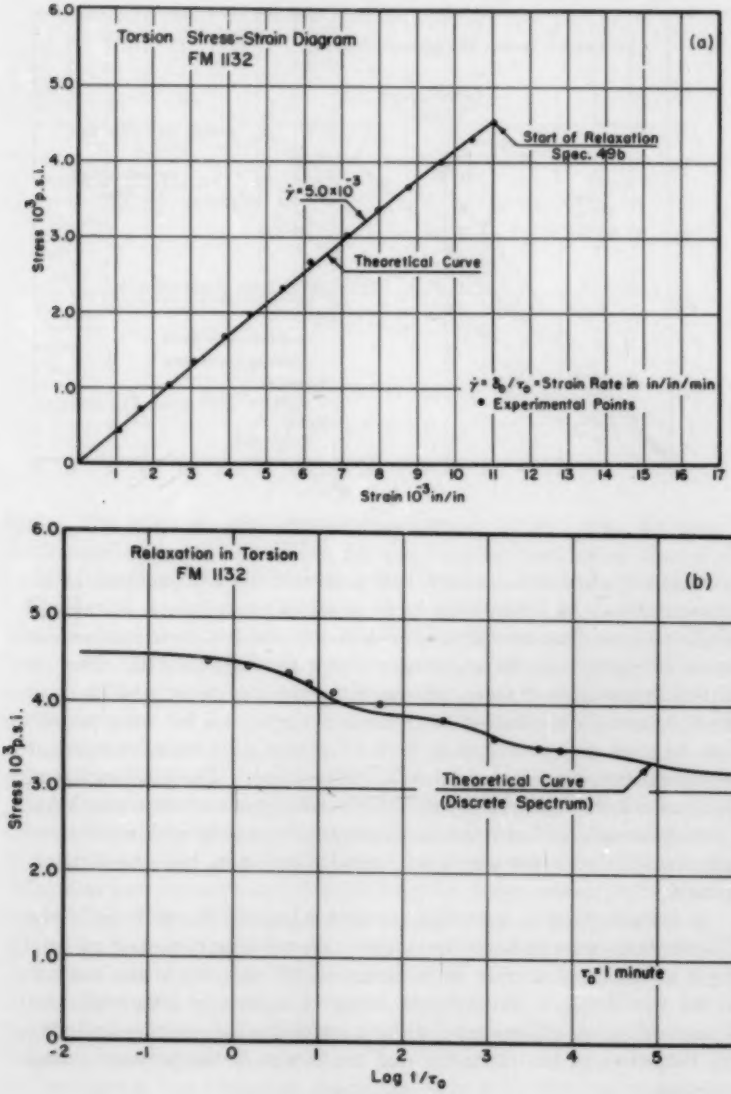
Torsion Stress-Strain Diagram
FM 1132
(a)
Start of Relaxation
Spec. 49b
$\dot{\gamma}=5.0\times10^{-3}$
Theoretical Curve
$\dot{\gamma}=\delta_0/\tau_0$ = Strain Rate in in/in/min
• Experimental Points
Stress 10^3 p.s.i.
Strain 10^{-3} in/in
Relaxation in Torsion
FM 1132
(b)
Theoretical Curve
(Discrete Spectrum)
τ_0 = 1 minute
Log $1/\tau_0$

Figure 22.

The research has been supported by the Army Ordnance Corps., Picatinny Arsenal, Plastics Research Laboratory, under the supervision of Dr. L. Gilman and Miss E. McAbee, whose continued interest is gratefully acknowledged.

APPENDIX

The inverse Laplace transform of the function

$$H(p) = \frac{1}{p[\ln(p\tau_2 + 1) - \ln(p\tau_1 + 1)]} \tag{30}$$

is defined as

$$h(t) = \lim_{\beta \to \infty} \frac{1}{2\pi i} \int_{\gamma-\beta i}^{\gamma+\beta i} \frac{e^{pt}}{p[\ln(p\tau_2 + 1) - \ln(p\tau_1 + 1)]}\, dp \tag{30a}$$

where p is a complex variable.

The function

$$f(p) = \frac{e^{pt}}{[\ln(p\tau_2 + 1) - \ln(p\tau_1 + 1)]} \tag{30b}$$

has a pole of the second order at $p = 0$ and branch points at $p = -1/\tau_2$ and $-1/\tau_1$. Making branch cuts along the negative axis of reals from $-1/\tau_2$ to $-\infty$, we can choose a line integral as shown in Figure 23.

With the path and direction of integration as shown in Figure 23, we can write

$$\oint_{C_1} f(p)dp = \oint_{C_2} f(p)dp \tag{30c}$$

but

$$\oint_{C_2} f(p)dp = 2\pi i b_1$$

where b_1 is the residue of the function $f(p)$ at the point $p = 0$. Evaluation gives

$$\oint_{C_2} f(p)dp = 2\pi i \left[\frac{t}{(\tau_2 - \tau_1)} + \frac{\tau_2 + \tau_1}{2(\tau_2 - \tau_1)}\right] \tag{30d}$$

The line integral along the curve C_1 will be broken into a number of line integrals, each evaluated separately. It can be shown that

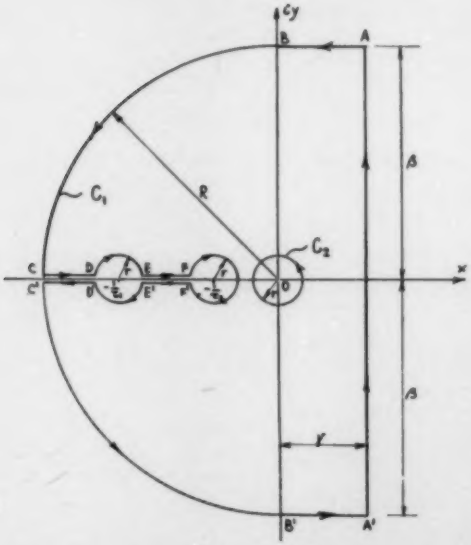

Fig. 23. Note that $\tau_2 > \tau_1$; $-\pi < arg(\tau_2 p + 1) < \pi$, $-\pi < arg(\tau_1 p + 1) < \pi$.

$$\int_A^B f(p)dp = \int_B^C f(p)dp = \int_{C'}^{B'} f(p)dp = \int_{B'}^{A'} f(p)dp = 0$$

when the radius R is increased indefinitely. The integral along the path C–D is

$$\int_C^D f(p)dp = \int_R^{1/\tau_1+r} \frac{e^{-\rho t}}{[\ln(\tau_2\delta - 1) - \ln(\tau_1\rho - 1)]\rho} d\rho \quad (30e)$$

and for the path D'–C'

$$\int_{D'}^{C'} f(p)dp = -\int_R^{(1/\tau_1)+r} \frac{e^{-\rho t}}{[\ln(\tau_2\rho - 1) - \ln(\tau_1\rho - 1)]\rho} d\rho \quad (30f)$$

The two integrals are identical but of opposite sign and therefore cancel each other.

Furthermore, it can be shown that

$$\lim_{r\to 0} \int_D^E f(p)dp = \lim_{r\to 0} \int_{E'}^{D'} f(p)dp = \lim_{r\to 0} \int_F^{F'} f(p)dp = 0 \quad (30g)$$

For the path E–F, the integral is

$$\lim_{r\to 0}\int_E^F f(p)dp = \int_{1/\tau_1}^{1/\tau_2} \frac{e^{-\rho t}}{[\ln(\tau_2\rho - 1) + i\pi - \ln(1 - \tau_1\rho)]\rho}\,d\rho \quad (30h)$$

and similarly for the path F'–E':

$$\lim_{r\to 0}\int_{F'}^{E'} f(p)dp = \int_{1/\tau_2}^{1/\tau_1} \frac{e^{-\rho t}}{[\ln(\tau_2\rho - 1) - i\pi - \ln(1 - \tau_1\rho)]\rho}\,d\rho \quad (30i)$$

Assembling all integrals as R approaches infinity and r approaches zero, the result is

$$\lim_{\beta\to 0}\int_{\gamma-\beta i}^{\gamma+\beta i} f(p)dp + 2\pi i\int_{1/\tau_2}^{1/\tau_1} \frac{e^{-\rho t}}{\left\{\left[\ln\dfrac{\tau_2\rho - 1}{1 - \tau_1\rho}\right]^2 + \pi^2\right\}\rho}\,d\rho$$

$$= 2\pi i\left\{\frac{t}{\tau_2 - \tau_1} + \frac{\tau_2 + \tau_1}{2(\tau_2 - \tau_1)}\right\} \quad (30j)$$

Rearranging the terms,

$$h(t) = \lim_{\beta\to\infty}\frac{1}{2\pi i}\int_{\gamma-\beta i}^{\gamma+\beta i} \frac{e^{pt}}{p[\ln(p\tau_2 + 1) - \ln(p\tau_1 + 1)]}\,dp$$

$$= \frac{t}{\tau_2 - \tau_1} + \frac{\tau_2 + \tau_1}{2(\tau_2 - \tau_1)} - \int_{1/\tau_2}^{1/\tau_1} \frac{e^{-\rho t}}{\left\{\left[\ln\dfrac{\tau_2\rho - 1}{1 - \tau_1\rho}\right]^2 + \pi^2\right\}\rho}\,d\rho \quad (30k)$$

References

1. Nolle, A. W., *J. Polymer Sci.*, **5**, 1 (1950). Mason, W. P., Baker, W. O., McSkimin, H. J., and Heiss, J. H., *Phys. Rev.*, **73**, 1074 (1948); **75**, 936 (1949). Marvin, R. S., Aldrich, R., and Sack, H., *J. Appl. Phys.*, **25**, 1213 (1954).

2. Baker, W. O., and Heiss, J. H., *The Bell System Tech. J.*, **31**, 306 (1952). Hopkins, I. L., *Trans. Am. Soc. Mech. Engrs.*, **73**, 195 (1951).

3. Donnell, L. H., *Trans. Am. Soc. Mech. Engrs.*, **56**, 795 (1934).

4. Kuhn, W., Künzle, O., and Preissmann, A., *Helv. Chim. Acta*, **30**(1), 307 (1947).

5. Kuhn, W., Künzle, O., and Preissmann, A., *Helv. Chim. Acta*, **30**(2), 464 (1947).

6. Andrews, R. D., Hofman-Bang, N., and Tobolsky, A. V., *J. Polymer Sci.*, **3**, 669 (1948). Tobolsky, A. V., *J. Am. Chem. Soc.*, **74**, 3786 (1952).

7. Alfrey, T., Jr., *Mechanical Behavior of High Polymers*, Interscience, New York-London, 1948, pp. 130–132.

Synopsis

The spectrum of relaxation times has been constructed for a fabric-filled phenolic of commercial type by combining the results of torsion tests on cylindrical specimens over a relatively wide range of strain rates and temperatures. The resulting spectrum is not unimodal and extends over almost sixty orders of magnitude; thus the mechanical response of high polymers at a certain combination of strain rate and temperature can be determined only by tests at this same combination. Prediction of such performance requires a knowledge of the spectrum over its entire range.

TRANSACTIONS OF THE SOCIETY OF RHEOLOGY, II : 131–151 (1958)

Approximate Equations for Interconverting the Various Mechanical Properties of Linear Viscoelastic Materials*

THOR L. SMITH, *Jet Propulsion Laboratory, California Institute of Technology, Pasadena, California*

INTRODUCTION

The mathematical theory of linear viscoelasticity has been developed rather completely.[1–3] Gross, who has made important contributions to this theory, has presented the exact equations for interconverting the various time-dependent mechanical properties.[3–5] However, many of these exact equations are difficult and tedious to use, since suitable analytical expressions which fit experimental data over an extended time-scale are not available, and so graphical or numerical methods are often required. Consequently, instead of the exact equations, various approximate relations have frequently been used for interconverting different time-dependent mechanical quantities and for calculating derived quantities such as the relaxation and retardation spectra.

There are several reasons why it is desirable to be able to interconvert the various experimental and derived time-dependent quantities: (*1*) Several experimental techniques are often used to cover the time-scale of interest, and it is then often necessary to convert the different experimental quantities into a single form. (*2*) Although in principle any time-dependent property, when known over the complete time-scale, gives a complete picture of the viscoelastic properties of a material, different methods of representing these properties emphasize different aspects of the overall behavior. So, to study these differ-

* This paper presents one phase of research carried out at the Jet Propulsion Laboratory, California Institute of Technology, under Contract No. DA-04-495-Ord 18, sponsored by the Department of the Army Ordnance Corps.

ent aspects, it is necessary to derive from available data various related quantities. (3) For the solution of applied problems, different viscoelastic quantities are needed. For example, stress-strain behavior under a constant strain rate is closely related to the stress-relaxation modulus, but stress-strain behavior under a constant loading rate is closely related to the creep compliance. Also, the heat build-up in a material subjected to sinusoidal deformation is proportional to the loss modulus G'' when the amplitude of the strain is constant but is proportional to the loss compliance J'' when the amplitude of the stress is constant.

In this paper, some approximate methods for interconverting different viscoelastic properties are described. Included are approximate equations for interconverting the relaxation and retardation spectra, and thus for interconverting the quantities directly related to these spectra. The equations have been tested by interconverting published data on the NBS polyisobutylene.

EQUATIONS BASED ON GENERALIZED MAXWELL MODEL

When strain as a function of time is controlled by the experimental method, the observed viscoelastic response can be represented conveniently by the continuous Maxwell model which consists of an infinite number of Maxwell elements and an isolated spring, all connected in parallel. This model is completely characterized by the relaxation spectrum H and the equilibrium modulus G_e, which is represented by the isolated spring.* For uncrosslinked polymers, such as polyisobutylene, the equilibrium modulus can be set equal to zero. The stress-relaxation modulus $G(t)$, the storage modulus $G'(\omega)$, the loss modulus $G''(\omega)$ and the stress-strain curve at a constant strain rate R ($\epsilon = Rt$, where R is a constant) are given exactly in terms of H by the following equations:

$$G(t) = G_e + \int_{-\infty}^{\infty} H(\tau)e^{-t/\tau}d \ln \tau \qquad (1)$$

* The symbols proposed by the Committee on Nomenclature of the Society of Rheology[4] are used in this paper. The symbols for primary quantities measured in shear are used, although the equations are equally applicable to quantities measured in bulk or longitudinal deformation.

$$G'(\omega) = G_e + \int_{-\infty}^{\infty} \frac{H(\tau)\omega^2\tau^2}{1 + \omega^2\tau^2} d \ln \tau \tag{2}$$

$$G''(\omega) = \int_{-\infty}^{\infty} \frac{H(\tau)\omega\tau}{1 + \omega^2\tau^2} d \ln \tau \tag{3}$$

$$\sigma(\epsilon) = G_e\epsilon + R \int_{-\infty}^{\infty} \tau H(\tau)(1 - e^{-\epsilon/R\tau}) d \ln \tau \tag{4}$$

Differentiating eq. (4) with respect to strain ϵ and substituting eq. (1) gives

$$\frac{d\sigma}{d\epsilon} = G\left(\frac{\epsilon}{R}\right) \tag{5}$$

Thus, the stress-strain curve at any desired rate can be obtained by integrating $G(t)$. Conversely, $G(t)$ can be obtained from the slopes of stress-strain curves, as experimentally demonstrated previously.[7]

When either $G(t)$ or G' is known, the other one can be calculated quite accurately with only a rough estimate of H by using Marvin's difference method.[8] This method is based on the fact that the difference between G' and $G(t)$ is relatively small and is given exactly by the equation:

$$G'(1/\omega) - G(t) = \int_{-\infty}^{\infty} H(\tau) \left[\frac{1}{1 + (t/\tau)^2} - e^{-t/\tau}\right] d \ln \tau \tag{6}$$

The quantity in the brackets, which approximates a delta-function, is significantly greater than zero over only a relatively narrow range of $\ln \tau$. Catsiff and Tobolsky[9] integrated eq. (6) by assuming that $H = k\tau^{-m}$ over the range of τ in which the quantity in the brackets is significantly greater than zero. They give the following equation, obtained by integration:

$$G(t) = G' - H\left[\frac{\pi}{2} \csc \frac{m\pi}{2} - \Gamma(m)\right] \quad -1 < m < 2 \tag{7}$$

It can be shown that this equation represents the integral when $-1 < m < 2$, and that when $m = 0$ the quantity in the brackets converges to Euler's or Mascheroni's constant which equals approximately 0.5772.

The storage modulus G'' can be calculated approximately from H by substituting $H = k\tau^{-m}$ in eq. (3). Integration gives

$$G'' = H \frac{\pi}{2} \sec \frac{m\pi}{2} \qquad -1 < m < 1 \qquad (8)$$

This equation is valid approximately since the quantity $\omega\tau/[1 + \omega^2\tau^2]$ in eq. (3) approximates a delta-function. To calculate H from G'', various investigators[10,11] have given as a zero-order approximation $H = 2G''/\pi$. This is obtained from eq. (8) when $m = 0$.

EQUATIONS BASED ON GENERALIZED VOIGT MODEL

When the stress as a function of time is controlled by the experimental method, the measured viscoelastic properties can conveniently be represented by the continuous Voigt model. This model contains an infinite number of Voigt elements in series, all in series with an isolated spring; for uncrosslinked polymers, the model also contains an isolated dashpot in series. The isolated spring represents the glassy compliance J_g and the isolated dashpot the steady-flow viscosity η. This model is characterized completely by J_g, η and the retardation spectrum L.

The creep compliance $J(t)$, the storage compliance $J'(\omega)$, the loss compliance $J''(\omega)$, and stress-strain curves measured under a constant loading rate R ($\sigma = Rt$, where R is a constant), are given by the equations:

$$J(t) = J_g + \int_{-\infty}^{\infty} L(\tau)(1 - e^{-t/\tau}) d \ln \tau + t/\eta, \qquad (9)$$

$$J'(\omega) = J_g + \int_{-\infty}^{\infty} \frac{L(\tau)}{1 + \omega^2\tau^2} d \ln \tau \qquad (10)$$

$$J''(\omega) = \frac{1}{\omega\eta} + \int_{-\infty}^{\infty} \frac{L(\tau)\omega\tau}{1 + \omega^2\tau^2} d \ln \tau \qquad (11)$$

$$\epsilon = J_g\sigma + R \int_{-\infty}^{\infty} L(\tau) \left[\frac{\sigma}{R} - \tau\left(1 - e^{-\sigma/R\tau}\right)\right] d \ln \tau + \frac{\sigma^2}{\eta R} \qquad (12)$$

Differentiating eq. (12) with respect to stress σ and substituting eq. (9) gives

$$\frac{d\epsilon}{d\sigma} = J\left(\frac{\sigma}{R}\right) + \frac{\sigma}{\eta R} \qquad (13)$$

Thus, $J(t)$ and stress-strain curves measured at constant loading rates can be interconverted in a manner similar to that described earlier for interconverting $G(t)$ and stress-strain curves measured at constant strain rates. To date, experimental data are not available which demonstrate the applicability of eqs. (12) and (13).

To obtain the difference between $J(t)$ and J', an equation analogous to eq. (7) can be derived. By assuming $L = g\tau^n$ over a narrow range of τ, the following is obtained:

$$J(t) = J' - L\left[\frac{\pi}{2}\csc\frac{n\pi}{2} + \Gamma(-n)\right] + \frac{t}{\eta} \quad -2 < n < 1 \tag{14}$$

This equation represents the integral when $-2 < n < 1$, and for $n = 0$, the quantity in the brackets again equals 0.5772.

The loss compliance J'' is likewise given by the approximate equation

$$J''(\omega) = \frac{1}{\omega\eta} + L\frac{\pi}{2}\sec\frac{n\pi}{2} \qquad -1 < n < 1 \tag{15}$$

APPROXIMATE EQUATIONS FOR INTERCONVERTING THE RELAXATION AND RETARDATION SPECTRA

Gross[4,5] has given the exact relations between the relaxation spectrum H and retardation spectrum L and these relations can be written as follows:

$$L(\tau) = \frac{H(\tau)}{\left[G_g - \int_{-\infty}^{\infty} \frac{H(\xi)}{1 - \xi/\tau}\, d\ln\xi\right]^2 + \pi^2 H^2(\tau)} \tag{16}$$

$$H(\tau) = \frac{L(\tau)}{\left[J_g + \int_{-\infty}^{\infty} \frac{L(\xi)}{1 - \xi/\tau}\, d\ln\xi - \tau/\eta\right]^2 + \pi^2 L^2(\tau)} \tag{17}$$

where the integrals are principal values. Although these equations are relatively simple, a series of graphical integrations are required to convert $H(\tau)$ into $L(\tau)$ and *vice versa*. As a result, these exact equations apparently have not been used, although Silva and Gross[12] have evaluated somewhat analogous equations to check the validity of the superposition principle applied to solid dielectrics. Their

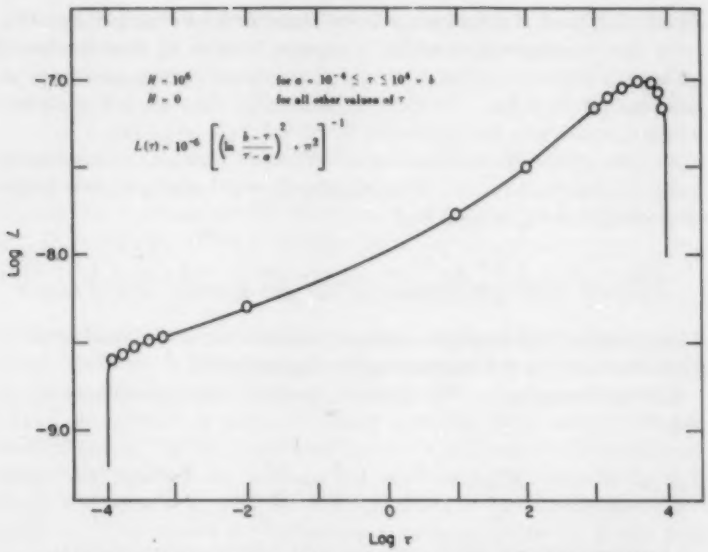

Fig. 1. Retardation spectrum L calculated exactly from a box relaxation spectrum H.

method shows that eqs. (16) and (17) can be evaluated, although the evaluation is tedious. Hence, the approximations to these equations, discussed subsequently, are not recommended when highly accurate conversions are desired.

Equations (16) and (17) can be integrated readily under the following two special conditions: (*1*) When either H or L is constant for $a \leq \tau \leq b$ and equals zero outside this range; and (*2*) when $H = k\tau^{-1/3}$ or $L = g\tau^{1/3}$ for $a \leq \tau \leq b$ and equals zero for all other values. (For H, these two cases correspond to the box and wedge distribution proposed by Tobolsky.[13]) When H is constant, integration of eq. (16) gives:

$$L(\tau) = \frac{1}{H\left[\left(\ln \frac{b-\tau}{\tau-a}\right)^2 + \pi^2\right]} \qquad a \leq \tau \leq b \qquad (18)$$

$$L(\tau) = 0 \quad \text{for } \tau < a \text{ and } \tau > b \qquad (18)$$

Figure 1 shows a plot of log L vs. log τ for eq. (18) with $H = 10^6$, $a = 10^{-4}$, and $b = 10^4$. It is seen that in the vicinity of log $\tau = -2$ the slope is about 0.15, and in the vicinity of log $\tau = 3$ the slope is about 0.3. The slope changes rapidly as log $\tau = 4$ is approached from the left and as log $\tau = -4$ is approached from the right. For log $\tau = -4$ and 4, L equals zero.

When $H = k\tau^{-1/2}$, integration of eq. (16) gives:

$$L(\tau) = \frac{1}{H(\tau)\left[\left(\ln \frac{\sqrt{b}+\sqrt{\tau}}{\sqrt{b}-\sqrt{\tau}} \cdot \frac{\sqrt{\tau}-\sqrt{a}}{\sqrt{\tau}+\sqrt{a}}\right)^2 + \pi^2\right]}$$

$$a \leq \tau \leq b \qquad (19)$$

$$L(\tau) = 0 \quad \text{for } \tau < a \text{ and } \tau > b$$

Figure 2 shows a plot of log L vs. log τ for eq. (19) with $H = 10^6\,\tau^{-1/2}$ for $-4 \leq \log \tau \leq 4$. It is seen that $L = 10^{-6}\,\tau^{1/2}/\pi^2$ accurately, except over about half a decade of τ near the extremes. This is expected since when $a \ll \tau \ll b$, eq. (19) reduces to $L = 1/\pi^2 H$.

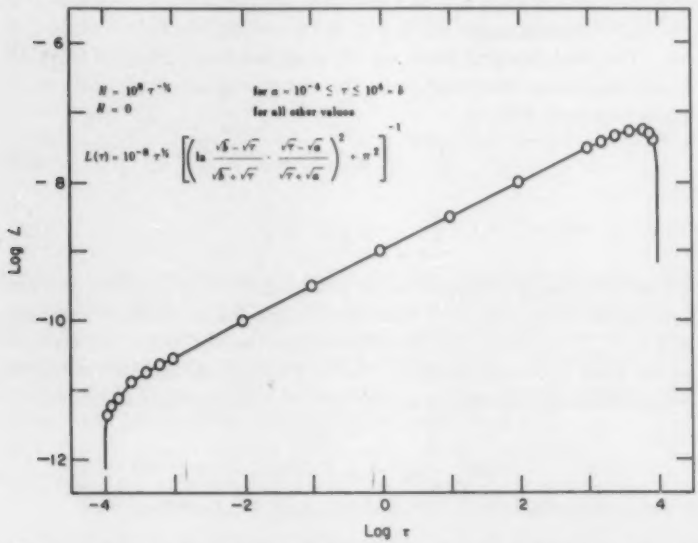

Fig. 2. Retardation spectrum L calculated exactly from a wedge relaxation spectrum H.

To obtain an approximate relation between H and L, eq. (16) can be written in the following form by recalling that the integral of $Hd \ln \tau$ over all values of τ equals $(G_\infty - G_o)$.

$$L(\tau) = \frac{H(\tau)}{\left[G_\infty - \int_0^\infty \frac{H(\xi)}{\tau - \xi}\, d\xi\right]^2 + \pi^2 H^2(\tau)} \tag{20}$$

Now, if we assume that $(\tau - \xi) = \tau$ when $\xi \leq 0.1\tau$ and that $(\tau - \xi) = -\xi$ when $\xi \geq 10\tau$, the integral in eq. (20) becomes:

$$\int_0^\infty \frac{H(\xi)}{\tau - \xi}\, d\xi = \int_0^{0.1\tau} \frac{H(\xi)}{\tau}\, d\xi + \int_{0.1\tau}^{10\tau} \frac{H(\xi)}{\tau - \xi}\, d\xi - \int_{10\tau}^{\infty} \frac{H}{\xi}\, d\xi \tag{21}$$

The first and third integrals on the right-hand side of eq. (21) can be written in terms of G' and G'' in the following way: Let us take eqs. (2) and (3) which define G' and G'' in terms of H and break both integrals up into three integrals which cover the same ranges of time (i.e., ξ) as used in eq. (21). After replacing in eqs. (2) and (3) the variable of integration τ with ξ and then setting $\omega = 1/\tau$, assume that $1 + (\xi/\tau)^2$ equals unity when $\xi \leq 0.1\tau$ and equals $(\xi/\tau)^2$ when $\xi \geq 10\tau$. The first integral from eq. (2) and the third integral from eq. (3) are negligible compared with the remaining integrals and can be equated to zero, i.e.,

$$\int_0^{0.1\tau} \frac{\xi}{\tau^2} H(\xi) d\xi = 0 \tag{22}$$

$$\int_{10\tau}^{\infty} \frac{\tau}{\xi^2} H(\xi) d\xi = 0 \tag{23}$$

To evaluate the two integrals over the range $0.1\tau \leq \xi \leq 10\tau$ and also the integral in eq. (21) over this same range, let us set H = constant for $0.1\tau \leq \xi \leq 10\tau$. (In this discussion, the symbols t, τ, and $1/\omega$ can be used interchangeably.) After evaluating the two integrals and substituting the results in eq. (20), the following is obtained:

$$L(\tau) = \frac{H(\tau)}{[G' - G'' + 1.37H(\tau)]^2 + \pi^2 H^2(\tau)} \tag{24}$$

By using a similar set of assumptions, eq. (17) becomes:

$$H(\tau) = \frac{L(\tau)}{[J' - J'' + 1.37L(\tau)]^2 + \pi^2 L^2(\tau)} \tag{25}$$

The numerical constant 1.37 comes from evaluating ($\tan^{-1} 10 - \tan^{-1} 0.1$) which more accurately equals 1.3714.

Although eqs. (24) and (25) give reasonably accurate transformations, as discussed subsequently, these equations are no doubt of limited practical value. This is true since if G' and G'' are known, J' and J'' can be calculated directly, and then $L(\tau)$ can be obtained from these by using the ordinary first and second approximation methods.[14-17,11] However, more useful equations can be obtained by substituting the quantities given by eqs. (7) and (8) for G' and G'' and the quantities given by eqs. (14) and (15) for J' and J''. These substitutions lead to the following equations:

$$L(\tau) = \frac{H(\tau)}{\left\{G(t) + H(\tau)\left[\frac{\pi}{2}\left(\csc\frac{m\pi}{2} - \sec\frac{m\pi}{2}\right) - \Gamma(m) + 1.37\right]\right\}^2 + \pi^2 H^2(\tau)} \qquad -1 < m < 1 \qquad (26)$$

$$H(\tau) = \frac{L(\tau)}{\left\{J(t) + L(\tau)\left[\frac{\pi}{2}\left(\csc\frac{n\pi}{2} - \sec\frac{n\pi}{2}\right) + \Gamma(-n) + 1.37\right] - 2t/\eta\right\}^2 + \pi^2 L^2(\tau)} \qquad -1 < n < 1 \qquad (27)$$

Thus, eq. (26) can be used to calculate $L(\tau)$ from experimental values of $G(t)$, although it is necessary first to calculate $H(\tau)$ from $G(t)$ by the common methods. In a similar manner, eq. (27) can be used to calculate $H(\tau)$ from experimental values of $J(t)$. After these calculations are made, either $J(t)$ or $G(t)$ can be calculated using equations, obtained by rearranging eqs. (26) and (27).

$$G(t) = \left[\frac{H(\tau)}{L(\tau)} - \pi^2 H^2(\tau)\right]^{1/2} - H(\tau)\left[\frac{\pi}{2}\left(\csc\frac{m\pi}{2} - \sec\frac{m\pi}{2}\right) - \Gamma(m) + 1.37\right] \qquad -1 < m < 1 \qquad (28)$$

$$J(t) = \left[\frac{L(\tau)}{H(\tau)} - \pi^2 L^2(\tau)^{1/2} - L(\tau)\left[\frac{\pi}{2}\left(\csc\frac{n\pi}{2} - \sec\frac{n\pi}{2}\right) + \Gamma(-n) + 1.37\right] + \frac{2t}{\eta} \qquad -1 < n < 1 \quad (29)$$

Another set of approximate equations interrelating the spectra can be derived by assuming that $H = k\xi^{-1/2}$ and $L = g\xi^{1/2}$ over the range $0.1\tau \leq \xi \leq 10\tau$, instead of assuming that H and L are constant over this range. In this way two sets of approximate equations could be obtained: the set given by eqs. (26) and (27) should be more accurate over the range of time in which H and L are more closely proportional to the zero power of ξ than to the $-1/2$ or $+1/2$ power of ξ; and the second set—not derived and tested in this paper—should be more accurate over the range of time in which H and L are more nearly proportional to the $-1/2$ or $+1/2$ powers of ξ than to the zero power.

RELATION BETWEEN STRESS RELAXATION MODULUS AND CREEP COMPLIANCE

Instead of using the continuous Maxwell and Voigt models to represent linear viscoelastic behavior, two equivalent expressions of the superposition principle can be used.[18,19,4,6] For a material in an unstressed state at zero time, these expressions are as follows:

$$\epsilon(t) = \int_0^t \frac{d\sigma(\xi)}{d\xi} J(t - \xi)d\xi \quad (30)$$

$$\sigma(t) = \int_0^t \frac{d\epsilon(\xi)}{d\xi} G(t - \xi)d\xi \quad (31)$$

Now, by taking the Laplace transforms of eqs. (30) and (31), the following single transform equation is readily obtained:

$$\bar{G}(p)\bar{J}(p) = 1/p^2 \quad (32)$$

The inverse transform of this equation is

$$\int_0^t G(\xi)J(t - \xi)d\xi = \int_0^t G(t - \xi)J(\xi)d\xi = t \quad (33)$$

This integral equation gives the relationship between $G(t)$ and $J(t)$. Further, it has been shown[19] that $J(t)G(t) \leq 1$. The inequality

holds in transition regions and the equality holds for equilibrium or quasi-equilibrium states. As a crude approximation, the equality holds, i.e., $J(t) = 1/G(t)$.

For certain functional forms of either $G(t)$ or $J(t)$, eq. (33) can be solved analytically to give the desired quantity. For example, if $G(t) = a(b/t)^m$, then eq. (33) can be solved readily to give

$$J(t) = \frac{\sin m\pi}{am\pi}\left(\frac{t}{b}\right)^m \tag{34}$$

For more detailed discussions and other examples, the reader is referred to the literature.[3,4,20,21]

TEST OF APPROXIMATE EQUATIONS

To test the various approximate equations that have been discussed, calculations were made using published data on the NBS polyisobutylene.[8] This uncrosslinked material has a viscosity-average molecular weight of 1.35×10^6 and has been studied extensively by various experimental techniques in a number of laboratories. Table I gives selected viscoelastic data, including the derived spectra H and L along with m and n. All data are reduced to 25°C. and at this temperature the polyisobutylene has a shear viscosity of 6.17×10^{10} poises. Since several sources of data exist, a certain amount of arbitrariness was used in selecting the data, especially in choosing values of H and L from literature data.

The stress relaxation modulus was measured by Tobolsky and Catsiff[22,9] and G'' and G' were measured by Fitzgerald and Ferry[23,24] and by Philippoff.[25] The values given in Table I for these three quantities were obtained by interpolating the data given in Table II of the paper by Tobolsky and Catsiff.[22] Values for G' and G'' at $\log t(\text{sec}) = 4$ and 5 were calculated by Tobolsky and Catsiff from their derived relaxation spectrum and are probably quite accurate, since at other values of time their calculated values agree very well with the experimental data. The values of J' and J'' were calculated directly from the values of G' and G'' listed in Table I. Since the stress relaxation data were measured in tension, they were converted into the shear modulus $G(t)$ by assuming $3G(t) = E(t)$. This assumption breaks down as the glasslike state is approached, but over the range of time covered in Table I, the assumption is quite accurate.

TABLE I

Viscoelastic Properties of the NBS Polyisobutylene at 25°C.

Log t, sec.	Log $G(t)$[a]	Log G'[a]	Log G''[a]	Log $J(t)$[b]	Log J'[c]	Log J''[c]	Log H[d]	m	Log L[d]	n
−9	9.85	—	9.41	—	—	—	9.18	−0.54	—	—
−8	9.57	9.62	9.51	−9.62	−9.83	−9.94	9.36	0.177	−10.37	0.513
−7	9.02	9.05	9.14	−9.19	−9.45	−9.36	8.84	0.600	− 9.84	0.540
−6	8.35	8.49	8.60	−8.63	−8.92	−8.80	8.25	0.647	− 9.27	0.587
−5	7.68	7.83	8.03	−8.00	−8.37	−8.17	7.60	0.700	− 8.70	0 657
−4	7.08	7.22	7.35	−7.36	−7.68	−7.53	6.90	0.633	− 7.92	0.680
−3	6.65	6.77	6.70	−6.81	−7.01	−7.08	6.30	0.577	− 7.32	0.440
−2	6.48	6.54	6.10	−6.50	−6.59	−7.03	5.73	0.503	− 7.21	−0.360
−1	6.42	6.45	5.56	−6.42	−6.46	−7.34	5.29	0.347	− 7.68	−0.705
0	6.39	6.41	5.35	−6.40	−6.41	−7.47	5.05	0.159	− 7.92	0.362
1	6.33	6.35	5.43	−6.32	−6.36	−7.30	5.15	−0.159	− 7.58	0.278
2	6.22	6.27	5.55	−6.23	−6.29	−7.00	5.31	−0.155	− 7.29	0.226
3	6.06	6.13	5.65	−6.08	−6.18	−6.67	5.43	−0.065	− 7.00	0.349
4	5.76	5.85[e]	5.52[e]	−5.82	−5.95	−6.26	5.41	0.077	− 6.62	0.434
5	5.19	5.34[e]	5.32[e]	−5.40	−5.62	−5.65	5.11	0.475	− 6.15	0.473

[a] Interpolated from experimental data given in Table II of Ref. 22.

[b] Calculated from $G(t)$ by Hopkins and Hamming.[26]

[c] Calculated from the values of G' and G'' listed in this table.

[d] For $\log t \leq -1$, values selected from data of Ferry, Grandine, and Fitzgerald.[24] For $0 \leq \log t \leq 5$, values reported by Marvin[8] but corrected by the second approximation method of Ref. 15.

[e] Values calculated by Tobolsky and Catsiff.[23]

Reliable experimental values for the creep compliance $J(t)$ are not available. However, Hopkins and Hamming[26] have recently calculated $J(t)$ from $G(t)$ by a numerical solution of eq. (33). Their values, listed in Table I, appear to be quite accurate and are used here in place of experimental data.

Values for the relaxation spectrum H for $-9 \leq \log t \leq -1$ were selected from the values reported by Ferry, Grandine, and Fitzgerald (FGF).[24] Values at longer times were obtained from the first-approximation data of Marvin[8] by applying the second-approximation method of Ref. 15. Similarly, values of the retardation spectrum over the range $-8 \leq \log t \leq -1$ were selected from the data of FGF, and for longer times the values were again obtained from the data of Marvin by applying the second-approximation correction.

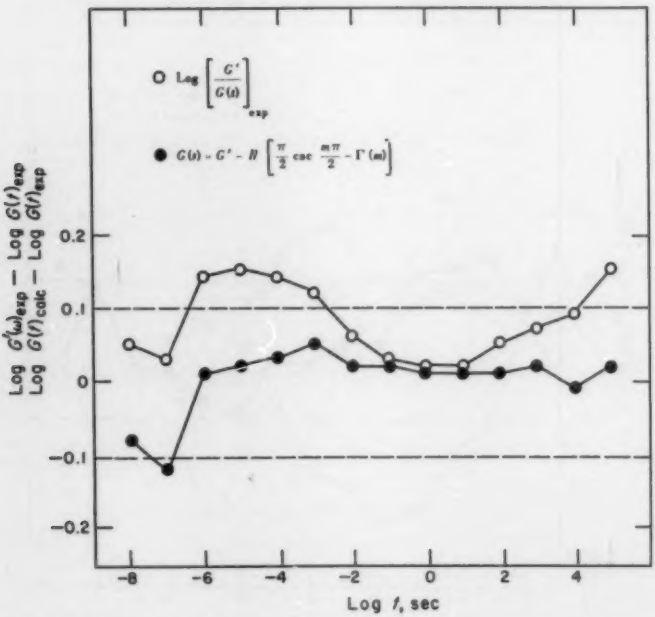

Fig. 3. Differences between experimental values of log G' and log $G(t)$ (○). Differences between experimental values of log $G(t)$ and values calculated from eq. (7) (●).

As a first approximation $G'(1/\omega)/G(t) = 1$, and the logarithm of this ratio is plotted as a function of log t in Figure 3. It is seen that this approximation is reasonably good but that the logarithm of the ratio becomes as large as 0.15 (at log $t = -5$) in the region of transition from rubberlike to glasslike properties and also at long times—the region of transition to liquidlike properties. $G(t)$ was also calculated from values of G', H, and m using eq. (7), and Figure 3 shows that the calculated and experimental values are in very close agreement, except at the shortest times. (The same calculations have been made and discussed previously by Catsiff and Tobolsky[9] but were repeated here.)

Figure 4 compares experimental values of log G'' with values calculated from eq. (8) and also with values calculated from the rough

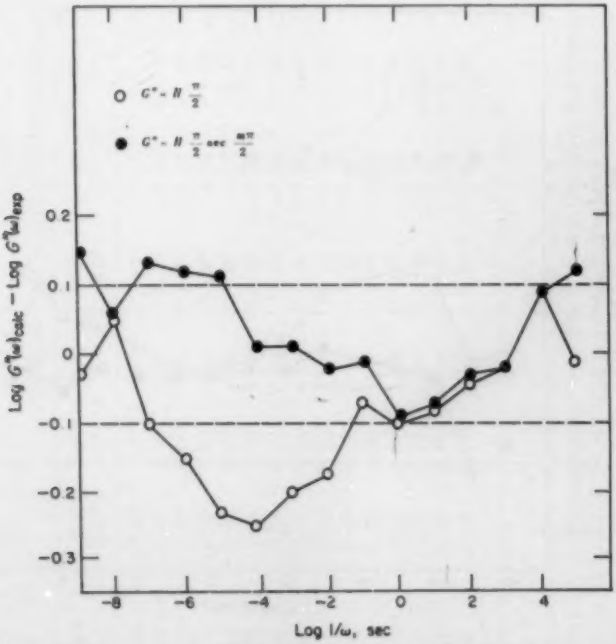

Fig. 4. Differences between experimental values of log G'' and log $H\pi/2$ (○), and values of log G'' calculated from eq. (8) (●).

approximate equation $G'' = \pi H/2$. It is seen that log G'' values calculated from eq. (8) deviate from the experimental values by less than 0.1 logarithmic units over most of the time scale. In evaluating the accuracy of all calculations discussed in this paper, deviations of 0.1 or less between the logarithms of the calculated and experimental quantities are considered to indicate satisfactory agreement. Such deviations might be expected due to some uncertainties in the experimental data and, more important, due to uncertainties in the spectra which have been derived from the experimental data by approximation methods.

Figure 5 shows the accuracy of the rough approximation $J(t) = 1/G(t)$ and that $J(t)$ and $1/G(t)$ can differ by a factor of two in the transition region. Using eq. (14), $J(t)$ was calculated from J', L, and n and the calculated values are compared in Figure 5 with the

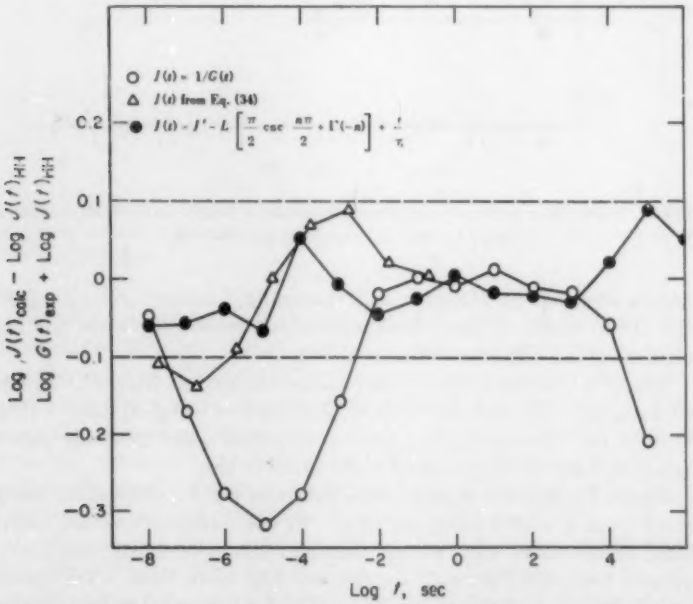

Fig. 5. Differences between log $1/G(t)$ and Hopkins and Hamming values of log $J(t)$ (○). Differences between Hopkins and Hamming values of log $J(t)$ and values calculated from eq. (34) (△) and from eq. (14) (●).

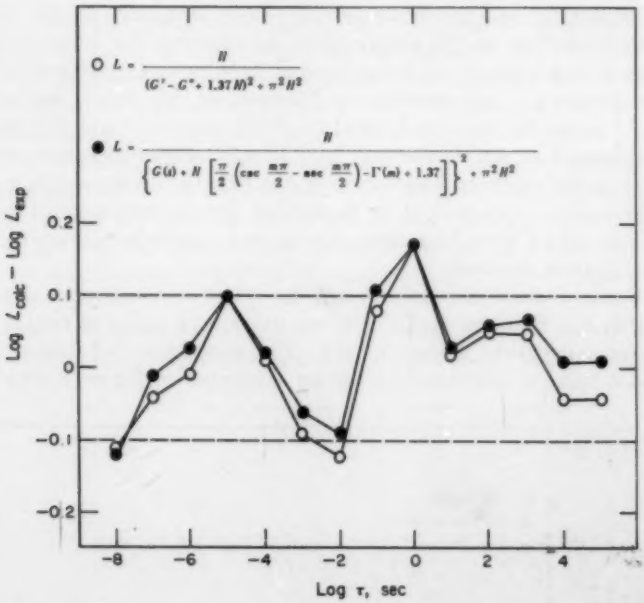

Fig. 6. Differences between experimental values of log L and values calculated from eq. (24) (○) and from eq. (26) (●).

values reported by Hopkins and Hamming,[26] labeled $J(t)_{HH}$. Over the entire range of time, the maximum difference between the logarithms of the two sets of values is 0.09.

Figure 6 compares log L with values calculated from H, G', and G'' using eq. (24), and also from $G(t)$, H, and m using eq. (26). Over most of the time range, the calculated values differ from the values listed in Table I by 0.1 logarithmic units or less.

Figure 7 compares experimental values of log J'' with values calculated from L and n using eq. (15). It also compares values calculated in the same way, except that the values of L calculated previously from $G(t)$, H, and m using eq. (26) were used. This latter calculation essentially means that only experimental values of $G(t)$ were used to calculate J''. For the most part, the agreement between calculated and experimental values is reasonably good.

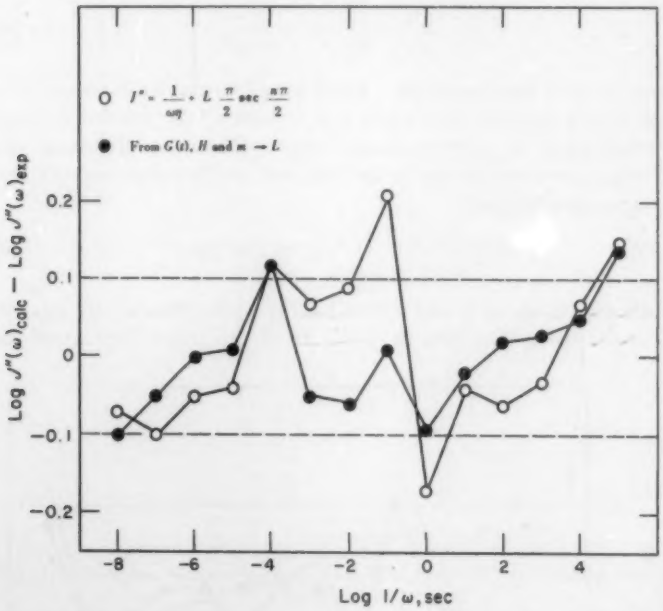

Fig. 7. Differences between experimental values of log J'' and values calculated from eq. (15) (○), and from eq. (15) but using values of L and n obtained from eq. (26) (●).

Figure 8 compares the values of log $J(t)$ given by Hopkins and Hamming with values calculated in two ways: (*1*) from values of H, L, and n using eq. (29), and (*2*) in the same way except that the values used for L and n were obtained from $G(t)$, H, and m using eq. (26). (Actually, smoothed values were used.) Again, at most values of time, the agreement between calculated and experimental values is moderately good. Figure 9 compares values of log H given in Table I with values calculated from L, J', and J'' using eq. (25).

In the present study, various direct methods for interconverting $G(t)$ and $J(t)$ were not carefully considered. However, eq. (34) was applied to the data on polyisobutylene in the rubber-to-glass transition zone. To do this, the experimental stress-relaxation data were first fitted to the following empirical equation:

$$\frac{E(t) - E_e}{E_g - E_e} = \frac{1}{1 + at^b} \tag{35}$$

where a and b are constants. Since experimental data measured in tension were reported by Catsiff and Tobolsky,[9] the symbol E is used here instead of G. This empirical equation has the advantage that the constants a and b can be determined readily, since eq. (35) can be rearranged to give

$$\log \frac{E_g - E(t)}{E(t) - E_e} = b \log t + \log a \tag{36}$$

To obtain values of a and b, the log-log plot indicated by eq. (36) was made using the data in Table II of the paper by Catsiff and

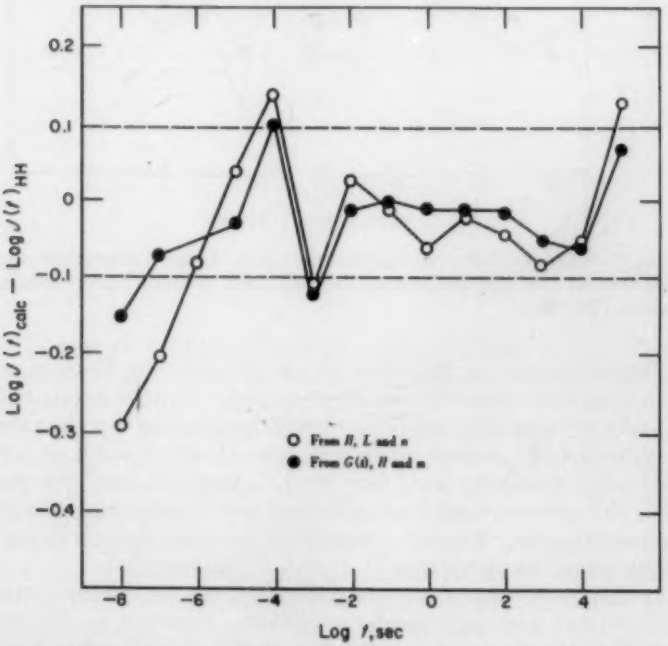

Fig. 8. Differences between Hopkins and Hamming values of log $J(t)$ and values calculated from eq. (29) (○), and from eq. (29) but using values of L and n obtained from eq. (26) (●).

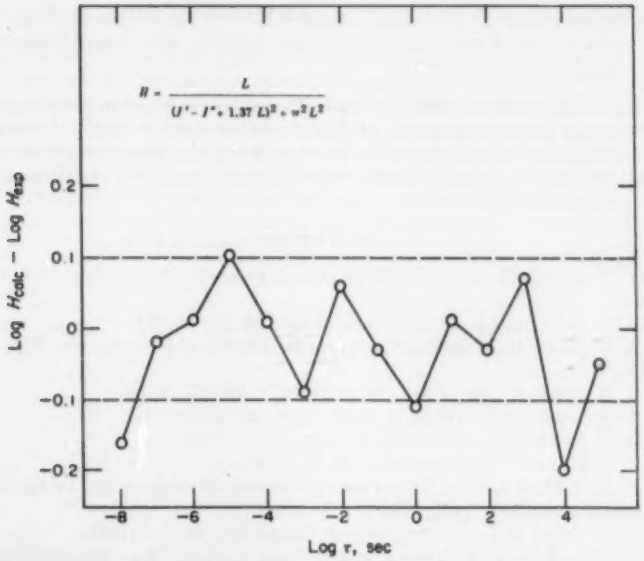

Fig. 9. Differences between experimental values of log L and values calculated from eq. (25).

Tobolsky[9] and log $E_g = 10.48$ and log $E_e = 6.88$. With time expressed in hours, the constants were found from the plot to be $a = 1.518 \times 10^8$ and $b = 0.6875$. With these values of a and b in eq. (35), values of $E(t)$ were then calculated at 45 different values of time in the range $-14.32 \leq \log t \leq -3.32$. The agreement between calculated and experimental values of $E(t)$ was excellent; the sum of the absolute values of the 45 deviations was 0.73. Catsiff and Tobolsky have used an equation of the Gauss Error Integral form to fit the same data, and from their calculations the sum of the deviations for the same set of time values is 0.89. (See Table II of Ref. 9.) Thus, eq. (35) fits the experimental data as well as, or perhaps slightly better than, the Gauss Error Integral equation.

Values of m needed to test eq. (34) were obtained by first differentiating eq. (35) to give $-m = d \log E(t)/d \log t$, and values of m were calculated from the resulting equation after substituting the known values of a and b. Values of $J(t)$ were calculated using eq. (34) and

are compared with the Hopkins and Hamming values in Figure 5. At most values of time, the two values differ by less than 0.1 logarithmic units.

The author wishes to thank Dr. R. F. Landel for assistance in assembling the data on the mechanical spectra of polyisobutylene and for helpful discussions. The author also expresses thanks to Mr. P. C. Hanzel for determining the convergence of certain expressions and to Mrs. Margaret Lecaro for carrying out the numerical calculations.

References

1. T. Alfrey, *Mechanical Behavior of High Polymers*, Interscience, New York, 1948.
2. T. Alfrey and P. Doty, *J. Appl. Phys.*, **16**, 700 (1945).
3. B. Gross, *Mathematical Structure of the Theories of Viscoelasticity*, Hermann & Cie, Paris, 1953.
4. B. Gross, *J. Appl. Phys.*, **18**, 212 (1947); **19**, 257 (1948).
5. B. Gross and H. Pelzer, *J. Appl. Phys.*, **22**, 1035 (1951).
6. H. Leaderman, *Trans. Soc. Rheology*, **1**, 213 (1957).
7. T. L. Smith, *J. Polymer Sci.*, **20**, 89 (1956).
8. R. S. Marvin, *Proc. Second Intern. Congress Rheology*, edited by Harrison, Academic Press, New York, 1954
9. E. Catsiff and A. V. Tobolsky, *J. Colloid Sci.*, **10**, 375 (1955).
10. D. G. Ivey, B. A. Mrowca, and E. Guth, *J. Appl. Phys.*, **20**, 486 (1949).
11. R. D. Andrews, *Ind. Eng. Chem.*, **44**, 707 (1952).
12. H. Silva and B. Gross, *Phys. Rev.*, **60**, 684 (1941).
13. A. V. Tobolsky, *J. Am. Chem. Soc.*, **74**, 3786 (1952).
14. For a general discussion see, A. J. Staverman and F. Schwarzl, Chap. I, *Die Physik der Hochpolymeren*, Vol. IV, H. A. Stuart, ed., Springer-Verlag, Berlin, 1956.
15. J. D. Ferry and M. L. Williams, *J. Colloid Sci.*, **7**, 347 (1952). M. L. Williams and J. D. Ferry, *J. Polymer Sci.*, **11**, 169 (1953).
16. F. Schwarzl, *Physica*, **17**, 830, 923 (1951).
17. F. Schwarzl and A. J. Staverman, *Physica*, **18**, 791 (1952).
18. H. Leaderman, *Elastic and Creep-Properties of Filamentous Materials and Other High Polymers*, Textile Foundation, Washington, D. C., 1943.
19. C. Zener, *Elasticity and Anelasticity of Metals*, Univ. Chicago Press, Chicago, 1948, p. 49.
20. R. Sips, *J. Polymer Sci.*, **5**, 69 (1950).
21. R. Simha, *J. Appl. Phys.*, **13**, 201 (1942).
22. A. V. Tobolsky and E. Catsiff, *J. Polymer Sci.*, **19**, 111 (1956).
23. E. R. Fitzgerald, L. D. Grandine, Jr., and J. D. Ferry, *J. Appl. Phys.*, **24**, 650 (1953).
24. J. D. Ferry, L. D. Grandine, Jr., and E. R. Fitzgerald, *J. Appl. Phys.*, **24**, 911 (1953).
25. Unpublished results. See Ref. 8.
26. I. L. Hopkins and R. W. Hamming, *J. Appl. Phys.*, **28**, 906 (1957).

Synopsis

Approximate equations are given for interconverting the storage modulus G', the loss modulus G'', and the stress relaxation modulus $G(t)$ by using the relaxation spectrum H, and similarly for interconverting the storage compliance J'', the loss compliance J'', and the creep compliance $J(t)$ by using the retardation spectrum L. Approximations to the exact equations of Gross are also given for interconverting H and L. All approximate equations are based on the assumption that $H = k\tau^{-n}$ and $L = g\tau^{n}$ over a relatively narrow region of the time-scale. To indicate the accuracy of the approximate equations, calculations were made using published data on the NBS polyisobutylene.

TRANSACTIONS OF THE SOCIETY OF RHEOLOGY II, 153–174 (1958)

The Principles of Plastico-Dynamics*

COSIMO TORRE,† *Department of Mechanical Engineering, Syracuse University, Syracuse, New York*

I. INTRODUCTION

An important problem in mechanics of continua is the *strength problem* for an arbitrary body, solid, fluid (liquid or gaslike), or cohesionless, which has been loaded by static or dynamic forces. A solution of this problem is not just the knowledge of the six stresses $\sigma_x, \ldots, t_{xy}, \ldots$ as functions of x, y, z, and t. It also includes the computation of the magnitude of the strength in comparison with a one-dimensional stress and the locus (x, y, z) at which the greatest strength of the loaded body occurs.

The general formulation of the strength problem includes the limit (or so-called "ultimate") strength which occurs not only in the range of plastic deformations and fracture but also in the range of elastic deformations. In other words, the principles of plastico-dynamics are the same as the principles of the strength problem of a solid or fluid body.

The equation of the limit strength (limiting condition) is mathematically a function of stresses, or of velocities and their gradients, and also of the pressure and density. It corresponds to the equation of state of matter (specifying equation[3]) in the dynamics of compressible fluids.

The authors of modern books on theoretical physics do not consider the strength problem. They stop their investigations when stresses, deformations, or vibrations have been computed. However, in gas dynamics the characteristics, which correspond to Mach lines, do represent a partial solution of the strength problem. The characteristics are the locus of the greatest strength.

* This paper was presented at the meeting of The Society of Rheology under a different title.

† Present address: Research and Development Laboratory, M. W. Kellogg Company, Jersey City, New Jersey.

St. Venant and Levy (1870) investigated the plane and the three-dimensional problem of plastico-dynamics. For these data see Nadai (ref. 1, pp. 527 and 530 and ref. 2, p. 465). Mises[3] and Hencky[4] have made suggestions for the solution of the three-dimensional problem of plastico-dynamics. Geiringer[5] investigated the plane problem, neglecting the acceleration terms in the equation of motion but considering the rate of strains in the stress-rate of strains relations. Therefore, these papers investigate the creeping flow of a plastic mass corresponding to the creeping flow in hydrodynamics.

Some results in the plane case of plastico-dynamics were computed by the author.[6] In these papers the author analyzes the stress circles of Mohr which are identical with Cauchy's stress relations. Since these relations are valid for a body under static or dynamic conditions, so also the equations computed by the author are valid in both the dynamic and the static case. They are valid for isotropic and anisotropic materials if the limiting condition is given in a general functional relation, and also for all kind of bodies: solids, fluids, and cohesionless materials.

Section II of this paper will discuss the general equations governing plastico-dynamics. Section III will contain a computation of the characteristics and velocities for the three-dimensional problems assuming a constant density. The limiting condition will be expressed in terms of velocities v_x, v_y, v_z. There will be some discussion of the plane strain problem in Section IV.

SYMBOLS

x, y, z, t = cartesian coordinates of space and time.

$\bar{i}, \bar{j}, \bar{k}$ = unit vectors in the x, y, z directions.

$\bar{r} = \bar{i}x + \bar{j}y + \bar{k}z$ = position vector.

u, v, w = displacements in the x, y, z directions.

$\bar{u} = \bar{i}u + \bar{j}v + \bar{k}w$ = displacement vector.

v_x, v_y, v_z = velocities in the x, y, z directions.

$\bar{v} = \bar{i}v_x + \bar{j}v_y + \bar{k}v_z$ = velocity vector.

$\sigma_x, \sigma_y, \sigma_z$ = normal stresses in the x, y, z directions.

$t_{xy} = t_{yx}$; $t_{yz} = t_{zy}$; $t_{zx} = t_{xz}$ = shear stresses in the x, y, z directions.

$\bar{S} = \bar{i}\bar{i}\sigma_x + \ldots + (\bar{i}\bar{k} + \bar{k}\bar{i})t_{xz}$ = stress dyadic.

$\epsilon_x, \epsilon_y, \epsilon_z$ = normal strains in the x, y, z directions; that is $\epsilon_x = \partial u/\partial x$ etc.

$\gamma_{xy} = \gamma_{yx}$; $\gamma_{yz} = \gamma_{zy}$; $\gamma_{zx} = \gamma_{xz}$ = shear strains in the x, y, z directions; that is, $\gamma_{xy} = {}^1/_2(\partial v/\partial x + \partial u/\partial y)$ etc.

$\bar{V} = \bar{i}\bar{i}\epsilon_x + \ldots + (\bar{i}\bar{k} + \bar{k}\bar{i})\gamma_{xz} +$ = strain dyadic.

$\dot{\epsilon}_x, \ldots, \dot{\gamma}_{xy}, \ldots$ = rate of normal and shear strains respectively; that is, $\dot{\epsilon}_x = \partial v_x/\partial x, \ldots, \dot{\gamma}_{xy} = {}^1/_2(\partial v_y/\partial x + \partial v_x/\partial y)$ etc.

$\dot{V} = \bar{i}\bar{i}\dot{\epsilon}_x + \ldots + (\bar{i}\bar{k} + \bar{k}\bar{i})\dot{\gamma}_{xz} +$ = rate of strains dyadic.

$\bar{J} = \bar{i}\bar{i} + \bar{j}\bar{j} + \bar{k}\bar{k}$ = unit dyadic.

$\omega_x, \omega_y, \omega_z$ = vortices in the x, y, z directions; that is $\omega_z = {}^1/_2(\partial v_y/\partial x - \partial v_x/\partial y)$ etc.

$\omega = \bar{i}\omega_x + \bar{j}\omega_y + \bar{k}\omega_z$ = vector of the vortex.

$\sigma_m = {}^1/_3(\sigma_x + \sigma_y + \sigma_z)$ = mean stress.

$p = -\sigma_m$ = mean pressure.

ρ = density.

μ, λ = viscosity coefficients.

$\nu = \mu/\rho$ = kinematical viscosity coefficient.

$\nabla = \bar{i}\partial/\partial x + \bar{j}\partial/\partial y + \bar{k}\partial/\partial_z$ = formal vector of differentiation.

$\Delta = \nabla.\nabla = \partial^2/\partial x^2 + \partial^2/\partial y^2 + \partial^2/\partial z^2$ = Laplace operator.

"." = the "dot" represents the scalar product.

"$\times$" = the "cross" represents the vector product.

$\bar{f} = \bar{i}X + \bar{j}Y + \bar{k}Z$ = vector of mass forces.

II. GENERAL FORMULATION OF PLASTICO-DYNAMICS

The complete system of the equations of motion of a plastic mass, written in the form of symbolic tensor calculus in cartesian coordinates, reads:

(*a*) The general equation of motion of a continuum

$$\rho \frac{d\bar{v}}{dt} = \nabla.\bar{S} + \bar{f} \tag{1}$$

(*b*) The continuity equation

$$\frac{\partial \rho}{\partial t} + \nabla.(\rho\bar{v}) = 0 \tag{2}$$

(*c*) The condition of the limit (ultimate) strength of materials (the limiting condition)

$$f(\sigma_x, \sigma_y, \sigma_z, t_{xy}, t_{yz}, t_{zx}) = 0 \tag{3}$$

(*d*) The stress-rate of strain relations (proposed by Stokes)

$$S = 2\mu\dot{V} + (-p + \lambda\nabla.\bar{v})\bar{J} \tag{4}$$

Equations (1) to (4) represent eleven equations in eleven unknowns; six stresses, σ_x, σ_y, σ_z, t_{xy}, t_{yz}, t_{zx}; three velocities, v_x, v_y, v_z; the value p; and the density ρ.

Criticism of eqs. (1) to (4) will be brought out in the following discussion.

The clarification of the relation of p and λ in eq. (4) will be made here as a purely formal but important step. The value

$$p = -\sigma_m + (^2/_3\mu + \lambda)\nabla.\bar{v} \tag{5}$$

is obtained by addition of the terms in the principal diagonal of the stress-rate of strain tensor matrix. Equation (5) is a known formula in which Stokes put $\lambda = -2\mu/3$ to show that the value p will be equal to the mean stress $-\sigma_m$.

In general a dependence of p upon σ_m, μ, λ, and $\Delta.\bar{v}$, as given in eq. (5), does not exist because if we substitute eq. (5) in eq. (4) we can eliminate the second viscosity coefficient λ and work with the mean stress σ_m and with only one viscosity coefficient μ. Similarly, in the theory of elasticity the lateral contraction number "m" can be eliminated. With the usual notation $\sigma_m = -p$, eq. (4) now reads

$$S = 2\mu\dot{V} - (p + {}^2/_3\mu\nabla.\bar{v})\bar{J} \tag{6}$$

In the place of eq. (6) we can use the following equivalent expression

$$S = 2\mu\dot{V} + \lambda\nabla.\bar{v}\bar{J} \tag{7}$$

The remarks of Sommerfeld[7] (p. 78) that $\lambda = -2\mu/3$ is valid for a monoatomic gas, may be correct for eq. (7) but not for eq. (4).

Equation (6) will most frequently be used in hydrodynamics, while eq. (7) is used in solid mechanics, as for instance in rheology (see ref. 9). The stress-strain relations

$$S = 2\mu_0\dot{V} + \lambda_0\nabla.\bar{v}\bar{J} \tag{7a}$$

proposed by Hooke, are the only relations which are completely independent from stress-rate of strain relations eq. (7). The dimensions of μ_0 and λ_0 in eq. (7a) are $[PL^{-2}]$, those of μ and λ in eqs. (6) and (7), $[PTL^{-2}]$. Other relations used in rheology (Maxwell's relations and others) are combinations of eqs. (7) and (7a). Equation (7) was first

proposed by Newton as a relation between the shear stress and rate of shear strain. Later it was extended by Stokes to a tensor relation eq. (6) of second rank and of dimension three.

Equation (7a) will be applied for an elastic body. It expresses the elastic behavior of matter in which the increasing stresses also cause increasing strains. Vice versa, the vanishing stresses cause the vanishing strains. Therefore, the reversibility of eq. (7a) corresponds to the physical behavior of an elastic body. However, eq. (7) is also a reversible stress-rate of strains relation although it will represent dissipative nonreversible processes in physics. Substituting eq. (7) in the eq. (1) of motion, we obtain a parabolic differential equation in $\bar{v}$ whose solution contains a time decay corresponding to the physical process of dissipation. On the other hand, substituting eq. (7a) in the eq. (1) of motion we obtain a hyperbolic differential equation in $\bar{u}$ whose solution contains periodic functions of time corresponding to the behavior of an elastic body. We see that the eq. (1) of motion actually decides which relation will be used for elastic and which for dissipative processes and not the relation as such without the equations of motion. This should be considered in the developing science of rheology.

If we subtract on the left and right of eq. (7) the expression

$$\sigma_m = (^2/_3\mu + \lambda)\nabla.\bar{v} \tag{5a}$$

we obtain eq. (6), taking $\sigma_m = -p$.

The equations above are valid for small deformations.

Substituting eq. (6) in eqs. (1) and (3), we reduce the system of eleven equations to a system of five equations in five unknowns: v_x, v_y, v_z, p, and ρ. Therefore, the new system of equations, without mass forces, reads

$$\rho \frac{d\bar{v}}{dt} = \mu\Delta\bar{v} - \nabla p + \frac{\mu}{3}\nabla(\nabla.\bar{v}) \tag{8}$$

$$\frac{\partial\rho}{\partial t} + \nabla.(\rho\bar{v}) = 0 \tag{9}$$

$$f\left(\frac{\partial v_x}{\partial x}, \ldots, p, \rho\right) = 0 \tag{10}$$

Using eq. (7) instead of eq. (6), eq. (8) reads

$$\rho \frac{d\bar{v}}{dt} = \mu \Delta \bar{v} + (\mu + \lambda) \nabla (\nabla . \bar{v}) \tag{11}$$

This equation is used for the most part in solid mechanics.

Equations (8), (9), and (10) are *equations of motion of a plastic mass* which permit the computation of magnitude of the strength of a loaded body and the locus of the greatest strength. The boundary conditions may be formulated separately for each problem. In solids the boundary conditions are usually given in terms of stresses, but they can also be given in terms of velocities (as in hydrodynamics), or in terms of displacements.

Equations (8), (9), and (10) are formally similar to the equations of motion of compressible frictional fluids. An interpretation of these equations follows in a discussion of the similarities and differences between the flow of a fluid and of a plastic mass. This is also a continuation of the criticism mentioned after eq. (4).

The appearance of the limiting condition eq. (10) instead of the equation of state of matter, which is usually given in terms of pressure and density $p(\rho)$, does not represent here a difference between fluid flow and motion of a plastic mass. The function $p = p(\rho)$ is only a special case of a general "specifying" equation which can be taken as a function of p, ρ, $\bar{v}$, $\bar{r}$, and t, and also of the velocity gradients; see v. Mises (ref. 8, p. 6). From a general point of view, eq. (10) can be taken also as the specifying condition in hydrodynamics.

A difference between fluids and solids is to be found, of course, in the magnitude of the viscosity coefficient μ. It is very large in solids, so that in solids only small velocities are possible; however, the acceleration terms in eq. (8) cannot be neglected without further consideration.[9] On the other hand, the small viscosity of fluids permits their velocities to be large.

Further differences are to be found in the interpretation of the expression "p." In fluid dynamics or statics it is still a pressure, although it represents the mean stress σ_m. Only on the upper free surface of a fluid can it be equal to zero (neglecting the atmospheric pressure). In solids the mean stress p represents in general a tension or a compression stress. It is equal to zero on the stress-free surfaces of a solid body if mass forces are neglected. In the static case a solid exerts a resistance against shearing forces while in a fluid only the principal normal stresses $\sigma_1 = \sigma_2 = \sigma_3 = -p$ are to be found.

In the special case of an *incompressible* fluid or solid further differences are to be considered. In the dynamics of fluids the assumption of a constant density (ρ = constant) replaces the specifying eq. (10) while the continuity equation now reads $\nabla . \bar{v} = 0$. However, for the computation of the general case of the strength of a material body, which may be taken as a fluid or solid, a very different situation is to be considered, namely that the expression $\nabla . \bar{v} = 0$ represents a special case of the limiting condition eq. (10) for an ideal plastic body. It is only a kinematical condition without any physical constants. Therefore one of these two eqs. (9) and (10) cannot be accepted. It is clear that we shall work with eq. (10), which in a special case will be represented by special functions set up from a physical point of view, while the condition $\nabla . \bar{v} = 0$ is only a kinematical equation as mentioned above.

Mises[3] in 1913 proposed equations of motion of a plastic mass in the three dimensional case. He applied eqs. (1) and (4) and worked with the value p. For ρ = constant he considered both eq. (2) and eq. (3); namely, the continuity equation for an incompressible fluid and the yield condition for an ideal plastic body. Considering the equation $\nabla . \bar{v} = 0$, Mises obtained ten unknowns but eleven equations. To remove this indeterminacy he took as an eleventh unknown the viscosity coefficient μ. The second viscosity coefficient λ does not appear, because of $\nabla . \bar{v} = 0$. The viscosity coefficient μ now becomes a function of the rate of strains $\partial v_x/\partial x$, etc. Thus for instance the stress $\sigma_x = 2\mu(\partial v_x/\partial x, \ldots).\partial v_x/\partial x + \ldots$. In other words, we have here a function of the form $y = y(x).x$, which can be written simply $y = y(x)$. (See also Schultz-Grunov.[10]) Similar proposals for a variable coefficient μ were made by many other authors. Nadai[11] has given numerical results for a few cases. However, μ can be a given function of $\bar{r}$ and t.

The next question is the acceleration term $d\bar{v}/dt$. It was taken from the dynamics of rigid bodies. Since, in a continuum, the velocity $\bar{v}$ is a continuous function of $\bar{r}$ and t with at least continuous first partial derivatives, it is possible to write

$$\frac{d\bar{v}}{dt} = \frac{\partial \bar{v}}{\partial t} + \frac{d\bar{r}}{dt} \cdot (\nabla \bar{v}) \tag{11a}$$

The question is, does $d\bar{r}/dt$ represent a velocity in a continuum? Since the definition of velocity in continua is the derivative of the

displacement $\bar{u}$ with respect to time t: $\bar{v} = d\bar{u}/dt$. We cannot replace $d\bar{u}$ by $d\bar{r}$ because there is a large difference between these two values, since

$$d\bar{u} = (\nabla\bar{u})\cdot d\bar{r} \tag{12}$$

There, the dyadic $(\nabla\bar{u})$ contains normal and shearing strains and rotations:

$$(\nabla\bar{u}) = \bar{i}\bar{i}\frac{\partial u}{\partial x} + \ldots + \bar{j}\bar{i}\frac{\partial u}{\partial y} + \bar{i}\bar{j}\frac{\partial v}{\partial x} + \ldots =$$
$$\bar{i}\bar{i}\epsilon_x + \ldots + (\bar{i}\bar{j} + \bar{j}\bar{i})\gamma_{xy} + (\bar{i}\bar{j} - \bar{j}\bar{i})\varphi_z + \ldots$$

where

$$\varphi_z = \frac{1}{2}\left(\frac{\partial v}{\partial x} - \frac{\partial u}{\partial y}\right)$$

is a very small angle of rotation and $\omega_z = \dot{\varphi}_z$.

Work on hydrodynamics usually contains the assumption $\bar{v} = d\bar{r}/dt$ without a statement of a satisfactory derivation. Lagally (ref. 12, p. 251) has written a noteworthy article about the time dependent displacements, but finally he uses $\bar{v} = d\bar{r}/dt$. Lamb (ref. 13, p. 3) asserts that any function $F(\bar{r}, t)$ has a convective term $\bar{v}.(\nabla F)$. However, this is not the case with the function of the displacement vector $\bar{u}$ which also depends upon $\bar{r}$ and t. Thus, since $\bar{v} = d\bar{u}/dt = \partial\bar{u}/\partial t + \bar{v}.(\nabla\bar{u})$, we obtain further difficulties. Lamb also assumed that the infinitesimal increase of $\bar{r}$ is equal to $\bar{v}dt$, while $\bar{v}dt$ is actually equal to $d\bar{u}$ but not to $d\bar{r}$. It is $\bar{r} + d\bar{r}$ but not $\bar{r} + d\bar{u}$.

Lagrange derived the equation of motion of a continuum by computing the motion of a fluid particle. He now loses the independent variables x, y, z since they are functions of t only. To replace this loss, he took the (initial) coordinates called a, b, c of the particle as independent variables. The acceleration here reads $\partial^2\bar{r}/\partial t^2$, but the function $\bar{r}$ which is to be computed also appears in the denominator of $\partial p/\partial\bar{r}$. The new variables a, b, c helped to put $\bar{r}$ in the numerator. For Lagrange's equations see for example Lamb (ref. 13, pp. 12, 13).

Expressing the momentum in the form of a differential equation and using the *continuity equation*, Oswatitsch (ref. 14, p. 34) obtains the convective term of acceleration for the one dimensional flow: $v_x dv_x/dx$. The other two terms in the x direction for a three-dimen-

sional flow, namely $v_y \partial v_x/\partial y$ and $v_z \partial v_x/\partial z$, can be expressed as a product of the velocities v_y and v_z and the tangents $\partial v_x/\partial y$ and $\partial v_x/\partial z$ of the angle between the velocity profile $v_x(x, y, z)$ and the directions y and z, respectively. So far as we are concerned, this appears to be only a partially satisfactory derivation of the convective terms of acceleration in a continuum.

Equation (11a) written in the form

$$\frac{d\bar{v}}{dt} = \frac{\partial \bar{v}}{\partial t} + \bar{v}.(\nabla \bar{v}) \tag{13}$$

is useful, for instance, in the investigation of laminar stationary jets and wakes flow.

To justify the change from $d\bar{u}$ to $d\bar{r}$ in the equation of velocity in a continuum, it is often explained that we are dealing with moving coordinates fixed on a fluid element. This assumption implies that the strains and stresses are related to deformed lengths and areas, respectively, of an instantaneous volume element. These strains and stresses are called *natural* strains and *true* stresses (see Nadai, ref. 2, pp. 74, 130, and 71, respectively), and will be used mostly for large deformations. Neither is applied yet in hydrodynamics.

III. THE THREE DIMENSIONAL PROBLEM

As mentioned in Section I, the knowledge of six stresses, three velocities, p and ρ as functions of x, y, z, and t is not a solution of the strength problem. The solution is closely connected with the general problem of plastico-dynamics. There remains the computation of the greatest strength of a loaded body and the locus at which the greatest strength occurs.

In this section we will assume that the density ρ is constant and we will neglect the expression $\nabla.\bar{v} = 0$ as a duplication of the limiting condition; eq. (14) can be assumed as a generalization of $\nabla.\bar{v} = 0$. It will also be assumed that $d\bar{v}/dt = \partial\bar{v}/\partial t$. We shall compute the differential equations of the characteristics whose solutions correspond (*1*) to the slip lines in the range of plastic deformation, (*2*) to cracks in the case of fracture, or, in general, (*3*) to the locus of greatest strength. The value of the greatest strength is to be computed immediately from the limiting condition, which can be applied also to a loaded elastic solid body.

The limiting condition eq. (10) will be expressed in terms of velocities. It reads

$$v_z = v_z(v_x, v_y) \tag{14}$$

Each term in eq. (8) will be multiplied by $\nabla\times$, so that

$$\nabla\times\bar{v} = 2\bar{\omega}, \qquad \nabla\times\nabla = 0 \tag{15}$$

Then eq. (8) reads

$$\rho\frac{\partial\bar{\omega}}{\partial t} = \mu\Delta\bar{\omega} \tag{16}$$

$\nabla\times\rho$, the rotor of a scalar, is not defined. The density ρ can be taken as a given scalar function of $\bar{r}$ and t.

The three eqs. (16) contain three unknowns v_x, v_y, v_z. These three unknowns cannot be computed from eqs. (16), because $\nabla.\bar{\omega} \equiv 0$; divrotor of any vector is equal to zero. To overcome this difficulty, we will consider the following. Also the creeping flow ($\partial\bar{\omega}/\partial t = 0$) can be considered using the potential differential equation $\Delta\bar{\omega} = 0$ instead of eq. (16) without changing the theoretical results in eqs. (20) to (23).

The three eqs. (16) are parabolic differential equations and, in the present case, they are valid for dissipative frictional processes. Their solutions are well known, and are formally the same as the solutions of the differential equations for heat transfer or diffusion. The solutions can be found using Fourier's series or also other additional solutions which are described in treatises on differential equations; see for instance Webster.[15]

We will carry out further derivations using only the remark that the solutions of eqs. (16) are known and that they are in general (neglecting "$^1/_2$")

$$\frac{\partial v_z}{\partial y} - \frac{\partial v_y}{\partial z} = \omega_x(x, y, z, t) \tag{17a}$$

$$\frac{\partial v_x}{\partial z} - \frac{\partial v_z}{\partial x} = \omega_y(x, y, z, t) \tag{17b}$$

$$\frac{\partial v_y}{\partial x} - \frac{\partial v_x}{\partial y} = \omega_z(x, y, z, t) \tag{17c}$$

Considering eq. (14) we obtain from eqs. (17a and 17b)

$$\frac{\partial v_z}{\partial v_x}\frac{\partial v_z}{\partial y} + \frac{\partial v_z}{\partial v_y}\frac{\partial v_y}{\partial y} - \frac{\partial v_y}{\partial z} = \omega_x(x, y, z, t) \tag{18}$$

$$\frac{\partial v_z}{\partial v_x}\frac{\partial v_z}{\partial x} + \frac{\partial v_z}{\partial v_y}\frac{\partial v_y}{\partial x} - \frac{\partial v_z}{\partial z} = -\omega_y(x, y, z, t) \tag{19}$$

The term $\partial v_y/\partial x$ from eq. (17c) will be substituted in eq. (19) and the term $\partial v_z/\partial y$ from eq. (17c) will be substituted in eq. (18). Thus we obtained the following two quasi-linear differential equations of first order in v_x and v_y separately:

$$F \equiv \frac{\partial v_z}{\partial v_x}\frac{\partial v_x}{\partial x} + \frac{\partial v_z}{\partial v_y}\frac{\partial v_x}{\partial y} - \frac{\partial v_x}{\partial z} + \frac{\partial v_z}{\partial v_y}\omega_z + \omega_y = 0 \tag{20}$$

$$G \equiv \frac{\partial v_z}{\partial v_x}\frac{\partial v_y}{\partial x} + \frac{\partial v_z}{\partial v_y}\frac{\partial v_y}{\partial_y} - \frac{\partial v_y}{\partial z} - \frac{\partial v_z}{\partial v_x}\omega_z - \omega_x = 0 \tag{21}$$

$F = 0$ and $G = 0$ are Hamilton-Jacobi differential equations.

Using s as a parameter, the differential equations of characteristics obtained from eqs. (20) and (21), which are Hamilton's or canonic differential equations (in particle mechanics s is to be replaced by t), read [cf. Lense (ref. 16, pp. 104–105; Webster (ref. 15, p. 73)]

$$\frac{dx}{ds} = \frac{\partial v_z}{\partial v_x} \tag{22a}$$

$$\frac{dy}{ds} = \frac{\partial v_z}{\partial v_y} \tag{22b}$$

$$\frac{dz}{ds} = -1 \tag{22c}$$

$$\frac{dv_x}{ds} = -\frac{\partial v_z}{\partial v_y}\omega_z - \omega_y \tag{22d}$$

$$\frac{d}{ds}\left(\frac{\partial v_z}{\partial x}\right) = -\frac{\partial}{\partial x}\left(\frac{\partial v_z}{\partial v_y}\omega_z + \omega_y\right) \tag{22e}$$

$$\frac{d}{ds}\left(\frac{\partial v_z}{\partial y}\right) = -\frac{\partial}{\partial y}\left(\frac{\partial v_z}{\partial v_y}\omega_z + \omega_y\right) \tag{22f}$$

$$\frac{d}{ds}\left(\frac{\partial v_x}{\partial z}\right) = -\frac{\partial}{\partial z}\left(\frac{\partial v_z}{\partial v_y}\,\omega_z + \omega_y\right) \tag{22g}$$

$$\frac{dx}{ds} = \frac{\partial v_z}{\partial v_x} \tag{23a}$$

$$\frac{dy}{ds} = \frac{\partial v_z}{\partial v_y} \tag{23b}$$

$$\frac{dz}{ds} = -1 \tag{23c}$$

$$\frac{dv_y}{ds} = \frac{\partial v_z}{\partial v_x}\,\omega_z + \omega_x \tag{23d}$$

$$\frac{d}{ds}\left(\frac{\partial v_y}{\partial x}\right) = \frac{\partial}{\partial x}\left(\frac{\partial v_z}{\partial v_x}\,\omega_z + \omega_x\right) \tag{23e}$$

$$\frac{d}{ds}\left(\frac{\partial v_y}{\partial y}\right) = \frac{\partial}{\partial y}\left(\frac{\partial v_z}{\partial v_x}\,\omega_z + \omega_x\right) \tag{23f}$$

$$\frac{d}{ds}\left(\frac{\partial v_y}{\partial z}\right) = \frac{\partial}{\partial z}\left(\frac{\partial v_z}{\partial v_x}\,\omega_z + \omega_x\right) \tag{23g}$$

Here $x = x(s)$, $y = y(s)$, $z = -s$; $v_x(s)$ or $v_y(s)$ are integral curves. Equations (22e–g) and (23e–g) say the same as eqs. (22d and 23d), respectively. If dS is the arc element and s the parameter, we obtain

$$\frac{dS}{ds} = \pm\sqrt{1 + \left(\frac{\partial v_z}{\partial v_x}\right)^2 + \left(\frac{\partial v_z}{\partial v_y}\right)^2} \tag{23h}$$

The direction cosines at any point of the characteristics are

$$\cos\alpha = \frac{dx}{dS} = \frac{dx/ds}{dS/ds} = \pm\frac{\partial v_z}{\partial v_x}\Big/\sqrt{1 + \left(\frac{\partial v_z}{\partial v_x}\right)^2 + \left(\frac{\partial v_z}{\partial v_y}\right)^2}$$

$$\cos\beta = \frac{dy}{dS} = \pm\frac{\partial v_z}{\partial v_y}\Big/\sqrt{1 + \left(\frac{\partial v_z}{\partial v_x}\right)^2 + \left(\frac{\partial v_z}{\partial v_y}\right)^2}$$

$$\cos\gamma = \pm(-1)\Big/\sqrt{1 + \left(\frac{\partial v_z}{\partial v_x}\right)^2 + \left(\frac{\partial v_z}{\partial v_y}\right)^2} \tag{23i}$$

The total derivative of the parameter s is equal, according to eqs. (22c) or (23c), to

$$ds = -dz \tag{24}$$

Therefore we obtain from eqs. (22) and (23) the following relations

$$\frac{dy}{dx} = \frac{\partial v_z}{\partial v_y} \Big/ \frac{\partial v_z}{\partial v_x} \tag{25a}$$

$$\frac{dx}{dz} = -\frac{\partial v_z}{\partial v_x} \tag{25b}$$

$$\frac{dy}{dz} = -\frac{\partial v_z}{\partial v_y} \tag{25c}$$

$$\frac{dv_x}{dz} = \frac{\partial v_z}{\partial v_y}\omega_z + \omega_y \tag{25d}$$

$$\frac{d}{dz}\left(\frac{\partial v_x}{\partial x}\right) = \frac{\partial}{\partial x}\left(\frac{\partial v_z}{\partial v_y}\omega_z + \omega_y\right) \tag{25e}$$

$$\frac{d}{dz}\left(\frac{\partial v_x}{\partial y}\right) = \frac{\partial}{\partial y}\left(\frac{\partial v_z}{\partial v_y}\omega_z + \omega_y\right) \tag{25f}$$

$$\frac{d}{dz}\left(\frac{\partial v_x}{\partial z}\right) = \frac{\partial}{\partial z}\left(\frac{\partial v_z}{\partial v_y}\omega_z + \omega_y\right) \tag{25g}$$

$$\frac{dv_y}{dz} = -\frac{\partial v_z}{\partial v_x}\omega_z - \omega_x \tag{26a}$$

$$\frac{d}{dz}\left(\frac{\partial v_y}{\partial x}\right) = -\frac{\partial}{\partial x}\left(\frac{\partial v_z}{\partial v_x}\omega_z + \omega_x\right) \tag{26b}$$

$$\frac{d}{dz}\left(\frac{\partial v_y}{\partial y}\right) = -\frac{\partial}{\partial y}\left(\frac{\partial v_z}{\partial v_x}\omega_z + \omega_x\right) \tag{26c}$$

$$\frac{d}{dz}\left(\frac{\partial v_y}{\partial z}\right) = -\frac{\partial}{\partial z}\left(\frac{\partial v_z}{\partial v_x}\omega_z + \omega_x\right) \tag{26d}$$

The solution of eqs. (22) and (23) or (25) and (26) give the characteristics of the differential eqs. (20) and (21) along which can be found some discontinuities.

According to eqs. (22b and 22d) and (23a and 23d) we obtain

$$\frac{dv_y}{dx} = \omega_z + \frac{\omega_x}{\partial v_z/\partial v_x}, \qquad \frac{dv_x}{dy} = -\omega_z - \frac{\omega_y}{\partial v_z/\partial v_y} \tag{27}$$

Eliminating ω_z from eqs. (27), we obtain

$$\frac{dv_x}{dy} + \frac{dv_y}{dx} = \frac{\omega_x}{\partial v_z/\partial v_x} - \frac{\omega_y}{\partial v_z/\partial v_y} \tag{28}$$

Since the velocities v_x and v_y are functions of x, y, and z, then eq. (28), representing the differential equation of the projections of the characteristics ("base" characteristics) in the plane (x, y), can be written as follows:

$$\left(\frac{dy}{dx}\right)_{1,2} = -\frac{\dot{A}}{\dot{\epsilon}_y} \pm \sqrt{\left(\frac{\dot{A}}{\dot{\epsilon}_y}\right)^2 - \frac{\dot{\epsilon}_x}{\dot{\epsilon}_y} - \frac{1}{\dot{\epsilon}_y}\frac{\partial v_x}{\partial z}\frac{dz}{dx}} \tag{29}$$

where

$$\dot{A} = \frac{dA}{dt} = \dot{\gamma}_{xy} + \frac{1}{2}\left(\omega_z + \frac{\partial v_y}{\partial z}\right)\frac{dz}{dx} - \frac{1}{2}\left(\omega_z - \frac{\partial v_x}{\partial z}\right)\frac{dz}{dy} - \frac{1}{2}\frac{\partial v_x}{\partial z}\frac{dz}{dy} \tag{30}$$

The values dz/dx and dz/dy in eqs. (29) and (30) have to be taken from eqs. (25b and 25c). Substituting in eqs. (29) and (30) the values ω_x and ω_y (see symbols), further taking $\partial v_z/\partial v_x = \dot{\epsilon}_z/(\partial v_z/\partial z)$, $\partial v_z/\partial v_y = \dot{\epsilon}_z/(\partial v_y/\partial z)$, and $\partial v_x/\partial z = \dot{\gamma}_{xz} + \omega_y$, $\partial v_y/\partial z = \dot{\gamma}_{yz} - \omega_x$, eqs. (29) and (30) read

$$\left(\frac{dy}{dx}\right)_{1,2} = \frac{\dot{A}}{\dot{\epsilon}_y} \pm \sqrt{\left(\frac{\dot{A}}{\dot{\epsilon}_y}\right)^2 - \frac{\dot{\epsilon}_x}{\dot{\epsilon}_y} + \frac{(\dot{\gamma}_{xz} + \omega_y)^2}{\dot{\epsilon}_y\dot{\epsilon}_z}},$$

$$\dot{A} = \dot{\gamma}_{xy} - \frac{1}{2\dot{\epsilon}_z}(\dot{\gamma}_{xz}\dot{\gamma}_{yz} + \omega_x\omega_y) \tag{31}$$

The limiting condition corresponding to eqs. (31) reads

$$f(\dot{\epsilon}_x, \ldots, \dot{\gamma}_{xy}, \ldots, \omega_z, \ldots) = 0 \tag{32}$$

The terms involving $\dot{\gamma}_{xz}$, $\dot{\gamma}_{yz}$ and ω_x, ω_y in eqs. (31) represent the influence of the three-dimensional state of strain on the characteristic directions.

Because $\dot{\epsilon}_x = d\epsilon_x/dt$ etc., eqs. (31) can be written in terms of total derivatives of strains; that is, using $\omega_x = \dot{\varphi}_x$ etc.,

$$\left(\frac{dy}{dx}\right)_{1,2} = -\frac{dA}{d\epsilon_y} \pm \sqrt{\left(\frac{dA}{d\epsilon_y}\right)^2 - \frac{d\epsilon_x}{d\epsilon_y} + \frac{(d\gamma_{xz} + d\varphi_y)^2}{d\epsilon_y d\epsilon_z}} \tag{33}$$

where

$$dA = d\gamma_{xy} - \frac{1}{2d\epsilon_z}(d\gamma_{xz}d\gamma_{yz} + d\varphi_x d\varphi_y) \tag{34}$$

The limiting condition corresponding to eqs. (33) and (34) reads

$$g(\epsilon_x, \ldots, \gamma_{xy}, \ldots, \varphi_x, \ldots) = 0 \tag{35}$$

The *general* integral of the partial quasi-linear non-homogeneous differential eqs. (20) and (21) of the first order can be investigated if the limiting condition of eq. (14) is given in a particular form, and the integral of eq. (16) is finally determined. Because dv_x in eq. (25d) and dv_y in eq. (26a) do not depend upon their partial derivatives eqs. (25e–g) and (26b–d), the characteristics of the differential eq. (20) [and similarly eq. (21)] read, taking $\vartheta_i = \vartheta_i(x, y, z, v_x, v_y)$, $i = 1, 2, 3$,

$$\vartheta_1 = v_x - \int\left(\frac{\partial v_z}{\partial v_y}\omega_z + \omega_y\right)dz = a$$

$$\vartheta_3 = v_x + \int\left(\frac{\partial v_z}{\partial v_y}\omega_z + \omega_y\right)dy\Big/\frac{\partial v_z}{\partial v_y} = b$$

$$\vartheta_2 = v_x + \int\left(\frac{\partial v_z}{\partial v_y}\omega_z + \omega_y\right)dx\Big/\frac{\partial v_z}{\partial v_x} = c$$

where a, b, c are constants. The general integral is a functional relation $\Phi(\vartheta_1, \vartheta_2, \vartheta_3) = 0$. The intersections of the surfaces ϑ_1, ϑ_2, ϑ_3 are characteristics or finally slip lines (with some restrictions; see ref. 6, Fig. 14, p. 338) of the three dimensional problem of plastico-dynamics. All these characteristics form an integral hyper-surface of v_z (or v_y) passing through an arbitrary twisted curve C.

IV. THE PLANE STRAIN PROBLEM

In the plane strain problem $\dot{\gamma}_{zz}$, $\dot{\gamma}_{yz}$, ω_z, ω_y, and γ_{zz}, γ_{yz}, ϑ_x, ϑ_y are equal to zero. Then $\dot{A} = \dot{\gamma}_{xy}$ and $dA = d\gamma_{xy}$. Therefore, according

to eqs. (31), (33) and (34), the differential equation of characteristics reads

$$\left(\frac{dy}{dx}\right)_{1,2} = -\frac{\dot{\gamma}_{xy}}{\dot{\epsilon}_y} \pm \sqrt{\left(\frac{\dot{\gamma}_{xy}}{\dot{\epsilon}_y}\right)^2 - \frac{\dot{\epsilon}_x}{\dot{\epsilon}_y}} \tag{36}$$

and

$$\left(\frac{dy}{dx}\right)_{1,2} = -\frac{d\gamma_{xy}}{d\epsilon_y} \pm \sqrt{\left(\frac{d\gamma_{xy}}{d\epsilon_y}\right)^2 - \frac{d\epsilon_x}{d\epsilon_y}} \tag{37}$$

The limiting conditions here read

$$f(\dot{\epsilon}_x, \dot{\epsilon}_y, \dot{\gamma}_{xy}) = 0 \qquad \text{or} \qquad g(\epsilon_x, \epsilon_y, \gamma_{xy}) = 0 \tag{38}$$

In the principal directions 1, 2 of strains, the shear strain γ_{xy} vanishes. Equation (37) now reads

$$\left(\frac{dy}{dx}\right)_{1,2} = \pm \sqrt{-\frac{d\epsilon_1}{d\epsilon_2}} \tag{39}$$

with the limiting condition

$$\epsilon_1 = \epsilon_1(\epsilon_2) \tag{40}$$

Similarly as in the plane stress problem (see ref. 6), the negative values of $d\epsilon_1/d\epsilon_2$ with imaginary characteristic directions are also allowed. Physically, they represent brittle fracture (see ref. 17). Geiringer[5] means correctly that the rate of strain $\dot{\epsilon}$ along the characteristics is equal to zero.

We return to the question of the validity of the continuity equation for the plane problem. It reads: $\dot{\epsilon}_1 + \dot{\epsilon}_2 = 0$. We can write also $d\epsilon_1 + d\epsilon_2 = 0$ or $-d\epsilon_1/d\epsilon_2 = 1$. Here the characteristic directions $dy/dx = \pm 1$ will still be at an angle of 45° with the x and y axes. The angle between the slip lines will still be 90°. This corresponds to the situation in an ideal plastic body. We see that the continuity equation is a special case of the limiting condition, and hence we are quite ready to apply here the more general case represented in eqs. (38) or (40). The continuity equation must now be neglected for the case of constant density, as mentioned in Section II, because it duplicates and specializes the limiting condition.

According to eq. (28), we obtain now in the plane strain problem ($\omega_x = \omega_y = 0$) the following relation

$$dy/dx = -(dv_x/dv_y) \tag{42}$$

Equation (42) says that a tangent to the curve $y(x)$ in the plane (x, y) is perpendicular to a tangent to the curve $v_y(v_x)$ in the plane (v_x, v_y). This corresponds to the mapping of the Prandtl-Busemann nets in plane supersonic flow. Equation (42) is derived also by Geiringer (ref. 5, p. 243).

In the plane problem eq. (16) with $\omega_x = \omega_y = 0$, $\omega_z = \omega$ reads

$$\rho \frac{\partial \omega}{\partial t} = \mu \Delta \omega \tag{43}$$

where $\omega = \omega(x, y, t)$ is a solution of the parabolic differential eq. (43). Equation (43) is one equation in two unknowns v_x and v_y. The second equation is the limiting condition

$$v_y = v_y(v_x) \tag{44}$$

Equation (43) corresponds to the vorticity transport equation in hydrodynamics; see, for instance, Schlichting (ref. 18, p. 54). In this equation the time variation of vorticity is equal to the rate of dissipation of vorticity through friction. In hydrodynamics the stream function $\psi(x, y)$ is applied which satisfies the continuity equation $\nabla . \bar{v} = 0$. Because eq. (44) replaces the continuity equation here, we shall now proceed similarly as in Section III. The equation of the vortex with $\omega(x, y, t)$ as a solution of eq. (43) reads (neglecting "$^1/_2$")

$$\frac{\partial v_y}{\partial x} - \frac{\partial v_x}{\partial y} = \omega(x, y, t) \tag{45}$$

Because the velocity v_y in eq. (45) is dependent on v_x by eq. (44), we obtain the differential equation of the plane strain problem as follows:

$$F \equiv \frac{dv_y(v_x)}{dv_x} \frac{\partial v_x}{\partial x} - \frac{\partial v_x}{\partial y} - \omega = 0 \tag{46}$$

Equation (46) is a partial quasi-linear differential equation of first order. The differential equation of characteristics reads (cf. Webster, ref. 15, p. 54).

$$\frac{dx}{dv_y/dv_x} = \frac{dy}{-1} \tag{47a}$$

$$\frac{dy}{-1} = \frac{dv_x}{\omega} \tag{47b}$$

$$\frac{dv_x}{\omega} = \frac{d\partial v_x/\partial x}{\partial\omega/\partial x} \tag{47c}$$

$$\frac{d\partial v_x/\partial x}{\partial\omega/\partial x} = \frac{d\partial v_x/\partial y}{\partial\omega/\partial y} \tag{47d}$$

Rearrangement of eq. (47a) gives eq. (42). Equation (47d) says the same as eq. (47c). The characteristics of the differential eq. (46) according to eqs. (47a) and (47b), with $\vartheta_i(x, y, v_x)$, $i = 1, 2$, are

$$\vartheta_1 = v_x + \int \omega dy = a = \text{constant},$$

$$\vartheta_2 = v_x - \int \frac{\omega}{dv_y/dv_x}\, dx = b = \text{constant} \tag{48}$$

The general integral is a functional relation $\Phi(\vartheta_1, \vartheta_2) = 0$. There are ∞^1 arbitrary intersections of the ϑ_1 and ϑ_2 surfaces. All these characteristics form an integral surface of v_x passing through an arbitrary twisted curve C.

If the velocities v_x, v_y for the three dimensional problem are known, the velocity v_z will be computed from eq. (14). Similarly, if the velocity v_x in the plane problem is known, the velocity v_y will be computed from eq. (44). Then the pressure p will be computed according to eq. (8). The stresses will be computed according to eq. (6).

V. THE PLANE PROBLEM OF AN IDEAL PLASTIC BODY

We consider here the plane problem with $\sigma_z = t_{xz} = t_{yz} = 0$ and with $\partial \ldots/\partial z = 0$. We do not consider the convective terms of the acceleration. Therefore, $dv_x/dt = \partial v_x/\partial t$ and $dv_y/dt = \partial v_y/\partial t$. The equation of motion (1) without mass forces reads

$$\rho\frac{\partial v_x}{\partial t} = \frac{\partial \sigma_x}{\partial x} + \frac{\partial t_{xy}}{\partial y}, \qquad \rho\frac{\partial v_y}{\partial y} = \frac{\partial \sigma_y}{\partial y} + \frac{\partial t_{xy}}{\partial x} \tag{49}$$

The continuity eq. (2) is neglected here, because we assume that the density ρ is a given function of r and t. For the limiting condition eq. (3) we shall take here a special yield condition for an ideal plastic

body. This is a quadratic expression in stresses without linear terms. It is

$$(\sigma_x - \sigma_y)^2 + 4t_{xy}^2 = 4t_0^2 \tag{50}$$

The stress-rate of strain relations for the plane problem are according to eq. (6)

$$\left.\begin{aligned} \sigma_x &= 2\mu \frac{\partial v_x}{\partial x} - \dot{p} - \frac{2}{3}\mu\left(\frac{\partial v_x}{\partial x} + \frac{\partial v_y}{\partial y}\right) \\ \sigma_y &= 2\mu \frac{\partial v_y}{\partial y} - p - \frac{2}{3}\mu\left(\frac{\partial v_x}{\partial x} + \frac{\partial v_y}{\partial y}\right) \\ t_{xy} &= \mu\left(\frac{\partial v_y}{\partial x} + \frac{\partial v_x}{\partial y}\right) \end{aligned}\right\} \tag{51}$$

If we put eq. (51) in eqs. (49) and (50), we obtain the differential equations of motion of an ideal plastic body, which read—compare with eqs. (8) and (10)—

$$\rho \frac{\partial v_x}{\partial t} = \mu \Delta v_x - \frac{\partial p}{\partial x} + \frac{\mu}{3}\frac{\partial}{\partial x}(\nabla . \bar{v}) \tag{52a}$$

$$\rho \frac{\partial v_y}{\partial t} = \mu \Delta v_y - \frac{\partial p}{\partial y} + \frac{\mu}{3}\frac{\partial}{\partial y}(\nabla . \bar{v}) \tag{52b}$$

$$\left(\frac{\partial v_x}{\partial x} - \frac{\partial v_y}{\partial y}\right)^2 + \left(\frac{\partial v_y}{\partial x} + \frac{\partial v_x}{\partial y}\right)^2 = \left(\frac{t_0}{\mu}\right)^2 \tag{53}$$

Equations (52) and (53) are three equations in three unknowns, v_x, v_y, and p.

If we differentiate eq. (52a) with respect to y and eq. (52b) with respect to x, and we subtract these two equations, we obtain

$$\rho \frac{\partial \omega}{\partial t} = \mu \Delta \omega \tag{54}$$

If we add the differentiated equations instead of subtracting, we have

$$\rho \frac{\partial \dot{\gamma}}{\partial t} = \mu \Delta \dot{\gamma} - \frac{\partial^2 p}{\partial x \partial y} + \frac{\mu}{3}\frac{\partial^2}{\partial x \partial y}(\nabla . v) \tag{55}$$

With the assumptions for the mean pressure p and the rate of the volume dilatation $\nabla . \bar{v}$

$$p = f_1(x, y) + g_1(y, t), \qquad \nabla . \bar{v} = f_2(x, t) + g_2(y, t) \tag{56}$$

Equation (55) simplifies as follows

$$\rho \frac{\partial \dot{\gamma}}{\partial t} = \rho \Delta \dot{\gamma} \tag{57}$$

Both equations (54) and (57) are parabolic differential equations. We can also carry out further derivations with the remark that the solutions of eqs. (54) and (57) are

$$\omega = \omega(x, y, t) \tag{58a}$$

$$\dot{\gamma} = \dot{\gamma}(x, y, t) \tag{58b}$$

If we substitute eq. (58b) in the yield condition eq. (53), we obtain with eq. (58a) two simultaneous differential equations which read

$$\frac{\partial v_x}{\partial x} - \frac{\partial v_y}{\partial y} = \pm \sqrt{\left(\frac{t_0}{\mu}\right)^2 - \dot{\gamma}^2(x, y, t)} \tag{59}$$

$$\frac{\partial v_y}{\partial x} - \frac{\partial v_x}{\partial y} = \omega(x, y, t) \tag{60}$$

Separating the velocities v_x, v_y each in one differential equation, we obtain two linear hyperbolic differential equations which read

$$\frac{\partial^2 v_y}{\partial x^2} - \frac{\partial^2 v_y}{\partial y^2} = \frac{\partial \omega}{\partial x} \pm \frac{\partial}{\partial y} \sqrt{\left(\frac{t_0}{\mu}\right)^2 - \dot{\gamma}^2} \tag{61}$$

$$\frac{\partial^2 v_x}{\partial x^2} - \frac{\partial^2 v_x}{\partial y^2} = \frac{\partial \omega}{\partial y} \pm \frac{\partial}{\partial x} \sqrt{\left(\frac{t_0}{\mu}\right)^2 - \dot{\gamma}^2} \tag{62}$$

These differential equations have the equations of characteristics

$$dy/dx = \pm 1 \tag{63}$$

As a consequence, eq. (63) yields two families of straight lines

$$x + y = \text{constant}, \qquad x - y = \text{constant} \tag{64}$$

These straight lines are inclined to the x and y axes at the angle of 45°. Each one of these straight lines is perpendicular to the other, as is known in the behavior of slip lines of an ideal plastic body.

Using the transformation in the direction of characteristics eq. (64): $u = x + y$, $v = x - y$, we obtain the integrals of eqs. (61) and (62) which read

$$v_x = -\frac{1}{2}\int [\omega dy \pm \sqrt{(t_0/\mu)^2 - \dot{\gamma}^2}\, dx] + F(x + y) + G(x - y) \tag{65}$$

$$v_y = \frac{1}{2}\int [\omega dx \pm \sqrt{(t_0/\mu)^2 - \dot{\gamma}^2}\, dy] + f(x + y) + g(x - y) \tag{66}$$

The boundary conditions will be taken separately for each special case.

If w and z are the orthogonal curvilinear coordinates, eq. (63) reads

$$dz/dw = \pm 1 \tag{67}$$

Its solution is

$$z \pm w = \text{constant} \tag{68}$$

Investigating the polar and bipolar coordinate systems with $w = \ln r$, $z = \phi$, and $w = \ln r_1/r_2$, $z = \phi_1 - \phi_2$, we obtain, according to eq. (68), $r/r_0 = e^{\pm\phi}$ and $r_1/r_2 = k \exp. \pm (\phi_1 - \phi_2)$. These are logarithmic and bipolar logarithmic spirals, respectively. These are valid, for instance, if the boundary conditions and the loading coincide with the principal stress trajectories along the coordinate curves.

References

(1) A. Nádai, *Plastizität und Erddruck*, article in *Handbuch der Physik*, Vol. VI, Springer, Berlin, 1928, p. 428.

(2) A. Nadai, *Theory of Flow and Fracture of Solids*, McGraw-Hill, New York, 1950.

(3) R. v. Mises, *Mechanik der festen Körper im plastisch-deformablen Zustand*, Göttinger Nachrichten, 1913.

(4) H. Hencky, *Z. angew. Math. Mech.*, **5**, 144 (1925).

(5) H. Geiringer, *Adv. Appl. Mech.*, **3**, 197 (1953). See also *The Ideal Plastic Body*, Article in *Encyclopedia of Physics*, Vol. VI, Springer, Berlin, 1958, p. 322.

(6) C. Torre, *Österr. Ing. Arch.*, **1**, 36, 316 (1946).

(7) A. Sommerfeld, *Vorlesungen über Theoretische Physik*, Vol. II, *Mechanik der deformierbaren Medien*, Wiesbaden, 1947.

(8) R. v. Mises, *Mathematical Theory of Compressible Fluid Flow*, Academic Press, New York, 1958. Completed by H. Geiringer and G. S. S. Ludford.

(9) C. Torre, *Österr. Ing. Arch.*, **4**, 417 (1952).

(10) F. Schultz-Grunov, *Kolloid-Z.*, **141**, 173 (1955).

(11) A. Nadai, *Inst. Mech. Eng. London J., Appl. Mech. Proc.*, **157**, 121 (1947). Translation in German: *Österr. Ing. Archiv.* **3**, 261, 421 (1949); **5**, 182 (1951).

(12) M. Lagally, *Vorlesungen über Vektor-Rechnung, Leipzig*, 1934.

(13) M. Lamb, *Hydrodynamics*, 6th ed., Dover, New York, 1932.

(14) K. Oswatitsch, *Gasdynamik*, Springer Verlag, Wien, 1952.

(15) A. G. Webster, *Partial Differential Equations of Mathematical Physics*, Dover, 1955.

(16) J. Lense, *Partielle Differentialgleichungen, Encyclopedia of Physics*, Vol. 1, Springer Verlag, Berlin, 1956, p. 90.

(17) C. Torre, *Spödbruch von Schweissverbindungen. Das Nichtschmelzschweissen. Jahrbuch 1953, der Wiss. Ges. f. Luftfahrt*, F. Vieweg & Sohn, Braunschweig, 1954, p. 182. *Osterr. Ing. Arch.*, **4**, 174 (1950).

(18) H. Schlichting, *Boundary Layer Theory*, McGraw-Hill, 1955. Translated from German by J. Kestin.

TRANSACTIONS OF THE SOCIETY OF RHEOLOGY II, 175–194 (1958)

The Creep of Snow under Combined Stress

J. K. LANDAUER,* *U. S. Army Snow, Ice, and Permafrost Research Establishment, Wilmette, Illinois*

I. INTRODUCTION

A considerable amount of work has been done in the field of creep under combined stress, but generally on materials for which the compressibility can be neglected.[1,2] These tests involve combinations of torsional and tensile stresses. Their applicability to snow is severely limited, however, by the great compressibility of snow. For typical creep tests, snow density may change 5 to 10% in a few hundred seconds. Bucher[3] studied the creep of low-density snow under tension, compression, and shear, using low stresses. He developed theoretical relationships to compare his results under different stress conditions, but his data are insufficient to establish a useful correlation.

Some uniaxial tests have been performed on snow.[4,5] They indicate a flow law for creep varying from a linear law at low stresses to a power relationship at high stresses. In-place compactive tests have been run on natural snow,[6–8] but these are difficult to analyze because of the variable snow conditions.

The present experiments were run under three different stress conditions: (*1*) uniaxial compressive; (*2*) confined-side compactive; and (*3*) hydrostatic, all at constant stress between 4 and 40 psi. For the uniaxial case both vertical and lateral creep were determined; under the confined-side compactive stress, vertical creep and lateral stress were measured; and change in volume was determined for the hydrostatic tests. Tests were run at various temperatures from −3.6 to −13.6°C. and for snow densities between 0.36 and 0.63 g./cm.^{3}. For each experimental condition, several samples were measured to obtain an average value.

* Present address: University of California Radiation Laboratory, Livermore, California.

II. EXPERIMENTAL

A. General

The snow used for the tests reported here was natural snow that had been stored at low temperatures (−25 to −50°C.) for periods ranging from a few months to a few years. Grain size and shape characteristic of these snows varied, depending on the original deposition and on the conditions of storage. In all cases, the stored natural snow was mixed and sieved into suitable containers and allowed to harden for periods of 1 to 4 weeks. During the first week most of the hardening process had occurred and tests performed after this did not involve an appreciably varying hardness.[9]

Because of differences in the natural snows used, the densities after sifting varied between 0.36 and 0.5 g./cm.^{3}. Higher-density snows were obtained by compacting freshly sieved snows and allowing them to harden in the same manner as for uncompacted snows. No change in density occurs during the hardening process.

The tests were performed in cold rooms where the temperature varied less than 1°C. For some experiments the temperatures were controlled to ±0.1°C. by placing the experimental apparatus in a constant temperature enclosure.

B. The Apparatus

The uniaxial and confined-side experiments were performed on an electrically operated press. Stress was maintained approximately constant by an on-off action of the press. Actually, therefore, a roughly sinusoidal stress was applied. The amplitude of the sinusoidal component was a few per cent of the applied stress and it was determined that the resulting deformations were the same as if a truly constant stress was maintained.

Vertical stress was measured using a 500-lb. Baldwin Type U load cell. Vertical strain was measured with a millimeter scale for large deformations and a 0.001 in. Starrett dial gage for small deformations.

The lateral expansion accompanying vertical compaction for uniaxial stress was measured using four 0.001 in. dial gages at the center of each of the sides of the specimen as shown in Figure 1.

The confined-side compactive experiments were run in square cross-section steel prisms lined with a thin coat of Teflon to reduce friction. Inside dimensions were 5.75 × 5.75 × 12.7 cm. high. The apparatus

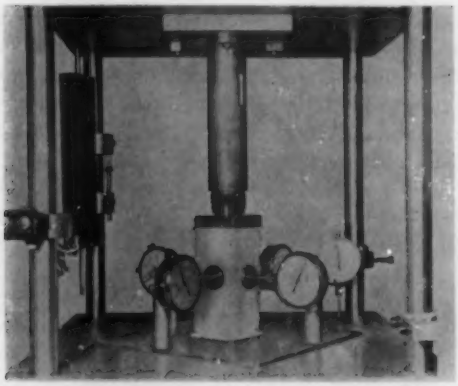

Fig. 1. The uniaxial apparatus.

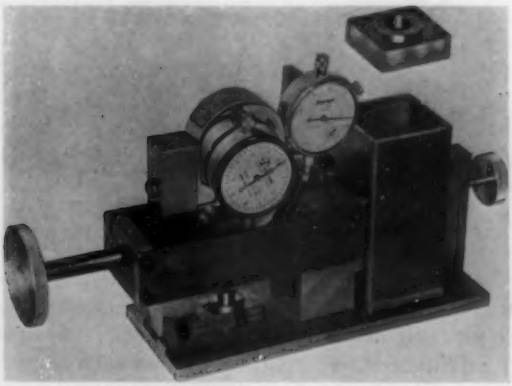

Fig. 2. The confined-side apparatus.

is shown in Figure 2. A circular hole 3.60 cm. in diameter was at the center of one side. A 3.46 cm. diameter pressure plate fitting coaxially into this hole was used to measure the lateral stress. Force was measured with a 5 kg. Dillon dynamometer. A fine screw arrangement allowed the lateral pressure plate to be kept flush with the inner wall of the steel cylinder. For this purpose a 0.0001 in. Starrett dial gage was used as reference indicator.

Hydrostatic stress was applied using compressed air and measured with a 200-lb. Baldwin SR-4 pressure cell. The snow sample rested on a porous base and was enclosed in a snugly fitting thin rubber envelope extending over the junction with the base (Fig. 3). A brass can was used to enclose the pressure system. A manometer arrangement served to measure the air expelled from the snow through the porous base and thus provided a measure of the deformation.

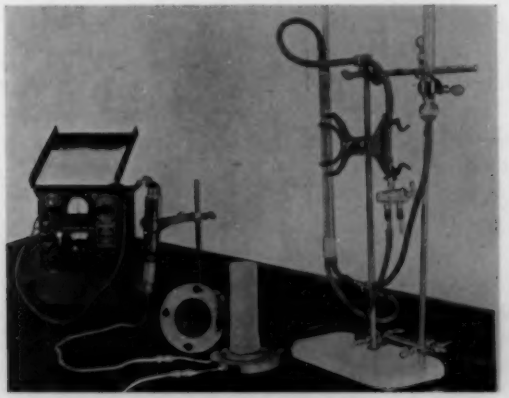

Fig. 3. The hydrostatic apparatus.

C. Procedure

A large group of uniaxial and hydrostatic experiments (Group I) were made with cylindrical snow samples 5.8 cm. in diameter and 18.9 cm. high. In these tests deformation was measured at each of a series of increasing stresses for constant time increments. Stresses of about 4, 10, 16, 22, and 28 psi were applied successively for several hundred seconds each. The total deformation of a sample was usually less than 10% and most of this occurred at the higher stresses. These experiments were performed on snows near 0.4 g./cm.^{3} density and at various temperatures between -3.6 and -13.6°C.

Because of the relatively large change in density between the beginning and end of these experiments, a second set of experiments (Group II) was performed at constant stress with the deformation continuing until the snow had densified a given small amount. In

these experiments initial densities were from 0.37 to 0.63 g./cm.^{3}. The temperature was maintained at -10°C. For the uniaxial and confined-side experiments the square prismatic samples (5.75 × 5.75 × 12.7 cm.) were used but the circular cylinders were again used for the hydrostatic experiments.

For all of the experiments the snow was brought to temperature several hours prior to testing. In the uniaxial and hydrostatic cases the snow sample was removed from its container and tested immediately. The snow for the confined-side experiments was not removed from the container, but loosened slightly to break any side bonding.

Usually a small initial pressure was applied (less than 10% of the test pressure) to assure good seating and to provide an adequate zero point from which to measure deformation.

III. THEORETICAL RELATIONS

A. Additive Theory

On the basis of an additive concept, deformation under combined stress is the sum of the deformations which would occur for separate uniaxial stresses. If this assumption is correct, deformation under combined stress can be predicted from uniaxial experiments. As will be seen later, the uniaxial creep law for snow can be taken as:

$$\dot{\epsilon}_{zu} = k\sigma_z(1 + a\sigma_z^2) \tag{1}$$

where $\dot{\epsilon}_{zu}$ and σ_z are the compressive strain rate and stress in the z-direction, and k is a constant depending on temperature, density, time, and snow-grain characteristics.

Snow under uniaxial compression undergoes horizontal expansion. The ratio

$$-\dot{\epsilon}_{xu}/\dot{\epsilon}_{zu} = m \tag{2}$$

is a measure of this effect. $1/m$ is the visco-plastic analogue of Poisson's ratio.

For combined stress the strain rate in the i-direction, using eqs. (1) and (2), is:

$$\dot{\epsilon}_i = k\sigma_i(1 + a\sigma_i^2) - \frac{k\sigma_j}{m}(1 + a\sigma_j^2) - \frac{k\sigma_k}{m}(1 + a\sigma_k^2) \tag{3}$$

where j and k are directions normal to i. Under uniaxial compression, the lateral strain rate, $\dot{\epsilon}_{zu}(= \dot{\epsilon}_{yu})$, is simply:

$$\dot{\epsilon}_{zu} = -(k\sigma_z/m)\,(1 + a\sigma_z^2) \tag{4}$$

For hydrostatic stress, the strain rate, $\dot{\epsilon}_{zh}(= \dot{\epsilon}_{zh} = \dot{\epsilon}_{yh})$ is, using eq. (3):

$$\dot{\epsilon}_{zh} = \frac{m-2}{m} k\sigma_z(1 + a\sigma_z^2) \tag{5}$$

In the case of confined-side compaction:

$$\dot{\epsilon}_{zc}(= \dot{\epsilon}_{yc}) = 0$$

For this case, using eq. (3), the ratio of vertical to lateral stress is found to be:

$$\frac{\sigma_z}{\sigma_x} = (m-1)\frac{1 + a\sigma_x^2}{1 + a\sigma_z^2} \tag{6}$$

For a linear creep law this reduces to:

$$\sigma_z/\sigma_x = m - 1$$

Creep in the z-direction should be less for the confined-side than for the uniaxial case. From eqs. (3) and (6) the strain rate is

$$\dot{\epsilon}_{zc} = \frac{(m-2)\,(m+1)}{m(m-1)} k\sigma_z(1 + a\sigma_z^2) \tag{7}$$

Creep rates for uniaxial, hydrostatic, and confined-side stresses can be compared on the basis of the additive concept. The ratios of the creep rates are:

$$\frac{\dot{\epsilon}_{zu}}{\dot{\epsilon}_{zh}} = \frac{m}{m-2} \tag{8}$$

and

$$\frac{\dot{\epsilon}_{zu}}{\dot{\epsilon}_{zc}} = \frac{m(m-1)}{(m-2)\,(m+1)} \tag{9}$$

B. Relationship between Tests Run for Constant Change in Density and Tests for Constant Time

Group I experiments were performed for constant time increments. An average velocity was determined which was the total strain di-

vided by the time, t, during which constant stress was applied. Thus, a generalized creep curve of the form

$$\overline{\Delta z}/z\dot{} = ABST \tag{10}$$

was found, where A is a constant depending on density, temperature, and grain characteristics, B is a constant of the stress condition (i.e., the factor to represent combined stress behavior which is equal to unity for the uniaxial case), S is the uniaxial stress function, and T is a function depending only on time.

The time dependent function was found to be well represented by

$$\epsilon = (\Delta z/z) \propto t^r \tag{11}$$

The average strain rate is, therefore,

$$(\overline{\Delta z}/zt) \propto t^{r-1} \equiv T \tag{12}$$

while the strain rate, $\dot{\epsilon}$, is

$$\dot{\epsilon} \propto rt^{r-1} \tag{13}$$

Thus, in terms of strain rate, the generalized creep curve for constant time becomes

$$\dot{\epsilon}_t = ABSrT \tag{14}$$

Owing to changing density during deformation, it is reasonable to compare creep rates at a chosen density as done for Group II experiments. To attain a given change in density (initial densities being equal) it is necessary to produce a larger z-axis strain for the uniaxial case than for the confined-side or hydrostatic cases. The z-axis strains to reach constant density will be in the ratio:

$$\epsilon_u : \epsilon_c : \epsilon_h = 1 : (m - 2)/m : (m - 2)/3m \tag{15}$$

To express the constant-time creep curve [eq. (14)] in terms of creep rates at constant density, it is first necessary to express the curve at constant z-axis strain. Since the time to attain a given strain is:

$$t_\epsilon = (\epsilon/ABS)^{1/r} \tag{16}$$

the creep rate at constant z-axis strain becomes:

$$\dot{\epsilon}_\epsilon = (ABS)^{1/r} r\epsilon^{(r-1)/r} \tag{17}$$

At constant density the ratios of the strain rates under confined-side and hydrostatic stresses to strain rate under an equal uniaxial stress are:

$$\left(\frac{\dot{\epsilon}_c}{\dot{\epsilon}_u}\right)_\gamma = B_c^{1/r}\left(\frac{(m-2)}{m}\right)^{(r-1)/r}$$

and

$$\left(\frac{\dot{\epsilon}_h}{\dot{\epsilon}_u}\right)_\gamma = B_h^{1/r}\left(\frac{(m-2)}{3m}\right)^{(r-1)/r}$$

From eqs. (8) and (9) the values of B can be taken as $B_c = [(m-2)(m+1)]/m(m-1)$ and $B_h = (m-2)/m$. The above equations can be rewritten

$$\left(\frac{\dot{\epsilon}_c}{\dot{\epsilon}_u}\right)_\gamma = \frac{m-2}{m}\left(\frac{m+1}{m-1}\right)^{1/r}$$

and (18)

$$\left(\frac{\dot{\epsilon}_h}{\dot{\epsilon}_u}\right)_\gamma = \frac{m-2}{m}\,3^{(1-r)/r}$$

IV. RESULTS AND DISCUSSION

A. Group I Experiments

Group I experiments provide information on the stress and temperature dependence of the uniaxial and hydrostatic cases. Thirty-five samples were tested. Typical creep curves for the two stress conditions are shown in Figure 4. An average strain rate was determined for each pressure by dividing the total strain by the time increment. A few tests at 300 and 500 sec. increments were converted to the predominant 200 sec. basis by eq. (12), using $r = 0.5$. The volume deformations determined for the hydrostatic experiments were converted to z-axis strain rates by dividing the volume strain rates by 3.

Either of two stress functions can be used to represent these data. A very good fit of the data is obtained using a hyperbolic sine stress dependence and a slightly inferior fit is obtained from the sum of linear and cubic stress terms. In Figure 5 the experimental results at -8.4°C. are compared with hyperbolic sine and linear plus cubic

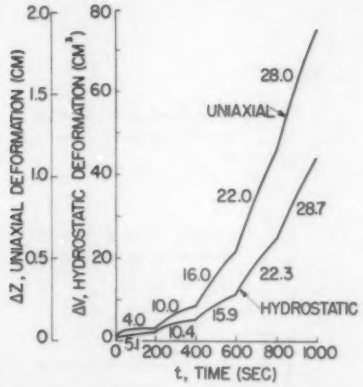

Fig. 4. Deformation vs. time. Group I experiment at −13.55°C. Numbers on curves indicate stress in psi.

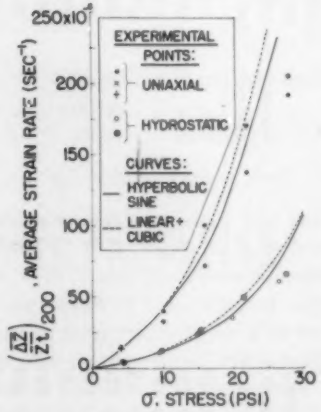

Fig. 5. Empirical creep curve for Group I test at −8.4°C. using coefficients from Table I.

stress curves. Some deviation occurs at the higher stresses due to the continuously increasing density of the sample. The coefficients, C, for a hyperbolic sine creep law

$$(\overline{\Delta z/zt})_{200} = C \sinh (\sigma/\sigma_0) \tag{19}$$

TABLE I

200-Sec. Average Z-Axis Strain Rates Represented by Creep Curves of the Form $(\overline{\Delta z}/zt)_{200} = C \sinh (\sigma/\sigma_0)$ and $(\overline{\Delta z}/zt)_{200} = k\sigma(1 + a\sigma^2)$ for Group I Tests under Uniaxial and Hydrostatic Stresses

The constants have been calculated using $\sigma_0 = 10$ psi and $a = 3 \times 10^{-3}$ psi^{-2}

Batch	Snow density (g./cm.^{3})	Temp. (°C.)	Stress condition	t, Time at each stress (sec.)	No. of samples averaged	C ($\times 10^{-6}$ sec.$^{-1}$)	k ($\times 10^{-6}$ sec.$^{-1}$)
1	0.420	−4.2	h	500	2	8.0	0.8
1	0.420	−8.8	h	500	2	5.3	0.45
1	0.420	−12.2	h	500	2	3.3	0.35
2	0.422	−4.2	u	300	1	16.4	1.3
2	0.422	−4.2	u	200	4	22.7	2.3
3	0.420	−4.2	u	200	3	18.5	1.5
3	0.420	−4.2	h	200	3	8.0	1.0
4	0.380	−3.6	u	200	2	80.5	7.4
4	0.380	−3.6	h	200	2	20.0	1.8
4	0.380	−5.1	u	200	3	54.0	4.5
4	0.380	−5.1	h	200	3	18.0	1.6
4	0.380	−8.4	u	200	3	34.4	3.3
4	0.380	−8.4	h	200	2	10.6	1.0
4	0.380	−13.55	u	200	2	32.2	3.0
4	0.380	−13.55	h	200	1	8.8	0.8

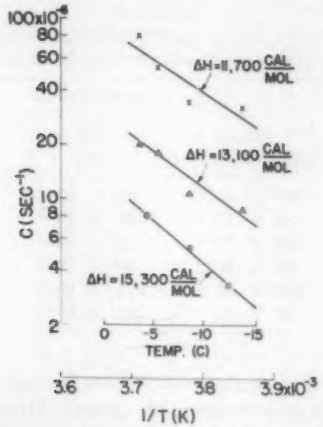

Fig. 6. The coefficient, C, for the hyperbolic sine creep curve plotted vs. inverse absolute temperature. (×) Uniaxial $\gamma = .38$. (△) Hydrostatic $\gamma = .38$. (⊙) Hydrostatic $\gamma = .42$.

are given in Table I. For both uniaxial and hydrostatic experiments σ_0 is a constant equal to 10 psi.

Representation of the data in a creep curve of the form

$$(\overline{\Delta z}/zt)_{200} = k\sigma(1 + a\sigma^2) \tag{20}$$

is advantageous for some applications. The values of the constants, k, are shown in Table I. The constant, a, does not vary appreciably from the value 3.0×10^{-3}, and k has been calculated on that basis.

Comparison of the values of C at different temperatures leads to a value of the activation energy for creep. Figure 6 is a plot of the C's versus inverse absolute temperature. An average activation energy of 13,400 cal./mole is found. The differences between hydrostatic and uniaxial activation energies are probably less than the experimental error.

B. Group II Experiments

One hundred and four samples prepared in six batches were run to the strains indicated in Table II. Uniaxial samples were tested first, the m number calculated and then, using eq. (15), limits for confined-side and hydrostatic experiments were determined. The dense snows

TABLE II
Limits of Deformation and Density Change for Group II Experiments
The average density for each batch is shown

Batch	γ_0 (g./cm.^{3})	Deformation Δz_u (in.)	Deformation ΔZ_c (in.)	Δv_h (cm.^{3})	$\Delta\gamma$ (g./cm.^{3})
6	0.369	240×10^{-3}	160×10^{-3}	15.7	0.012
5	0.451	240×10^{-3}	160×10^{-3}	15.7	0.015
10	0.477	150×10^{-3}	125×10^{-3}	12.5	0.012
8	0.503	60×10^{-3}	50×10^{-3}	5.0	0.006
9	0.503	150×10^{-3}	125×10^{-3}	13.0	0.015
7	0.626	50×10^{-3}	33×10^{-3}	3.3	0.004

required a smaller change in density than the light snows in order to run the experiments over comparable times. However, for a particular batch, all samples were run to the same final density. The strain rates and parameters m and r were determined at this final density. Results of the Group II tests are compiled in Table III.

C. Stress Dependence for Group II Tests

Stress dependence can be derived from the tests at 10, 15, and 20 psi at initial density of 0.369 g./cm.^{3}. Uniaxial, confined-side, and hydrostatic data indicate a creep rate varying closely to the cube of the stress. The difference between this result and that obtained for constant time tests rests on several factors. First, reference to eq. (17) shows that the exponent of the stress function in the case of constant strain should be a factor of $1/r$ times the exponent of the function for constant time. Second, increasing density during the course of Group I tests tends to reduce the strain rates for the higher stresses. This makes the effective value of the exponent lower than it would be for Group II tests involving small total deformation. Third, the linear term in Group I stress functions would become fairly inconspicuous for the somewhat higher stresses used in Group II experiments.

D. Variability

Considerable variability exists between samples of the same density prepared at different times, and less, but still a large variability exists between samples prepared under identical conditions at the

TABLE III. Results of Group II Tests. (The indicated errors are mean deviations.)

TABLE III. Results of Group II Tests. (The indicated errors are mean deviations.)

Batch	Initial density, γ_0 (g./cm.^{3})	σ_z (psi)	$\dot{\epsilon}_z$ ($\times 10^{-7}$ sec.$^{-1}$)	m	r_z	r_x	σ_z/σ_x	No. averaged
			A. Uniaxial Tests					
5	0.457 ± 0.002	17.5	180 ± 17	4.3 ± 0.5	0.45 ± 0.04	0.29 ± 0.02		3
6	0.370 ± 0.001	10	220 ± 40	5.2 ± 0.1	0.45 ± 0.01	0.30 ± 0.04		2
6	0.372 ± 0.003	15	550 ± 10	3.1 ± 0.1	0.49 ± 0.05	0.40 ± 0.04		2
6	0.371 ± 0.007	20	1400 ± 0	3.8 ± 0.3	0.64 ± 0.07	0.53 ± 0.07		2
7	0.620	20	1.4	4.6	0.09	0.02		1
7	0.619	30	2.2	5.2	0.12	0.05		1
7	0.625 ± 0.005	40	4.4 ± 1.0	3.7 ± 1.1	0.15 ± 0.01	0.10 ± 0.06		6
8	0.507 ± 0.004	20	11 ± 4	6.7 ± 0.1	0.19 ± 0.01	0.04 ± 0.01		5
9	0.502 ± 0.004	20	250 ± 30	5.0 ± 1.3	0.45 ± 0.01	0.25 ± 0.04		7
10	0.476 ± 0.006	20	300 ± 30	4.5 ± 0.4	0.42 ± 0.04	0.20 ± 0.03		5
			B. Confined-Side Compactive Tests					
5	0.458 ± 0.002	17.5	150 ± 10		0.42 ± 0.07		22 ± 7	3
6	0.371 ± 0.009	10	98 ± 22		0.50 ± 0.04		34 ± 10	3
6	0.37[illegible] ± 0.006	15	670 ± 197		0.46 ± 0.08		23 ± 7	3
6	0.37[illegible] ± 0.008	20	1600 ± 230		0.60 ± 0.02		25 ± 6	3
7	0.610 ± 0.002	40	2.5 ± 0.5		0.15 ± 0.01		46 ± 10	3
8	0.496 ± 0.008	20	12 ± 0.7		0.24 ± 0.02		39 ± 10	8
9	0.497 ± 0.009	20	130 ± 40		0.45 ± 0.04		20 ± 10	7
10	0.478 ± 0.004	20	220 ± 60		0.41 ± 0.01		25 ± 14	6
			C. Hydrostatic Tests					
5	0.445 ± 0.007	16.7 ± 0.6	1130 ± 43		0.49 ± 0.15			9
6	0.367 ± 0.004	9.2 ± 0.5	430 ± 100		0.34 ± 0.06			3
6	0.360 ± 0.002	15.4 ± 0.7	2250 ± 100		0.61 ± 0.12			4
7	0.634 ± 0.007	40.0 ± 1.2	3.4 ± 0.05		0.15 ± 0.04			7
8	0.513 ± 0.012	19.0 ± 0.8	2.6 ± 0.1		0.38 ± 0.01			5
9	0.516 ± 0.014	19.5 ± 0.9	430 ± 110		0.34 ± 0.07			3
10	0.476 ± 0.018	20.1 ± 0.5	350 ± 110		0.25 ± 0.06			3

same time. Samples produced under identical conditions may differ in creep rate by 20 to 30% and occasionally by 100% or more. The parameters r and m show similar variability.

When snows are prepared at different times out of similar, but not identical snows, and aged under roughly similar, but again not identical, conditions of time and temperature, the differences in measured creep parameters can be as great as a factor of 10 although the densities are nearly equal.

The densities of samples prepared under identical conditions vary several per cent but no correlation is apparent between these small variations and the variations in creep behavior. Apparently, the differences in creep are the result of differences in the aging process. This process is the change from a loose aggregate of angular snow particles to a bonded aggregate of rounded particles. The rate and degree of bonding depend to a large extent on temperature variations which are not well controlled during the aging process. Variability in creep is due, therefore, to differences in the bonding structure of the aged snow. Since variations in creep are large for constant density, the dominant creep mechanism is probably intergranular rather than intragranular, for the former is strongly dependent on the structure but the latter would be structure-independent.

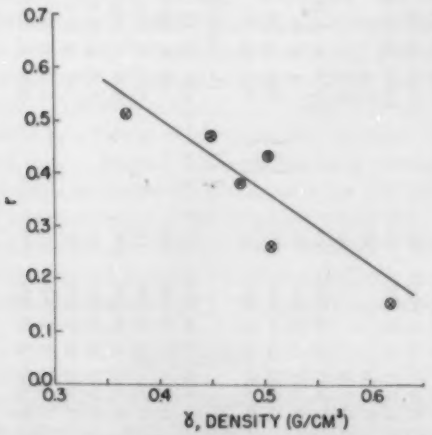

Fig. 7. Variation of average values of time-dependent parameter r with initial density for Group II tests.

E. Time Dependence

Creep curves for snow show a continuously decreasing creep rate which can be represented, with fair accuracy, by a function of the form $\epsilon \propto t^r$. The dependence of r on density is shown in Figure 7, where the average values are plotted for the 6 batches of snow used in Group II tests.

Consider deformation of snow at low stress to be essentially intergranular. As density increases, each particle has more neighbors and more points of contact. For the same externally applied stress, the stress acting on the contact between particles decreases as the number of contact points per particle increases. At low densities this stress is large, resulting in predominantly visco-plastic flow. At higher densities, the stress is small and elastic deformation becomes significant. A value of r equal to unity, as predicted for low densities by extrapolation in Figure 7, is correct for viscous flow. The value of r at high density approaches zero as for purely elastic behavior. Therefore, the observed creep-rate time dependence is mainly due to increasing density and is not the approach to an equilibrium condition.

F. Activation Energy

The activation energy for creep of about 13,400 cal./mole, determined from the Group I tests, agrees adequately with the value 14,000 cal./mole previously reported[5] for uniaxial compression of snow between -5 and $-20°$C.

The value 16,100 cal./mole for polycrystalline ice reported by Jellinek and Brill[10] is based on the purely viscous (and therefore time-independent) component of creep.

Glen[11] obtained a value of 31,800 cal./mole from the minimum creep rates of polycrystalline ice at -1.5, -6.7, and $-12.8°$C. The reliability of his activation energy is strongly dependent on the use of a single value at $-12.8°$C., and therefore a liberal possible error could be assigned to his value.

The activation energy for snow based on creep rates at constant time may not be directly compared with the values based on time-independent creep rate values for ice. From eq. (17) the activation energy determined at constant strain is increased by a factor of $1/r$ over the value at constant time. This would increase the observed value for snow near 0.4 g./cm.^{3} density by a factor of about 2.

Because of the change in density of snow during creep, no steady state creep occurs and the creep rate decreases continuously. In terms of an actual creep mechanism, such as described by Weertman,[12] the pertinent activation energy is for steady state conditions where the production and blocking of imperfections has reached equilibrium. The activation energy for snow, comparable with the steady state value, will lie between the constant time and constant strain values of 14,000 to 27,000 cal./mole. Assuming the activation energy for creep is the same for snow as for ice, the present data do not settle the discrepancy between the values of Jellinek and Brill, and those of Glen.

G. Relations between Creep Rates under Different Stress Conditions

The ratios of creep rates for confined-side and hydrostatic stress conditions to uniaxial creep rates were determined in Group II tests. In Table IV, values of these ratios averaged for tests performed at the same stress are compared to those calculated for constant time and constant change in density. Observed values are seen to fall between the calculated ones in five cases, with the remainder scattered above and below these limits.

From these results it is concluded that the present method of analysis, although leading to some very rough agreement, is not adequate for a complete understanding of triaxial behavior of snow.

H. Density Dependence

Creep rate is a very strong function of density, as can be seen from results in Table III. No analytical representation of the density function has been attempted because of differences in aging of the snow from batch to batch.

Variation of the parameter m with density is erratic as shown in Table IV, and does not agree well with the average curve determined by Bader.[13] However, the values fall within his range of scatter. Differences in the bonding structure of the snows prevent an undistorted picture of the variation of m with density.

I. Lateral Stress for Confined-Side Tests

The lateral stress developed under confined-side conditions is much lower than expected. Observed ratios of vertical to lateral stress

TABLE IV

Comparison of Ratio of Compactive to Uniaxial and Hydrostatic to Uniaxial Strain Rates with Values Calculated on Constant Time and Constant Density Change Basis

Average values for Group II tests are given

γ_0, initial density (g./cm.^{3})	m	r	$\dot{\epsilon}_{zc}/\dot{\epsilon}_{zu}$			$\dot{\epsilon}_{zh}/\dot{\epsilon}_{zu}$		
			Observed	Calc. constant time	Calc. constant density change	Observed	Calc. constant time	Calc. constant density change
0.369	4.2	0.51	0.94	0.85	1.4	3.0	0.52	1.5
0.451	4.3	0.47	0.83	0.86	1.4	6.3	0.54	1.9
0.477	4.5	0.38	0.73	0.88	1.8	1.2	0.56	3.3
0.503	6.7	0.26	1.09	0.95	2.2	0.23	0.70	16
0.503	5.0	0.43	0.52	0.90	1.5	1.72	0.60	2.6
0.626	3.7	0.15	0.58	0.80	18	0.80	0.46	235

vary considerably but are always greater than 20:1. Equation (4), based on the additive theory, predicts ratios of from approximately 3:1 to 6:1. Side friction can be eliminated as a possible cause for this discrepancy, for tests were run which showed that the stress reaching the bottom of the sample was within a few per cent of the applied vertical stress.

An explanation for the low lateral stress is based on the open structure of the snows used. The tendency for snow to expand when subjected to uniaxial compression is erratic, as indicated by the parameter m. This expansion can take place inwardly almost as easily as outwardly and a small lateral stress is sufficient to prevent outward expansion.

V. CONCLUSIONS

Deformation of snow occurs predominantly by intercrystalline sliding. The magnitude of the creep rate depends on the bonding structure between grains. Because of the relative openness of the snows studied, there is no difference in the mode of deformation for uniaxial, confined-side, or hydrostatic stress conditions. In all cases the applied stress ultimately becomes a shear stress acting between individual grains.

The concept of combined stresses producing deformations which are the same as would occur for separate uniaxial stresses is not valid. Openness of structure allows deformation to take place under combined stresses in a somewhat different manner than for uniaxial stress. In particular, the tendency for uniaxial specimens to expand laterally when compressed is easily overcome by small lateral stresses which alter the directed motion to random displacements. Z-axis strain rates, measured at a particular density, as in Group II tests, are not strongly dependent on the type of stress applied. This means that strain rate is a function of the state of the material but does not depend on other simultaneously applied stresses.

Further investigation must be made in order to determine the relationship between combined stress behavior in the laboratory and under natural conditions. The slow process of compaction occurring in the névé regions of glaciers may not necessarily follow the behavior of the faster laboratory tests.

The author wishes to thank Mr. Warren Schlueter for carrying out the Group II experimental work.

References

1. A. E. Johnson, *Proc. Inst. Mech. Engrs. London*, **164,** 432 (1951).

2. L. F. Coffin, Jr., *Mechanics of Creep and Design for Combined Stress*, Proceedings for a short course in Mechanics of Creep, Joseph Marin, Ed., Pennsylvania State University, 1954.

3. E. Bucher, *Beitrage zur Geologie der Schweiz, Geotechnische Serie, Hydrologie* Lieferung 6, 1948. U. S. A. Snow Ice and Permafrost Research Establishment, Translation 18, 1956.

4. Z. Yosida and T. Huzioka, *Some Studies on the Mechanical Properties of Snow*, Union géodesique geophys. intern. Assoc. Hydrologie sci. Compt. rend. Assemb. gén. Rome, 1954.

5. J. K. Landauer, *J. Appl. Phys.*, **26,** 1493 (1955).

6. A. S. Kondrat'eva, I. V. Kragel'skii, and A. A. Shakhov, *Uvelichenie plotnosti snega pod vliianiem szhimaiushchei nagruzki* (*Increase of Density of Snow under Compressive Loading*), in *Fizikomekhanicheski svoistva snega i ikh ispol'zovanie v aerodromnom i dorozhnom stroitel'stva* (*The Physico-Mechanical Properties of Snow*), Izd. Akademii Nauk, Moscow-Leningrad, 1945. Translation: Bureau of Yards and Docks, U. S. Navy, 1949.

7. T. Fujimoto, *Seppyō*, **12,** 207 (1950). (Text in Japanese.)

8. K. Kojima, *Teion-kagaku* (Low Temperature Science, Hokkaido University), **A14** (1955). (Text in Japanese.)

9. J. A. Bender, *Testing of a Compacted Snow Runway*, in *Proc. Am. Soc. Civil Engrs., J. Air Transport Div.*, 1956.

10. H. H. G. Jellinek and R. Brill, *J. Appl. Phys.*, **27,** 1198 (1956).

11. J. W. Glen, *Proc. Roy. Soc. London*, **A228,** 519 (1955).

12. J. Weertman, *J. Appl. Phys.*, **28,** 362 (1957).

13. U. S. Army Snow Ice and Permafrost Research Establishment, *Preliminary Investigations of Some Physical Properties of Snow, SIPRE Report* 7, 1951.

Synopsis

Experiments have been performed on the creep of sifted snows under uniaxial, hydrostatic, and confined-side compressive stresses. The dependence of creep rate on stress (in the range 4 to 40 psi), time (up to several thousand seconds), temperature (between −3.6 and −13.6°C.) and density (from 0.36 to 0.63 g./cm.^{3}) was investigated. For one group of tests, stress was applied for constant time increments, while for another group, stress was continued until an arbitrarily selected small change in density was reached. The results are discussed on the basis of an additive theory for combined stresses.

TRANSACTIONS OF THE SOCIETY OF RHEOLOGY II, 195–218 (1958)

Time Dependence of Mechanical Breakdown in Bundles of Fibers. III. The Power Law Breakdown Rule

BERNARD D. COLEMAN, *Mellon Institute, Pittsburgh 13, Pennsylvania*

INTRODUCTION

This paper represents an extension of previous work[1,2] on the relationships between the strength of a bundle and the strength of its constituent filaments. The calculations presented here are based on the theory of breaking kinetics.[1,3] This phenomenological theory of tensile strength distributions differs from the classical statistical theories of tensile strength[4–8] in that it represents an attempt to account explicitly for the time dependence of mechanical breakdown.

The words *fiber* and *filament* are used interchangeably in this paper. They refer to a single cylindrical entity whose stress history in simple extension can be described by a single-valued scalar function of time. The term *bundle*, as used here, indicates a collection of filaments which are bearing nonseparate loads such that the stress at a particular cross-sectional plane of a given filament depends on the size of the collection and (perhaps) the location of the plane.

Consider a large collection of separated fibers, all of length l, which are bearing equal loads of sufficient magnitude so that some of the fibers will break. We can measure the size of the applied load at time t by means of a function, $f(t)$, which is equal to the total load in dynes at time t divided by the cross-sectional area before loading ($t \leq 0$). In the theory of breaking kinetics the function $f(t)$ is referred to as either "the stress at time t" or "the loading history." It is always assumed that $f = 0$ for $t \leq 0$. The present theory is limited to noncompressive loading histories for which $\infty > f(t) \geq 0$ for all t. We denote the time at which a particular fiber breaks by t_B, the number

that survive without breaking to the time t by $n(t)$, and the size of the collection at zero time by N.

We say that the collection of fibers has been drawn from a *first-order ensemble* if we can write, in the limit of large N, the following deterministic equation,[2]

$$-dn/dt = n(t)l\,\kappa[f(t)] \tag{1}$$

as representing the rate of decrease of n. Here, κ is a function only of f. It is independent of l, it depends on t only insofar as f depends on t, and for separated fibers it is independent of n and N.

The cumulative distribution function, $Q_l(t_B)$, for the lifetimes, t_B, of separated fibers of length l drawn from a first-order ensemble can be obtained by integrating eq. (1):

$$\begin{aligned} Q_l(t_B) &= 1 - n(t_B)/N \\ &= 1 - \exp\left\{-l\int_0^{t_B}\kappa[f(t)]dt\right\} \end{aligned} \tag{2}$$

It has been previously shown[1,3] that eqs. (1) and (2) are compatible with the weakest-link hypothesis; that is, with the notion that the lifetime of a fiber under a given loading history, $f(t)$, must be equal to the lifetime of that cross-sectional region of the fiber which has the *shortest* lifetime under $f(t)$. It has also been pointed out that the first-order ensemble represents the simplest time-dependent breakdown behavior[1,3] compatible with the weakest-link hypothesis. It will be noticed that eq. (1) implies that the probability that a given unbroken fiber breaks in a time interval dt, at t, depends only on the force on the fiber at time t and is independent of the fiber's past loading history. In spite of this probable deficiency of not accounting for any "memory" of past loadings, the theory of the first-order ensemble appears to furnish a reasonably good approximation to the experimentally observed[3] breakdown behavior of real textile fibers.

It is possible to write theories of mechanical breakdown which start with equations of greater generality than eqs. (1) and (2) and which are compatible with the weakest-link hypothesis.[9] These theories do account for some memory of past loading histories. However, it is the purpose of the present paper to calculate distributions of breaking times for bundles of filaments, and it has been found that the mathematical development of stochastic processes[10,11] which represent finite bundles composed of fibers which obey the more general

theories is fraught with serious computational difficulties. This is because it is only in the case of first-order ensembles that the behavior of bundles can be represented by Markov processes[10–12] for which the state of the system is a simple scalar quantity. We shall, therefore, restrict the present discussion to bundles composed of filaments which have been drawn from a first-order ensemble.

The article will be further restricted to bundles composed of untwisted, continuous filaments arranged into parallel arrays which are sufficiently loose to permit the neglect of all effects of interfiber friction (including abrasion). In particular, we shall discuss a special class of twist-free, frictionless bundles, called "ideal bundles."[1]

When the fibers of a first-order ensemble are tested separately under a constant stress, f, their average lifetime is

$$E\{t_B\} = \int_0^\infty t_B \frac{dQ_t}{dt_B}\, dt_B = [l\kappa(f)]^{-1} \tag{3}$$

In previous work on mechanical breakdown in ideal bundles[1,2] it was assumed that κ is an exponential function of f:

$$\kappa[f(t)] = a^{-1}e^{\beta f(t)} \tag{4}$$

Here, a and β are constants which define the fiber ensemble under consideration. Equation (4) might be called the *exponential breakdown rule*. This particular form was chosen for κ because existing experimental evidence indicates[13–17] that for a large class of polymeric fibers (including cottons, rayons, drawn polyesters, and drawn nylons), $E\{t_B\}$ in eq. (3) can be well represented by an exponential function of f over a range of several decades in $E\{t_B\}$. It turned out, however, that for the exponential breakdown rule of eq. (4) the calculation of the lifetime distributions for ideal bundles containing a finite number of filaments was possible only for the special case of constant total load.[1] The systems of differential equations which describe finite ideal bundles under time-dependent total loads (e.g., loads proportional to time and oscillating periodic loads) could not be integrated. The calculation of the lifetimes of infinite ideal bundles composed of filaments obeying eq. (4) was, in general, also difficult when the total load varied with time, and it was found to be necessary to use numerical integration procedures even in the simple case in which the total load was proportional to time.[2]

In this paper we shall investigate the behavior of bundles composed of filaments which obey a *power law* breakdown rule when tested separately:

$$\kappa[f(t)] = c\,[f(t)]^{\rho} \tag{5}$$

where c and ρ are positive constants. In general, we expect to have $\rho > 1$. From eq. (3), we see that the assumption of eq. (5) implies a linear relationship between $\log E\{t_B\}$ and $\log f$ in lifetime-under-dead-load measurements on separated fibers:

$$\log E\{t_B\} = -\log (cl) - \rho \log f \tag{6}$$

Equation (6) furnishes a satisfactory approximation to the dead-load behavior of real systems over limited ranges in $E\{t_B\}$. The main justification, however, for studying in detail the behavior of bundles whose constituent filaments obey the power law breakdown rule is that the functional form assumed in eq. (5) is such as to permit the integration, even for time-dependent loads, of the differential equations which describe both finite and infinite ideal bundles. For systems which obey eq. (5) we can do the mathematics required for the calculation of the loss in mean strength and decrease of the variance in strength that occur when filaments are plied up into bundles.

THE IDEAL BUNDLE

Definitions

The concept of an ideal bundle was introduced in Ref. 1 and defined as a parallel array of filaments of equal length for which the stress distribution has the following properties: (*a*) all unbroken filaments support equal loads, (*b*) broken filaments support no load, and (*c*) all transverse sections of a given filament bear equal stresses.

We shall here consider the behavior of an ideal bundle in a testing apparatus which controls the total load, F (in dynes), on the bundle, so that $F(t)$ is a known function of time.

Let N be the size of the bundle at $t = 0$, and let $n(t)$ be the number of filaments which survive to t without breaking. The lifetime, t_B, of

the bundle is defined to be the time required for $n(t)$ to reach zero.* The cross-sectional area of the bundle before loading (but not including the space between filaments) is taken to be A.

We write

$$f(t) = F(t)/A \tag{7}$$

and thus, for a bundle, $f(t)$ is the stress in dynes cm.$^{-2}$ which would be attributed to each component filament if one did not account for the chance that $n(t) < N$. The actual stress (in dynes per unit of initial cross-sectional area) in each filament at time t is $f(t)N/n(t)$. If $F(t)$ is a monotonic-increasing function of time, then we can define a tensile strength, f^*, for the bundle, as follows:

$$f^* \equiv f(t_B) = \lim_{n(t) \to 0} F(t)/A \tag{8}$$

Equation (8) is the customary operational definition of tensile strength, or tenacity, as measured in apparatus which control the applied load, such as constant-rate-of-loading machines.

We say that an ideal bundle is in the state $\mathcal{E}_{N,n}$ at time t if it contains n unbroken filaments at that time and was originally of size N. We note that the bundle can undergo transitions of the type

$$\mathcal{E}_{N,N} \to \mathcal{E}_{N,N-1} \to \mathcal{E}_{N,N-2} \to \ldots \mathcal{E}_{N,1} \to \mathcal{E}_{N,0} \tag{9a}$$

When it is known that an ideal bundle is in the state $\mathcal{E}_{N,n}$ at a particular moment, the probability of $\mathcal{E}_{N,n} \to \mathcal{E}_{N,n-1}$ occurring in dt is given by

$$\lambda_{N,n}(t)dt + o(dt) \tag{9b}$$

where

$$\lambda_{N,n}(t) = nl\,\kappa[f(t)N/n] \tag{9c}$$

The probability of transitions of the form $\mathcal{E}_{N,n} \to \mathcal{E}_{N,n-j}$, $j > 1$, involves terms of higher order in dt. Equations (9) are valid if, and

* If the bundle were to be placed in apparatus which controls the elongation, such as an Instron tester, then $F(t)$ would be a random variable. If, in addition, the elongation were controlled to be a monotonic-increasing function of time, $F(t)$ could pass through a maximum. In such a case it would be quite reasonable to let t_B be the time at which $F(t)$ reaches its greatest value and to define the tensile strength of the bundle as $F(t_B)/A$.

only if, the filaments in the bundle have been randomly drawn from a first-order ensemble.

The probability that a bundle which is known to be in the state $\mathcal{E}_{N,N}$ at zero time is found in a state $\mathcal{E}_{N,n}$ at time t will be denoted by $P_{N,n}(t)$. Equations (9) define a stochastic process which obeys the following system of differential equations:

$$\begin{aligned}
\frac{\partial P_{N,N}(t)}{\partial t} &= -\lambda_{N,N}(t)P_{N,N}(t) \\
\frac{\partial P_{N,N-1}(t)}{\partial t} &= -\lambda_{N,N-1}(t)P_{N,N-1}(t) + \lambda_{N,N}(t)P_{N,N}(t) \\
\frac{\partial P_{N,n}(t)}{\partial t} &= -\lambda_{N,n}(t)P_{N,n}(t) + \lambda_{N,n+1}(t)P_{N,n+1}(t) \\
\frac{\partial P_{N,0}(t)}{\partial t} &= \lambda_{N,1}(t)P_{N,1}(t)
\end{aligned} \tag{10}$$

subject to the conditions that

$$0 \leq P_{N,n}(t) \leq 1 \tag{11a}$$

$$P_{N,N}(0) = 1 \tag{11b}$$

$$P_{N,n}(0) = 0 \qquad \text{for } n \neq N \tag{11c}$$

Small Ideal Bundles

When F, and thus f, are constant in time, $\lambda_{N,n}$ is independent of t. In this case, we say that the stochastic process is time-homogeneous, and we can easily integrate eqs. (10) to obtain, for $N \geq n \geq 1$:

$$P_{N,n}(t) = \lambda_{N,n}{}^{-1} \sum_{i=N}^{n} \phi_{N,n,i}\, \lambda_{N,i} \exp\left\{-\lambda_{N,i}t\right\} \tag{12a}$$

where

$$\phi_{N,n,j} = \prod_{\substack{i=N \\ i \neq j}}^{n} (1 - \lambda_{N,j}/\lambda_{N,i})^{-1} \tag{12b}$$

When the total load depends on time, we have a nonhomogeneous process, and we cannot write an explicit expression for $P_{N,n}(t)$ un-

less the functional form of $\lambda_{N,n}(t)$ is specified. We note, however, that if we use eq. (5), we can factor $\lambda_{N,n}(t)$ into two parts:

$$\lambda_{N,n}(t) = \alpha(t)\, B_{N,n} \tag{13a}$$

one of which,

$$\alpha(t) = lc\, [f(t)]^p \tag{13b}$$

depends only on time; the other depends only on n and N:

$$B_{N,n} = n(N/n)^p \tag{13c}$$

When this is the case, the stochastic process can be made homogeneous by a simple change of the time scale[18,19] from t to $\theta(t)$:

$$\theta(t) \equiv \int_0^t \alpha(\tau) d\tau \tag{14}$$

It is clear that the assumption that $\infty > f(t) \geq 0$ implies that θ is a continuous, monotonic-increasing function of t. Therefore, the inverse function, $t(\theta)$, is single-valued and monotonic-increasing; and further, finite t implies finite θ. One usually is concerned with loading histories that are sustained long enough to make $\theta(\infty) = \infty$. For such loading histories finite θ implies finite t.

If we now put

$$Q_{N,n}(\theta) \equiv P_{N,n}(t) \tag{15}$$

then we find that in place of eqs. (10) we have

$$\begin{aligned} \frac{\partial Q_{N,N}}{\partial \theta} &= -B_{N,N} Q_{N,N} \\ \frac{\partial Q_{N,n}}{\partial \theta} &= -B_{N,n} Q_{N,n} + B_{N,n+1} Q_{N,n+1} \\ \frac{\partial Q_{N,0}}{\partial \theta} &= B_{N,1} Q_{N,1} \end{aligned} \tag{16}$$

with boundary conditions determined by the relations $Q_{N,n}(0) = P_{N,n}(0)$ and eqs. (11). Since the coefficient of $Q_{N,n}$ in eq. (16) is independent of θ, the solution of eq. (16) is given by eqs. (12) with $P_{N,n}$, $\lambda_{N,j}$ and t replaced, respectively, by $Q_{N,n}$, $B_{N,j}$ and θ:

$$P_{N,n}(t) = Q_{N,n}(\theta) = B_{N,n}^{-1} \sum_{j=N}^{n} \phi_{N,n,j} B_{N,j} \exp\left\{-B_{N,j}\,\theta\right\} \tag{17a}$$

$$= \lambda_{N,n}^{-1} \sum_{j=N}^{n} \phi_{N,n,j} \lambda_{N,j} \exp\left\{-\int_0^t \lambda_{N,j}(\tau)d\tau\right\} \tag{17b}$$

$$\phi_{N,n,j} = \prod_{\substack{i=N \\ i \neq j}}^{n} (1 - B_{N,j}/B_{N,i})^{-1} \tag{17c}$$

$$= \prod_{\substack{i=N \\ i \neq j}}^{n} (1 - \lambda_{N,j}/\lambda_{N,i})^{-1} \tag{17d}$$

The probability, $p_{N,n}(t)\,dt$, that the transition $\mathcal{E}_{N,n} \to \mathcal{E}_{N,n-1}$ occurs in a small time interval at t is simply $\lambda_{N,n}(t)P_{N,n}(t)\,dt$:

$$p_{N,n}(t)dt = \sum_{j=N}^{n} \phi_{N,n,j} \lambda_{N,j}(t) \exp\left\{-\int_0^t \lambda_{N,j}(\tau)d\tau\right\} dt \tag{18}$$

The probability density function for the lifetime of the bundle is $p_{N,1}(t_B)$. The cumulative distribution function for t_B is

$$P_{N,0}(t_B) = \int_0^{t_B} p_{N,1}(t)dt \tag{19a}$$

$$= 1 - \sum_{j=N}^{1} \phi_{N,1,j} \exp\left\{-\int_0^{t_B} \lambda_{N,j}(t)dt\right\} \tag{19b}$$

When $N = 1$, eq. (19b) reduces to eq. (2) for single filaments.

In the special case $\rho = 1$, all the $\lambda_{N,n}$ are identical and the $\phi_{N,n,j}$ are all infinite in magnitude (although some are positive and some negative). This yields a pathological situation in which eqs. (17) and (19b) are indeterminate, and suggests that for $\rho = 1$ it is advisable to re-examine the original differential equation and seek a special solution. If this is done, we find that when $\rho = 1$ our stochastic process is homogeneous in both θ and n, and possesses a modified Poisson distribution[10] for $P_{N,n}(t)$, $N \geq n \geq 1$:

$$P_{N,n}(t) = \frac{e^{-N\theta(t)}\,[N\theta(t)]^{N-n}}{(N-n)!}$$

We shall not go into this special case any further, because in physical applications of the theory we expect to have $\rho > 1$, not $\rho = 1$.

We note that according to eq. (19b) a necessary and sufficient condition to have, for finite N,

$$P_{N,0}(\infty) = 1 \tag{20a}$$

is that

$$\lim_{t \to \infty} \int_0^t \lambda_{N,n}(\tau) d\tau = \infty \tag{20b}$$

or $\theta(\infty) = \infty$. In other words, if the loading history is such that $\theta(\infty) = \infty$, it is "almost certain" that the last fiber in the bundle will break if we wait long enough. If $\theta(\infty) < \infty$, there is a positive probability, $1 - P_{N,0}(\infty)$, that the bundle will never break down completely.

Let $E_{N,n}\{t^m\}$ be the mth moment of the distribution of times of occurrence of the transition $\mathcal{E}_{N,n} \to \mathcal{E}_{N,n-1}$:

$$E_{N,n}\{t^m\} = \int_0^\infty t^m p_{N,n}(t) dt \tag{21}$$

The average lifetime of the bundle, $E\{t_B\}$, is the same as $E_{N,1}\{t\}$. The direct computation of moments by means of eq. (21) is possible but usually leads to expressions which rapidly increase in complexity with increasing N. For example, if we consider the behavior of an ideal bundle in a constant-rate-of-loading apparatus, so that $F(t)$ is proportional to time:

$$f(t) = \alpha t \tag{22a}$$

$$f^* = \alpha t_B \tag{22b}$$

then eqs. (13), (18), and (21) yield

$$E_{N,n}\{t^m\} = \left[\frac{\rho + 1}{lc\ \alpha^\rho N^\rho}\right]^{m/(\rho+1)} \Gamma\left(1 + \frac{m}{\rho + 1}\right) \sum_{j=N}^{n} \phi_{N,n,j} j^{m\omega} \tag{23a}$$

where Γ denotes the gamma function, and

$$\omega = \frac{\rho - 1}{\rho + 1} \tag{23b}$$

It is quite clear that eqs. (23) are useful only for small N. When $N = 1$, eqs. (23) give the following expression for the average tenacity, $E_1\{t^*\}$, of separated filaments:

$$E_1\{f^*\} = E\{\alpha t_B\} = \alpha E_{1,1}\{t\} = \left[\frac{(\rho+1)\,\alpha}{lc}\right]^{1/(\rho+1)} \Gamma\left(1 + \frac{1}{\rho+1}\right) \tag{24}$$

The average tenacity, $E_2\{f^*\}$, of a bundle of two filaments is

$$E_2\{f^*\} = \alpha E_{2,1}\{t\}$$
$$= \left[\frac{(\rho+1)\alpha}{lc\,2^\rho}\right]^{1/(\rho+1)} \Gamma\left(1 + \frac{1}{\rho+1}\right) \times \left\{\frac{2^\rho}{1-2^{1-\rho}} + \frac{1}{1-2^{\rho-1}}\right\} \tag{25}$$

The Semi-Invariants for θ_B

Let Δt_n be the time the bundle spends in the state $\mathcal{E}_{N,n}$. Regardless of the time-dependence of the total load, the probability density function for Δt_n is

$$q(\Delta t_n)d(\Delta t_n) = \exp\left\{-\int_t^{t+\Delta t_n} \lambda_{N,n}(\tau)d\tau\right\}\lambda_{N,n}(t+\Delta t_n)\,d(\Delta t_n) \tag{26}$$

The value of t at the moment that $\mathcal{E}_{N,n+1} \rightarrow \mathcal{E}_{N,n}$ occurs (i.e., the time required to reach the state $\mathcal{E}_{N,n}$) is simply the sum of the time spent in all states between $\mathcal{E}_{N,N}$ and $\mathcal{E}_{N,n}$:

$$t = \sum_{j=N}^{n+1} \Delta t_j \tag{27}$$

This is the value of t to be used in eq. (26).

When the total load is *constant*, $\lambda_{N,n}$ is constant and the N quantities Δt_n constitute a set of independent random variables, each with its own probability density function:

$$q(\Delta t_n)d(\Delta t_n) = \exp\{-(\Delta t_n)\lambda_{N,n}\}\lambda_{N,n}d(\Delta t_n) \tag{28}$$

Equation (28) is the well-known Laplace (or exponential) distribution,[10] which frequently occurs in the theory of time-homogeneous stochastic processes. It possesses a moment generating function, $G_n(s)$, given by:

$$G_n(s) = \int_0^\infty \exp\{s\Delta t_n\}q(\Delta t_n)d(\Delta t_n) \tag{29a}$$
$$= (1 - s/\lambda_{N,n})^{-1} \tag{29b}$$

Here, s is a pure imaginary number. The mth semi-invariant,[11,20] $x_{n,m}\{\Delta t_n\}$, of the distribution of Δt_n is defined as follows

$$x_{n,m}\{\Delta t_n\} \equiv \frac{\partial^m \log G_n(s)}{\partial s^m}\bigg|_{s=0} \tag{30}$$

The first semi-invariant, $x_{n,1}$, is the average value, $E\{\Delta t_n\}$, of Δt_n. The second, $x_{n,2}$, is the variance, $\sigma^2\{\Delta t_n\}$, for Δt_n. The third, $x_{n,3}$, is the third central moment, $\mu^3\{\Delta t_n\}$.

For the time-homogeneous stochastic process of eqs. (28) and (29), we have

$$\log G_n(s) = \sum_{m=1}^{\infty} m^{-1} s^m \lambda_{N,n}^{-m} \tag{31a}$$

so that

$$x_{n,m} = (m-1)!\,\lambda_{N,n}^{-m} \tag{31b}$$

The semi-invariants of independent random variables are additive.[20] It follows that the semi-invariants, $X_{N,n,m}\{t\}$, of the time occurrence of the transition $\varepsilon_{N,n} \rightarrow \varepsilon_{N,n-1}$ are, when F is constant,

$$X_{N,n,m}\{t\} = \sum_{j=N}^{n} x_{j,m}\{\Delta t_j\} = (m-1)! \sum_{j=N}^{n} \lambda_{N,j}^{-m} \tag{32a}$$

For example:

$$E_{N,n}\{t\} = \sum_{j=N}^{n} E\{\Delta t_j\} = \sum_{j=N}^{n} \lambda_{N,j}^{-1} \tag{32b}$$

$$\sigma_{N,n}^2\{t\} = \sum_{j=N}^{n} \sigma^2\{\Delta t_j\} = \sum_{j=N}^{n} \lambda_{N,j}^{-2} \tag{32c}$$

$$\mu_{N,n}^3\{t\} = \sum_{j=N}^{n} \mu^3\{\Delta t_j\} = 2\sum_{j=N}^{n} \lambda_{N,j}^{-3} \tag{32d}$$

When F varies with time, eqs. (28), (29b), (31), and (32) no longer hold. Our stochastic process is always homogeneous, however, on the time scale $\theta(t)$. Thus, if we let $\Delta\theta_n$ be the change in θ while the bundle stays in the state $\varepsilon_{N,n}$, we can immediately write, for any $f(t)$, the following expression for the semi-invariants of the distribution of the

total value* of θ at the moment that $\mathcal{E}_{N,n} \to \mathcal{E}_{N,n-1}$ occurs:

$$X_{N,n,m}\{\theta(t)\} = \sum_{j=N}^{n} x_{j,m}\{\Delta\theta_j\} = (m-1)! \sum_{j=N}^{n} B_{N,j}^{-m} = (m-1)! \sum_{j=N}^{n} j^{-m}(j/N)^{\rho m} \tag{33}$$

Equation (33) is identical to eq. (32a) except that θ is substituted for t and $B_{N,j}$ for $\lambda_{N,j}$.

According to eq. (33), the distribution of the value of θ at the moment the last fiber breaks [i.e., the lifetime, θ_B, of the bundle on the time-scale $\theta(t)$] possesses the semi-invariants, $X_{N,1,m}$:

$$X_{N,1,m}\{\theta\} = (m-1)! \sum_{n=N}^{1} n^{-m}(n/N)^{\rho m} \tag{34a}$$

In particular, the first three semi-invariants of the lifetime, θ_B, on the time-scale $\theta(t)$ are:

$$E\{\theta_B\} \equiv X_{N,1,1}\{\theta\} = \sum_{n=N}^{1} n^{-1}(n/N)^{\rho} \tag{34b}$$

$$\sigma^2\{\theta_B\} \equiv X_{N,1,2}\{\theta\} = \sum_{n=N}^{1} n^{-2}(n/N)^{2\rho} \tag{34c}$$

$$\mu^3\{\theta_B\} \equiv X_{N,1,3}\{\theta\} = 2 \sum_{n=N}^{1} n^{-3}(n/N)^{3\rho} \tag{34d}$$

If one is interested in the behavior of small bundles with $\rho >> 1$, it is convenient to write eqs. (34a) and (34b) in the following form:

$$X_{N,1,m}\{\theta\} = \frac{1}{N^m}\left[1 + \sum_{r=1}^{N-1}\left(\frac{N-r}{N}\right)^{m\rho-m}\right] \tag{34a}'$$

$$E\{\theta_B\} = \frac{1}{N}\left[1 + \sum_{r=1}^{N-1}\left(\frac{N-r}{N}\right)^{\rho-1}\right] \tag{34b}'$$

Thus, if $\rho \to \infty$ with N and m kept finite, $X_{N,1,m}\{\theta\} \to N^{-m}$; it follows that $E\{\theta_B\}$ is inversely proportional to N for small N and $\rho >> 1$.

* We use the symbol $x_{n,m}$, with two subscripts, for the mth semi-invariant (or cumulant) of random variables such as Δt_n and $\Delta\theta_n$ which involve only one transition, $\mathcal{E}_{N,n} \to \mathcal{E}_{N,n-1}$. We use the symbol $X_{N,n,m}$, with three subscripts, for the mth semi-invariant of random variables such as t and θ, which involve several transitions, i.e., all the transitions between $\mathcal{E}_{N,N}$ and $\mathcal{E}_{N,n-1}$.

Infinite Ideal Bundles

To evaluate the sums in eqs. (34) for the limit of large N, we make the substitution $y = n/N$ and note that $\Delta y = 1/N$ when n increases by 1. Equation (34a) yields the Riemann integral:

$$\lim_{N\to\infty} X_{N,1,m}\{\theta\} \to (m-1)!\,N^{-m+1}\int_0^1 y^{m\rho-m}\,dy = \frac{(m-1)!}{N^{m-1}(m\rho-m+1)} \tag{35a}$$

and, in particular:

$$\lim_{N\to\infty} E\{\theta_B\} \to \rho^{-1} \tag{35b}$$

$$\lim_{N\to\infty} \sigma^2\{\theta_B\} \to N^{-1}(2\rho-1)^{-1} \tag{35c}$$

$$\lim_{N\to\infty} \mu^3\{\theta_B\} \to 2N^{-2}(3\rho-2)^{-1} \tag{35d}$$

From eqs. (35) it is clear that for $\rho > 0$, $E\{\theta_B\}$ is always finite. Sufficient conditions to have $\sigma^2\{\theta_B\}$ and $\mu^3\{\theta_B\}$ finite for all N are to have, respectively, $\rho > 1/2$ and $\rho > 2/3$. If $\rho > 1$, all the $X_{N,1,m}\{\theta_B\}$ with $\infty > m \geq 1$ are finite and go to zero as $N \to \infty$.

There is a famous theorem in probability theory which states the following: If $\gamma_1, \gamma_2, \ldots, \gamma_n, \ldots$ be mutually independent random variables, then the probability of convergence of the series

$$\sum_{n=1}^{\infty} \gamma_n$$

is either *zero* or *one*. In particular, this probability equals one when both the series

$$\sum_{n=1}^{\infty} E\{\gamma_n\} \quad \text{and} \quad \sum_{n=1}^{\infty} \sigma^2\{\gamma_n\}$$

converge. It follows from this powerful theorem that whenever $\rho > 1/2$, θ_B is, *with probability one*, finite, for all bundle sizes—finite or infinite.

All experimental evidence indicates that for single filaments mechanical breakdown is "autocatalytic" in the sense that the increase in the rate of breakdown [as measured, say, by $(E\{t_B\})^{-1}$] with an increase in stress is always greater than that predicted by a linear

relationship between rate of breakdown and stress. This means that we can expect to find $\rho > 1$; and thus both θ_B and t_B will be finite whenever $\theta(\infty) = \infty$, regardless of N.

We note that according to eqs. (34) the semi-invariants of θ_B for separate filaments ($N = 1$) are

$$E\{\theta_B\} = 1 \tag{36a}$$

$$\sigma^2\{\theta_B\} = 1 \tag{36b}$$

$$\mu^3\{\theta_B\} = 2 \tag{36c}$$

$$X_{1,1,m}\{\theta_B\} = (m-1)! \tag{36d}$$

On the time scale θ, the average lifetime of an infinite ideal bundle is ρ^{-1} times the average lifetime of its component filaments. A detailed examination of the sum in eq. (34b) indicates that for $\rho > 1$, $E\{\theta_B\}$ decreases monotonically toward the limiting value shown in eq. (35b). For $\rho = 1$, $E\{\theta_B\}$ is independent of bundle size. For $\rho < 1$, $E\{\theta_B\}$ increases monotonically with increasing bundle size.

It is clear from eqs. (35) that, for $\rho > {}^2/_3$, as N approaches infinity the distribution of θ_B becomes perfectly sharp with the coefficient of variation, $\sigma\{\theta_B\}/E\{\theta_B\}$, and the coefficient of skewness, $\mu^3\{\theta_B\}/\sigma^3\{\theta_B\}$, both decreasing as $N^{-1/2}$.

We wish to apply the central limit theorem to θ_B. To do this, we define a new random variable $T_B \equiv N\theta_B$ which is the sum of a set of independent random variables, ΔT_n, defined as $\Delta T_n \equiv N\Delta\theta_n$. We note that for all N, finite or infinite, the mean value of ΔT_n, $E\{\Delta T_n\} = NE\{\Delta\theta_n\}$, and the variance for ΔT_n, $\sigma^2\{\Delta T_n\} = N^2\sigma^2\{\Delta\theta_n\}$, are finite and positive. Further

$$\lim_{N\to\infty} \sigma^2\{T_B\} = \lim_{N\to\infty} \sum_{n=N}^{1} \sigma^2\{\Delta T_n\} \to \infty$$

which is a necessary condition for the application of the central limit theorem. We now examine the third absolute central moment for ΔT_n:

$$C_{n,3} \equiv E\{|\Delta T_n - E\{\Delta T_n\}|^3\}$$

The variables ΔT_n are always positive. Therefore,

$$C_{n,3} < E\{(\Delta T_n + E\{\Delta T_n\})^3\}$$

or

$$C_{n,3} < E\{(\Delta T_n)^3\} + 3E\{(\Delta T_n)^2\}\, E\{\Delta T_n\} + 3[E\{(\Delta T_n)\}]^2 E\{\Delta T_n\} + [E\{\Delta T_n\}]^3$$

$$C_{n,3} < E\{(\Delta T_n)^3\} + 3E\{\Delta T_n\}\, E\{\Delta T_n^2\} + 4[E\{\Delta T_n\}]^3$$

The following relations between the moments of a distribution and the first three semi-invariants are completely general[20] and follow from the definition of the semi-invariants:

$$E\{\Delta T_n\} = x_{n,1}\{\Delta T_n\}$$

$$E\{(\Delta T_n)^2\} = x_{n,2}\{\Delta T_n\} + x_{n,1}^2\{\Delta T_n\}$$

$$E\{(\Delta T_n)^3\} = x_{n,3}\{\Delta T_n\} + 3x_{n,1}\{\Delta T_n\}x_{n,2}\{\Delta T_n\} + x_{n,1}^3\{\Delta T_n\}$$

Our last inequality for $C_{n,3}$ may therefore be written as follows

$$C_{n,3} < x_{n,3}\{\Delta T_n\} + 6x_{n,1}\{\Delta T_n\}x_{n,2}\{\Delta T_n\} + 8x_{n,1}^3\{\Delta T_n\}$$

If we now note that $x_{n,3}\{\Delta T_n\} = NB_{N,n}^{-1}$, $x_{n,2}\{\Delta T_n\} = N^2B_{N,n}^{-2}$, and $x_{n,3}\{\Delta T_n\} = 2N^3B_{N,n}^{-3}$, we finally obtain a simple upper bound for $C_{n,3}$:

$$C_{n,3} < 16N^3B_{N,n}^{-3} = 8\,N^3x_{n,3}\{\Delta\theta_n\}$$

It follows that

$$\frac{\sum_{n=N}^{1} C_{n,3}}{\sigma^3\{T_B\}} < \frac{8N^3\sum_{n=N}^{1} x_{n,3}\{\Delta\theta_n\}}{N^3\sigma^3\{\theta_B\}} = \frac{8\mu^3\{\theta_B\}}{\sigma^3\{\theta_B\}}$$

and thus, for $\rho > {}^2/_3$, eqs. (35c) and (35d) yield

$$\lim_{N\to\infty} \frac{\sum_{n=N}^{1} C_{n,3}}{\sigma^3\{T_B\}} = O(N^{-1/2}) \to 0$$

According to Liapounoff's form of the central limit theorem,[20] this means that, for $\rho > {}^2/_3$, in the limit as N approaches infinity the distribution of T_B is asymptotically normal. It follows that for $\rho > {}^2/_3$, as $N \to \infty$, the variable θ_B becomes asymptotically normal with its mean equal to ρ^{-1} and its variance equal to $N^{-1}(2\rho - 1)^{-1}$. Thus we have solved the problem of calculating the distribution of t_B for large N. In the limit as $N \to \infty$, eqs. (19) become

$$\lim_{N\to\infty} P_{N,0}(t_B) = \lim_{N\to\infty} Q_{N,0}[\theta(t_B)] = \Phi[(\theta_B - \rho^{-1})\sqrt{N(2\rho - 1)}] \tag{37a}$$

where Φ is the error integral:

$$\Phi(y) = \frac{1}{\sqrt{2\pi}} \int_{-\infty}^{y} \exp\{-z^2/2\} dz \tag{37b}$$

The probability density function for t_B becomes

$$\lim_{N\to\infty} p_{N,1}(t_B) dt_B = \sqrt{\frac{N(2\rho - 1)}{2\pi}} \exp\left\{-\frac{N}{2}\left(lc \int_0^{t_B} [f(t)]^\rho dt - \rho^{-1}\right)^2 (2\rho - 1)\right\} \times lc[f(t_B)]^\rho dt_B \tag{38}$$

According to eq. (35b), when $N = \infty$ the expected value of t_B is the real, positive root of

$$\rho^{-1} = \theta(t_B) \equiv lc \int_0^{t_B} [f(t)]^\rho dt \tag{39}$$

and according to eq. (35c), the fluctuations from this value of t_B are negligible for $N = \infty$ if $\rho > 1/2$. It will be noticed that eq. (39) can be obtained from the solution of the deterministic equation

$$-dn/dt = [f(t)N/n]^\rho lc \tag{40}$$

subject to the conditions $n(0) = N$, $n(t_B) = 0$. The almost intuitive fact that eq. (40) is valid for large N may be derived by replacing j/N by y in eq. (33) to obtain the Riemann integral

$$\lim_{N\to\infty} X_{N,n,m}\{\theta(t)\} = \frac{(m-1)!}{N^{m-1}} \int_{n/N}^{1} y^{m\rho - m} dy \tag{41a}$$

$$= \frac{(m-1)!}{N^{m-1}(m\rho - m + 1)} [1 - (n/N)^{m\rho - m + 1}] \tag{41b}$$

If we put $m = 1$ and $m = 2$ in eq. (41b) we obtain

$$\lim_{N\to\infty} E_{N,n}\{\theta(t)\} = \rho^{-1}[1 - (n/N)^\rho] \tag{42a}$$

$$\lim_{N\to\infty} \sigma^2_{N,n}\{\theta(t)\} = N^{-1}(2\rho - 1)^{-1}[1 - (n/N)^{2\rho - 1}] \tag{42b}$$

Differentiation with respect to t of eq. (42a) yields eq. (40). Equation (42b) makes it clear that when $\rho > 1/2$, and $N = \infty$, there are no fluctuations from eq. (40).

We shall now use eq. (39) for explicit calculations of the lifetime of infinite ideal bundles under various loading histories, $f(t)$, that can occur in practical applications. We shall then compare the resulting expressions for t_B with calculated values of the average lifetime, $E\{t_B\}$, which the component filaments would exhibit if the filaments were tested *separately* under the same $f(t)$.

When f is a constant, eq. (39) yields

$$t_B = \rho^{-1}(lcf^\rho)^{-1} \tag{43}$$

According to eq. (3), if the filaments were tested individually, under the same load, f (in dynes cm.$^{-2}$), the average lifetime would be

$$E\{t_B\} = (lcf^\rho)^{-1} \tag{44}$$

confirming the result that for $\rho > 1$, a bundle is weaker than its components.

When $f(t)$ is a periodic function of time, with a frequency, ν, high enough so that $\nu t_B \gg 1$, eq. (39) may be written

$$\rho^{-1} = lc \langle f^\rho \rangle_{AV} t_B + O(1/\nu) \tag{45}$$

where $\langle f^\rho \rangle_{AV}$ denotes the average value of f^ρ averaged over one cycle in time:

$$\langle f^\rho \rangle_{AV} = \nu \int_0^{1/\nu} [f(t)]^\rho dt \tag{46}$$

Thus, for high frequencies, the lifetime of an infinite ideal bundle under a periodic loading history is

$$\lim_{\nu t_B \gg 1} t_B = \rho^{-1}(lc \langle f^\rho \rangle_{AV})^{-1} \tag{47}$$

The average lifetime of the individual filaments under the same periodic $f(t)$ may be calculated from eq. (2). The following result is obtained:

$$\lim_{\nu t_B \gg 1} E\{t_B\} = (lc \langle f^\rho \rangle_{AV})^{-1} \tag{48}$$

For a particular example of a periodic load we may consider a sequence of saw-tooth pulses of maximum amplitude, g (in dynes cm.$^{-2}$), which are repeated at intervals, $1/\nu$:

$$f(t) = \begin{cases} gt\nu, & t < 1/\nu \\ 0, & t = 1/\nu \\ f(t - 1/\nu), & t > 1/\nu \end{cases} \tag{49}$$

When eq. (49) is substituted into eqs. (46) and (47), the following expression is obtained for the lifetime of an infinite ideal bundle:

$$t_B = (\rho + 1)\,(\rho\, lcg^\rho)^{-1} \tag{50}$$

The average lifetime of the component filaments tested separately under the same stress is

$$E\{t_B\} = (\rho + 1)\,(lcg^\rho)^{-1}$$

For both static loads, and periodic loads of high frequency, t_B for the infinite bundle differs from $E\{t_B\}$ for separate filaments only in the presence of the factor ρ^{-1}. This observation is really a direct consequence of the remark made under eqs. (36) and the fact that for such loading histories $\theta(t)$ is proportional to t. [See eq. (14).]

When $\theta(t)$ is not proportional to t, the relation between t_B for a bundle and $E\{t_B\}$ for the component filaments is more complicated. Consider, for example, the breaking of an infinite ideal bundle in a constant-rate-of-loading apparatus which produces the loading history described by eqs. (22). In this case, eq. (39) yields

$$f_\infty^* = \alpha t_B = \left(\frac{\alpha(\rho + 1)}{lc\rho}\right)^{1/(1+\rho)} \tag{52}$$

When eq. (52) is compared with eq. (24) we see that for $\rho > 2$, the tenacity, f_∞^*, of the infinite bundle is less than the average tenacity, $E_1\{f^*\}$, of its component filaments. But when $\rho = 1$, f_∞^* is greater than $E_1\{f^*\}$, because then $E_1\{f^*\} = \Gamma(1 + 0.5)f_\infty^* \simeq 0.886 f_\infty^*$. Thus, there exists a critical value of ρ between 1 and 2 which must be exceeded to have $f_\infty^* < E_1\{f^*\}$. This strange result is due to the lack of proportionality between θ_B and t_B. The "natural" measure of strength, $E\{\theta_B\}$, always decreases with increasing N when $\rho > 1$ and is always invariant to changes in N when $\rho = 1$. It does not follow that the same is true for $E\{t_B\}$ or $E\{f^*\}$, even though the functions $t(\theta)$ and $\theta(t)$ are monotonic and single-valued for each $f(t)$. It does

appear to be generally true, however, that for each loading history, $f(t)$, there exists a critical value of ρ, say ρ_c, such that if $\rho > \rho_c$, then $E\{t_B\}$ is a monotonic-decreasing function of N. When f is constant, $\rho_c = 1$; when $f = \alpha t$, ρ_c lies between 1 and 2.

Intermediate Values of N

For the rest of our discussion of the distribution of lifetimes for ideal bundles of size N it will be convenient to talk in terms of a new random variable, $y_N(t_B)$, defined as follows:

$$y_N(t_B) = \frac{\theta_B - E\{\theta_B\}}{\sigma\{\theta_B\}} \tag{53a}$$

$$= \frac{\sum_{n=N}^{1} \Delta\theta_n - \sum_{n=N}^{1} B_{N,n}^{-1}}{\left[\sum_{n=N}^{1} B_{N,n}^{-2}\right]^{1/2}} \tag{53b}$$

In mathematical statistics,[20] y_N is called the "standardized sum" of the independent random variables, $\Delta\theta_n$. This standardized sum of the $\Delta\theta_n$ is simply related to the true sum, θ_B, but is so defined that for all N it has a mean value equal to zero and a variance equal to unity.

It is clear that

$$\lim_{N\to\infty} y_N = (\theta_B - \rho^{-1})\sqrt{N(2\rho - 1)} \tag{54}$$

Let $Y_N(y_N)$ be the cumulative distribution function for y_N: $Y_N(y_N) = Q_{N,0}(\theta_B) = P_{N,0}(t_B)$.

Equations (37) and (38) give expressions for the distribution of t_B that are valid for very large N. According to some results of Cramér,[21] eq. (37) may be regarded as the first term in an asymptotic expansion of $Y_N(y_N)$ in powers of $N^{-1/2}$:

$$\lim_{N\to\infty} Y_N[y_N(t_B)] = \Phi[y_N(t_B)] + O(N^{-1/2}) \tag{55}$$

The error involved in using eqs. (37) and (38) is of the order $N^{-1/2}$. This error may be too large when one is dealing with bundles that contain, say, 20 to 200 filaments. For such bundles, N is already rather large for arithmetical evaluation of the complicated, yet exact, expressions in eqs. (18) and (19). On the other hand, bundles of such a size frequently occur in textile technology.

This practical problem may be overcome by using a series introduced by Edgeworth[20,22] which permits the expansion of the distribution function for a standardized sum in terms of the derivatives, $\Phi^{(m)}$, of the error integral,

$$\Phi^{(m)}(y) = \frac{\partial^m \Phi(y)}{\partial y^m} \tag{56}$$

and a set of quantities, $\gamma_{m,N}$, which, in the present problem, are simply related to the semi-invariants for θ_B:

$$\gamma_{m,N} = \frac{X_{N,m,1}\{\theta_B\}}{\sigma^m\{\theta_B\}} \tag{57a}$$

$$= \frac{(m-1)! \sum_{n=N}^{1} n^{-m}(n/N)^{m\rho}}{\left[\sum_{n=N}^{1} n^{-2}(n/N)^{2\rho}\right]^{m/2}} \tag{57b}$$

Cramér[21] has presented sufficient conditions for the use of Edgeworth's series as an asymptotic expansion in powers of $N^{-1/2}$ of the distribution of a standardized sum of N independent random variables drawn from different populations. His results are general enough to apply directly to our standardized sum, y_N, of the independent random variables, $\Delta\theta_n$, and to permit us to say that for $\rho \geq 1$ Edgeworth's series can be carried out to any desired power of $N^{-1/2}$. The asymptotic evaluation of $Y_N(y_N)$ to within terms of order $N^{-3/2}$ is

$$\begin{aligned} Y[y_N(t_B)] = \Phi(y_N) &- \left[\frac{\gamma_{3,N}}{3!}\Phi^{(3)}(y_N)\right] + \\ &\left[\frac{\gamma_{4,N}}{4!}\Phi^{(4)}(y_N) + \frac{10\,\gamma_{3,N}^2}{6!}\Phi^{(6)}(y_N)\right] - \\ &\left[\frac{\gamma_{5,N}}{5!}\Phi^{(5)}(y_N) + \frac{35\,\gamma_{3,N}\gamma_{4,N}}{7!}\Phi^{(7)}(y_N) + \right. \\ &\left. \frac{280\,\gamma_{3,N}^3}{9!}\Phi^{(9)}(y_N)\right] + O(N^{-2}) \end{aligned} \tag{58}$$

The term in the first square bracket is $O(N^{-1/2})$; the terms in the second and third square brackets are, respectively, $O(N^{-1})$ and $O(N^{-3/2})$. It is not claimed that the series of eq. (58) converges for fixed, finite N, but merely that it represents an asymptotic expansion

of $Y_N(y_N) = P_{N,0}(t_B)$ for large N. The following expression which is obtained from eqs. (35) and (57a) should be of use in evaluating eq. (58) for $N > 100$:

$$\lim_{N\to\infty} \gamma_{m,N} = \frac{(m-1)!(2\rho-1)^{m/2}}{N^{(m/2)-1}(m\rho - m + 1)} \tag{59}$$

However, for each particular set of values of N, m, and ρ, one should carefully investigate the error involved in approximating eq. (57b) by eq. (59).

SUMMARY AND CONCLUSIONS

We have investigated the breakdown behavior of ideal bundles composed of filaments which obey eqs. (1) and (5) when tested separately. By a change of the time scale from the true time, t, to an artificial time, $\theta(t)$ [see eqs. (14) and (13b)], it was possible to formulate the behavior of such an ideal bundle as a time-homogeneous stochastic process,[12,18] even when the total load depends on time. One conclusion that immediately followed from this observation is that the quantity, θ_B, defined as $\theta_B \equiv \theta(t_B)$, furnishes a convenient measure of the strength of the bundle. Becasue θ_B is the sum of a set of independent random variables, $\Delta\theta_n$, it could be shown by use of the central limit theorem that, subject to very general conditions, in the limit as N approaches infinity, θ_B is distributed according to a normal (Gaussian) distribution [see eqs. (37) and (38)]. It was shown that for large, but far from infinite, N it is possible to develop an asymptotic expansion for the distribution of θ_B as a power series in $N^{-1/2}$ [see eqs. (53), (56), (57), and (58)].

It was also pointed out that for each given $f(t)$ the average strength, as measured by $E\{\theta_B\}$, decreases with increasing N whenever $\rho > 1$, and actual fibers are expected to have $\rho > 1$. When θ is proportional to t, as in the case of dead loads or periodic loads of high frequency, the average true lifetime, $E\{t_B\}$, for a given $f(t)$ increases, decreases, or remains constant with increasing N depending, respectively, on whether ρ is greater than, less than, or equal to unity.

The rate of breakdown of very large bundles is described, in the limit $N \to \infty$, by eq. (40) which is a deterministic equation (that is, it ignores any possibility of fluctuations) analogous to the equations of chemical kinetics. Equation (42a) is the solution of eq. (40). A

measure of the fluctuations from this solution for large, yet finite, N was presented in eq. (42b).

It is possible to criticize all of the calculations of this paper for their reliance on eq. (5) which is used to furnish a definite functional form for $\kappa(fN/n)$ in eq. (9c). It was pointed out that eq. (5), which implies eq. (6), was chosen mainly for mathematical convenience. It is suspected that eq. (6) can be accurate only for limited ranges of $E\{t_B\}$ and f; yet, for large values of N the argument of κ in eq. (9c) changes over a wide range, even for constant f, as n gets close to unity. This is not really a serious matter, however, for a practical bundle with $\rho > 1$, because when N is large and $\rho > 1$ the bundle does not spend much time in those states $\mathcal{E}_{N,n}$, $n > 1$, for which $n \ll N$. In other words, when $n \ll N$, and $\rho > 1$, Δt_n makes a very small relative contribution to t_B. Most of the time required for complete breakdown is spent in those states for which n is close to N, and the transition probabilities for departure from such states are accurately described by eqs. (5) and (9c) whenever eq. (6) has been experimentally verified over a small range in f.

There does exist, however, a serious limitation on the present calculations which must be clearly emphasized. In comparisons of the predictions of the present calculations with experiment it will be very important to first make sure that one is dealing with bundles that obey items (*a*), (*b*), and (*c*) of the definition of an ideal bundle given on page 198.

Relation of This Work to the Classical Theory of Daniels

An elegant theory of the relations between the strength of bundles and the strength of their component filaments has been developed by Daniels.[8] Daniels makes assumptions in his work which are in effect almost equivalent to items (*a*), (*b*), and (*c*) of page 198 of the present paper, and his theory is also restricted to low-friction, low-twist bundles for which all the constituent filaments have stress-strain curves of the same shape. He considers the behavior of bundles which have been placed in an apparatus which controls elongation rather than total load, so that his criterion for failure is that given in the footnote on page 199, rather than our failure criterion of $n(t_B) = 0$.

The principal difference between Daniels' theory and the present one is that he is concerned with bundles whose tensile strength is independent of the speed of measurement (i.e., independent of the rate-

of-loading for $f = \alpha t$, or the time allowed for failure when f is a constant), whereas in the present work we have accounted for the dependence of strength on speed of measurement but have assumed that our fibers have been sampled from a first-order ensemble. We have also assumed a very definite functional form for the dependence of the strength of isolated filaments on time allowed for failure, namely, that shown in eq. (6).

Since Daniels' theory does not make any mention of the time dependence of the elongation of the bundle, aside from assuming that it is monotonic-increasing in time, his theory implicitly assumes (*a*) that the strength of the constituent filaments is independent of loading history, and (*b*) that the stress-strain curves of the filaments are independent of rate of stretching. It is also implicitly assumed in his work that (*c*) a fiber breaks instantly when its critical strength is exceeded. Now, for fibers which obey these three assumptions, the strength of a bundle has the same value if one controls the elongation to be monotonic in time and takes the maximum in $F(t)$ as the point of failure or if one controls $F(t)$ to be monotonic and takes the time of occurrence of $\varepsilon_{N,1} \rightarrow \varepsilon_{N,0}$ as the point of failure. Of course, such an equivalence of the two failure criteria does not apply to the systems discussed in the present paper.

Daniels' theory should be applicable to bundles made of fibers, such as steel wires, whose strength properties are not very sensitive to rate of testing. The present theory should be applicable to textile yarns such as those made of rayon, drawn nylon, and drawn polyester fibers.

References

1. B. D. Coleman, *J. Appl. Phys.*, **28**, 1058 (1957).
2. B. D. Coleman and D. W. Marquardt, *J. Appl. Phys.*, **28**, 1065 (1957).
3. B. D. Coleman, *J. Appl. Phys.*, **27**, 862 (1956); Errata, *ibid.*, **28**, 1514 (1957).
4. F. T. Peirce, *J. Textile Inst. Trans.*, **17**, 355 (1956).
5. W. Weibull, *Ing. Vetenskaps Akad. Handl.*, **No. 151** (1939); **No. 153** (1939).
6. J. I. Frenkel and T. A. Kontorova, *J. Phys.* (*U.S.S.R.*), **7**, 108 (1943).
7. B. Epstein, *J. Appl. Phys.*, **19**, 140 (1948).
8. H. E. Daniels, *Proc. Roy. Soc.* (*London*), **183**, 405 (1945).
9. B. D. Coleman, *J. Appl. Phys.*, **29**, 968 (1958).
10. W. Feller, *An Introduction to Probability Theory and Its Applications*, Wiley, New York, 1950, Chapter 17.

11. M. S. Bartlett, *An Introduction to Stochastic Processes*, Cambridge Press, Cambridge, 1956.
12. W. Feller, *Trans. Am. Math. Soc.*, **48**, 488 (1940).
13. J. C. Mann and F. T. Peirce, *Shirley Inst. Mem.* **5**, 7 (1926).
14. E. Midgley and F. T. Peirce, *Shirley Inst. Mem.*, **5**, 102 (1926).
15. W. F. Busse, E. T. Lessig, D. L. Loughborough, and L. Larrick, *J. Appl. Phys.*, **13**, 715 (1942).
16. B. D. Coleman, *J. Polymer Sci.*, **20**, 447 (1956).
17. B. D. Coleman and A. G. Knox, *Textile Research J.*, **27**, 393 (1957).
18. O. Lundberg, *On Random Processes and Their Application to Sickness and Accident Statistics*, Almqvist and Wiksells, Uppsala, 1940, pp. 55–58.
19. M. Frechet, *Recherches Theoriques Modernes sur le Calcul des Probabilités, Livre II*, Gauthier-Villars, Paris (1st ed., 1938, or 2nd ed., 1953).
20. H. Cramér, *Mathematical Methods of Statistics*, Princeton Univ. Press, Princeton, 1946, pp. 185–192, 213–218, 227–231.
21. H. Cramér, *Random Variables and Probability Distributions*. Cambridge Tracts in Mathematics and Mathematical Physics, No. 36, Cambridge Press, Cambridge, 1937, Chapter VII, Particularly Theorem 26.
22. F. Y. Edgeworth, *Proc. Cambridge Phil. Soc.*, **20**, 36 (1905).

Synopsis

The problem of calculating relationships between the strength of a bundle and the strength of its constituent filaments is discussed. Detailed calculations are done for the case in which the filaments are drawn from a first-order ensemble with the special property that the average lifetime of the filaments, when tested separately under static loads, varies as a power of the applied stress. For this special case it is possible to derive some general results which are valid whatever the time dependence of the total load. The distribution functions for the lifetime of ideal bundles are calculated for both small and large bundles subjected to arbitrary loading histories. The conditions under which the strength of a bundle decreases with increasing number of filaments are examined.

TRANSACTIONS OF THE SOCIETY OF RHEOLOGY II, 219–238 (1958)

The Tensile Strength of GR-S Elastomers

LAWRENCE M. EPSTEIN* and ROBERT P. SMITH,† *Mellon Institute, Pittsburgh 13, Pennsylvania*

I. INTRODUCTION

Recently various attempts have been made to develop a theory of tensile strength for amorphous polymeric materials.[1–3] Taylor[1] observed the dependence of tensile strength upon the degree of crosslinking using GR-S crosslinked with decamethylene bismethylazodicarboxylate, hereafter abbreviated (10-1). He proposed that the tensile strength of a noncrystallizable elastomer was proportional to the concentration of active chains and to an orientation factor calculated from the observed length at break. He obtained good agreement between theory and experiment, especially in the region of low degrees of crosslinking where a sharp maximum in tensile strength was observed. This work was undertaken to test Taylor's theory over a wider range of conditions including swelling and rate of extension.

Taylor suggested that, instead of relying completely upon the per cent (10-1) as a measure of crosslinking, we determine the network activity (i.e., the number of stress bearing chains per unit volume) by independent methods as well. This was done by static modulus measurements and by swelling ratio in benzene.

II. MATERIALS AND THEIR STATIC PROPERTIES

Experimental Procedures

The polymer used was a commercially produced GR-S 1006. The number-average molecular weight, M_n, for rubber of this type is

* Present address: Westinghouse Electric Corp., Materials Engineering Department, Engineering Center, East Pittsburgh, Pennsylvania.

† Present address: Operations Evaluation Group, Navy Department, Washington, D. C.

ordinarily about 70,000 according to information supplied by R. Pearson of the Goodyear Tire and Rubber Co. The raw material was dissolved in benzene, filtered, and precipitated with methanol to remove gel, dirt, and very low molecular weight material including the anti-oxidant (Wingstay). After this treatment the viscosity-average molecular weight, M_v, was 350,000. (We are indebted to Miss Dorothy Pollock for this measurement.) The precipitated polymer was mixed with about 1% of phenyl-β-naphthylamine (PBNA), dried in vacuum, and stored on dry ice.

Portions of polymer containing varying amounts of decamethylene-bismethylazodicarboxylate, called (10-1), were dissolved in benzene, cast onto glass plates with glass walls, dried, and cured for 2 hours at 60–70°C. In the case of low percentages of (10-1) there was a great tendency for the sheets to ripple. This could be mitigated only by partly covering the dishes to reduce the rate of solvent evaporation. Unfortunately this may have reduced the efficiency of the (10-1) by allowing intramolecular linkage to occur during drying. The extent of this error was not determined.

For tensile strength measurements small dumbbells with an approximately 2.8 × 6.0 mm. uniform test section were cut with a die. For swelling and for most of the equilibrium tension measurements, strips about 2.0 × 20.0 mm. were cut with a die.

Accurately measured and weighed strip specimens were soaked in shallow glass dishes of benzene (containing PBNA) overnight at room temperature. The swollen lengths were measured while the specimens were immersed for determining the swelling ratio. Swelling appeared to be isotropic, and the effect of sol polymer on the swelling ratios of the lightly crosslinked gels was minimized by using a very large excess of solvent and by the fact that very low molecular weight polymer had been previously removed. The swollen specimens were then soaked in baths of benzene and acetone containing successively more acetone until shrunken replicas were obtained in pure acetone. These were vacuum dried and weighed to determine per cent gel. This procedure gave lower values and more reproducible results for per cent gel than simply drying the swollen specimens, and in addition the extracted specimens were obtained undistorted.

The equilibrium modulus was obtained by essentially the procedure described by Flory, Rabjohn, and Schaffer[4] using low boiling petroleum ether to equilibrate the specimens at constant extension.

Calculation of Network Activity

To calculate the network activity of the lightly crosslinked materials from the percentage of (10-1), it is necessary to account for the partitioning of the (10-1) between sol and gel as well as the segregation of the lower molecular weights in the sol portion. The equations of Charlesby[5] provide a basis for the calculation which is outlined below. It must be admitted that the per cent (10-1) and the per cent gel data were not entirely consistent with the molecular weight distribution implied by the figures given above for M_n and M_v. This necessitated some compromise as noted below. The discrepancy was such that the experimental gel fraction was less than that calculated on the basis of the M_n and M_v noted.

The bulk crosslinking density q is defined as the probability that a butadiene unit is crosslinked and is related to P, the grams of (10-1) per 100 grams of polymer by

$$q = \left(\frac{P}{100}\right)\left(\frac{M_B/b}{M_{(10-1)}/2}\right) \tag{1}$$

where M_B and $M_{(10-1)}$ are the molecular weights of butadiene and (10-1), respectively, and b is the weight fraction of butadiene in the polymer.

The crosslinking density of the gel, q_g, is given by

$$q_g = q(1 + s) \tag{2}$$

where s is the measured sol fraction. Then

$$\left(\frac{\nu}{V_x}\right) = \frac{q_g\rho}{M_B/b} = \frac{P\rho(1 + s)}{100M_{(10-1)}/2} \tag{3}$$

where (ν/V_x) is the moles of crosslinked units per cm.^{3} of gel and ρ is the density of the polymer.

The effective number of chains per unit volume (ν_{eff}/V_x) is obtained by multiplying (ν/V_x) by the usual Flory factor[6] and can be written

$$\frac{\nu_{eff}}{V_x} = \frac{\nu}{V_x}\left\{1 - \frac{2M_B/b}{[M_n(g)]q_g}\right\} = \frac{\nu}{V_x}\left\{1 - \frac{100M_{(10-1)}}{[M_n(g)](1 + s)P}\right\} \tag{4}$$

where $[M_n(g)]$, the number-average molecular weight of molecules which formed the gel is calculated by

$$M_n(g) = M_n \frac{(1 - s)}{(1 - r)} \tag{5}$$

$(1 - r)$ is the fraction of the original polymer molecules present in the gel, and may be calculated graphically from the relation

$$1 - r = \frac{M_n}{M_w} \int_0^{\delta g} s d(\delta g) \tag{6}$$

Here g is the measured gel fraction and δ, the number of crosslinked units per initial weight-average polymer molecule, is given by

$$\delta = q \frac{M_w}{M_B/b} = \frac{PM_w}{100M_{(19-1)}/2} \tag{7}$$

The value 350,000 was used for M_w.

The measured gel fraction and the results of the above calculations are listed in Table I.

TABLE I
Calculated Network Activity

P	g $(= 1 - s)$	$1 - r$	$[M_n(g)]$	$\nu/V_s \times 10^5$	$\nu_{eff}/V_s \times 10^5$
0.2	0.447	0.219	143,000	1.44	0.137
0.3	0.549	0.348	110,500	2.02	0.337
0.4	0.626	0.468	93,600	2.55	0.559
0.5	0.700	0.585	83,800	3.01	0.780
0.6	0.733	0.673	76,100	3.53	1.08
0.8	0.798	(0.828)	70,000	4.47	1.80
1.0	0.822	—	70,000	5.47	2.80
2.0	0.895	—	70,000	10.28	7.61
4.0	0.955	—	70,000	19.40	16.73

The incongruity of the data is evidenced by the fact that $1 - r$ becomes greater than g (which is impossible) at $P = 0.8$. As a compromise therefore $[M_n(g)]$ was assumed the same as M_n from there on. As can be seen, the variation of $[M_n(g)]$ and its effect on ν_{eff}/V_s has become small at this value of P.

Network Activity from Swelling Ratio

The equation used to calculate network activity from swelling measurements[7] applies to a network which was crosslinked in the presence of soluble polymer.

$$\frac{\nu_{eff}}{V_x} = \frac{1}{V_1} \frac{[(0.5 - \mu)v^2 + v^3/3 + \ldots]}{v^{1/3} g^{2/3} - v/2} \tag{8}$$

Here (ν_{eff}/V_x) is the effective chain density of the network (the gel portion), V_1 is the molar volume of the solvent, and v is the ratio of gel volume to final swollen volume. The parameter μ was chosen as 0.35,[8] which gives good agreement with modulus results at a high per cent of (10-1). (It was pointed out in review that μ probably is not constant over this large range of concentrations, but increases with increasing polymer concentration. Allowance for this would have improved the agreement with elasticity data.) Terms higher than v^3 in the numerator were found to be negligible.

Network Activity from Modulus

Application of simple elasticity theory to the unextracted specimens gives the effective chain density based on the original specimen volume V_0. Denoting the stress per unit undeformed cross-section area by τ and extension ratio by α,

$$\frac{\nu_{eff}}{V_0} = \frac{1}{RT} \frac{\tau}{(\alpha - 1/\alpha^2)} \tag{9}$$

To compare these results with the results of eq. (8) above, one must divide by g to get the chain density on the basis of the volume of the network polymer only.

When one measures the modulus of the extracted specimens, the appropriate expression becomes:

$$\frac{\nu_{eff}}{V_x} = \frac{1}{RT} \frac{\tau_x g^{-2/3}}{(\alpha - 1/\alpha^2)} \tag{10}$$

Here τ_x and α are based on the dimensions after extraction.

Results of Network Activity Measurements

The results of the above measurements are given in Figure 1. The agreement between extracted modulus, nonextracted modulus, and swelling methods is quite good above 1% (10-1). The swelling method in turn yields somewhat higher results than the calculation based on percentage of (10-1). Such a discrepancy between network activity based on swelling and modulus compared to that based on

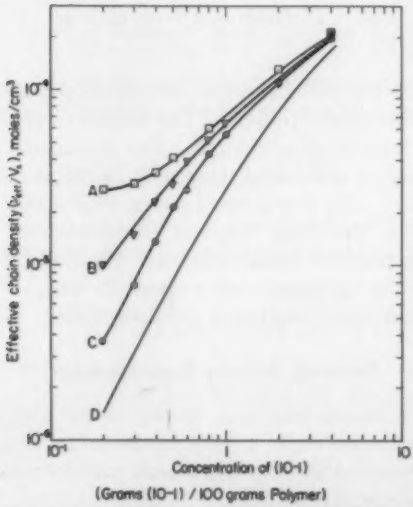

Fig. 1. Network activity of GR-S crosslinked with (10-1). (*A*) From modulus (extracted). (*B*) From modulus (unextracted). (*C*) From swelling ratio. (*D*) Calculated.

chemical composition was found also by Moore and Watson.[9] At about 1×10^{-4} moles of chains per cm.^{3} their swelling results were about 2.5 times their chemical results whereas that factor in our data is only about 1.5. Above this degree of crosslinking the ratio is decreased in both cases. Our data carry this comparison to much lower crosslinking and indicate that the network activity manifested by swelling behavior remains between 2.5 to 3 times the calculated value.

III. TENSILE STRENGTH MEASUREMENTS

For each specimen a complete stress-strain curve was obtained up to the point of break using a constant rate of clamp separation. Some preliminary experiments were performed on an Instron testing machine. In one set of preliminary experiments, ring specimens were compared to dumbbell specimens. The rings were mounted on double pulleys set in miniature precision bearings in order to permit free uniform extension of the specimens (see Fig. 2). Despite the use of the double

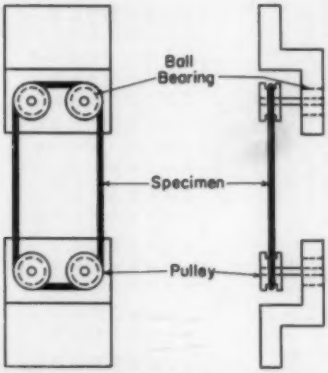

Fig. 2. Mounting for ring specimen.

pulleys, it was found that the rings broke somewhat shorter and at a considerably lower tension when the degree of crosslinking was low and when the end portion of the stress-strain curve was concave upwards and steep. Since the region of low degree of crosslinking was of greatest interest, no further ring specimens were used. This was despite the fact that with dumbbell specimens it was not possible to obtain a uniform rate of extension of the test portion. At higher degrees of crosslinking, ring and dumbbell specimens gave results in close agreement.

The great majority of the stress-strain curves were obtained on an instrument similar in principle to that described by Taylor. In this, the lower specimen clamp was mounted on a cantilever spring, the deflection of which was sensed by a differential transformer and recorded. The upper clamp was drawn at a uniform rate by a calibrated Graham drive. There was no temperature control except for the room thermostat.

The elongation of the specimens was followed by visually observing the spacing of the bench marks on the sample against a movable scale. Pips were recorded at fixed intervals of distance between the marks.

In Table II are summarized the tensile strengths and ultimate extension ratios obtained. The tensile strength has been referred as usual to the unstressed cross-sectional area, after treatment in the case of the swollen or extracted specimens. The extension ratios,

TABLE II
Tensile Strengths and Ultimate Extension Ratios of GR-S Vulcanizates

Per cent (10-1)	Untreated samples, 2"/min.		Untreated samples, 20"/min.	Extracted with benzene, 2"/min.		Swollen with light mineral oil, 70% by volume, 2"/min.		Extracted with benzene; then reswollen with light mineral oil to approximately original volume, 2"/min.	
	T.S., kg./cm.²	α Break	T.S., kg./cm.² $\alpha\beta$[a]	T.S., kg./cm.²	$\alpha\beta$[b]	T.S., kg./cm.²	$\alpha\beta$[c]	T.S., kg./cm.²	$\alpha\beta$[c]
0.2	12.9 ± 1.0	26.8 ± 0.9	22.2 ± 3.0	19.9 ± 2.8	26.0 ± 0.5	4.30 ± 0.80	24.5 ± 1.3	4.95 ± 0.73	24.3 ± 0.78
0.3	22.3 ± 1.4	21.4 ± 0.2	38.9 ± 2.9	49.8 ± 4.0	21.4 ± 0.5	8.28 ± 0.97	17.8 ± 0.6	8.83 ± 0.92	18.9 ± 0.13
0.4	28.0 ± 4.3	17.6 ± 0.6	55.0 ± 4.0	49.6 ± 8.8	17.3 ± 0.7	6.75 ± 0.74	13.5 ± 0.4	8.87 ± 1.31	15.9 ± 0.89
0.5	18.9 ± 2.8	13.8 ± 0.4	48.7 ± 5.5	49.2 ± 6.4	14.5 ± 0.2	6.88 ± 1.13	10.8 ± 0.9	8.80 ± 1.00	12.8 ± 0.31
0.6	19.4 ± 5.7	12.8 ± 0.7	51.6 ± 6.7	33.8 ± 5.8	13.7 ± 0.5	6.56 ± 0.73	9.55 ± 0.48	8.95 ± 1.17	11.1 ± 0.22
0.8	11.6 ± 1.68	9.02 ± 0.75	30.9 ± 5.0	26.3 ± 4.0	10.0 ± 0.37	7.59 ± 0.81	7.78 ± 0.42	8.19 ± 1.18	7.94 ± 0.65
1.0	10.1 ± 1.58	7.42 ± 0.78	21.8 ± 3.1	17.7 ± 3.2	7.87 ± 0.67	6.34 ± 0.80	5.70 ± 0.48	7.33 ± 1.12	6.30 ± 0.73
2.0	11.1 ± 1.1	4.83 ± 0.26	15.0 ± 1.7	18.6 ± 1.2	5.17 ± 0.11	7.67 ± 0.62	3.5 ± 0.17	9.42 ± 1.32	3.86 ± 0.35
4.0	14.5 ± 0.85	3.28 ± 0.22	17.7 ± 1.9	20.4 ± 1.0	3.53 ± 0.27	10.7 ± 0.83		12.6 ± 0.47	2.99 ± 0.5

[a] Could not be obtained because rate of stretching was too fast.
[b] Computed on the basis of the length before extraction.
[c] Computed on the basis of the length before swelling.

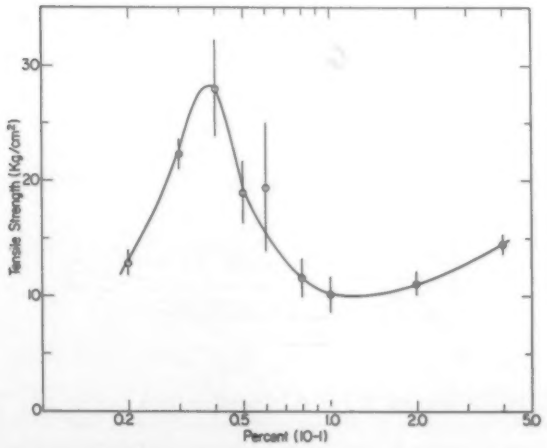

Fig. 3. Tensile strength of GR-S crosslinked with (10-1). Samples extended at rate of 2 in./min. Vertical lines indicate average deviation of the points.

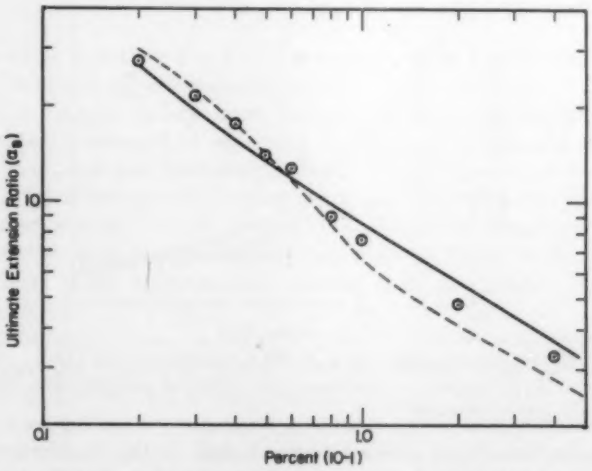

Fig. 4. Length at break of untreated specimens. Calculated (——). Observed (⊙). Results of Taylor (- - -). Parameters used in calculation: $\phi = 0.5$ at 0.2% (10-1) and $M_1 = 122.3$.

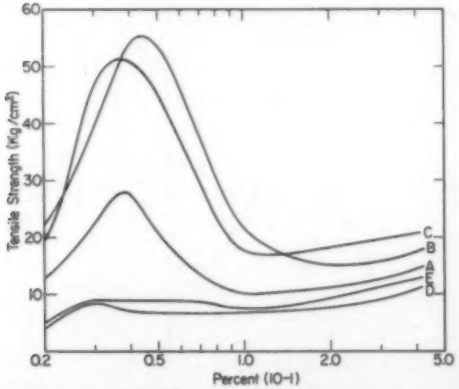

Fig. 5. Tensile strength of GR-S crosslinked with (10-1). (*A*) Untreated, stretched at 2 in./min. (*B*) Untreated, stretched at 20 in./min. (*C*) Extracted, stretched at 2 in./min. (*D*) Swollen with mineral oil, stretched at 2 in./min. (*E*) Extracted and reswollen, stretched at 2 in./min.

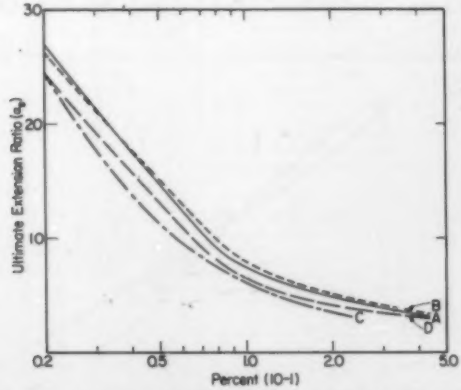

Fig. 6. Ultimate extension ratios of GR-S crosslinked with (10-1). (*A*) Untreated. (*B*) Extracted. (*C*) Swollen. (*D*) Extracted and reswollen. α_B based on length before treatment.

however, have been referred to the length of the undeformed network, that is, the specimen length before extraction or swelling, etc.

Figures 3 and 4 are plots of these data for the first set (i.e., untreated 2″/min.) showing the individual points and their average deviations.

Figures 5 and 6 are plots of the tensile strengths and extension ratios listed in Table II for all five sets of samples. For the sake of clarity individual points are not shown, only the smooth curves.

Occasionally a result was rejected when both the tensile strength and elongation were very much lower than the average. Since it is difficult to set a criterion for rejection, this was avoided as much as possible and altogether only eight out of about 400 observations were rejected.

IV. DISCUSSION

A. Application of Taylor's Theory

The initial objective of these experiments was to test Taylor's theory, which states that the tensile strength is proportional to the number of effective chains per unit volume and to an orientation factor, ω_0, which can be calculated from the extension ratio at break, α_B. Accordingly

$$TS = K \frac{\nu_{eff}}{V_0} \omega_0 \tag{11}$$

where $\omega_0 = 1 - (1 - \delta^2\alpha_B^2)^{-1/2}$ for small δ, where δ is the maximum angle for effectively oriented chains.

Our treatment differs from Taylor's in the following respects: (*1*) α_B was measured by observing the separation of marks on the specimen rather than clamp separation; (*2*) the accuracy of observation of α_B was improved further using only one-tenth the speed of clamp separation; (*3*) we have used ν_{eff}/V_0 as calculated from the equilibrium swelling measurement; in place of Taylor's $N\omega_a$ which was based on the stoichiometry of crosslinking and Flory's free end correction.

Accordingly, various values of δ^2 were tried in order to match the observed and calculated tensile strength values. The results displayed in Figures 7 and 8 were obtained using $\delta^2 = 5 \times 10^{-6}$, the same value used by Taylor, and corresponding to an angle of 0.4° for effectively oriented chains. This resulted in values for K similar to Taylor's but shifted the peak tensile strength to a higher percentage of (10-1). The value of K used was 0.63 times Taylor's value. For the fast stretch (20″/min.) data K was 1.15 times Taylor's value.

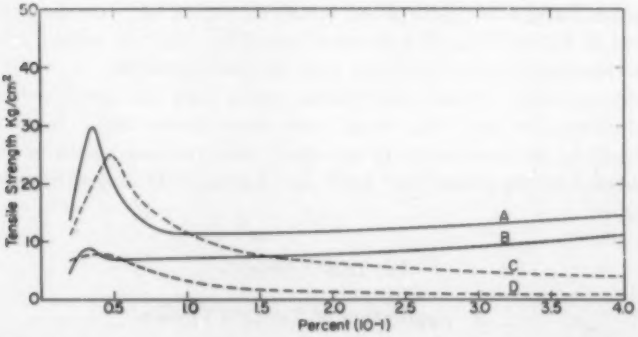

Fig. 7. Comparison of observed tensile strength and tensile strength calculated by Taylor's theory. (*A*) Dry observed. (*B*) Swollen observed. (*C*) Dry calculated. (*D*) Swollen calculated.

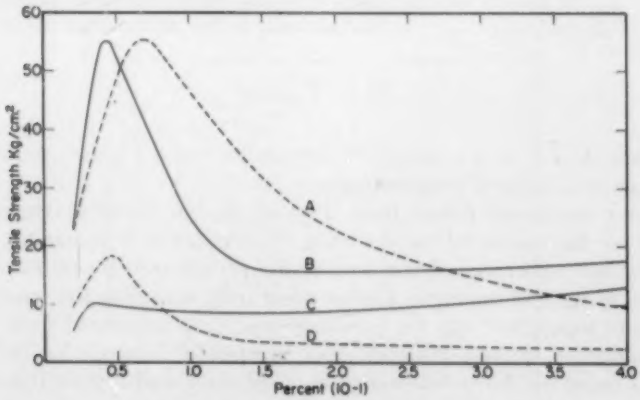

Fig. 8. Comparison of observed tensile strength and tensile strength calculated by Taylor's theory. (*A*) Fast stretch, calculated. (*B*) Fast stretch, observed. (*C*) Extracted and reswollen, observed. (*D*) Extracted and reswollen, calculated.

To move the calculated peak closer to the observed peak required a much smaller δ^2 and a drastically larger K. For even smaller δ^2, $\omega_0 \cong 1/2\delta^2\alpha_B^2$ and the position of the peak becomes independent of the choice of δ^2 and is determined instead by the α_B's.

As shown in Figures 7 and 8, in all cases the calculated curve has

a peak at low percentages of (10-1) which resembles the observed curve in shape but is definitely shifted to the right. In all cases the calculation yielded unreasonably low values at high percentages of (10-1). The calculation successfully correlated the drop in tensile strength on swelling with the drop in α_B for the low vulcanizates, but unfortunately also predicted an unreasonably low ratio for the tensile strength of the swollen high vulcanizates compared to the unswollen high vulcanizates. Again, when the same parameters were applied to the extracted and reswollen material the calculation predicted a peak for low vulcanizates which was not observed as well as an unusually low tensile strength for the high vulcanizates.

The discrepancies for the fast run were similar to those noted for the slow run.

The data obtained leads qualitatively to the conclusion that the large peak in tensile strength for these elastomers at low percentages of (10-1) is a viscous effect which cannot be explained in terms of equilibrium network structure. Particularly pertinent are the observations that:

(*a*) Variations in specimen treatment produced large changes only at low degrees of vulcanization. The tensile strength of the high vulcanizates was changed relatively slightly by higher speed, replacement of soluble polymer by oil, or swelling.

(*b*) The peak tensile strength of the low vulcanizates increased about 85% on increasing the speed, compared to an 18% increase at 4.0% (10-1).

(*c*) Upon replacing the soluble polymer with oil the peak tensile strength of the low vulcanizates dropped 65% compared to only 13% decrease at 4.0% (10-1).

(*d*) Upon swelling the comparison was similar to (c).

(*e*) To further substantiate the viscous nature of the tensile strength peak, several specimens with a low percentage of (10-1) were extended at the usual rate to just less than their ultimate elongation and allowed to relax. The swollen specimens relaxed very little whereas the dry specimens relaxed a great deal. Furthermore, if dry specimens were extended to an elongation corresponding to the ultimate elongation of the same specimen when swollen, they would relax to approximately the tensile strength of the swollen specimens and then break.

(*f*) The oil replaced and swollen tensile strength curves were re-

markably parallel. Here the sole difference was the initial deformation of the network; there was little difference in "lubrication."

B. Test of Bueche's Theory

According to a recent theory proposed by A. Bueche,[3] rupture occurs in some section of the specimen when the relative rate of bond breakdown equals the relative rate of increase of tension, i.e.

$$-\left(\frac{1}{n}\frac{\partial n}{\partial t}\right)_c = \left(\frac{1}{\phi}\frac{\partial \phi}{\partial \alpha}\right)_c \left(\frac{\partial \alpha}{\partial t}\right)_c \tag{12}$$

where n is the number of bonds, α is the extension ratio, $\phi(\alpha)$ gives the shape of the stress strain curve, and t is time. The subscript c refers this relationship to the critical section of the specimen and will be dropped in future discussion. For the left side of (12) Bueche has derived the expression

$$A \exp\left\{-\frac{\Delta F}{RT} + \frac{1}{Z}\left[\frac{W_e}{RT} + \frac{1}{2}\ln Z - \frac{3}{2}\ln\frac{8}{e} + \frac{\Delta H}{RT}\right]\right\}$$

where A is the frequency factor kT/h, Z is the number of main chain bonds in each chain, W_e is the work of extension, and the other parameters have physical significance as discussed by Bueche. We have examined Bueche's data (and our own) and found that the first three terms in the square brackets may be ignored for these specimens. For example, $\Delta H/RT$ is about 200 while the other terms amount to less than 10. These terms have thus not really been tested since we found that the points in Bueche's Figure 1 are hardly shifted when these terms are omitted.

Bueche set Z inversely proportional to the chain density determined by tension modulus measurements at low elongation and we have done likewise. One may then write

$$A \exp\left\{-\frac{\Delta F}{RT} + \frac{\Delta H}{RT}\frac{v_0}{V_0}\right\} = \left(\frac{1}{\phi}\frac{\partial \phi}{\partial \alpha}\right)_c \left(\frac{\partial \alpha}{\partial t}\right)_c \tag{13}$$

where v_0 is the molar volume per chain bond. Bueche calculated $(1/\phi)(d\phi/d\alpha)$ from the measured ultimate elongation using the simple theory of rubber elasticity. Our measurements extended to materials whose stress-strain curve inflected upward (implying serious departure from simple theory), so we used for the right-hand side $(1/\tau)(d\tau/$

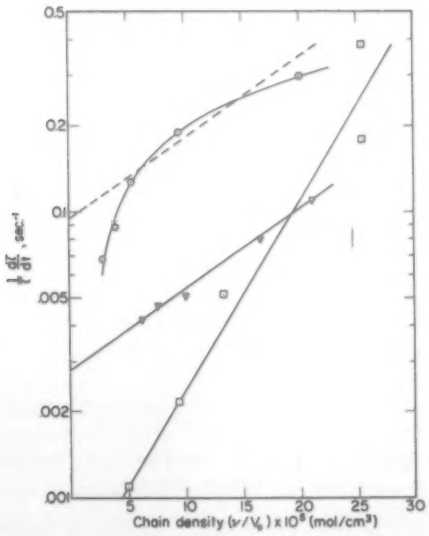

Fig. 9. Test of A. Bueche's theory. Swollen GR-S dumbbells (⊙). Swollen GR-S rings (▽). Bueche's data on silicones (⊡).

dt), i.e., the ultimate force and slope of the stress-strain curve obtained at constant chart speed. Taking logarithms then, one expects to find:

$$\log[(1/\tau)(d\tau/dt)] = C + B(\nu/V_0) \tag{14}$$

Figure 9 shows Bueche's data for radiation-crosslinked silicones and two sets of our swollen data plotted according to eq. (14). These specimens of ours fulfilled the requirement of displaying very little stress relaxation. The dumbbell data is for the same specimens as in Figure 5. The other points are taken from an older set of data obtained in this laboratory for the same GR-S crosslinked with (10-1) but died into 1″ diameter rings, which were also swollen about 1.7 times in mineral oil. They were extended at 2″/min., or $d\alpha/dt$ = 1.1 min.$^{-1}$ compared to Bueche's 0.25 min.$^{-1}$ It is seen that the data for the rings for which $d\alpha/dt$ is necessarily constant is well rectified in this manner. In the case of our dumbbells, $d\alpha/dt$ varied con-

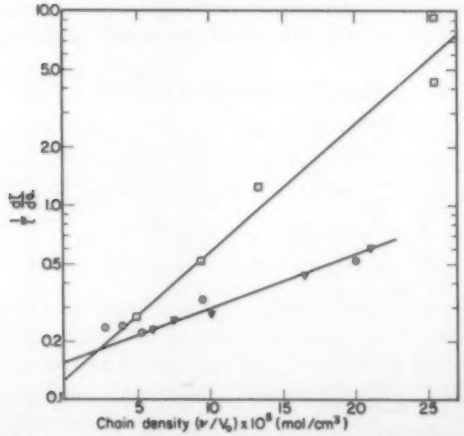

Fig. 10. Test of eq. (15). Swollen GR-S dumbbells (⊙). Swollen GR-S rings (▽). Bueche's data on silicones (⊡).

siderably because of excessive shoulder stretching, leading, we believe, to the curvature observed.

It is common experience that τ is approximately constant over a small range of $d\alpha/dt$. Accordingly, we attempted alternatively to rectify our data by means of the following empirical equation:

$$\log[(1/\tau)(d\tau/d\alpha)] = X + Y\nu/V_0 \tag{15}$$

Figure 10 shows the same data as in Figure 9 plotted instead according to eq. (15). In the case of our dumbbell data, pips had been put on the chart for each centimeter of travel of the bench marks on the test section of the specimen, so that we could compute $d\alpha/dt$ at the break, and so obtain $d\tau/d\alpha$. It is noted that the dumbbell data and the ring data are now in much better agreement. Furthermore, both Bueche's data and ours have nearly the same intercept. (If one wishes to interpret this intercept in terms of a ΔF, the difference observed in Fig. 10 corresponds to less than 0.1 kcal.)

C. Discussion of Ultimate Elongation Data

It is noteworthy that although swelling, extraction, etc. caused gross changes in the tensile strength of the lightly crosslinked materials, the ultimate extension ratio α_B, based on the untreated speci-

men dimensions, was changed by a relatively small amount. One is thus inclined to seek a fundamental correlation between network activity and α_B rather than with tensile strength. A naive estimate of the ultimate extension ratio is that $\alpha_B = n^{1/2}$ (n is the average number of statistical links per chain). It was obvious from our data as well as Bueche's and Taylor's that this relationship does not hold. Such a relationship is based on the premise that rupture occurs when the chain of average end-to-end displacement is stretched to its full contour length.

Obviously by the time the average chain has become fully extended a number of chains which were abnormally extended to begin with will have been broken. Suppose we postulate that a particular network snaps when only some small fraction ϕ of the chains, representing an upper percentile of r/nl, has been fully extended. Here l is the length of a link, n the number of links between junction points, and r is the undeformed end to end distance. To rationalize such a postulate one may argue that only after some threshold is reached does breakdown become catastrophic. We could try two ideas: (*1*) that ϕ is the same for all vulcanizates, and (*2*) that the critical number of breakdowns per unit volume is constant for all vulcanizates, necessitating that ϕ be decreased as the chain density is increased.

Before attacking this problem another difficulty should be pointed out. The same specimen treatments that cause the tensile strength to appear greater because of increased viscous effects also result in greater α_B. One would expect nonequilibrium effects, such as temporary entanglements, van der Waals' forces, and insufficient orientation time, all to lead to shorter α_B, if α_B were determined solely by network geometry. Some other idea, such as the occurrence of some chemical rate catastrophe, appears necessary to complete the picture.

In all calculations below we will ignore the fact that there is a distribution of n for each vulcanizate. Using an average n is simply compensated for by using a "statistical" l. The problem is further reduced to one dimension for simplicity, by visualizing a network consisting of three mutually perpendicular sets of chains. One set, with displacements, r, all in the direction of elongation, limits the ultimate extension.

Using the Gaussian distribution $p(r)$ for r, one calculates ϕ as

$$\phi = F(Z) = 1 - \int_0^r p(r)dr = 1 + (2/\sqrt{\pi})\, Ze^{-Z^2} - \operatorname{erf} Z \quad (16)$$

where

$$Z = (r/l)\sqrt{3/2n}$$

Then

$$r(\phi) = l\sqrt{2n/3}\, F^{-1}(\phi)$$

and

$$\alpha_B = nl/r(\phi) = \sqrt{3n/2}/F^{-1}(\phi) \tag{17}$$

Equation (17) tells us that if ϕ is a constant for all vulcanizates then we must still have $\alpha_B \sim \sqrt{n}$, which is denied by experiment. Consequently the second idea, which requires that ϕ be inversely proportional to the chain density, will be tested. The procedure was as follows: (*a*) The molecular weight per crosslinked unit, M_c, was calculated from the percentage of (10-1) accounting for soluble polymer and the partitioning of (10-1) between sol and gel. (*b*) A trial value of ϕ was assigned to the 0.2% vulcanizate and corresponding values proportional to M_c assigned to the others. From a graph of eq. (16) values of $F^{-1}(\phi)$ were found for each vulcanizate. (*c*) The value of n required to fit the smoothed data at 0.8% (10-1) was computed using eq. (17) and from that the necessary value of M_l, the molecular weight of a statistical link. (*d*) Using this M_l, the remaining n and α_B were then calculated.

After several trials (using the data for the untreated specimens) we chose $\phi = 0.5$ for the 0.2% (10-1) specimens. The fit is not strongly dependent on ϕ. It could have been improved slightly by choosing ϕ much larger, which seems unreasonable. Also $\phi = 0.5$ yields a rather sensible value for M_l, namely 122.3. Figure 4 shows the calculated and observed α_B's for the untreated specimens.

Although the data is in fair agreement with the calculated curve, it deviates in a systematic way, having a sigmoidal shape not predicted by the calculation. Such a shape is indeed difficult to account for theoretically, and may in fact represent a fault in the specimen preparation, such as intramolecular reaction of (10-1) at low percentages of (10-1). The only similar data, that of Taylor, although in error because it included shoulder stretching, does show this same trend.

A serious deficiency in the calculation presented is that no account

was taken of entanglements, which one might expect to reduce M_e below the stoichiometric value at low percentages of (10-1). Unfortunately, any attempt to correlate tensile data over a wide range of degrees of crosslinking is beset with the difficulty of obtaining a good measure of network activity for low vulcanizates.

The effect of the various specimen treatments on the length at break requires, for its understanding, more knowledge of the mechanism of rupture. However, the increase observed at the faster stretching rate could certainly not be attributed to a smaller M_l, but might be the result of a larger ϕ. Increasing ϕ to 0.6, for example, would increase the calculated extreme α_B's from 26.1 to 29.4, and from 3.7 to 3.8.

V. SUMMARY

GR-S rubber crosslinked with (10-1) generally exhibited a greater network activity in static modulus and swelling experiments than was calculated stoichiometrically. Results were close above 1% (10-1), but became increasing divergent at lower degrees of crosslinking.

The maximum in tensile strength at low degrees of crosslinking was greatly dependent on the rate of extension. In the case of the swollen specimens no maximum occurred. In general, attempts to fit the data by Taylor's theory were unsuccessful. Some success was had in fitting the data to an empirical equation suggested by the theory of A. M. Bueche.[3] Furthermore, a theory which has been proposed to relate the ultimate elongation to the degree of crosslinking is in good agreement with the observed data.

We wish to acknowledge helpful discussions with Hershel Markovitz.

This was work supported by the National Science Foundation at Mellon Institute.

References

1. G. R. Taylor and S. R. Darin, *J. Polymer Sci.*, **17**, 511 (1955).
2. F. Bueche, *J. Appl. Phys.*, **26**, 738 (1955); *J. Polymer Sci.*, **24**, 189 (1957).
3. A. M. Bueche, *J. Polymer Sci.*, **19**, 297 (1956).
4. P. J. Flory, N. Rabjohn, and M. C. Schaffer, *J. Polymer Sci.*, **4**, 225 (1949).
5. A. Charlesby, *Proc. Roy. Soc.*, **222A**, 542 (1954).
6. P. J. Flory, *Principles of Polymer Chemistry*, Cornell Univ. Press, Ithaca, N. Y., 1953.

7. A. M. Bueche, *J. Polymer Sci.*, **15**, 105 (1955).
8. J. Yanko, *J. Polymer Sci.*, **3**, 576 (1948).
9. C. G. Moore and W. F. Watson, *J. Polymer Sci.*, **19**, 237 (1956).

Synopsis

Specimens of purified GR-S were crosslinked with from 0.2 to 4.0% decamethylenebismethylazodicarboxylate. The network activity (i.e., number of stress-bearing chains per cc.) calculated from the quantity of crosslinking agent and polymer molecular weight was somewhat lower than that determined by swelling and equilibrium tension measurements, especially at low degrees of crosslinking. Ultimate strength and elongation were measured at extension rates of 2 and 20 in./min. These were also measured at 2 in./min. on sets of specimens which were swollen with 70% by volume of mineral oil, sets from which the soluble polymer was extracted, and sets from which the soluble polymer was extracted and replaced with an equal volume of mineral oil. Attempts were made to interpret the results according to theories previously proposed for amorphous crosslinked elastomers. It was observed that despite wide differences in tensile strength among the sets which received the various treatments noted above, the ultimate elongation varied relatively little. A theory for the ultimate elongation is proposed which is in good agreement with the data. It is based on the assumption that a specimen breaks when the number of broken chains per unit volume reaches a critical value. These broken chains are those which in the undeformed network have end-to-end distances closest to their contour lengths.

TRANSACTIONS OF THE SOCIETY OF RHEOLOGY II, 239–254 (1958)

Flow Behavior of Concentrated (Dilatant) Suspensions

A. B. METZNER and MALCOLM WHITLOCK, *University of Delaware, Newark, Delaware*

The objects of this work were to establish the effects of particle size, particle concentration, and carrier liquid viscosity on the flow behavior of concentrated suspensions; the ranges of variables of primary interest were those in which the phenomena of dilatancy may be observed. A rotational as well as a capillary-tube viscometer was used in the experimental studies to assure the absence of effects which might be solely attributable to the peculiarities of a particular type of measuring instrument.

REVIEW OF PRIOR ART

The classical experiment demonstrating "dilatant behavior" was performed by Reynolds.[11] One of the systems which Reynolds considered was sand in water. The sand was placed in a rubber balloon containing a small excess of water over that just necessary to fill the void between the sand grains, and the water level was shown by an attached glass tube. When Reynolds pressed or distorted the balloon the liquid level in the glass tube decreased. Obviously if the sand-water suspension originally had enough water to fill the voids between the sand grains and received more on application of pressure to the system, then the value of the suspension must have increased, i.e., the system must have dilated. da C. Andrade and Fox[1] extended Reynolds work using arrays of cylindrical polyethylene rods. The displacing force was that of a piston on the array of perfectly arranged rods. Volume increases were measured, in support of Reynolds original observations.

Freundlich and Roder,[4] working with starch-water and quartz-water systems, found that increases in the viscosity of a given system

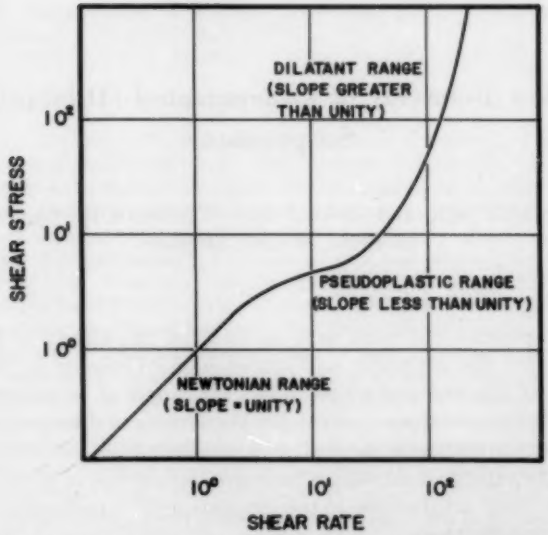

Fig. 1. General shape of the flow curve for concentrated suspensions.

sometimes occurred with increases in shear rate. This was also termed "dilatant" behavior since Reynolds had also noted similar increases in rigidity upon distortion (and volumetric dilation) of his systems. From this and related experiments a second definition of dilatancy has arisen; viz. that fluids for which a shear stress vs. shear rate plot is concave towards the stress axis be termed dilatant. Most fluids will not be dilatant rheologically at all shear rates; Figure 1 presents a qualitative picture of the behavior of many suspensions over a wide range of shear rates.

In general, the term "dilatancy" has been used to describe both of the above phenomena interchangeably, sometimes implying that volumetric dilation under shear is accompanied by sufficient increases in the slopes of the shear stress–shear rate diagrams to cause the fluid viscosity (defined as shear stress divided by the corresponding shear rate) to increase with increasing shear rate. Both means of identifying dilatancy have been largely on a qualitative basis. One purpose of this work was to quantitatively distinguish between these two types of dilatancy and to determine how they were related, if at all.

The ranges of particle concentrations over which rheologically dilatant behavior may be observed have been studied by three groups of investigators. Freundlich and Roder[4] reported dilatancy only in suspensions containing between 42 and 45 volume per cent solids. Above and below this range no dilatancy was encountered in either of the two systems studied (quartz-water and starch-water). However, no experimental data are reported, hence it is impossible to determine whether their statements are truly valid or not. It seems quite possible, for example, that their experimental equipment simply did not enable them to reach shear stresses sufficiently high to bring them into a region of dilatancy on the flow curves of the more concentrated suspensions. It would appear that any method used to estimate the volumetric concentrations of starch particles is open to serious question; it is not known to what extent their conclusions rest on data taken with this system. Verwey and de Boer[16] also report that sometimes dilatant behavior occurred only over very narrow concentration ranges in suspensions of metallic particles (coated with oleic acid) in organic liquids, although few specific values are given. While de Bruijn and Meerman[2] reported dilatancy in a suspension of glass particles at only 13.8 volume per cent solids, their data appear questionable in view of the experimental techniques used. Thus the available quantitative information on the relation between dilatancy and particle concentration, while of very limited utility, suggests that dilatancy may be confined to a narrow range of concentrations. Since the importance of concentration appears to be through its effect on the volume occupied by the particles, swelling or solvatable particles were not used in the present work.

The effects of particle size on dilatancy are somewhat clearer than the above data on concentration effects. Freundlich and Roder,[4] in the work discussed above, used particles with diameters between 1.5 and 5 microns. Robinson[13] encountered no dilatancy in the rheological sense with particle sizes in the 3–4, 4–10, and 10–30, micron ranges, even with particle concentrations as high as 52% by volume. However, it is possible that he may have missed the phenomenon if it is restricted to as narrow a range of concentrations as indicated above, since frequently none of his samples fell into the 40–45% range. Similarly, Vand[15] found no dilatancy in suspensions of 130 micron diameter glass beads,* and Ting and Luebbers[14] found no dilatancy

* Vand studied concentrations up to 47% by volume in a capillary tube viscometer. Higher concentrations were studied only in an unsatisfactory apparatus.

in their suspensions of 390 micron diameter glass beads (at concentrations up to about 50 volume per cent). While de Bruijn and Meerman report dilatancy for all particle sizes in their 0–50, 50–90, 90–250, 250–500, and 500–700 micron ranges, their results may be doubtful in view of the crude experimental techniques used. Thus, all the reliable data available on rheological dilatancy indicate it has been confined to suspensions of particles having diameters of less than 5 microns.

The viscosities of the suspending liquids used in studies of dilatancy have not been varied over an appreciable range; all studies have been in liquids having viscosities of a few centipoises or less. Freundlich and Roder[4] theorized that such low viscosities are probably necessary to bring out the phenomenon.

Pryce-Jones[9] and Verwey and de Boer[16] have studied the great importance of the surface or colloidal properties of the solids used to prepare dilatant suspensions. Freundlich and Kross[3] studied these colloidal properties extensively in titania suspensions similar to those used in the present work.

EXPERIMENTAL

Most of the data were obtained using a Stormer rotational viscometer of standard design except that a smooth cup with no internal obstructions was used. The bob was hollow; analytical balance weights were used for the loads. Check runs were made with a capillary tube viscometer described in detail by Riggs[12] and in general similar to a model available commercially from the Burrell Apparatus Co. Both instruments were calibrated with U. S. National Bureau of Standards oils. No correction of the measured capillary tube dimensions was found to be necessary; the Stormer data were corrected by interpolating from the following table to obtain "effective" bob lengths.

Viscosity of calibrating oil, poises	Ratio of effective to measured bob length
2	1.13
12	1.13
200	1.04

The usual rigorous equations[7] were used for calculating the true shear rates in both instruments.

The suspensions of titanium dioxide were mixed for 15–20 minutes in a small household Waring Blender. The glass bead suspensions were mixed by adding the beads to the carrier solution with intermittent paddle agitation with maximum care taken to exclude air intake. Volumetric concentrations were calculated from the known weights of the two phases used and their densities (a density of 4.2 g./ml. was assumed for the titania).

After the viscometer cup was filled, the bob was slowly lowered into the cup to insure escape of all air through the four holes in the top of the bob. The bob was inserted to the same depth into the cup for all runs and the cup filled to one-sixteenth of an inch from the cup lip. Weights were added and the time required for the bob to make 100 revolutions was measured. Prior to this measurement at least 15 revolutions were allowed to insure a constant speed during the test measurement. This was repeated for different weights until a speed of 100 revolutions per 7 seconds or a load of 3000 grams was reached, whichever came first.

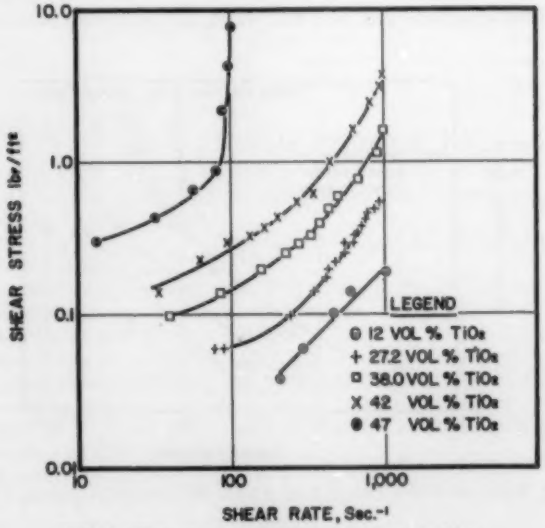

Fig. 2. Flow curves for TiO_2-water suspensions.

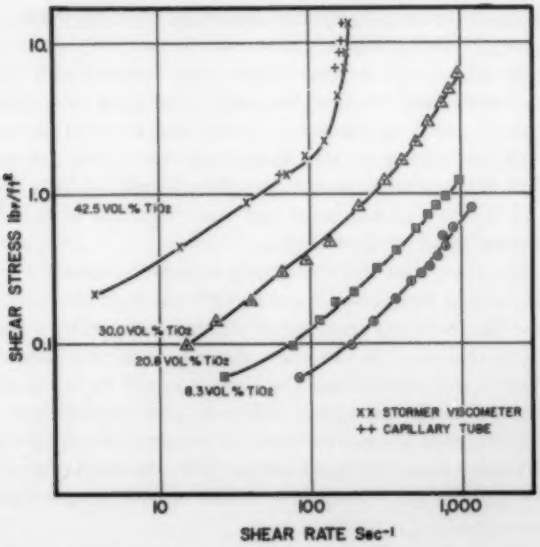

Fig. 3. Flow curves for TiO_2 in a 47.1 wt.-% (17 centipoise) sucrose solution.

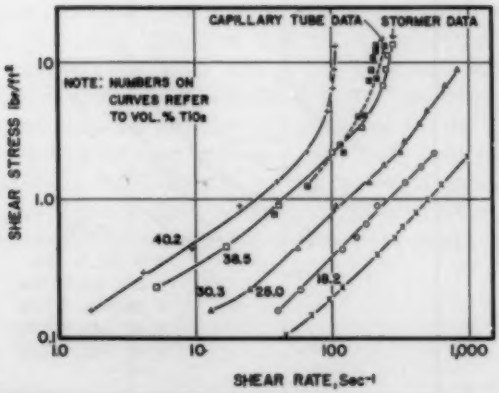

Fig. 4. Flow curves for TiO_2 in a 58 wt.-% (42 centipoise) sucrose solution.

Further details concerning equipment and the methods of calculation are available in a dissertation.[17]

RESULTS AND DISCUSSION OF RESULTS

The primary variables studied were the viscosity of the suspending medium used in preparing the suspension and the solids concentration of the suspension. The wide ranges used were chosen to determine the range over which dilatancy persisted, and, in the case of the solids content, the lowest concentration of solids which would produce dilatant behavior was also to be determined. The results are summarized in Figures 2–4 and in Tables I–V.

Dilatancy in the rheological sense was never obtained with certainty in any of the glass bead suspensions. As a result, detailed flow curves for these systems are not presented here. Inspection of the flow curves of the titania suspensions reveals that in all cases the

TABLE I
Summary of Experimental Conditions Studied and of Ranges in which Rheological Dilatancy Occurred

System	Concentration of solids, % by volume	Concentration exhibiting rheological dilatancy
Titania suspended in:		
water	12.1, 27.2, 38.0, 42.5, 47.0	27.2, 38.0, 42.5, 47.0
aqueous sucrose (μ = 17 cp.)	8.3, 20.8, 30.0, 42.5	30.0, 42.5
aqueous sucrose (μ = 42 cp.)	18.2, 25.2, 30.3, 38.5, 40.2	30.3, 38.5, 40.2
28-micron glass beads in 42 cp. sucrose solution	32.7, 39.2, 46.0, 58.6, 61.0, 64.4	None
57-micron glass beads in 42 cp. sucrose solution	46.0, 58.6, 64.4	None
100-micron glass beads in 42 cp. sucrose solution	46.0, 58.6, 64.4	None
Equal parts by weight of the above 3 glass beads, in 42 cp. sucrose solution	46.0, 58.6, 64.4	None
28-micron glass beads in an 18 cp. $CdCl_2$ solution	46.6, 52.7, 59.2, 62.7, 64.6	None

TABLE II

Comparison of the Minimum Shearing Stresses at which Volumetric Dilation, Rheological Dilatancy and Fracture of the Suspension First Occur

System	Concentration of solids, % by volume	Shear stress, lb.$_F$/ft.^{2} corresponding to: Volumetric dilation	Rheological dilatancy	Visual and audible fracture in viscometer
Titania in 42 cp. sucrose solution	25.0	0.9	Above 2.2	—
	30.3	1.3	2.0	6.8
	38.5	—	3.5	5.8[a]
	40.2	0.9	2.0	4.4
Titania in 18 cp. sucrose solution	30.0	0.8	1.0	2.9
	42.5	0.9	1.8	4.4[b]
Titania in water	27.2	—	0.14	0.43
	38.0	—	0.4	0.80
	42.5	0.4	0.6	1.0
	47.0	0.4	0.8	2.2

[a] Observed stress corresponding to audible cracking and fracture in the capillary tube was 5–6 psf.

[b] Observed stress corresponding to audible cracking and fracture in capillary tube was 5–6 psf for this suspension.

TABLE III

Variation in the Conditions Corresponding to Initial Dilatancy with Viscosity of the Carrier Medium

Particle concentration, % by volume	Carrier liquid viscosity, centipoises	Shearing conditions at onset of rheological dilatancy: Stress, lb.$_F$/ft.^{2}	Rate, sec.$^{-1}$
27.2	1	0.13	320
30.0	17	1.2	330
30.3	42	2.0	280
38.0	1	0.40	380
38.5	42	3.4	160
42.	1	0.60	300
42.5	17	1.9	110
40.2	42	2.0	60

TABLE IV
Effect of Particle Concentration on Conditions Corresponding to Initial Dilatancy

Liquid viscosity, cp.	Particle concentration, vol. %	Shear stress, $lb._F/ft.^2$	Shear rate, $sec.^{-1}$
1	27.2	0.13	320
	38.0	0.40	380
	42.5	0.60	300
	47.0	0.73	70
42	30.3	2.00	280
	38.5	3.40	160
	40.2	2.00	60

more dilute suspensions were essentially Newtonian in behavior. As the solids concentration was increased, non-Newtonian behavior of the type shown by Figure 1 occurred: at high shearing stresses the fluid was dilatant, passed through a Newtonian point (or small region) at decreasing stresses, and became pseudoplastic at still lower shearing stresses. Shearing stresses sufficiently low to study the fluid behavior in the Newtonian region at the lower end of the curve in Figure 1 were not obtained, since this region was not of primary interest, and in most cases there was little reason to doubt that Newtonian behavior would always be exhibited at sufficiently low shearing stresses.

Before attempting to explain the mechanisms responsible for the L- or S-shaped curves of Figures 1–4, it may be helpful to discuss the volumetric behavior of these systems under shear. Since volumetric dilation of concentrated suspensions may cause them to appear dry* visually, inspection of the appearance of the top of the suspension in the annulus of the rotational viscometer sheds direct light on the volumetric behavior of the fluid under steady (and nearly uniform) shear.

Surface drying,† under shear, was noted in all of the glass bead suspensions containing over 50 volume per cent solids. No dilatancy at all in the rheological sense was observed in 8 of these 13 systems studied, and, in the other 5 cases, was within experimental error.

* Reiner[10] discusses this point extremely well.

† This dryness of the surface was due to volumetric expansion of the system and not due to evaporation of liquid, as evidenced by its reversibility.

TABLE V
Data of Present Work Compared with Prior-Art Data

Solids studied	Investigator, ref.	Liquid viscosity, cp.	Particle diameter, μ	Dilatancy range volume, % solids	Max. volume, % solids tested	Max. shear stress, lb.$_F$/ft^2	Max. shear rate, sec.$^{-1}$
Iron powder	16	CCl_4 and other low viscosity liquids	3	46	—	—	—
TiO_2	This work	1, 17, 42	0.2–1.0	30–47	47	13.1	1000
Quartz	4	1	1–5	42–45	55	—	—
Glass beads	13	152, 241	3–4	None	37.4	35.	639
		136, 234	4–10	None	47.4	75.	639
		71, 94	10–30	None	52.4	17.	639
Glass beads	This work	18, 42	24–32	Possibly at 64.4	64.6	13.1	1300
		42	53–62	" " "	64.4	13.1	1300
		42	85–105	None	64.4	13.1	700
		42	24–105	None	64.4	13.1	1300
Glass beads	15	80	100–160	None	50.0	Variable; max. shear rate for concentrated suspensions about 100 sec.$^{-1}$	

Thus it is clear that volumetric dilation may occur quite separately from dilatancy in the rheological sense.

Further data on the differences between rheological and volumetric dilatancy are shown in Table II. These data, for the titanium dioxide suspensions, show that volumetric dilation as evidenced by "surface drying" of the suspension always was noticed at shearing stresses well below those at which the flow curve began to exhibit dilatancy in the rheological sense. Thus, at least for both of the systems studied in this work, the usual suggestion that rheological dilatancy and a dry appearance of a suspension go hand in hand is clearly incorrect.

The flow mechanisms which determine the shape of the flow curve may now be investigated in the light of the above knowledge concerning the volumetric behavior of suspensions under shear. At sufficiently low shearing stresses (Fig. 1) Newtonian behavior occurs in the absence of sufficient forces to affect either particle size or alignment (see, for example, references 7 and 8). In the range of slightly higher shearing stresses, the slope of the curve (Fig. 1) progressively decreases as the flowing particles either align (if asymmetric) or are progressively decreased in size due to the imposed shearing forces—which may break up loosely-bonded structures formed by groups of particles. The momentum transfer leading to viscous energy dissipation in liquids is not believed to be due so much to direct collisions between individual molecules or particles as to an "association" between molecules or particles in adjacent streamlines.[5] Progressive decrease in the size of the flowing aggregates decreases not only the mass, hence the excess momentum which an aggregate in one streamline possesses over that in an adjacent one, but also the total intermolecular or interparticle forces which account for the momentum transfer. Accordingly, the viscosity of the system decreases rapidly within a range of shearing stresses in which the particle size is decreasing, just as liquids with small molecules possess lower viscosities than otherwise similar liquids which are composed of larger molecules.

The above theories explain the shape of the lower half of the flow curve of Figure 1, i.e., up to the point of inflection. Two mechanisms may account for the inflection and subsequent increases in slope of the curve. In the first place, as the shearing stresses reach levels at which the size of the aggregates or flowing particles has been reduced to a minimum, the fluid system should approach Newtonian behavior

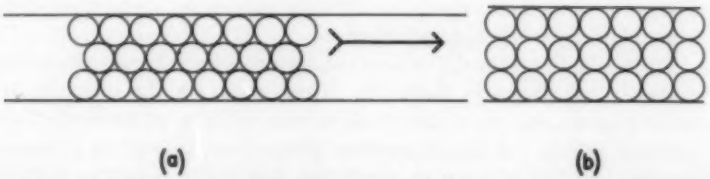

Fig. 5. Dilation (volumetric) of a closely packed suspension under shear. (*a*) Suspension at rest; particles fit into voids in next adjacent layer. (*b*) Suspension under rapid shear; particles have no time to fall into voids in adjacent layers and each layer glides over the adjacent one.

or constant viscosity. (This factor by itself should account for the inflections noted in the flow curves of other suspensions which approach Newtonian behavior at high shearing rates.) Second, and of much greater importance in suspensions which may become rheologically dilatant, at increasing stresses the system beings to expand volumetrically, as indicated by the data of Table II. Accordingly, the flow mechanism begins to change to one in which entire layers of particles begin to glide over adjacent layers, as pictured by Reiner's[10] diagrams depicting flowing dilatant suspensions. Figure 5 shows schematically why such expansion must occur in concentrated (closely packed) suspensions at high shear rates and indicates how this expansion may result in entire layers of particles gliding over the adjacent ones. However, to the present author's knowledge, no one has yet ventured to explain why such gliding of entire layers should lead to rheological dilatancy, i.e., increases in viscosity with increases in shear rate. The above picture of momentum transfer between adjacent layers or streamlines offers a possible explanation, however. At the lower shear rates discussed earlier, momentum transfer occurred between individual groups of particles in adjacent laminae. Now, however, with many particles in a given lamina or streamline moving past an adjacent one, momentum interchange, i.e., a change of velocity, of one particle in a lamina must concomitantly bring all the others following closely behind it to experience the same change in velocity. (If the particle in question moves from a region of high velocity to one of lower velocity. If the particle were to be accelerated, on the other hand, it would simultaneously need to accelerate all of the others in front of it.) Since, as one moves to progressively increasing shear rates within this high shear rate region the particles

become progressively more perfectly aligned into laminae, one progressively increases the effective mass of the particles which experience momentum transfer with adjacent laminae whenever only a single particle moves laterally. It is suggested that this mechanism becomes of importance as soon as some volumetric dilation occurs. However, since this dilation occurs while the flow is still pseudoplastic, it is not until one reaches considerably higher shear rates that this mechanism is able to predominate over those leading to pseudoplasticity, hence one does not experience rheological dilatancy until such higher shear stresses are reached.

If the above theories, which suggest that rheological dilatancy begins under conditions in which the counterbalancing effects leading to pseudoplasticity and dilatancy are first balanced in favor of the latter are correct, then dilatancy in various systems should begin at the same point of balance. This balance should be determined by the shear rates in the system—since the balance is between progressively increased *rates* of alignment by the velocity gradient and of disalignment due to Brownian motion. Thus, if particles of a given type are suspended in various liquids of increasing viscosity, one should find rheological dilatancy to begin at similar or decreasing shear rates and at progressively increasing shear stresses in these systems. The data tabulated in Table III show that this is indeed the case.

The theories also suggest that dilatancy in a given system should occur at progressively decreasing shear rates as the solids concentration in the suspension is increased, because the "slipping" or "gliding" of adjacent laminae over one another should be easier to achieve at high solids concentrating when there are fewer voids between the individual particles. Table IV shows that this is also the case.

The theory as developed to this point is incomplete insofar as its ability to predict the behavior of extremely concentrated suspensions is concerned. As one moves toward the limit represented by no liquid at all between the particles, one must again predict the observed low resistance to shear offered by dry solids themselves. Therefore, while the theory predicts increases in dilatancy with increases in both solids concentration and shear rate, a limit must finally be reached at which the theory no longer is applicable. This presumably happens when the liquid content becomes sufficiently low to prevent continuous laminae from forming and the solid phase again begins to behave as discrete particles rather than as large groups thereof.

The frequently-quoted "fracture" of dilatant suspensions was also studied briefly but quantitatively in the present work. In the rotational viscometer the fracturing of the fluid was not only visible but also audible. This "noise" corresponding to fracturing of the fluid served to detect its presence in the capillary tube viscometer as well. The stresses at which such fracture occurs are recorded in Table II. While no particular trends may be noted, the point of initial fracture was always close to that at which dilatancy first occurred. However, reproducible flow data could be obtained at shear stresses well within the fracturing region. The fact that it occurred at essentially the same stresses in two types of viscometers is of interest in theoretical discussions of fracture,[6] but no extensive data were obtained on this point.

The results of this study are combined with those of the prior art in Table V. It may be surprising to note how few and far between the available quantitative studies of dilatancy really have been. The data of Table V, while not nearly extensive enough to be entirely conclusive, indicate that strong dilatancy in the rheological sense is confined to suspensions having very small particles. (The data are inconclusive in that it is possible that dilatancy might occur at higher shear stresses than have been studied experimentally in the systems containing particles of larger size.) The data also refute the theory of Freundlich and Roder[4] which suggests that suspending liquids of low viscosity are necessary. It is strange that dilatancy was not always observed in the most concentrated suspensions studied by other authors —although it is possible, it does not seem likely that the higher solids concentrations at which some investigators found dilatancy to disappear would be in a region of "dry solids" flow. A more likely explanation would seem to be that all investigators except a few of the most recent ones confined their work to shear stresses below those at which dilatancy might be expected in the more concentrated suspensions.

In conclusion, it appears that this paper represents the first attempt to compile all the available quantitative data on dilatancy. In addition, the conditions under which mere volumetric dilatation occurred were clearly shown to be quite separate from those under which dilatancy, in the rheological sense, first occurs, although the prior art makes no such distinction.

Mechanisms were postulated for the Newtonian-pseudoplastic–

Newtonian-dilatant shape of the flow curve of concentrated suspensions (as one moves from low to high shear rates). Since only few data are yet available which quantitatively support the proposed mechanisms, they are offered tentatively rather than as a well-developed, inclusive theory in the hope that they will be useful until further facts become available.

The conditions under which dilatant suspensions fracture were studied quantitatively. While the data obtained were limited, they appear to represent the first quantitative study of this problem.

This work was sponsored by the Office of Ordnance Research, U. S. Army. Mr. J. H. Peters arranged for a donation of titania pigment from E. I. du Pont de Nemours and Co. Equipment was made available by the Atlantic Refining Co. The authors are grateful for the support given this work by all three organizations.

References

1. da C. Andrade, E. N., and Fox, J. W., *Proc. Phys. Soc.* (*London*), **62B,** 483 (1949).
2. de Bruijn, H., and Meerman, P. G., *Proc. Intern. Rheological Congress* (*Holland*), Vol. II, North Holland Pub. Co. (Amsterdam), Interscience, New York, 1948, p. 160.
3. Freundlich, H., and Kross, W., *Kolloid-Z.*, **52**, 37 (1930).
4. Freundlich, H., and Roder, H. C., *Trans. Faraday Soc.*, **34,** 308 (1938).
5. Lewis, W. K., Squires, L., and Broughton, G., *Industrial Chemistry of Colloidal and Amorphous Materials*, Macmillan, New York, 1942.
6. Metzner, A. B., *Ind. Eng. Chem.*, **50**, 1577 (1958).
7. Metzner, A. B., in *Advances in Chemical Engineering*, Vol. I, T. B. Drew and J. W. Hoopes, Jr., eds., Academic Press, New York, 1956.
8. Philippoff, W., *Viskosität der Kolloide*, Steinkopff, Germany, 1942, Edwards Bros., Ann Arbor, Michigan, 1944.
9. Pryce-Jones, J., *Proc. Univ. Durham Phil. Soc.*, **10,** 427 (1948).
10. Reiner, M., *Deformation and Flow*, H. K. Lewis & Co., London, 1949.
11. Reynolds, O., *Phil. Mag.*, **8,** 20 (1885).
12. Riggs, L. C., B.Ch.E. thesis, Univ. of Delaware, Newark, 1956.
13. Robinson, R. V., *J. Phys. and Colloid Chem.*, **55**, 455 (1951).
14. Ting, A. P., and Luebbers, R. H., *A.I.Ch.E. Journal*, **3,** 111 (1957).
15. Vand, V., *J. Phys. and Colloid Chem.*, **52,** 300 (1948).
16. Verwey, E. J. W., and de Boer, J., *Rec. trav. chim.*, **57,** 383 (1939).
17. Whitlock, M., M.Ch.E. thesis, Univ. of Delaware, Newark, 1957.

Synopsis

The purpose of this work was to study the factors influencing the flow behavior of concentrated suspensions; particular emphasis was placed on study of the factors which determine the conditions under which dilatancy may occur. The

most important variables studied were solids concentration and viscosity of the suspending medium.

It was found that the frequently quoted observation that dilatant non-Newtonian behavior occurs when a suspension has dilated volumetrically sufficiently to appear to be dry visually is not quantitatively correct. Instead, visual dryness was found to occur at shear stresses well below those at which rheological dilatancy, as determined by inspection of the flow curve, occurred. Rheological dilatancy was found to increase with increasing shear stress; at stresses only a few fold higher than those at which dilatancy first occurred the suspension was found to fracture.

The ranges of the variables studied were:

Viscosity of the suspending liquid	1–43 centipoises
Solids concentration	0–64% by volume
Shear rates	2–1,000 sec.$^{-1}$
Shear stresses	0.1–13 p.s.f. (50–6000 dynes/cm.^{2})

Particle diameters were varied from 0.5 to 100 microns, although most of the work was carried out with the smallest particles.

TRANSACTIONS OF THE SOCIETY OF RHEOLOGY II, 255–262 (1958)

Flow of an Incompressible Visco-Plastic Layer on an Inclined Plane

P. R. PASLAY, *General Electric Company, Schenectady, New York,*
and A. SLIBAR, *Technische Hochschule Stuttgart, Stuttgart, Germany*

INTRODUCTION

Many materials, such as emulsions for coating and paint, can be characterized, to a first approximation, as an incompressible visco-plastic (Bingham) material.[1] This material at any point has zero deformation rate until a certain combination of stresses at the point exceeds a critical value. When flow occurs the ratios of corresponding reduced stress and strain rate components have the same value which depends on the excess of the stress over the critical stress necessary to initiate flow.

Analytically, the behavior may be expressed as follows:

$$\begin{aligned} 2\mu d_{ij} &= \left(\frac{\sqrt{J_2} - \tau_0}{\sqrt{J_2}}\right) S_{ij} && \text{if } \sqrt{J_2} \geq \tau_0 \\ d_{ij} &= 0 && \text{if } \sqrt{J_2} < \tau_0 \end{aligned} \tag{1}$$

where d_{ij} is a component of the incompressible deformation rate tensor. In Cartesian spatial coordinates x_i with velocity components v_i, d_{ij} becomes:

$$d_{ij} = \frac{1}{2}\left(\frac{\partial v_i}{\partial x_j} + \frac{\partial v_j}{\partial x_i}\right)$$

Also,

$$\sqrt{J_2} = \sqrt{\frac{1}{2}\sum_{i,j} S_{ij}S_{ji}}$$

is the positive square root of the second invariant of the reduced stress tensor.

S_{ij} is a component of the reduced stress tensor. If σ_{ij} denotes a stress tensor component, then

$$S_{ij} = \sigma_{ij} - \frac{1}{3}\,\delta_{ij} \sum_{K=1}^{3} \sigma_{KK}$$

where δ_{ij} is the Kronecker delta.

μ and τ_0 are material constants (a viscosity and critical shear stress, respectively).

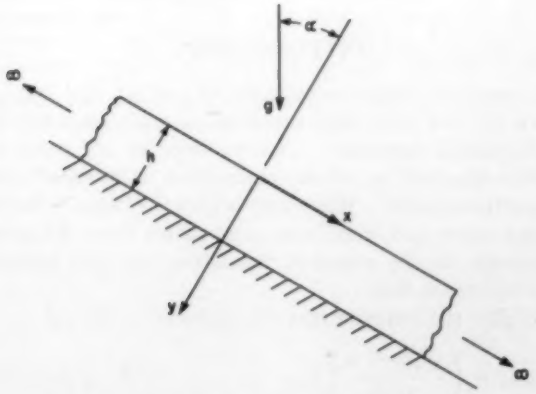

Fig. 1. Geometry of system under consideration.

The formulation of eqs. (1) was first proposed by Hohenemser and Prager[2] and later by Oldroyd.[3]

The Appendix of this paper considers means of selection of suitable values of the material constants μ and τ_0 for incipient flow from experimental data.

SOLUTION

Figure 1 shows the problem under consideration. The inward normal to the infinite plane is taken as the positive y-axis and is inclined at an angle α to the gravity acceleration vector, g. The layer thickness is denoted by h.

The stress solution which satisfies the force equilibrium equations and, as will be shown, leads to a compatible flow field under the prescribed boundary conditions is given as follows:

$$\begin{aligned} \sigma_{zz} &= \sigma_{yy} = \sigma_{xx} = -\rho g y \,(\cos \alpha) \\ \sigma_{xy} &= -\rho g y \,(\sin \alpha) \\ \sigma_{zx} &= \sigma_{yz} = 0 \end{aligned} \tag{2}$$

where ρ is the mass density of the material.

Substituting the stress field into the stress-deformation rate relations, eqs. (1), yields one nontrivial set of equations as follows:

$$\mu \frac{\partial v_x(y)}{\partial y} = -\rho g y \,(\sin \alpha) + \tau_0 \qquad \text{if } |\rho g y (\sin \alpha)| \geq \tau_0 \tag{3}$$

$$\mu \frac{\partial v_x(y)}{\partial y} = 0 \qquad \text{if } |\rho g y (\sin \alpha)| < \tau_0$$

Integration gives

$$\mu v_x = -\frac{1}{2} \rho g y^2 \,(\sin \alpha) + \tau_0 y + C \qquad \text{if } |\rho g y (\sin \alpha)| \geq \tau_0 \tag{4}$$

$$v_x = v_0 \qquad \text{if } |\rho g y \,(\sin \alpha)| < \tau_0$$

Equation (4) shows that as long as

$$y < \frac{\tau_0}{\rho g \,(\sin \alpha)} = h^* \tag{5}$$

the deformation rate is zero so that the region $y = 0$ to $y = h^*$ has a uniform velocity, v_0, in the x direction.

For values of

$$y \geq h^* \tag{6}$$

there is a finite velocity gradient.

The above shows that, in general, two circumstances can occur:

1. $h \leq h^*$ and, since $v_x = 0$ at $y = h$ because the material is assumed to adhere to the plate, no flow occurs.

2. $h > h^*$ and flow will occur.

For Case *2* the velocity v_x is zero at $y = h$ so that from the first of eqs. (4) there follows

$$\mu v_x = \frac{1}{2} \rho g \,(\sin \alpha)(h^2 - y^2) - \tau_0 (h - y) \tag{7}$$

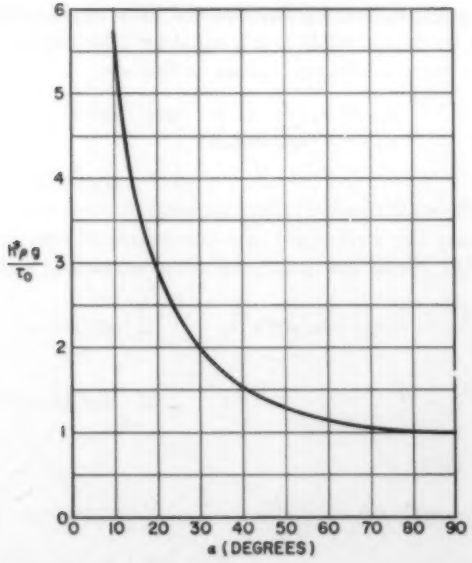

Fig. 2. Dimensionless critical thickness to initiate flow, h^*, as a function of angle of inclination of plane to gravity force, α.

The uniform velocity v_0 is given by the value of v_x at $y = h^*$, since the velocity field must be continuous, as

$$\mu v_0 = \frac{1}{2}\rho g (\sin\alpha)\left(h^2 - \frac{\tau_0^2}{\rho^2 g^2 (\sin\alpha)^2}\right) - \tau_0\left(h - \frac{\tau_0}{\rho g(\sin\alpha)}\right) \quad (8)$$

The volume flow, Q, past a unit width plane perpendicular to the x direction is given by

$$\mu Q = \mu v_0 \frac{\tau_0}{\rho g (\sin\alpha)} + \mu \int_{h^*}^{h} v_x dy \quad (9)$$

or, in dimensionless form, by

$$\frac{\mu Q}{\tau_0 h^2} = \frac{1}{3}\frac{h}{h^*} - \frac{1}{2} + \frac{1}{6}\left(\frac{h^*}{h}\right)^2 \quad (10)$$

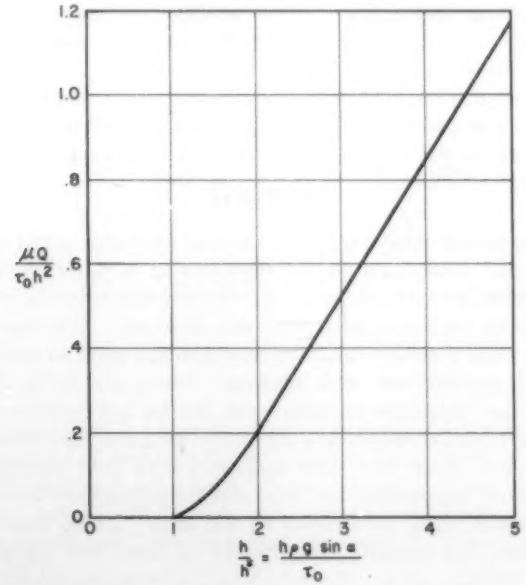

Fig. 3. Dimensionless volume rate of flow past unit width plane perpendicular to flow direction, Q, as a function of the ratio of the layer thickness to the critical layer thickness, h/h^*.

Figure 2 in dimensionless form shows the critical thickness h^* as a function of the angle of inclination α according to eq. (5).

Figure 3 in dimensionless form shows the volume flow rate past a unit width perpendicular to the flow direction as a function of the ratio of the thickness to the critical thickness to initiate flow.

DISCUSSION

By idealizing the behavior of a paint or emulsion as that of a Bingham plastic, the maximum layer thickness without "running" on an infinite flat surface can be predicted from material properties.

The effect on the maximum layer thickness of varying the angle, α, of inclination of the plane to the gravity field is given in Figure 2. The practical significance of this is that an estimate of the change of inclination of the plane necessary to prevent running of a layer is possible.

For practical application of these results, experimental data must be carefully interpreted. The Appendix considers means of arriving at representative values of μ and τ_0 to predict incipient flow. The necessity of reviewing the proper selection of μ and τ_0 is because these material constants are not normally measured directly. The usual measurement is the "effective viscosity" as a function of shear rate.

APPENDIX

The problem of selection of the material constants μ and τ_0 is considered here. The usual way of representing data for many paints and emulsions is to report values of "effective viscosity" as a function of some parameter associated with rate of shear. This implies that equations valid for Newtonian viscous flow are used to calculate an equivalent viscosity for each reading. Obviously, for a Bingham material, the "effective viscosity" will not be independent of shear rate. The means of selecting μ and τ_0 for incipient flow from "effective viscosity"–shear rate data suggested here is to predict "effective viscosity" dependence on shear rate for a Bingham material and then to match these predictions to the data. Three cases of predicting "effective viscosity" dependence on shear rate are given below:

1. For parallel plates separated by a layer of material of constant thickness h, and moved with a constant relative velocity v, the solution for the required shear stress for a Bingham material is (say τ versus v is measured),

$$\tau = \tau_0 + \mu \frac{v}{h} \qquad \text{if } v > 0 \qquad \text{(A.1)}$$

The "effective viscosity" is:

$$\text{effective viscosity} = \tau h/v \qquad \text{(A.2)}$$

and by eliminating τ between eqs. (A.1) and (A.2)

$$\text{effective viscosity} = \mu + (\tau_0 h/v) \qquad \text{(A.3)}$$

The best fit obtainable to the experimental data at low shear rates gives the desired value of μ and τ_0 for predicting incipient flow.

2. For a rotation viscometer with fixed outside cylinder, outer radius r_0, and inside radius r_i, the Bingham material slow flow solution gives[4] (say the moment M and angular velocity ω are measured):

$$\frac{M}{4\pi l_0 r_o^2}\left(\frac{r_o^2}{r_i^2} - 1\right) = \tau_0 \left(\log \frac{r_o}{r_i}\right) + \mu\omega \quad \text{if} \quad M > 2\pi l_0 \tau_0 r_o^2 \tag{A.4}$$

where l_0 is the length of the cylinders.

The effective viscosity is:

$$\text{effective viscosity} = \frac{M\left(\frac{r_o^2}{r_i^2} - 1\right)}{4\pi l_0 r_o^2 \omega} \tag{A.5}$$

Eliminating the moment M between eqs. (A.4) and (A.5) gives:

$$\text{effective viscosity} = \mu + \frac{\tau_0}{\omega}\left(\log \frac{r_o}{r_i}\right) \tag{A.6}$$

Again, as for Case *1*, μ and τ_0 are selected so that the prediction of eq. (A.6) matches experimental results for low shear rates.

3. The last case considered here is capillary flow in a long cylinder of inner radius R subjected to a pressure gradient $(\Delta p/l)$. The volume rate of flow Q resulting from this loading is[5] (say Δp and Q are measured)

$$\frac{\Delta p R}{l} = \frac{8}{3}\left(\tau_0 - 2\,\frac{\tau_0^4 l^3}{(\Delta p)^3 R^3}\right) + \mu\,\frac{8Q}{\pi R^3} \qquad \text{if } \Delta p > \frac{2\tau_0 l}{R} \tag{A.7}$$

The nonlinearity in τ_0 arises because there is a "plug" in the center of the pipe with rigid body motion, and the size of this "plug" depends on τ_0.

The effective viscosity for the capillary is given by:

$$\text{effective viscosity} = \pi R^4 \Delta p / 8Ql \tag{A.8}$$

Eliminating Δp between eqs. (A.7) and (A.8) gives

$$\text{effective viscosity} = \mu + \frac{\pi\tau_0 R^3}{3Q}\left[1 - 2\left(\frac{\tau_0 l}{\Delta p R}\right)^3\right] \tag{A.9}$$

Equation (A.9) is used to select μ and τ_0 for incipient flow calculations so that experiment and theory agree for low shear rates.

References

1. E. C. Bingham and H. Green, *Am. Soc. Testing Materials, Proc.*, **19**, 640 (1919).
2. K. Hohenemser and W. Prager, *Z. angew. Math. u. Mechanik*, **12**, 216 (1932).
3. J. G. Oldroyd, *Proc. Cambridge Phil. Soc.*, **43**, 100 (1947).
4. M. Reiner, *J. Rheol.*, **1**, 5 (1929).
5. E. Buckingham, *Am. Soc. Testing Materials, Proc.*, **21**, 1154 (1921).

Synopsis

The complete solution, stresses and velocities, of the flow of a Bingham plastic on an infinite flat plate due to gravity forces is given. This solution has practical application in emulsion coating and paint technology. Selection of appropriate material constants for incipient flow from experimental data is discussed in the Appendix.

TRANSACTIONS OF THE SOCIETY OF RHEOLOGY II, 263–284 (1958)

The Capillary Experiment in Rheology*

WLADIMIR PHILIPPOFF and FREDERICK H. GASKINS,
The Franklin Institute, Laboratories for Research and Development, Philadelphia 3, Pennsylvania

INTRODUCTION

The use of the flow through a cylindrical tube for the measurement of the viscosity of liquids was introduced by Poiseuille[1] in 1840 and has been used ever since. However, recently we have come across phenomena that show how careful one must be when utilizing this well-known experiment for the determination of the rheological properties of *viscoelastic* liquids. This led to a re-evaluation of some of the fundamental principles of rheology that have been generally accepted during the past 30 years. In the present paper we give a systematic survey of the problems involved in the flow of viscoelastic liquids through a cylindrical (capillary) tube.

THEORY FOR NEWTONIAN LIQUIDS

From Poiseuille's experiments, assuming Newton's law of flow, Wiedemann[2] (1856) calculated the so-called "Poiseuille Law." In the calculation it was assumed that the applied pressure is held in equilibrium by the viscous loss in the shearing layers of the liquid in the capillary. Explicitly stated, the exterior pressure is counterbalanced exclusively by the viscous loss inside the tube. This condition of equilibrium, that has been widely used in rheology, subsequently leads to the classical formula for the shear stress at the rim of the capillary:

$$\tau_R = \frac{Rp_T}{2L} \tag{1}$$

where R and L are the radius and length of the capillary and p_T is the applied pressure difference across the ends of the capillary.

* Part VI of a series, "Flow Birefringence and Stress."[11–15]

However, it was well known that all of Poiseuille's experiments (as well as Hagen's[1]) could not be described by "Poiseuille's Law." The reason for this behavior of normal liquids was the kinetic energy imparted to the liquid leaving the capillary at higher flow velocities. This meant that part of the energy determined by the pressure and volume of flow per second, Q, was destroyed outside the capillary and converted into heat. This led Hagenbach[3] (1860) to introduce the "kinetic energy correction" to Poiseuille's Law by subtracting the kinetic energy of the emerging liquid from the pressure drop across the ends of the capillary. If we call p_T the total pressure, p_c the pressure held in equilibrium inside the capillary, ρ the density of the liquid and $v = Q/\pi R^2$ the mean velocity of flow, we can then write, with m a constant coefficient:

$$p_T = p_c + m\rho v^2 \tag{2}$$

This equation results directly from the energy balance cancelling Q from both parts of the equation. Both Hagenbach and Boussinesq[4] calculated the value of m for the normal parabolic distribution of velocity across the capillary radius; the final value generally accepted is $m = 1.12$ (see Riemann[5]) instead of the value of $^1/_2$ which should be the case for a uniform velocity across the capillary. This treatment is adequate for Newtonian liquids under such pressures that the viscosity rise with hydrostatic pressure can be neglected and the energy loss inside the capillary does not lead to a measurable heating of the emerging liquid. Both these complicating phenomena exist and are important in the case of very high rates of shear with Newtonian liquids such as lubricating oils.

Of course a liquid flow cannot be supposed to terminate abruptly either at the geometrical entrance or in the end section of the cylindrical tube; it will continue outside and distort the flow on the inside near the end. The entrance contribution is generally termed "the end correction" or "Couette correction."[6] Schiller[7] (1932) determined l, the length necessary to accelerate a (Newtonian) liquid of viscosity η so as to obtain stationary laminar flow:

$$l = 0.037\, Q\rho/\eta \tag{3}$$

A numerical evaluation of this expression gives exceedingly small corrections to the length of the capillary, which can usually be neglected within the precision of the measurements, especially for the

long tubes, of $R/L = 1/100$ or less, used in viscometry. The Couette correction, n (see below), was experimentally determined for Newtonian liquids by Dorsey[8] to be $n = 0.57$ [see eq. (14)].

THEORY FOR NON-NEWTONIAN LIQUIDS

For non-Newtonian liquids, whose viscosity is different for each shearing stress, the mathematical calculations have been made by Weissenberg[9] and reported numerous times in the literature. Starting from an arbitrary function—the rate of shear, dv/dr, vs. shearing stress, τ:

$$dv/dr = f(\tau) \tag{4}$$

and assuming that the applied pressure is held in equilibrium in the capillary, the liquid being sheared in concentric cylinders (laminar flow) and no slippage occurring at the wall (same assumptions as those used by Wiedemann[2]), Weissenberg obtained the well-known equation:

$$dv/dr = {}^3/_4\, D + {}^1/_4\, \tau_R\, (dD/d\tau_R) \tag{5}$$

The quantity D introduced here is usually called "the mean rate of shear"; this must be discussed in some detail. The primary quantity measured is, of course, Q. In the case of a Newtonian liquid the viscosity is constant under all conditions. However in the non-Newtonian liquids it is quite important that the shearing stress and the rate of shear be referred to the same point of the material. Using this idea, inserting eq. (1) for the shear stress at the wall into Poiseuille's Law, and defining the viscosity according to Newton as τ_R/(rate of shear), one obtains without further calculation:

$$D = (4/\pi)(Q/R^3) \tag{6}$$

for the rate of shear at the wall for a Newtonian liquid, the point at which the maximum shear stress τ_R is calculated. Physically speaking, we calculate the rate of shear at the wall from the integrated value of the velocity across the whole capillary cross section, Q, assuming Newton's law or, what is identical, a parabolic distribution of velocity over the radius. Weissenberg's differential eq. (5) allows us to calculate the rate of shear at the wall from the integrated velocity which does not have a parabolic distribution. As the ranges of vari-

ables used in the investigation of viscoelastic liquids are quite large, it is usual to plot log D vs. log τ_R (flow curve). Under these conditions eq. (5) becomes:

$$\frac{dv}{dr} = \frac{N+3}{4} \cdot D = \frac{N+3}{\pi} \cdot \frac{Q}{R^3} \tag{7}$$

with N defined as the slope of the curve:

$$N = (d \log D)/(d \log \tau) \tag{8}$$

The value of D as defined in eq. (6) for viscoelastic non-Newtonian liquids is therefore not the true rate of shear at the wall of the capillary, which should be calculated according to eq. (5) or (7), but a somewhat smaller value. Equation (7) obviously corrects D to the true value at the wall of the capillary, the same point where the shear stress is calculated according to eq. (1).

The use of the so-called Kroepelin[10] equation for the "mean rate of shear" G,

$$G = (8/3)\ (Q/\pi R^3) \tag{9}$$

does not seem, therefore, to have any advantage over D for Newtonian liquids and has as little physical sense as D for non-Newtonian liquids. In many cases, when $N \sim 1$, the correction calculated from eqs. (5) and (7) can be disregarded within the experimental precision. It is not important in the comparison of capillaries of different sizes which at the same rate of shear have a correction independent of their dimensions. However, in comparing different modes of flow, such as rotational and capillary viscometers, the correction is important for strongly non-Newtonian liquids ($N > 1$).

CORRECTION FOR ELASTIC ENERGY

In our previous publications[11-15] we believe that we have proved beyond a reasonable doubt that flowing viscoelastic liquids have a measurable elastic potential energy in stationary flow. This elastic energy was first introduced by Herzog and Weissenberg[16] in 1928 and has been discussed by these authors extensively since that time. It was also discussed at length by Garner, Nissan, and Wood[17] in 1950. A measure of this elastic energy per unit volume, as has been shown especially in our latest publication,[15] is the product of the shearing

stress τ and the recoverable shear s, called the "normal stress," P_{11}, which is a constant for each rate of shear:

$$P_{11} = \tau s \tag{10}$$

This "normal stress" acts as a "pull" or tension in the direction of flow. In the case of a rotational viscometer, after application of a constant torque the deflection of the inner cylinder increases until the rate of increase with time becomes constant (stationary laminar flow). If we assume that the streaming viscoelastic liquid acquires an elastic energy in steady flow, this elastic energy remains constant with time; the outside force supplies only the additional energy required for overcoming the viscous resistance or energy loss.

In the capillary, however, the elastic energy is imparted to the liquid at the entrance of the capillary and is carried out of the capillary by the flowing liquid. It is then dissipated outside the capillary (in a manner not to be described here) much in the same way as the kinetic energy discussed previously. Herein lies the fundamental qualitative difference of the capillary and rotational viscometers for viscoelastic liquids. The energy balance for the capillary can be written as:

$$p_T Q = p_c Q + m\rho v^2 Q + E \tag{11}$$

where E is the elastic energy transported out at the capillary, in ergs. Dividing by Q we obtain, similarly to eq. (2):

$$p_T = p_c + m\rho v^2 + E/Q \tag{12}$$

E/Q is the mean elastic energy in ergs/cc. or dynes/cm.^{2} or, for that matter, the "axial normal force, P_{11}." Assuming as a first approximation (which we know is not completely right) that p_c is a constant over the capillary area and that $(P_{11})_R$ is the normal force at the rim of the capillary, we can write

$$p_T = p_c + m\rho v^2 + (P_{11})_R \tag{13}$$

At a constant rate of shear, D, assuming the viscous flow to occur in concentric cylinders along the whole length of the capillary, we can express p_c through the "shear stress" τ_{cR} at the radius R of the capillary. Any real "geometrical end correction" would increase the active length of the capillary by $\delta L = nR$. n is termed the "Couette Correction."[6]

$$p_c = \frac{2(L + \delta L)}{R} \tau_{cR} = \frac{2(L + nR)}{R} \tau_{cR} \tag{14}$$

Similarly we can formally calculate the "total or apparent shear stress" τ_T from the dimensions of the capillary and the applied pressure p_T:

$$p_T = (2L/R)\, \tau_T \tag{15}$$

τ_T is not an experimental shear stress, but a mathematical reference quantity. Furthermore, at the radius R [see eq. (10)] (with s_R the recoverable shear at radius R):

$$(P_{11})_R = \tau_{cR}\, s_R \tag{16}$$

We can rearrange eq. (13) to obtain:

$$\tau_{TR} = \tau_{cR}\left[1 + \frac{R}{L}\left(n + \frac{s_R}{2}\right)\right] + \frac{R}{2L}\, m\rho v^2 \tag{17}$$

Similarly, for $r = R$, eq. (13) can be rewritten as:

$$p_T = \tau_{cR}\left[\frac{2L}{R} + 2n + s_R\right] + m\rho v^2 \tag{18}$$

We have in practice calculated the "kinetic energy correction," $m\rho v^2$, and used a "corrected pressure," p_{corr} ($p_{corr} = p_T - m\rho v^2$). Then eq. (18) can be written as:

$$p_{corr} = \tau_{cR}\left(\frac{2L}{R} + 2n + s_R\right) \tag{19}$$

Equations (18) and (19) are independent of the particular velocity distribution in the capillary due to their being the result of a force equilibrium. τ_{cR} is the corrected shear stress at the wall taking into account both the geometrical end effect and the elastic energy.

Both equations are linear functions of R/L and L/R, respectively. They lead to intercepts on both coordinate axes and a slope. In Table I these quantities are tabulated. For each rate of shear we have assumed above that P_{11} is dependent only on the shear stress τ_{cR} or the rate of shear. Therefore, investigating τ_T and p_T *at a constant rate of shear* for capillaries of different ratios of R/L we can calculate τ_{cR} and $\left(n + \frac{s_R}{2}\right)$ and therefore have in principle the possibility

TABLE I

	X-intercept	Y-intercept	Slope
$\tau_T = f(R/L)$	$\left(\frac{R}{L}\right)_{\tau_T \to 0} = \frac{-1}{n + (s_R/2)}$	$(\tau_T)_{L \to \infty} = \tau_{cR}$	$\tau_{cR}[n + (s_R/2)]$
$p_T = f(L/R)$	$(L/R)_{p_T \to 0} = -[n + (s_R/2)]$	$(p_T)_{L \to 0} = \tau_{cR}(2n + s_R)$	$2\tau_{cR}$

of measuring P_{11} from a capillary experiment. The complete discussion of the physical significance of these equations will be given later.

We know that p_c is not independent of r. However, the exact calculations of the condition are very elaborate and not yet complete. We have presented this very approximate treatment to convey the general idea; in a later paper the exact calculation will be given.

ELASTIC DEFORMATION IN THE CAPILLARY

It is well known that the relation between the rate of shear and shear stress for a viscous liquid leads to a field of flow that is identical with the distribution of the elastic shear of a Hookean body stressed by the same shear stress. The equations for the shear stress are identical for both cases and the equations for the shear strain s result from the ones for the rate of shear by substituting the volume of deformation V for the volume of flow per second Q. Therefore if an elastic body such as a gel is put into a capillary and stressed by a pressure difference across the ends of the capillary, the elastic deformation over the radius forms a parabola analogous to the parabolic distribution of the velocity over the radius observed in laminar flow. From this relationship the shear at the wall can be easily calculated to allow the measurement of the shear modulus knowing the shearing stress at the wall in eq. (1). This leads to the equation for the shear modulus G if we measure the total volume V displaced by the pressure analogous to the Poiseuille equation:

$$G = \pi p_T R^4 / 8VL \tag{20}$$

Similarly the shear at the wall s_R is calculated as

$$s_R = (4/\pi)(V/R^3) \tag{21}$$

If, however, we measure the maximum axial displacement x_0 along the axis of the capillary under pressure, the equation for the shear at the wall s_R becomes:[18]

$$s_R = 2x_0/R \tag{22}$$

The last equations, especially (21) and (22), can be used for measuring the recoverable shear s using the capillary viscometer, and therefore the normal stress can be calculated through eq. (10).

In this connection it is important to give a precise definition of what we have called, in this and our previous articles, recoverable shear, s. If a viscoelastic system is stressed in any of the geometries suitable for the measurement of viscosity such as cone and plate, concentric cylinders, or capillary, the force is applied primarily as a shear stress. The elastic energy per unit volume is given by the product of force and deformation. In the case of the geometries discussed, by using rigid walls, all elastic deformations of the test body except the elastic shear deformation are eliminated. When the source of the shear stress is removed, the normal stresses can exist, but their elastic energy is zero due to the fact that they have not led to elastic deformations. (See definition of Weissenberg,[19] quoted in ref. 13.) Therefore the elastic energy recovered is exactly equal to the elastic energy put in.

DISCUSSION

The equations mentioned above are not new; however, a correlated discussion of them appears to be novel. The existence of an end effect in the capillary flow of Newtonian liquids is well known. It led Erk[20] to design a "normal viscometer" in which the indeterminate end correction (as well as the kinetic energy correction) is eliminated from the measurement by using two capillaries of the same diameter but different lengths in series. From pressure measurements including the junction point, the pressure gradient p_T/L is calculated. In the actual practice of viscometry, direct microscopic measurement of length and diameter usually does not lead to adequate precision. One has to resort to one single exact measurement (i.e., the length) and

calculate the radius by using a standard calibrating liquid such as water. The radius cannot be measured exactly enough for *real* capillaries, as they cannot be expected to be uniform along the bore. The radius so calculated obviously includes the end correction for Newtonian liquids. This value may or may not be the same for non-Newtonian liquids. However, the fact that in many cases a τ–D curve gives (within experimental error) a single plot independent of the dimensions of the capillary shows that this method can often be correct. From eq. (18) it is directly seen that long capillaries ($L/R \sim 100$), especially when calibrated in the way outlined above, make the influence of n and s negligible. τ_T is essentially equal to τ_{cR}. This is practically the case for the solutions of cellulose derivatives described in the accompanying paper[28] and for the numerous "flow curves" published. However, for liquids that have $s = 10$–100 this correction is important. Examples of such liquids seem to be the solutions of aluminum soaps in hydrocarbons and polyisobutylene solutions at high rates of shear as well as molten polyethylene. Equations (17) and (19) require a linear plot of τ_T or p_{corr} as a function of R/L or L/R, as has been stated. However, this is only true when the properties of the material do not change during the flow in the capillary. This condition is very difficult to analyze mathematically; we therefore resorted to experimental measurements to investigate the situation.

EXPERIMENTAL CHECK OF THE THEORY

We were fortunate in having some recently published experimental data that seemed to prove our point. We have carried out additional measurements on other materials which have confirmed the results described.

The investigations of Bauer and Weber[21] have shown that the properties of aluminum dilaurate solutions in toluene do not give a uniform τ–D curve at different ratios of R/L. They referred to this as the "end correction." They then replotted their values as shown in Figure 1, where the apparent shear stress τ_T is plotted over R/L following eq. (17). For the six values of D investigated, each curve is a straight line between the limits $L/R = 20.9$ to $L/R = 1{,}021$ independent of the value of R, as predicted by eq. (17). These very painstaking experiments with a considerable number of tubes prove

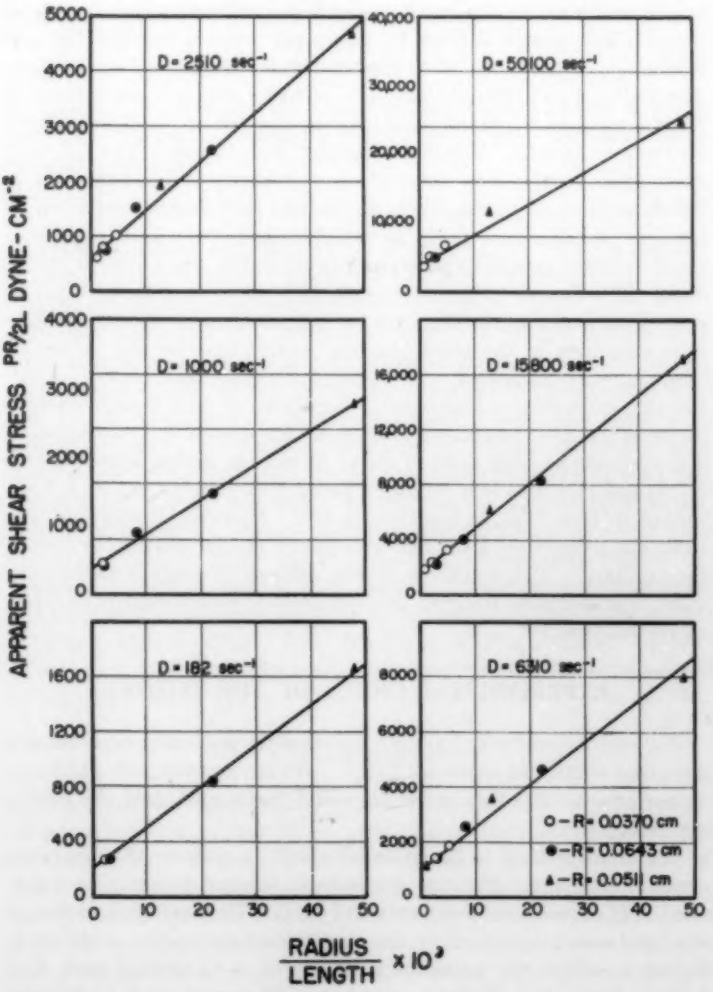
D = 2510 sec⁻¹
D = 50100 sec⁻¹
D = 1000 sec⁻¹
D = 15800 sec⁻¹
D = 182 sec⁻¹
D = 6310 sec⁻¹
APPARENT SHEAR STRESS PR/2L DYNE-CM⁻²
RADIUS / LENGTH x 10³
○ – R = 0.0370 cm
● – R = 0.0643 cm
▲ – R = 0.0511 cm

Fig. 1. Bauer and Weber's experiments on aluminum dilaurate in toluene at 25°C.: plot of τ_T vs. R/L [see eq. (18)] at stated values of D.

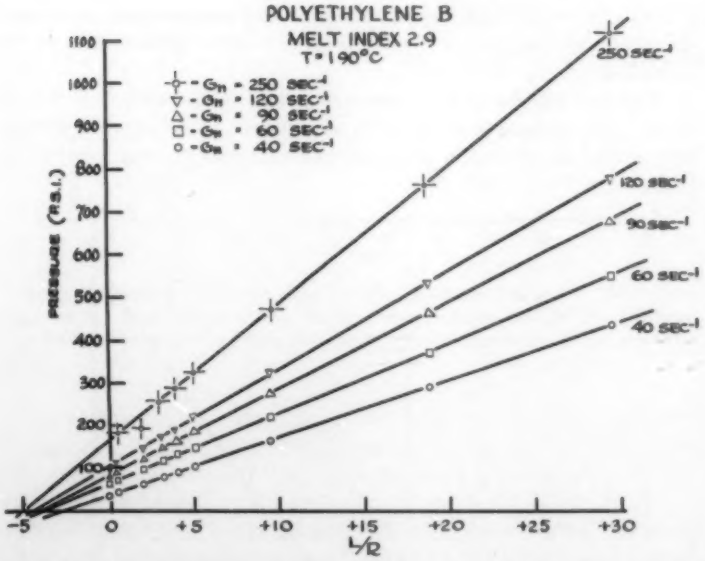

Fig. 2. Bagley's experiments on polyethylene B at 190°C.: plot of p_T vs. L/R [see eq. (19)] at stated values of D.

conclusively, in our opinion, that for the aluminum dilaurate solutions, at least, eq. (17) is valid.

The evaluation of the x-intercept gives a value of $n + (s_R/2) \sim 133$, which is approximately constant in the whole range of D investigated. Neglecting n we obtain a value of $s_R \sim 260$. Mathematically, we cannot decide if this large value of s is at all physically possible. We will discuss this subsequently. The plot of τ_{sR} vs. D, gives a value of D independent of R/L as it should.

Bagley[22] investigated molten polyethylene in a capillary viscometer using values of $L/R = 0$ to 29.69 ($L/R = 0$ being a sharp-rimmed orifice). He plotted his values as p_T vs. L/R as required in our eq. (19), and got straight lines in all cases, as seen in Figure 2. This shows very clearly that the state of flow along the capillary length is the same at $L = 0$ as at $L = 29.69R$. This means that the "end effect" for non-Newtonian liquids influences only the liquid *outside* the capillary. His evaluation of these measurements gave values of

$n + (s_R/2) = 2.5$ to 9.75, depending on the material and the rate of shear. Again his plot of τ_{cR} vs. D gave a curve independent of the ratio L/R for various R and L.

Tordella[23] published flow curves of polyethylene with $L/R = 1.78$ to 32. An evaluation of his data at constant D also gave a straight line, within the precision of measurement, when τ_{cR} was plotted vs. R/L.

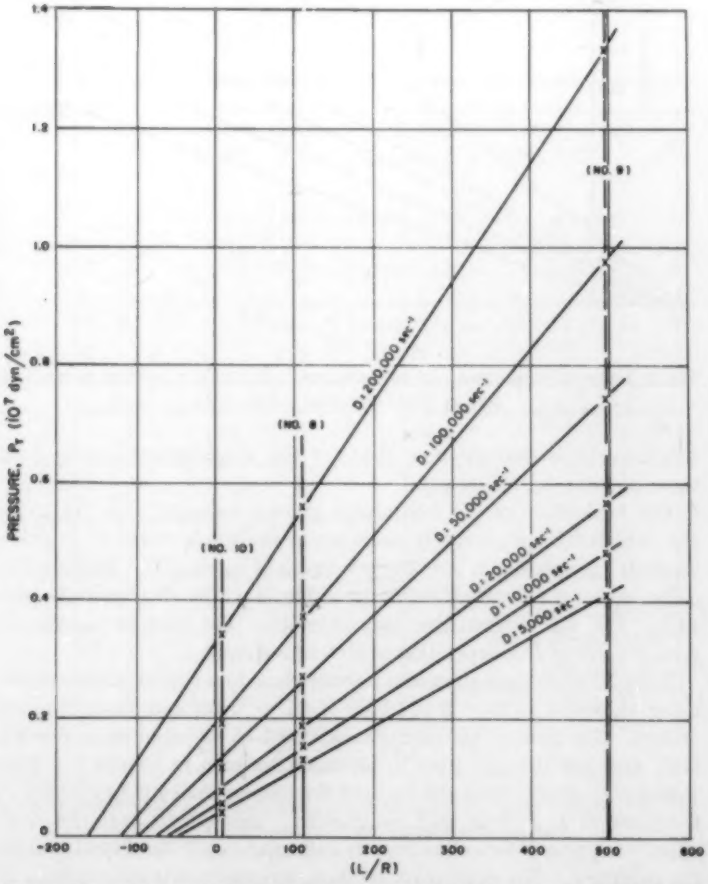

Fig. 3. Plot of p_T vs. L/R for jellied gasoline A at 25°C. at stated values of D.

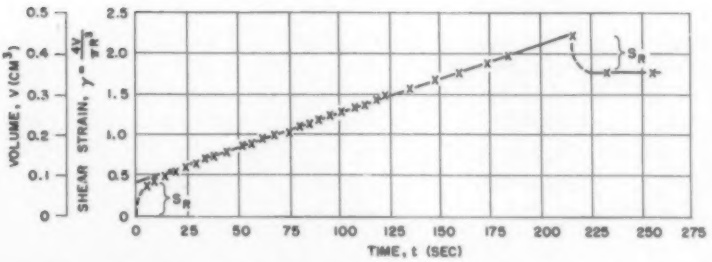

Fig. 4. Deformation-recoil vs. time for jellied gasoline A at 25°C. Tube diameter: 0.5 in. Tube length: 12 in. Shear stress: 139 dynes/cm.^{2}. Rate of shear: $D = 8.45 \times 10^{-3}$ sec.$^{-1}$. Recoverable shear: fore effect (deformation), $s = 0.42$; recoil, $s = 0.45$.

Measurements on a gasoline jellied with an aluminum soap (A) in Figure 3, investigated with three capillaries with $L/R = 500$, 120, and 5, gave straight lines when p_T was plotted vs. L/R at constant rates of shear.

Recoil measurements performed with the same material as above using a $^1/_2$ inch diameter tube, 12″ long as a "capillary" and a sensitive volume-measuring device gave the time-volume curve shown in Figure 4. Similar curves have been obtained and published by Bauer and Weber. However, they measured only the "fore-effect" (i.e., the phenomena occurring after application of pressure), whereas our measurements include both the fore- and after-effects (recoil, after the pressure is removed.) From these measurements we can evaluate s_R, using eq. (21) and from it P_{11} [eq. (10)].

We measured the above solution in the same way as described in a previous publication.[15] The recoil was measured directly in the rotational viscometer. In eq. (21) we have the relation between s and V, which is identical to the one between D and Q. Similarly in the rotational viscometer:

$$s = 2\phi/(1 - c^2) \tag{23}$$

where ϕ is the angle of recoil (in radians), and $c = R_i/R_0$, the ratio of inner to outer radius of the concentric cylinders. The normal stress P_{11} was measured in the Weissenberg Rheogoniometer and evaluated as $s = P_{11}/P_{12}$ (Note: $P_{12} \equiv \tau$). In the birefringence instrument we measured the extinction angle, χ, at the same rate of shear and deter-

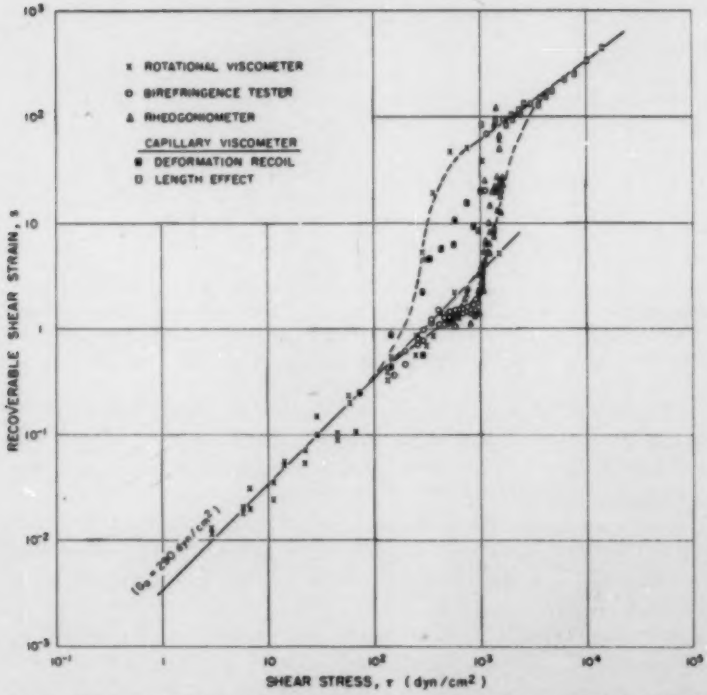

Fig. 5. Recoverable shear strain vs. shear stress for jellied gasoline A at 25°C.

mined $s = 2 \cot 2\chi$. From all the measurements on jellied gasoline we compiled a curve of s vs. τ that in the case of Hookean behavior should be a straight line. Figure 5 shows this plot. The lower portion of this plot, up to a shear stress $\tau = 100$ dynes/cm.^{2}, is essentially a straight line with a 45° slope: Hooke's Law in shear. From about $\tau = 100$ to 1000 dynes/cm.^{2} the deformation increases less than proportionally to τ; from 1000 to 2000 dynes/cm.^{2} s increases by nearly a factor of 100 and then continues to increase somewhat between $\tau = 2000$ to $\tau = 10{,}000$ dynes/cm.^{2}. This general picture is assembled from a variety of measurements. In the lower range of s the recoil values measured in the rotational or capillary viscometers are substantially equal. In the range of $\tau = 100$ to 2000 this particular material has two limits of stability: a lower one that is essen-

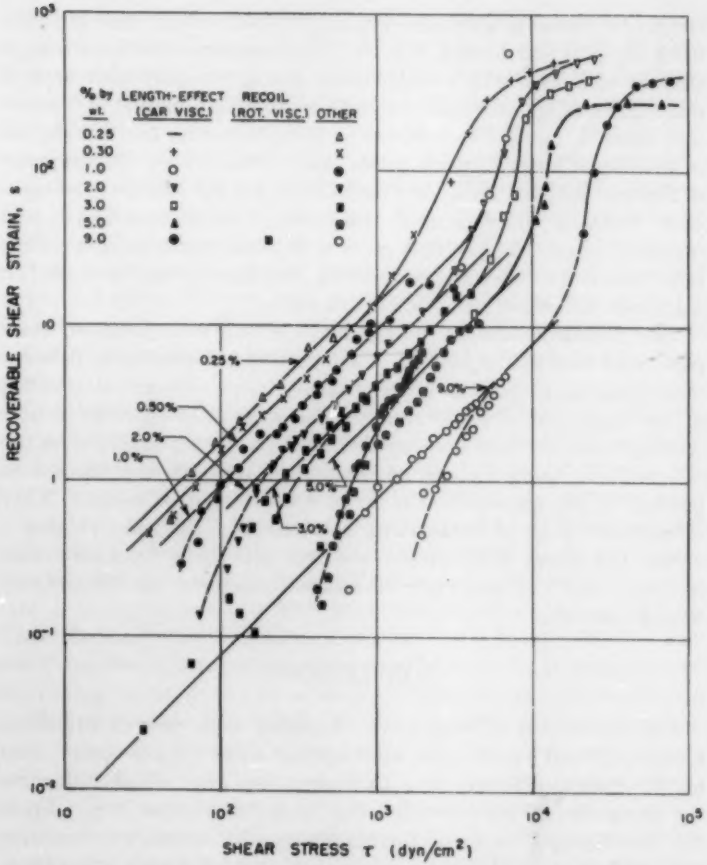

Fig. 6. Recoverable shear strain vs. shear stress for solutions of polyisobutylene in decalin at 25°C.

tially described by the "fore effect" of the rotational and capillary viscometers, the birefringence tester, and the Weissenberg Rheogoniometer; and a higher level of s determined by the recoil in both viscometers.

In the range of 500 to 1000 dynes/cm.^{2} the measurements with capil-

laries of different lengths were evaluated at a constant rate of shear, using eq. (19) and putting $n = 0$. The measurements show a large amount of scatter which is primarily due to the particular type of material investigated, which showed a considerable amount of recoverable shear, s, but is also unstable as is evidenced by the two regions of stability. From Figure 5 we see that s values above 100 computed in the way outlined above are found with several instruments, especially recoil in the rotational viscometer, birefringence tester, and capillary length effect. This gives a physical significance to these large values of s, especially considering that Bauer's measurements on a different material gave a similar value of s.

The measurements on polyisobutylene solutions reported were performed with two capillaries, which showed a displacement between measurements at the same rates of shear for two different R/L values in the high rate of shear range. The evaluation of these results (adding a new series of measurements with a shorter capillary for the 5% solution) using eq. (19) gave values of $s \sim 200$ that have been plotted on the same plot (Fig. 6) of s vs. τ reported before. They extend the range of measurable s values to considerably higher τ values and merge satisfactorily with the previously reported values of s measured with either the birefringence tester or the Weissenberg Rheogoniometer.

CONCLUSIONS

The theoretical developments, together with the experimental results reported above, show what appears to be the possibility of an elastic energy in steady flow through a capillary, which influences the properties of viscoelastic bodies in an unexpected way. From the experimental results on the aluminum soap solutions and molten polyethylene it is seen that eqs. (18) and (19) have been proved correct within the whole possible range of capillary lengths from 0 to ∞. The straight-line relationships are at least a good confirmation that the capillary flow does not change along the axis of the capillary after the entrance section has been passed. As has been mentioned by Bagley,[22] this also means that the time of transit through the capillary, which has been discussed by Smith,[24] is of no importance for the flow of viscoelastic liquids. As the flow pattern is completely developed at the entrance of the capillary it is obvious that the velocity profile

is the same at the entrance and along the capillary length. This leads to the conclusion that eq. (7), which allows us to calculate the rate of shear at the wall, is applicable also at the entrance of the capillary and has a more general meaning than the shear stress calculated according to eq. (1). Obviously the rate of shear in a sharp-edged orifice can be calculated from the volume of flow Q with the same precision as has been done previously in the flow through long capillaries. This is a very unexpected conclusion, but Bagley's experiments as well as our own seem to have proved it conclusively. The volume element at the rim of a sharp-edged orifice has a shear stress τ which is determined by D taken from a separately measured flow curve (D vs. τ_R) using long capillaries. However, the calculated τ_T for a sharp orifice is determined not by the length L which is 0, but by the quantity $n + (s/2)$.

In the development shown [especially in eqs. (18) and (19)], we see that the geometrical end correction, n, in terms of the radius is always added to the recoverable shear at the wall, $s_R/2$. From capillary experiments alone we cannot possibly distinguish between a large n or a large s_R. Only further experiments of the sort described here with the Weissenberg Rheogoniometer, the recoil in the rotational viscometer and/or the birefringence instrument, all used at the same rate of shear, allow us to distinguish between these two quantities. They obviously measure only s_R and are not influenced by n. The results presented here seem to indicate that n, in the particular cases where the correction has to be made, is negligible as compared to s_R, making it possible to measure the normal stress P_{11} in a capillary experiment. It has been stated before that the whole correction is only important when $(n + (s_R/2))\ (R/L)$ becomes comparable to unity. This means practically that only for values of $[n + (s_R/2)]$ of 10–100 and more is the correction necessary for long capillaries. However, in Bagley's experiments with short capillaries (small values of L/R) considerably smaller values of n are important. With such small values we probably cannot disregard n in comparison with $s_R/2$, but measurements of s under the same conditions have not yet been made.

This discussion of the short orifice is directly pertinent to the problem of extrusion of plastics through dies where the length is comparable to the diameter. It seems that the normal stress P_{11} makes the greatest contribution to the resistance to flow, the viscosity having a second-

ary effect. This gives a direct practical significance to P_{11} which has until now been considered somewhat of a scientific curiosity. Of further importance is the fact that τ and P_{11} have different types of dependence on D (as s is not necessarily a linear function of either τ or D) so that flow curve results are not directly applicable to extrusion through short dies.

The foregoing discussion applies only to the conditions inside the capillary. In a future paper, a discussion of what takes place both before and after the liquid passes through the capillary will be given.

The theory outlined above has shown that the transition from Newtonian to non-Newtonian flow in a capillary requires three corrections to Poiseuille's law:

(*1*) The correction for the rate of shear at the wall [eq. (7) of Weissenberg].

(*2*) The correction for the shear stress in the capillary due to the combined geometrical length effect and normal stress in eq. (18).

(*3*) The correction for the kinetic energy of the emerging liquid.

The experimental data seem to show that no further corrections are necessary for these phenomena.

The investigation of the solutions mentioned above showed that even for moderate N, such as for molten polyethylene, an end correction has to be applied; whereas in the case of the formerly reported nitrocellulose solutions, even very large values of N did not require it. We know in this case by direct measurement that s was small. Therefore attributing the large end corrections to the recoverable shear (s_R) seems to be plausible. It seems from our results that s_R is more important than n. The use of n values up to 100 as mentioned by Bauer seems improbable, as they become in some cases larger than the geometry of the viscometer allows.

The experimental proof of the theory presented above does not seem to be complete in all details. However, it is enough to prove a great probability of its validity and should lead to further exact determinations on more suitable materials.

The experimental results given here show very distinctly the importance of the recoverable shear s introduced by Weissenberg as a measure for the "anomalous behavior" of viscoelastic materials. Using eq. (10) we see that s determines the ratio of the normal stress to the shear stress. Normal liquids have $s = 0$ and no normal stresses. Most polymer solutions have $s \sim 1$: both normal and shear

stresses are of about the same magnitude; normal stresses can be measured (see the results on ethylcellulose solutions in ref. 28) but they do not dominate the conditions in steady flow. However, in the case of molten polyethylene and aluminum soap solutions, where values for s reach 10 to 100, the normal stresses dominate the whole behavior of the material and in the limit the viscous contribution to flow becomes unimportant. We see therefore that the suggestion of Weissenberg[16] is borne out by the results quoted: s in steady shear is indeed a good nondimensional parameter for describing the "anomalous" viscoelastic flow behavior of materials.

SUMMARY

It is shown that the elastic potential energy of the emerging liquid in a capillary experiment leads to a new kind of correction. The "end correction" is increased by $^1/_2$ the recoverable shear s_R. The implications arising are discussed and compared with available experimental results.

APPENDIX I

In ref. 13 we quoted Rivlin and Mooney regarding the calculation of the stresses in finite elongations. The equation used by both authors was (referring to the deformed state):

$$\sigma_1 = (\partial W/\partial \lambda_1)\, \lambda_2 \lambda_3$$

with λ_1 the principal extension in Cauchy measure, λ = deformed length/initial length, and W = the strain-energy function.

For incompressible materials $\lambda_1\lambda_2\lambda_3 = 1$ and

$$\sigma_i = \lambda_i(\partial W/\partial \lambda_i)$$

This is however identical with

$$\sigma_i = \partial W/\partial \lambda_i^H$$

with $\lambda_i^H = \ln \lambda_i$, the deformation in "Hencky-measure." This may be compared with the classical definition:

$$\sigma_i = \partial W/\partial \lambda_i$$

Reiner[25] quotes a number of "deformation measures" for finite deformations. For the case discussed above, having one single shear modulus G, we obtain the following *identity* for the principal stresses σ_i, as a function of the principal extension λ_i in Cauchy measure (the formulation with I, according to Rivlin):

$$\sigma_i = \lambda_i(\partial W/\partial\lambda_i) = \partial W/\partial\lambda_i^H = \partial\lambda_i^2\,(\partial W/\partial I_1)$$

$$-p = 2G\,\lambda_i^G = G\,\lambda_i^2 - p$$

where:

I_1 = the strain-invariant $= \lambda_1^2 + \lambda_2^2 + \lambda_3^2$

$\lambda^G = (\lambda_1^2 - 1)/2$ = deformation in "Green-measure"

We see that λ^H and I_1 are directly related to W whereas λ^G occurs in the tensor-equation. This simplest possible case applies to experimental results as we have shown in our publications. [In ref. 13 an error occurred: $C_1 = (G + H)/4$, not $(G + H)/2$.]

APPENDIX II

Cerf[26] introduced the quantity ω (which was also called "the intrinsic orientation constant" by Peterlin[27]) by the relation:

$$\omega = \left(\frac{45 - \chi}{D}\right)_{D\to 0}$$

In order to connect it with the calculations published in ref. 12, we calculate it in other terms: (η_0 = "initial viscosity" at $D = 0$)

$$\left(\frac{1}{G}\right)_{D\to 0} = \left(\frac{s}{\tau}\right)_{D\to 0} = \left[\frac{2\cot 2\chi}{\eta D}\right]_{D\to 0}$$

$$= \left[\frac{2\tan 2(45 - \chi)}{\eta_0 D}\right]_{D\to 0} = \frac{4\omega}{\eta_0}$$

$$\omega = \frac{1\eta_0}{4G}$$

We therefore see that ω has the dimensions of a relaxation time.

This work was supported under a research contract with the U. S. Army Chemical Warfare Laboratories, Army Chemical Center, Maryland. The assistance of this agency is gratefully acknowledged.

We express our thanks to Prof. Bauer for permission to reproduce one of his figures as our Figure 1, and to Dr. Bagley for the same courtesy (our Fig. 2).

References

1. G. Hagen, *Ann. phys.*, **16,** 423 (1839). J. L. M. Poiseuille, *Compt. rend.*, **11,** 961 (1840); *Rec. Savants Etrangers*, **IX** (1846).
2. G. Wiedemann, *Ann. phys.*, **99,** 221 (1856).
3. E. Hagenbach, *Ann. Phys.*, **109,** 385 (1860).
4. J. Boussinesq, *Compt. rend.*, **110,** 1160, 1238, 1292 (1890); **113,** 9, 49 (1891).
5. W. Riemann, *J. Am. Chem. Soc.*, **50,** 46 (1928).
6. M. Couette, *Ann. chim. phys.*, **21,** 433 (1890).
7. L. Schiller, *Handb. d. Experimentalphysik*, Vol. IV, 2, Leipzig, 1932.
8. N. E. Dorsey, *Phys. Rev.*, **28,** 833 (1926).
9. R. Eisenschitz, B. Rabinowitsch, and K. Weissenberg, *Mitt. deut. Materialp. Anst. Sonderh.*, **9,** 91 (1929). B. Rabinowitsch, *Z. physik. Chem.*, **145,** 1 (1929).
10. H. Kroepelin, *Ber.*, **62,** 3056, 3061 (1929).
11. W. Philippoff, *Nature*, **178,** 811 (1956).
12. W. Philippoff, *J. Appl. Phys.*, **27,** 984 (1956).
13. W. Philippoff, *Trans. Soc. Rheology*, **1,** 95 (1957).
14. J. G. Brodnyan, F. H. Gaskins, and W. Philippoff, *Trans. Soc. Rheology*, **1,** 109 (1957).
15. W. Philippoff, F. H. Gaskins, and J. G. Brodnyan, *J. Appl. Phys.*, **28,** 1118 (1957).
16. R. Herzog and K. Weissenberg, *Kolloid-Z.*, **46,** 277 (1928).
17. F. H. Garner, A. H. Nissan, and G. F. Wood, *Phil. Trans. Roy. Soc.*, **A241,** 379 (1950).
18. F. Michaud, *Compt. rend.*, **174,** 1282 (1922); *Ann. phys. chim.*, **19,** 63 (1923).
19. K. Weissenberg, *Conf. British Rheology Club*, 1946.
20. S. Erk, *Forsch. Gebiete Ingenieurw.*, **Nr. 288** (1927). S. Erk and A. Schmidt, *Physik. Z.*, **37,** 489 (1936).
21. W. H. Bauer and N. Weber, *J. Phys. Chem.*, **60,** 270 (1956).
22. E. B. Bagley, *J. Appl. Phys.*, **28,** 624 (1957).
23. J. P. Tordella, *J. Appl. Phys.*, **27,** 454 (1956).
24. T. Smith, *J. Polymer Sci.*, **14,** 37 (1954).
25. M. Reiner, *Rheology*, Vol. I., F. Eirich, ed., Academic Press, New York, 1956, Chap. II.
26. R. Cerf, Thesis, Strasbourg, 1951; *J. Phys. Rad.*, **15,** 145 (1954).
27. A. Peterlin, Chapter XV in ref. 25, p. 628.
28. J. G. Brodnyan, F. H. Gaskins, W. Philippoff, and E. G. Lendrat, *Trans. Soc. Rheology*, **2,** 285 (1958).

Synopsis

In previous publications we have shown that the potential energy in flow can be calculated from the applied shear stress, τ, and the "recoverable shear," s. Here the concept of a potential elastic energy existing in a liquid emerging from a capillary gives a means of determining s from the predicted and experimentally-found linear relationship between τ and the L/R ratio. With polyisobutylene solutions the calculated recoverable shears correlate satisfactorily with the measurements previously reported. This condition of potential energy in flow has also been noted with molten polyethylene and solutions of aluminum dilaurate.

TRANSACTIONS OF THE SOCIETY OF RHEOLOGY II, 285-302 (1958)

The Rheology of Various Solutions of Cellulose Derivatives*

JOHN G. BRODNYAN, FREDERICK H. GASKINS, and WLADIMIR PHILIPPOFF, *The Franklin Institute, Laboratories for Research and Development, Philadelphia, Pennsylvania,* and E. G. LENDRAT, *American Viscose Corporation, Marcus Hook, Pennsylvania*

1. INTRODUCTION

In the past there has been some controversy over the relative merits of various geometries in the measurement of the viscosity of non-Newtonian materials. The purpose of the work described here was to show that different geometries and loadings give the same results when the data are treated properly. This was done with a number of solutions of cellulose derivatives which are non-Newtonian materials.

Also, recent publications[1-6] have shown a correlation between "normal stresses" as measured by a Weissenberg Rheogoniometer and the optical extinction angle as measured in a birefringence instrument. This correlation was also checked in a wide range of rates of shear using solutions of cellulose derivatives. The solutions used did not exhibit the considerable recoil in the rotational viscometer at low rates of shear that was reported for the very high polymer nitrocellulose solutions.

2. MATERIALS USED

A. The ethyl cellulose was a commercial grade N-100 supplied by Hercules Powder Co., Wilmington, Delaware, and the cyclohexanone was supplied by Eastman Kodak. This 11% solution was homogenized on a roller mill for two weeks and filtered through a 200-

* Part VII of a series, "Flow Birefringence and Stress" [3,4,5,13,15,16]

mesh screen. It was not so homogeneous as solutions of cellulose derivatives generally are, but still had no noticeable yield value.

B. The 1.7% solution of carboxymethyl cellulose in water was supplied by the Army Chemical Center, Edgewood, Maryland. This is the same material used by Gill and Gavis[6] in their investigation of the tensile stress in jets of viscoelastic fluids.

C. The viscose solutions were supplied by the American Viscose Company, Marcus Hook, Pennsylvania.

3. INSTRUMENTS USED

The instruments used in these investigations have been described in the literature, either partially or fully. A more detailed description of the first-mentioned instrument is given below. They vary in geometry and type of loading. We used (*1*) a coni-cylindrical (rotational) viscometer which has a constant shearing stress; (*2*) a Ferranti-Shirley viscometer[7] which is a cone and plate instrument having a constant rate of shear; (*3*) a high pressure capillary viscometer[8] which gives a constant shearing stress; (*4*) a McKee Consistometer[4] which is a capillary instrument driven at a constant rate, the pressure being measured; (*5*) a Weissenberg Rheogoniometer[3] which is a cone and plate instrument giving a constant rate of shear; (*6*) a birefringence instrument[3] with a constant rate of shear; and (*7*) the dynamic tester of the Franklin Institute[9] which has a constant frequency. The Weissenberg Rheogoniometer differs from the Ferranti-Shirley instrument in that it measures the force normal to the plate as well as the shearing stress.

The coni-cylindrical rotational viscometer used in the work is pictured in Figure 1. The coni-cylindrical design as first developed by Mooney and Ewart[10] was modified so that the bob has the shape of a cylinder with two end cones instead of one, giving a constant rate of shear in the whole viscometer. Thus the whole cup was filled with the material to be investigated. The bottom cone rests on a bearing in the stationary cup consisting of a carboloy point on a hardened steel bearing surface. The cup has a 25.4 cm. diameter which determines a large shearing area. The hollow bobs will float in the materials to be investigated so this upward force must be counteracted by adding a weighted ring to the shaft. Proper adjustment of the weights keeps

1	UPPER BEARING (SLEEVE)	12	SHAFT
2	COLUMN	13	BEARING RETAINER
3	PLATFORM	14	BEARING SUPPORT
4	MIRROR BRACKET	15	BEARING SUPPORT BRACKET
5	PULLEY VERNIER	16	LOWER COLUMN
6	SPECIMEN CUP BEARING	17	WASHER
7	BELT RETAINER	18	PULLEY
8	COVER	19	PULLEY BUSHING
9	CONE	20	CUP STUD
10	SPECIMEN CUP	21	CONE BEARING
11	LOWER PLATFORM		

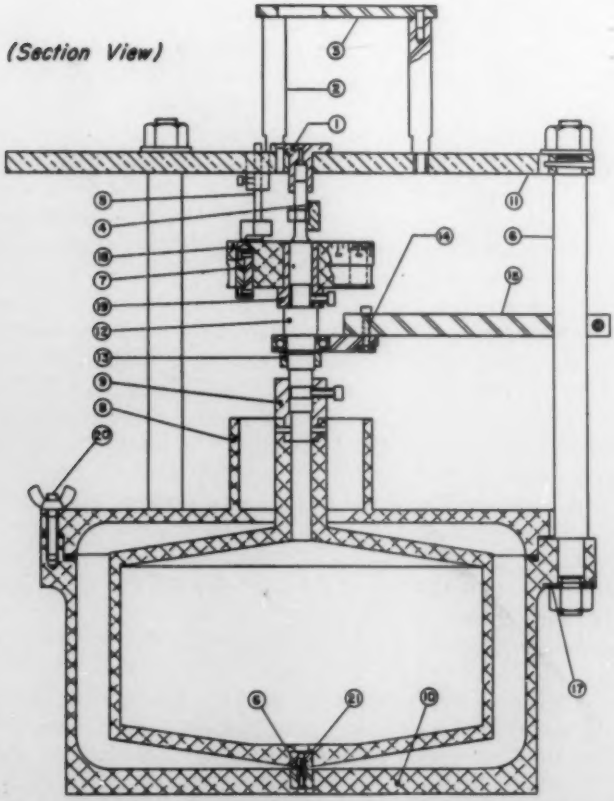

Fig. 1. Assembly drawing of rotational (coni-cylindrical) viscometer.

the friction low and this together with the large shearing area allows measurements at very low shearing stresses (0.1 dyne/cm.^{2}). The shaft from the top of the bob has a pulley with a degree scale etched on it, which allows a force to be applied by using weights over pulleys in the usual way. The shaft is held above the pulley by a bronze sleeve bearing, with a third bearing in the center of the shaft to take up the thrust when extremely high forces are applied.

The two bobs have clearances of 18 and 4 mm., respectively. The conditions can be calculated according to the formulas elaborated by Mooney and Ewart, and the actual calibrations show that the values measured correlated within 8 and 14%, respectively, with the ones calculated from the dimensions. The differences are caused by such things as the neglect of the edge effects of the viscometer.

The smallest shearing stress already mentioned is 0.1 dyne/cm.^{2}; the maximum, 6500 dyne/cm.^{2}. With the two bobs, this instrument gives rates of shear between 10^{-7} and 100 sec.$^{-1}$.

The Ferranti-Shirley cone and plate viscometer has a stipulated range of rates of shear of 20 to 20,000 sec.$^{-1}$.

In the high-pressure capillary viscometer we use six stainless steel capillaries of different diameters and different lengths giving ratios of length to diameter of 60, 120, and 240. They enable the capillary viscometer to measure the flow properties of substances in a range of rates of shear from 3×10^{-3} to 5×10^5 sec.$^{-1}$ with pressures from 0.5 cm. Hg to 1400 psi. These pressures give shearing stresses varying from 28 to 1,000,000 dyne/cm.^{2}.

The McKee Consistometer allows one to make measurements at rates of shear from 24 to 6.51×10^5 sec.$^{-1}$ by using three different capillaries with ratios of length to diameter of 24.0, 63.5, and 107.5.

The Weissenberg Rheogoniometer can be used, adding reduction gears, in the range of rates of shear of 4×10^{-4} to 4×10^2 sec.$^{-1}$.

The flow birefringence instrument can be used in the range of rate of shear of 7.9×10^{-5} to 3.46×10^4 sec.$^{-1}$ by using three interchangeable inner cylinders.

The dynamic tester has a frequency range of 3.4×10^{-4} to 6.17 cycles per second.

The viscometers were calibrated using a National Bureau of Standards Oil, and these experimentally obtained constants correlated very well with those calculated theoretically.

The capillary viscometer values were corrected in the well-known[5] way for non-Newtonian flow to insure a comparison with the other values.

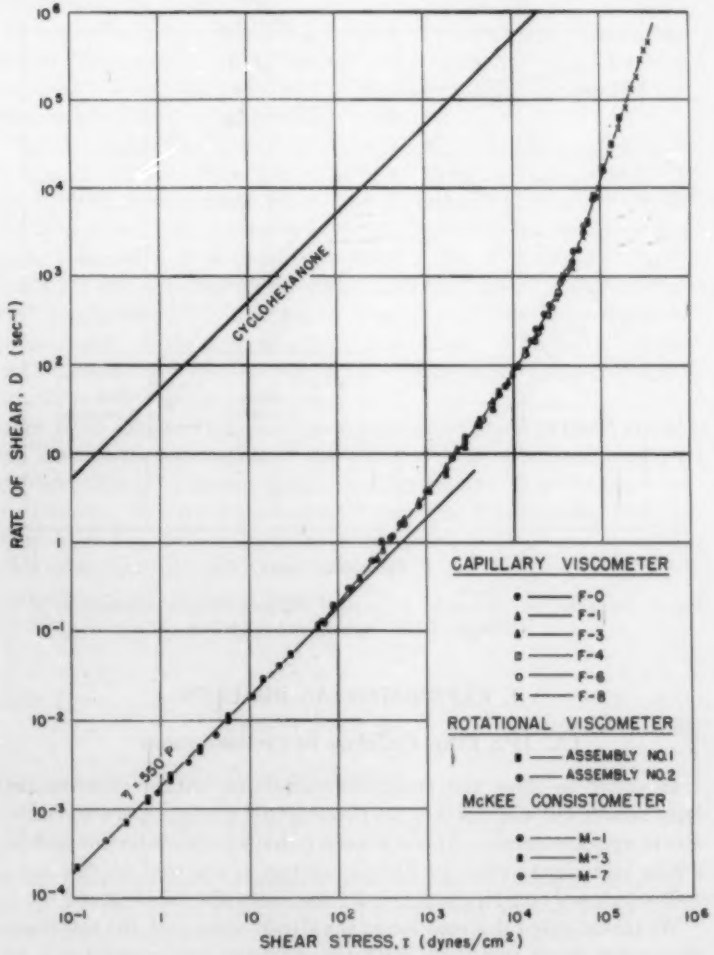

Fig. 2. Flow curve for 11% ethyl cellulose in cyclohexanone at 25°C.

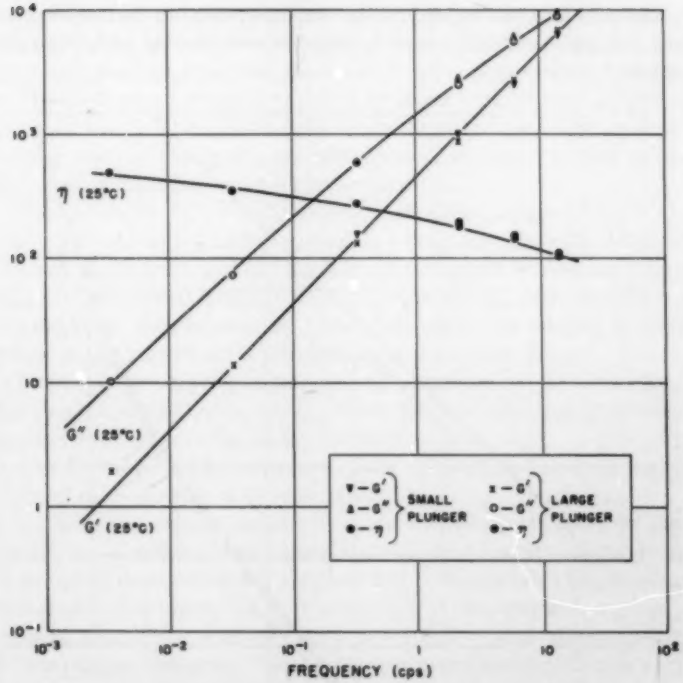

Fig. 3. Dynamic test curves for 11% ethyl cellulose in cyclohexanone at 25°C. Ordinate: G',G'' (dynes/cm.^{2}) η (poises).

4. EXPERIMENTAL RESULTS

A. 11% Ethyl Cellulose in Cyclohexanone

In order to show the complete correlation within experimental error among our viscometers, we investigated a solution of ethyl cellulose in cyclohexanone. It was chosen to have a concentration and intrinsic viscosity so that the Newtonian region was well defined and a well-developed non-Newtonian behavior could also be observed.

We investigated this solution in the steady state with the rotational viscometer using two bobs, with the capillary viscometer using six capillaries, and with the McKee consistometer using three capillaries.

The results are shown in Figure 2. Within the precision of the measurements, all the results fall on one single τ–D curve beginning with a rate of shear of 2×10^{-4} up to 5×10^{5} sec.$^{-1}$, a range of more than nine decades.

It might be noted that in one hundred consecutive runs in the McKee consistometer there was no irreversible viscosity decrease measured. This indicates that the effects published by Bestul[11] are apparently confined to rubberlike polymers.

The dynamic behavior of this viscoelastic solution was also investigated at 25°C. from 3.4×10^{-3} to 16 cycles per second. A plunger-type arrangement previously described[12] was used. However, it was modified to give two interchangeable inner cylinders, one giving a gap of 2.40 mm. and the other a gap of 6.40 mm. From Figure 3 it can be seen that the mechanical properties—storage modulus G', loss modulus G'', and dynamic viscosity η—were independent of the geometry of the testing arrangement used. The region of the initial viscosity was not reached and therefore could not be compared with the steady state measurements.

The ethyl cellulose solution was finally investigated in the Weissenberg Rheogoniometer to check experimentally the distribution of P_{22} over the radius. This was done in a different way than the one used by Roberts. We have mentioned[13] that the Weissenberg relation $P_{22} = P_{33}$ can be deduced from Roberts' experiments without resorting to his measurements with three different liquids.

Experimentally Roberts found:

$$\frac{\partial P_{22}}{\partial \ln r} = K \tag{1}$$

$$P_{22} = P_{33} = 0 \qquad \text{at } r = R \tag{2}$$

Theoretically from the force equilibrium:

$$\partial P_{33}/\partial \ln r = P_{11} - P_{22} = \text{const.} \tag{3}$$

for the cone-and-plate arrangement, in which s = constant independent of r. The experimental relation is observed for a different force than the theoretical one: P_{22} instead of P_{33}.

From all the existing *theories* the differences of the normal stresses are functions of the shear s, or more exactly s^2. Therefore they are

sometimes called "secondary stresses." They are constant for a constant s, which is the case for the narrow cone-and-plate arrangement used here. Then quite generally,

$$P_{22} - P_{33} = const. = Bs^2 \tag{4}$$

Differentiating with respect to $\ln r$ we get

$$\frac{\partial P_{22}}{\partial \ln r} - \frac{\partial P_{33}}{\partial \ln r} = 0 \tag{5}$$

or using the relations mentioned above we obtain:

$$K = P_{11} - P_{22} \tag{6}$$

$$P_{22} = P_{33} + const. \tag{7}$$

The observed relation $P_{33} = P_{33} = 0$ for $r = R$ results in: $P_{22} = P_{33}$ and $B = 0$.

Jobling developed the formula for the determination of $P_{11} - P_{22}$ from the total thrust F of the cone in the following way:

$$F = \int_0^R 2\pi r \, dr P_{22}(r) \tag{8}$$

Introducing the relation

$$P_{22}(r) = (P_{11} - P_{22}) \ln (r/R) \tag{9}$$

from eqs. (2) and (3), which was found by Roberts and required by Weissenberg for $P_{22} = P_{33}$, we obtain, by setting $r/R = x$:

$$F = 2\pi(P_{11} - P_{22})R^2 \int_0^1 x \ln x \, dx \tag{10}$$

where:

$$\int_0^1 x \ln x dx = \left| \frac{x^2}{2} \ln x - \frac{x^2}{4} \right|_0^1 = -\frac{1}{4}$$

because:

$$\left| \frac{x^2}{2} \ln x \right|_{x \to 0} = 0 . \infty = \frac{1}{2} \frac{1/x}{-2/x^3} = -\frac{x^2}{4} \to 0$$

therefore:

$$P_{11} - P_{22} = -2F/\pi R^2 \tag{11}$$

F is a pressure, $P_{11} - P_{22}$ a tension, therefore the $-$ sign. We see that Jobling's formula is derived for the logarithmic distribution of P_{22} over the radius.

Therefore to prove the logarithmic distribution we need only prove that eq. (11) holds at a given rate of shear for various radii of the top plate. This has been done with two different radii (using two solid upper plates and one "torque assembly," by which shear stresses could also be measured); the results are given in Table I. They show that the normal stresses calculated in this way correlate for the two radii, hence that the logarithmic distribution of P_{22} over the radius is confirmed in this new manner. This is in principle similar to the use of the volume flowing through the capillary to determine the velocity distribution over the radius. Birefringence tests on this solution could not be made as it was dark brown in color, due to the cyclohexanone used.

Molecular weight calculation

Concn., g./cm.^{3}	T, °K	$\frac{d(\cot 2\chi)}{d\tau}$	M
0.1135	~298	1.01×10^{-3}	2.85×10^6

$M \approx 50{,}000$

$M = cRT \frac{d(\cot 2\chi)}{d\tau}$

$R = 8.314 \times 10^7$

Density = 1.032 g./cm.^{3}

B. 1.7% Carboxymethylcellulose in Water

This solution was measured in the rotational viscometer, the Weissenberg Rheogoniometer, and the birefringence tester. The flow curve determined with the rotational viscometer covers a range of rates of shear from 10^{-3} to 10^2 sec.$^{-1}$, Figure 4, with an initial viscosity of 320 poises.

The Weissenberg Rheogoniometer was primarily used for the investigation of the normal stresses at rates of shear of 0.6 to 200 sec.$^{-1}$ using the "torque head." These data are plotted in Figure 4.

TABLE I

Rheogoniometer[a] Data for 11% Ethyl Cellulose in Cyclohexanone (Ambient Temp.)

Rate of shear, D, sec.$^{-1}$	Normal stress $P_{11} - P_{22}$, dyne-cm.$^{-2}$				Shear stress, τ, dyne-cm.$^{-2}$	Rec. shear, s	Shear modulus, G, dyne-cm.$^{-2}$	Viscosity, η, poises
	Torque head	Plate No. 1	Plate No. 2	Mean				
0.0656	0	0	0	0	40	0		610
0.131	0	0	0	0	75	0		572
0.197	0	0	0	0	95	0		482
0.328	0	22	0	7	130	0.054	2400	396
0.459	52	52	46	50	195	0.257	759	425
0.656	124	124	116	120	270	0.445	607	410
0.984	259	238	277	260	370	0.705	525	376
1.31	466	435	508	455	475	0.958	497	363
1.31	415							
1.97	620	672	715	670	620	1.08	574	315
3.28	1040	993	1080	1040	890	1.17	760	271
4.59	1500	1350	1520	1460	1150	1.27	905	251
6.56	1970	1890	2240	2020	1580	1.28	1230	241
6.56	1970				1580			
9.84	2630	2500	2820	2650	2110	1.26	1680	214
13.1	3150	3080	3390	3210	2610	1.23	2120	200
19.7	4040	3630	4480	4050	3500	1.16	3020	178
26.2	4550			4550	4350	1.05	4140	166
32.8	5280		5630	5450	5500[b]	0.992	5550	167
34.6	5290			5290	5700[b]	0.928	6150	165
45.9			6900	6900	7000[b]	0.985	7120	153
65.6			8800	8800	8800[b]	1.00	8800	134

[a] Rheogoniometer: Spring No. 3, 4° cone.

[b] Values taken from Flow-Curve.

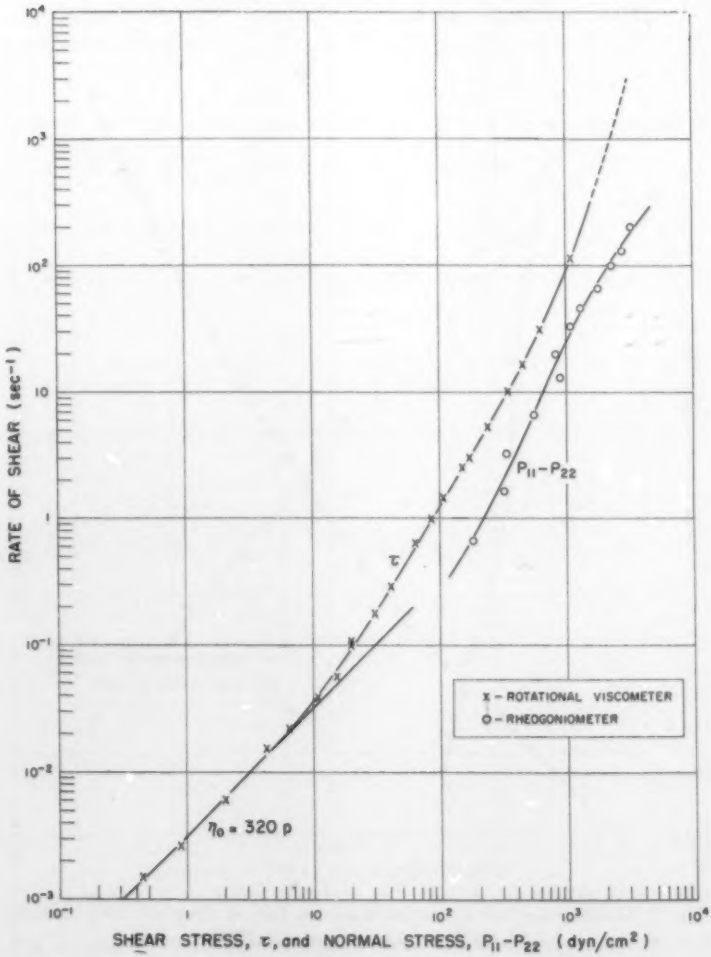

Fig. 4. Shear stress and normal stress vs. rate of shear for 1.7% carboxymethylcellulose in water at 25°C.

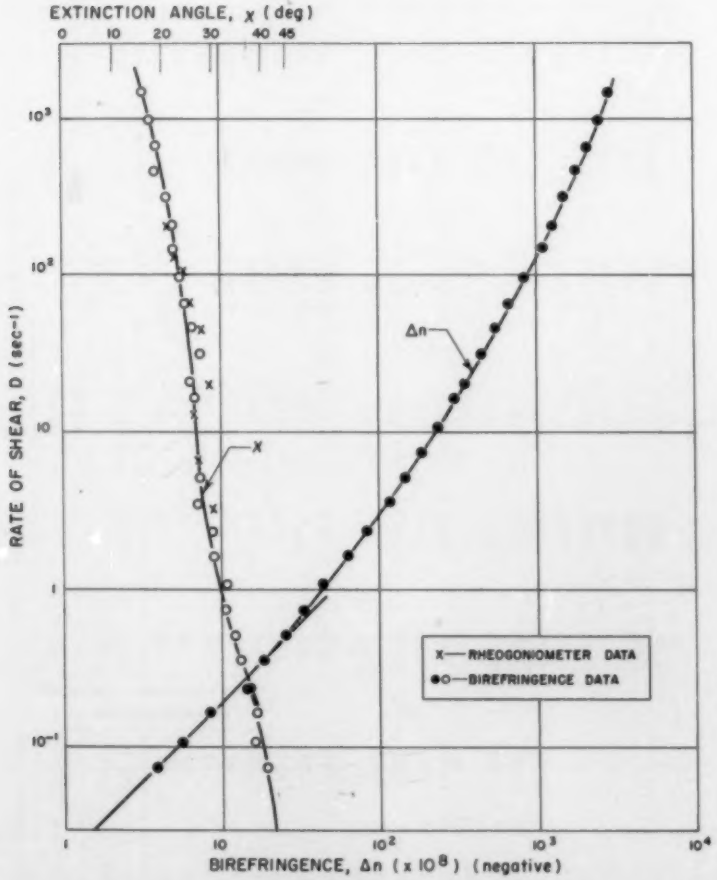

Fig. 5. Birefringence and extinction angle vs. rate of shear for 1.7% carboxymethylcellulose in water at 25°C.

The degree of birefringence, Δn, and extinction angle, χ, were measured in the birefringence instrument as functions of the rate of shear from 10^{-1} to 2×10^{3} sec.$^{-1}$. The curves are given in Figure 5. The rheogoniometer data are also superimposed on the extinction

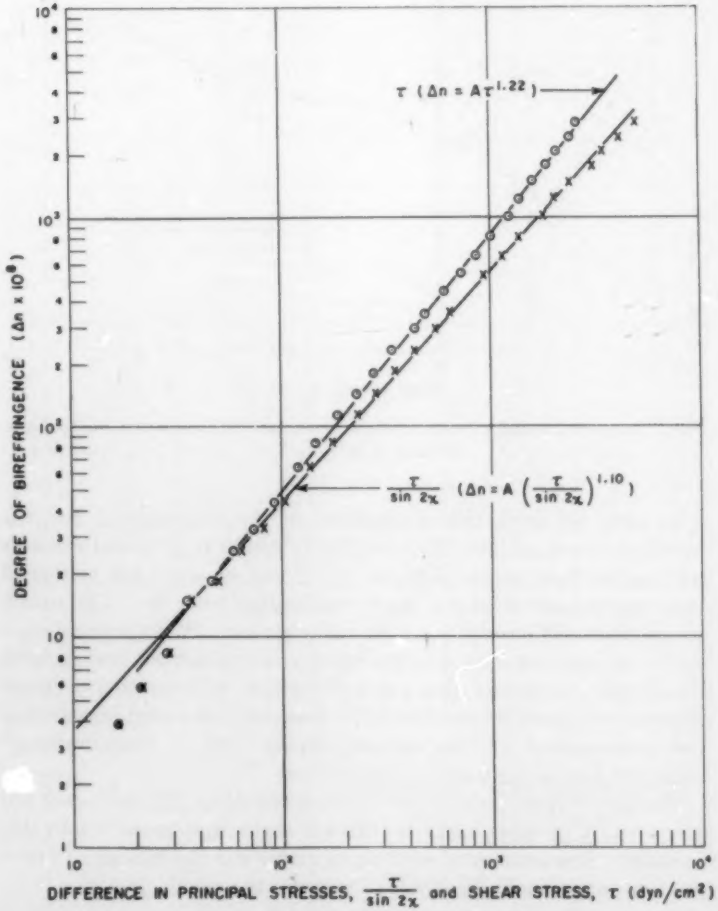
DEGREE OF BIREFRINGENCE (Δn x 10⁸)
DIFFERENCE IN PRINCIPAL STRESSES, τ/sin 2χ and SHEAR STRESS, τ (dyn/cm²)
τ (Δn = Aτ^1.22)
τ/sin 2χ (Δn = A (τ/sin 2χ)^1.10)

Fig. 6. Degree of birefringence vs. difference in principal stresses and vs. shear stress for 1.7% carboxymethylcellulose in water at 25°C.

angle curve where $2 \cot 2\chi = (P_{11} - P_{22})/\tau$. The results show good correlation between the optical and mechanical measurements of the angle χ.

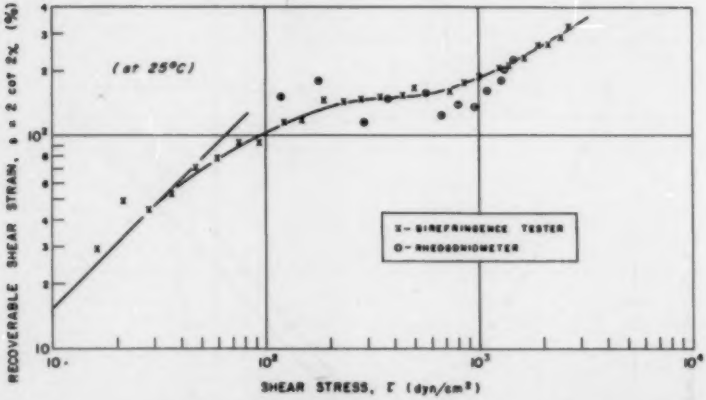

Fig. 7. Recoverable shear strain vs. shear stress for 1.7% carboxymethylcellulose in water at 25°C.

In order to check the applicability of the stress-optical law, the birefringence was plotted against the difference in principal stress as well as the shear stress in Figure 6. It can be seen that neither of these parameters display a linear relationship with Δn. The reason for this lack of linearity is not completely clear. With polyisobutylene[4] a constant coefficient independent of concentration and molecular weight was found; this was not the case with another cellulose derivative (nitrocellulose[5] in *n*-butyl acetate). It would appear that the stress-optical law, so defined, applies only to "free-draining" coils (soft bodies) such as polyisobutylene.

The plot of recoverable shear versus shear stress, Figure 7, does not give a constant shear modulus ("steady state compliance") with this solution. The amount of solution available was not enough to use in the large rotational viscometer to measure the recoil.

C. Viscose Solutions

Four viscose solutions were investigated using a Ferranti-Shirley viscometer, a capillary viscometer, and a rotational viscometer. The Ferranti-Shirley measurements were carried out at the American Viscose Corporation by Mr. E. G. Lendrat at the same time as the

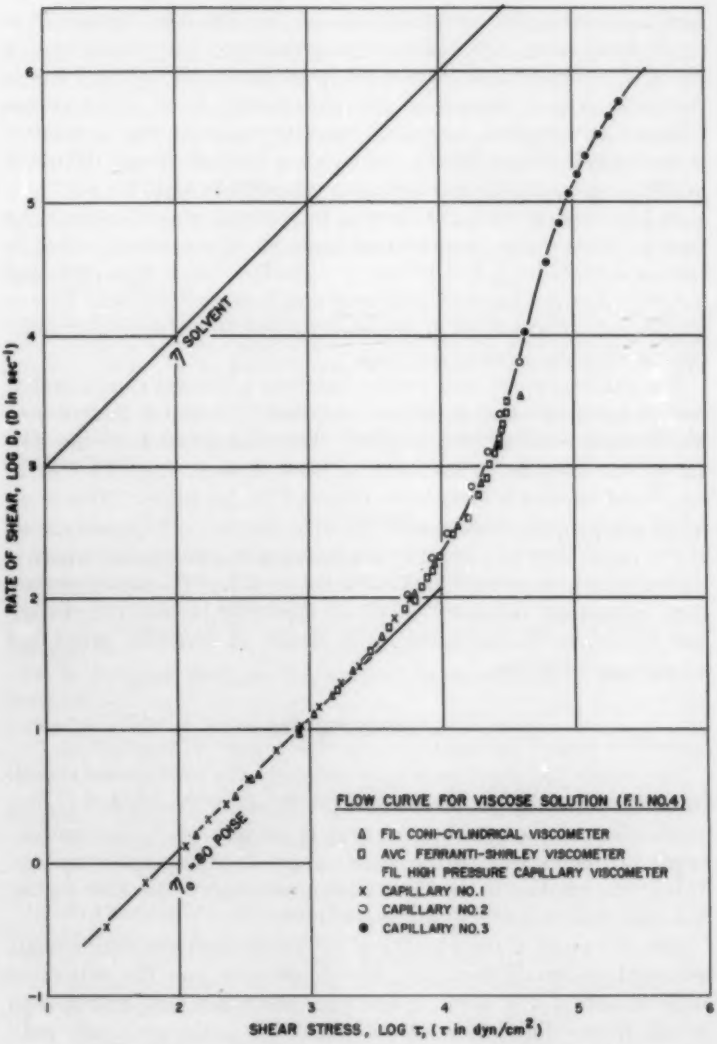
RATE OF SHEAR, LOG D, (D in sec⁻¹)
SHEAR STRESS, LOG τ, (τ in dyn/cm²)
η SOLVENT
η₀ = 80 POISE
FLOW CURVE FOR VISCOSE SOLUTION (F.I. NO.4)
Δ FIL CONI-CYLINDRICAL VISCOMETER
□ AVC FERRANTI-SHIRLEY VISCOMETER
FIL HIGH PRESSURE CAPILLARY VISCOMETER
x CAPILLARY NO.1
○ CAPILLARY NO.2
● CAPILLARY NO.3

Fig. 8. Flow curve for viscose solution (F.I. #4) at 25°C.

capillary viscometer measurements at the Franklin Institute, to insure equal aging. All of the curves showed very close coincidence in the whole range of operation of all three viscometers. One curve in particular (Fig. 8) showed no deviation at all. In all of the viscose solutions investigated, an initial viscosity was obtained at rates of shear between 10 and 100 sec.$^{-1}$ which was between 40 and 100 poises at 25°C., although the measurements extended down to 0.3 sec.$^{-1}$.

At high rates of shear the Ferranti instrument tended to splash the material around due to centrifugal force, so its range was limited to rates of shear of 10^1 to 3×10^3 sec.$^{-1}$. The flow curves were very similar to the ones published by Philippoff and Krueger[14] in 1940. Due to the larger available range in D an S-shape was found, which is characteristic for high polymer solutions.

The question of the recoverable shear was investigated on a similar viscose using the large rotational viscometer which for this purpose was sprayed with acrylic lacquer. The measurement of the flow curves was possible in the range of rates of shear from 10^{-2} to 10 sec.$^{-1}$ and showed a Newtonian behavior in this range. This is directly comparable to the results reported above. The investigation of the recoil showed a considerable amount of scatter, but where it was possible to measure it gave values of $s \sim 0.1$. The measurements were exceedingly difficult to perform, especially because the viscometer was made of aluminum. The danger of corrosion prohibited a longer investigation.

5. DISCUSSION

The results described show very definitely the experimental possibility of measuring the mechanical properties of viscoelastic liquids independent of the geometry or type of loading when the measurements are performed in the same range of mechanical variables. This is true whether in the Newtonian or non-Newtonian flow region, in steady state or under dynamic conditions.

Also, the proof of the equality of the mechanical orientation angle measured in the Weissenberg Rheogoniometer and the extinction angle measured in a birefringence instrument has been extended to include these cellulose derivatives in addition to the previously published results on polyisobutylene and nitrocellulose solutions.

The use of plates of two different radii for the measurements of the normal stresses supplied additional evidence for the reported logarithmic distribution of the normal stress P_{22} over the radius of the cone-and-plate arrangement which together with a separate theoretical treatment contributed toward an understanding of the relation $P_{22} = P_{33}$. All the solutions reported had comparatively small values of $s \sim 1$. Under these conditions, the complications of capillary measurements with large values of s discussed in the accompanying article[16] were below the experimental sensitivity or scatter of the instruments used.

The authors wish to thank the U. S. Army Chemical Warfare Laboratories, Army Chemical Center, Edgewood, Maryland, and the American Viscose Corporation, Marcus Hook, Pennsylvania, for the support which made this work possible.

The authors also sincerely thank Mr. Gwynn McConnell who carried out most of the capillary measurements and Mr. Richard Keyser who did the work with the dynamic tester.

References

1. A. S. Lodge, *Nature*, **176**, 838 (1955).
2. A. S. Lodge, *Trans. Faraday Soc.*, **52**, 120 (1956).
3. W. Philippoff, *J. Appl. Phys.*, **27**, 984 (1956).
4. J. G. Brodnyan, F. H. Gaskins, and W. Philippoff, *Trans. Soc. Rheology*, **1**, 109 (1957).
5. W. Philippoff, F. H. Gaskins, and J. G. Brodnyan, *J. Appl. Phys.*, **28**, 10, 1118 (1957).
6. S. J. Gill and J. Gavis, *J. Polymer Sci.*, **20**, 287 (1956).
7. R. McKennell, *Proceeding of the Second International Congress on Rheology*, London, 1954, p. 350.
8. S. A. McKee and H. S. White, *ASTM Bull.*, **No. 153**, 90 (1948); *J. Research Natl. Bur. Standards*, **46**, 18 (1951).
9. W. Philippoff, *J. Appl. Phys.*, **24**, 685 (1953).
10. M. Mooney and R. M. Ewart, *Physics*, **5**, 350 (1934).
11. A. B. Bestul, *J. Appl. Phys.*, **25**, 1069 (1954).
12. W. Philippoff, *J. Appl. Phys.*, **25**, 1102 (1954).
13. W. Philippoff, *Trans. Soc. Rheology*, **1**, 95 (1957).
14. W. Philippoff and H. E. Krueger, *Kolloid-Z.*, **88**, 215 (1939).
15. W. Philippoff and F. H. Gaskins, *Trans. Soc. Rheology*, **2**, 263 (1958).
16. W. Philippoff, *Nature*, **178**, 811 (1956).

Synopsis

An investigation of the rheological properties of solutions of various cellulose derivatives in different solvents has been carried out in order to correlate the measurements using different instruments. In each investigation several of the following instruments, representing a variety of geometrical configurations, were used: (*1*) a coni-cylindrical viscometer, (*2*) a high-pressure capillary viscometer, (*3*) a birefringence tester, (*4*) a Weissenberg Rheogoniometer, (*5*) a McKee Consistometer, and (*6*) a Ferranti-Shirley Viscometer. The results clearly prove the independence of the mechanical properties of the solutions from any particular geometry when the measurements are performed in the same range of mechanical variables.

TRANSACTIONS OF THE SOCIETY OF RHEOLOGY II, 303–312 (1958)

Abstracts of Additional Papers Presented at the Society of Rheology Meeting, November 7–9, 1957

Flow Phenomena with Oleogels

A. BONDI

Shell Development Company, Emeryville, California

The flow properties of oleogels (= oils gelled by small organic or inorganic particles) are not uniquely characterizable for two reasons: (*a*) the flow properties change with time as a function of mechanical history of the sample, and (*b*) flow at the apparatus-gel interface cannot be neglected, relative to bulk movement of the gel, especially at shear stresses of the order of the initial yield point.

Time effects occur at essentially three levels of time scale. The application of shear stresses of the order of the yield stress for several seconds to minutes may result in strain acceleration which passes through a maximum (Fig. 1). In some instances negative strain acceleration (hardening) is observed. A true steady-state strain rate is rarely observed. The yield stress of the gel is generally reduced by preceding flow measurements.

Shearing at high strain rates, i.e., with shear stresses of the order of 10 to 100 times the yield stress, causes drastic reductions in the instantaneous flow resistance (Figs. 2 and 3) of the gels (and in the size and density of its structural components[1]). Interruption of the shear degradation leads to slow, usually partial, recovery of flow resistance during prolonged rest periods.

The dielectric constant of gels composed of anisometric and anisotropic particles changes (usually decreases) as shear is applied, as one would expect to result from the flow orientation of the gel par-

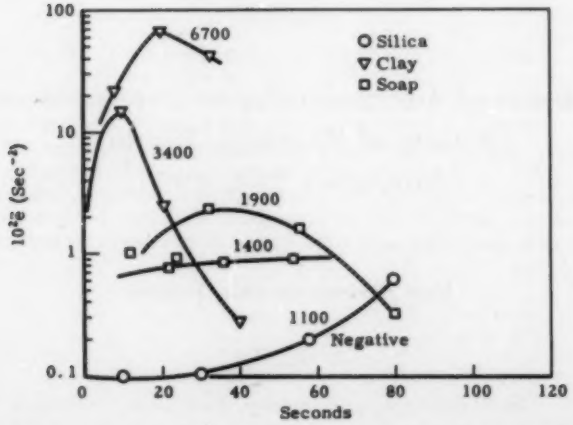

Fig. 1. Change in strain acceleration with time of stress application (in Couette viscometer) for three different oleogels. The curves are numbered with the constant shear stresses (dynes/cm.^{2}) applied.

ticles.[2] Strangely enough, this orientation effect decays instantly as shearing ceases, whereas one would have expected, from the particle dimensions and from substrate viscosity, decay periods of the order of 100 sec. or more.

These observations might be reconciled by the hypothesis that oleogels are sheared along (irregular) planes of structural weaknesses, so that lumps with relatively strong internal structure flow past each other. Elastic deformation of the structure within each lump causes the observed dielectric constant reduction, and the stored elastic energy restores the random configuration of structure components as shearing stops. The size of the "lumps" decreases with increasing shear stress and duration of shearing. There is some evidence[3] that the "primary" gel structure components flow as independent particles at very high ("infinite") shear stress.

Flow at the apparatus-gel interface is evident as yielding far below the bulk yield stress of the gel, described by Bonner and Blott[4] as "first yield point." Both the first and the second yield points are observed in the concentric cylinder and the capillary viscometer. The

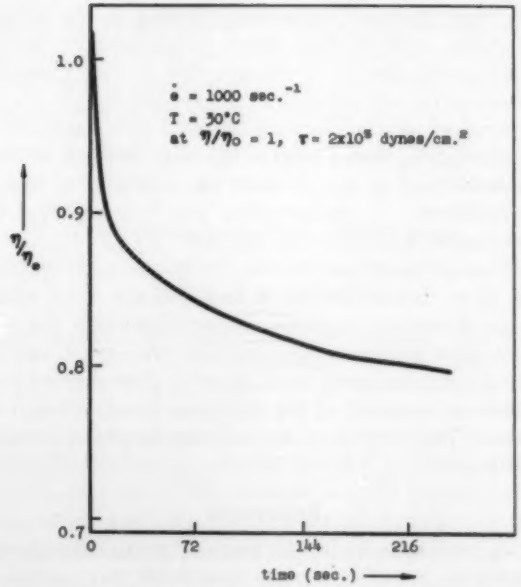

Fig. 2. Change of flow resistance with time at high shear rates (1000 sec.$^{-1}$) in Couette viscometer. Typical for soap fiber gels. $\eta_0 = \eta$ at $t = 0$.

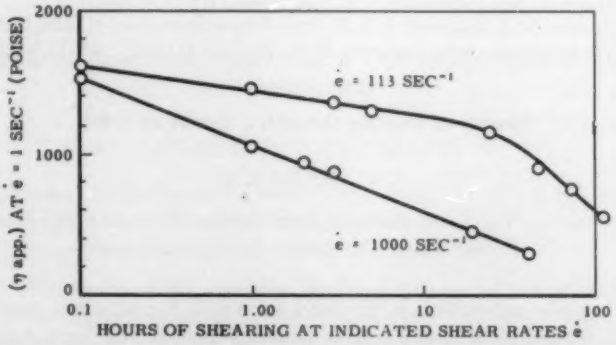

Fig. 3. Change in consistency (expressed as apparent viscosity at $\dot{e}$ = 1 sec.$^{-1}$) with time at high shear rates. Typical for soap fiber gels.

first yield point probably represents yielding in the gel-apparatus interface. Over a short shear stress range between the first and second yield points, pseudo-Newtonian flow is often observed. The gel plug seems to slip on a layer of oil and gel debris.

One of the most striking memory effects in gels composed of anisometric particles (e.g., soap fibers) is the large increase in yield stress (and flow resistance) as one reverses the direction of rotation in a Couette viscometer. A similar effect has been reported by Vinogradov[5] for the reversal of flow in a capillary.

The above-mentioned complications in flow measurements on oleogels, while quite understandable in terms of the weak forces which hold the gel structures together, rather discourage the search for general principles governing quantitative rheology of such systems. The utility of empirical gross descriptions of flow curves by means of various methods proposed in the literature is not affected by these observations. They only serve as a warning to those looking for more detailed answers.

References

1. (a) Bondi, A., Moore, R. J., and Peterson, W. H., *Institute Spokesman*, **1950** (3), 12.
   (b)Moore, R. J., and Cravath, A. M., *Ind. Eng. Chem.*, **43**, 2892 (1951).
   (c)Peterson, W. H., Accinelli, J. B., and Bondi, A., *Lubrication Eng.*, **12**, 45 (1956).
2. Bondi, A., and Penther, C. J., *J. Phys. Chem.*, **57**, 72 (1953).
3. Moses, E., and Puddington, I. A., *Can. J. Res.*, **B27**, 616 (1949).
4. Bonner, W. B., and Blott, J. F. T., *Proc. Intern. Rheol. Congr.*, **1948**, II-265.
5. Vinogradov, G., et al., *Neftyanoe Khoz.*, **25**, (12), 47 (1947); **26** (1), 52 (1948).

Theory of Peeling through a Hookean Solid

J. J. BIKERMAN

Department of Civil and Sanitary Engineering, Massachusetts Institute of Technology, Cambridge 39, Massachusetts

When the adhesive is a Hookean solid and the adhesive joint between a rigid plate and a flexible ribbon is peeled, the force required for peeling is $0.3799\ w\sigma\ (E/E_1)^{1/4}\ \delta^{3/4}\ y_0^{1/4}$, if w denotes the width of the ribbon, σ the tensile strength of the adhesive, E and E_1 the moduli

of elasticity of the ribbon and the adhesive, respectively, δ the thickness of the ribbon, and y_0 the initial thickness of the adhesive film. If $\delta = y_0$, the ratio of tensile force to stripping force needed for separation is of the order of l/y_0, l being the length of the ribbon.

[Published in *J. Appl. Phys.*, **28**, 1484 (1957).]

The Coalescence of Latex Dispersions

GEORGE L. BROWN

Research Laboratories, Rohm & Haas Company, Philadelphia, Pennsylvania

The process of coalescence of discrete polymer particles into a continuous polymer film is governed by the flow processes of the dispersion and of the polymer. It is proposed that the particles are brought into juxtaposition and then fused under the influence of the evaporating water, which acts by virtue of the adhesive force (between the polymer surface and the water) and the cohesive (tensile) strength of the water. This "capillary force" must be sufficient in magnitude and duration to overcome the resistance of the particles to deformation. An approximate mathematical solution is proposed.

Mechanical Resonance Dispersion in Crystalline Solids at Audio-Frequencies

EDWIN R. FITZGERALD

Department of Physics, The Pennsylvania State University, University Park, Pennsylvania

Measurements of the complex shear compliance ($J^* = J' - iJ''$) of various crystalline solids at closely spaced frequencies in the audio-frequency range have resulted in the discovery of multiple frequency dispersions of the resonance type. Values of the loss compliance (J'') have sharply defined maxima in the region from 100 to 5000

cycles/sec.; values of the storage compliance (J') rise to a maximum and then drop to pass through a minimum as a narrow (50 to 100 cycles/sec. wide) dispersion region is traversed in the direction of increasing frequency. Pure polycrystalline metals, crystalline polymers, and inorganic crystalline compounds have been found to exhibit the effect. The results indicate the presence of a dispersion mechanism different from those leading to the relaxation dispersions previously found for polymers and metals. The magnitudes and locations of the resonances depend on the static stress history and state of the material as well as temperature. In some cases the resonances are removed by annealing at a raised temperature (e.g., 150°C. for lead) and can be reintroduced by slight cold working. The dependence of the effect on static stress history suggests that motions of dislocations or other imperfections in the crystalline structure may be important in producing this type of dispersion. At present, however, there is no satisfactory explanation for these phenomena. In addition to their theoretical implications, the results are of considerable practical importance since they indicate that certain materials may undergo large changes in mechanical properties at a particular frequency or frequencies.

The Low-Temperature Transition in Polytetrafluoroethylene

N. G. McCRUM

Polychemicals Department, E. I. du Pont de Nemours & Co., Inc., Du Pont Experimental Station, Wilmington, Delaware

The internal friction and torsion modulus of polytetrafluoroethylene have been measured from −160 to −40°C. The experiment proved unambiguously that there is a transition in the region of −100°C. (1 cycle/sec.) and that it occurs in the amorphous regions of the polymer. A comparison is made of the experimental measurements with the predictions of a standard linear solid model.

[To be published in *J. Polymer Sci.*]

The Steady Flow of a Slightly Viscoelastic Fluid between Rotating Spheres

WILLIAM E. LANGLOIS

Polychemicals Department, E. I. du Pont de Nemours & Co., Inc., Du Pont Experimental Station, Wilmington, Delaware

The following case is considered: An incompressible, slightly viscoelastic fluid is contained between two concentric spheres which rotate slowly about a common axis of symmetry with different constant angular velocities. The motion thereby produced in the fluid is quite different from that which would result if the space between the spheres were filled with a Newtonian fluid. In addition to the rotary flow about the axis of symmetry, a secondary flow occurs in the meridianal planes. The feasibility of designing a rheometer based upon this fluid motion is discussed.

Use of Viscosity Measurements for Study of Entanglement in Polymer Solutions

S. H. MARON, N. NAKAJIMA, and I. M. KRIEGER

Department of Chemistry and Chemical Engineering, Case Institute of Technology, Cleveland, Ohio

Application of the Ree-Eyring theory to the non-Newtonian flow of polymer solutions permits separation of the contribution of solvent to the total viscosity of the solution. From a study of this solvent contribution as a function of polymer concentration, it is possible to evaluate a "swelling factor," and to study the effects of solvent, polymer concentration, and temperature upon this factor.

Such a study has been made with solutions of polystyrene in a number of solvents at several temperatures. The results obtained permit deductions to be made with respect to the state of entanglement of the polymer chains as a function of the above variables in both dilute and concentrated solutions.

Flow Experiments with Special Capillaries in the McKee Worker-Consistometer

HOBART S. WHITE and HARRIET V. BELCHER

National Bureau of Standards, Washington, D. C.

The McKee worker-consistometer consists essentially of two coaxial steel cylinders and mating pistons with a capillary shearing element between them. The material being tested is forced repeatedly through the shearing element, back and forth from one cylinder to the other. A special shearing element with a tapered capillary has been constructed, and flow data obtained with it have been compared with data obtained with a uniform bore capillary and a uniform bore capillary chamfered at one end. With polyisobutene-cetane solutions, degradation occurs at lower rates of flow and persists for a greater number of passes with flow entering the smaller end, compared to flow entering the larger end, of the tapered capillary. When degradation occurs in both directions at high rates of flow, the pressure is larger for flow entering the larger end, though after degradation has ceased the pressure (used to overcome viscous resistance) is less for flow in this direction, compared to flow entering the smaller end in each case.

Cooling Time of Strong Glass Fibers

O. L. ANDERSON

Bell Telephone Laboratories, Inc., Murray Hill, New Jersey

Simplified equations for the cooling time of glass fibers to the solid state are deduced from the well-known general theory of heat conduction. The approximations made are based upon a value of the order of 1 for Nusselts number. This value of N_U holds for comparable metallic fibers, as measured by Mueller, and is assumed to hold for glass fibers. The relation of pulling speed and flow rate to cooling time is shown. Calculations of cooling time of typical glass fibers

are made, and it is observed that they are of the same order as the Maxwell relaxation time of the glass at the orifice temperature. The consequence of this correlation is discussed in terms of the high strength of fibers, and the high "fictive" temperature of fibers.

[Published in *J. Appl. Phys.*, **29**, 9 (1958).]

The Viscosity of Gases

J. ROSS and R. V. HANKS

Department of Chemistry, Brown University, Providence, Rhode Island

Measurements have been made of the absolute viscosity of some gases in a new capillary flow viscometer as a function of temperature in the range of −78 to 100°C. and as a function of pressure in the range of 5–300 atm. The apparatus permits the determination of the viscosity as a function of flow rate at a given temperature and pressure. The precision of the measurements is of the order of 0.02% and the accuracy is estimated to be better than 0.1%.

Shear Rate Dependence of the Viscosity and Elastic Compliance of Polymer Melts—Correspondence with a Hydrodynamic Theory of Viscoelastic Flow

R. H. BOYD

Polychemicals Department, E. I. du Pont de Nemours & Co., Inc., Du Pont Experimental Station, Wilmington, Delaware

The variation of viscosity and steady state elastic compliance with shear rate of several typical polymer melts has been measured. The results are compared with the predictions of a hydrodynamic flow theory proposed by Y. H. Pao [*J. Appl. Phys.*, **28**, 591 (1957)]. The agreement is satisfactory.

[Published in *J. Appl. Phys.*, **29**, 953 (1958)]

Stress Relaxation in Glass

I. L. HOPKINS

Bell Telephone Laboratories, Inc., Murray Hill, New Jersey

Successive stress relaxation experiments on glass both at and below the fictive temperature show that in the latter case there is a gradual change in the glass during the test, resulting in this particular instance in a change in the total viscosity of over ten times. If it is assumed that the change in the glass is a shift of the relaxation spectrum with time, such that all the relaxation times are multiplied by the same function of time—analogous to the a_T of Ferry and the $K(T)$ of Tobolsky associated with a temperature change—it is possible to find the manner in which this factor changes with time.

If the glass is preconditioned at constant temperature, not under stress, for a time sufficient to reach approximate equilibrium and a relaxation test then made, the relaxation curve differs in shape from those obtained from successive runs on another specimen of the same material which has been continually under stress. The latter curves have a greater negative slope than the former. This suggests that some structural change—perhaps devitrification—is inhibited by the presence of stress.

Fracture of Non-Newtonian Fluids at High Shear Stresses

A. B. METZNER

University of Delaware, Newark, Delaware

While the fracture of polymer melts during extrusion has been the subject of several recent papers, no similarly quantitative data have been reported on suspensions of solids in liquids. This paper presents such data on TiO_2 suspensions in water and syrups.

Theories of the fracture phenomena of fluids are reviewed in the light of all available data. No definite choice of only one theory may be made at this time, but several theories are shown to be at sufficient variance with experimental facts to warrant their rejection.

TRANSACTIONS OF THE SOCIETY OF RHEOLOGY II, 313–314 (1958)

Corrigenda

A Stochastic Process Model for Mechanical Breakdown

[*Trans. Soc. Rheology*, 1, 153–168 (1957)]

BERNARD D. COLEMAN

Mellon Institute, Pittsburgh 13, Pennsylvania

Equations (10) and (15) should read as follows:

$$p_{N,n}(t \mid f)dt = \sum_{j=N}^{n} \phi_{N,n,j}\, \lambda_{N,j}\, e^{-\lambda_{N,j} t}\, dt \tag{10}$$

$$E_{N,n}\{e^{i\psi t}\} = \prod_{j=N}^{n} (1 - i\psi/\lambda_{N,j})^{-1} \tag{15}$$

The condition for the convergence of all of the integrals in eqs. (22) was incorrectly stated in the sentence which includes eq. (23), (page 160). This sentence says that the integrals in eqs. (22) will converge if

$$\lim_{y \to 0} k(f/y) \to \infty \tag{23}$$

at least as fast as $(f/y)^{\epsilon}$, $\epsilon > 0$. This condition is necessary for the convergence of all the integrals, but is not sufficient. It is sufficient for (22a) but not for (22b) and (22c). Actually, a sufficient condition which is strong enough to apply to all three of these integrals is obtained if we say that the limit shown in eq. (23) must be approached at least as fast as $(f/y)^{3/2+\epsilon}$. This new condition will still be met by any real physical system.

The convergence of the integrals in eqs. (22) implies that

$$\lim_{N \to \infty} E_{N,1}\{t\} < \infty \tag{a}$$

$$\lim_{N \to \infty} \sigma_{N,1}/E_{N,1}\{t\} = O(N^{-1/2}) \to 0 \tag{b}$$

$$\lim_{N \to \infty} \mu_{N,1}{}^3/\sigma_{N,1}{}^3 = O(N^{-1/2}) \to 0 \tag{c}$$

$$\lim_{N \to \infty} E_{N,1}\{|t - E_{N,1}\{t\}|^3\}/\sigma_{N,1}{}^3 = O(N^{-1/2}) \to 0 \tag{d}$$

The last of the above equations is the hypothesis in Liapounoff's form of the central limit theorem. In other words, equation (d) implies that the distribution of lifetimes is normal (Gaussian) for separate slabs. In the original article it was stated that the distribution of lifetimes is normal, but equation (d), which is needed to make this statement evident, was not given. Equation (d) is easily derived directly from (b) and (c) through the use of the fact that t is always ≥ 0, and therefore, $E_{N,1}\{|t - E_{N,1}\{t\}|^3\} \leq E_{N,1}\{(t + E_{N,1}\{t\})^3\}$. Equations (a), (b), (c), and (d) are, of course, all valid when $k(f) = \alpha \exp\{\beta f\}$.